The molecular basis of G_s protein efficacy at the β_2-adrenoceptor

Clare R. Harwood, MSci (Hons)

Thesis submitted to the University of Nottingham for the degree of Doctor of Philosophy

July 2022

This thesis is entirely the candidates own work. The experiments described in the this were performed between 2018 and 2022 in the Cell Signalling Research Group, University of Nottingham. No part of this work has been submitted previously for a degree or any other qualification at any university,

Abstract

GPCRs are the largest family of transmembrane receptors in the human genome and currently represent 34% of all FDA approved medicines. The β_2-adrenoceptor (β_2AR) is a prototypical class A GPCR which is therapeutically relevant in asthma, whereby β_2AR agonists relieve bronchoconstriction. Despite the therapeutic importance of the β_2AR and other GPCRs the molecular basis of agonist efficacy is not well understood.

The hypothesis underlying this study was that ligand residence time effects β_2AR receptor conformational dynamics to affect efficacy of G_s protein activation. To this end, this thesis investigated β_2AR agonist ligand binding kinetics and purified mini-G_s binding kinetics to β_2AR that had been extracted from the mammalian cell membrane using detergent. This study found no correlation between ligand residence time and G_s protein efficacy for β_2AR agonists but found differences in the affinity of full agonist bound β_2AR complexes for the mini-G_s compared to partial agonist bound complexes.

These results do not support a role for kinetics in the molecular basis of efficacy at the β_2AR but suggest a model in which agonists of higher efficacy stabilise a conformation of the β_2AR which is more likely to recruit a G_s protein. Moreover, this thesis shows the development and application of novel methods to study isolated GPCR dynamics and pharmacology. Further application of this approach to a greater number of GPCRs and agonists would elucidate if the model presented in this study is relevant to other receptors and if this shows a general mechanism of efficacy.

Publications arising from this thesis

Papers

Harwood, CR. Sykes, DA. Hoare, BL. Poyner, PR. Briddon, SJ. Veprintsev, DB. (2021). Functional solubilisation of the β_2-adrenoceptor using diisobutylene maleic acid. iScience 24, 103362

Abstracts

Harwood, CR. Sykes, DA. Hoare, BL. Poyner, PR. Briddon, SJ. Veprintsev, DB. (2019/2020). Functional solubilisation of the β_2-adrenoceptor using diisobutylene maleic acid. Poster Pharmacology, Edinburgh 2019, Oral presentation European SMALP conference 2020 (cancelled due to COVID-19)

Harwood, CR, Briddon, SJ. Veprintsev, DB (2022)
Agonist efficacy at the β_2-adrenoceptor (β_2AR) is driven agonist induced conformational differences that increase the affinity of the β_2AR for the G_s protein.
Poster Keystone: GPCRs: An Odyssey from structure, signaling and regulations to therapeutics, Snowbird Utah 2022

Acknowledgments

I would like to thank my supervisors, Professor Dmitry Veprintsev and Dr Stephen Briddon, for their help, support, and guidance over the last 3.5 years, as for well as the opportunity to work on such an interesting project.

I would also like to thank past and present members of Dmitry's lab group for their instruction and discussion. Particularly, Dr David Sykes for his help and advice with the kinetic experiments in this thesis.

I am very grateful to the whole Cell Signalling research group, for creating such a positive and collaborative working environment. Their encouragement and engagement in scientific discussion was enormously helpful, and fun in and out of the lab.

Of course, this was done in a pandemic, among other crises, and I would like to thank my all my friends and family for their love and support during this time. Especially, my parents, who for some reason always seemed to believe in me, and my friends and 'households' in Nottingham for their companionship during this time. A special thanks to Fi, Charlie, Rhi, Beth, Desi, and Lydia[2].

Abbreviations

$A_{2A}R$	Adenosine-2A receptor
AC	Adenylyl cyclase
ATP	Adenosine triphosphate
β_1AR	β_1-adrenoceptor
β_2AR	β_2-adrenoceptor
B_{max}	Maximal specific binding of the system
BSA	Bovine Serum Albumin
C26	7-[(R)-2-((1R,2R)-2-benzyloxycyclopentylamino)-1-hydroxyethyl]-4-hydroxybenzothiazolone
cAMP	3,'5'-cyclic adenosine monophosphate
CHO cells	Chinese Hamster Ovary cells
CMV	Cytomegalovirus
CV	Column Volume
Cyanopindolol hemifumerate	1-(1H-indol-4-yloxy)-3-(propan-2-ylamino)propan-2-ol
DDM	n-dodecyl-β-D-maltoside
DIBMA	Diisobutylene Maleic Acid
DIBMALP	Diisobutylene Maleic Acid Lipid Particle
DMEM	Dulbecco's Modified Eagle's Medium
DMSO	Dimethyl Sulphoxide
EC_{50}	Concentration at which half the system maximal response occurs
E_{max}	Maximal response of the system
E.coli	Esherichia coli
Epinephrine hydrochloride	4-[1-hydroxy-2-(trideuterio(113C)methylamino)ethyl]benzene-1,2-diol;hydrochloride
F-propranolol	Fluorescent propranolol
F-XAC	Fluorescent Xanthine Amine Cogener
FBS	Fetal Bovine Serum
FSEC	Fluorescence Size Exclusion Chromatography

GDP	Guanosine diphosphate
GPCR	G Protein-Coupled Receptor
GTP	Guanosine triphosphate
HBSS	Hank's Balanced Salt Solution
HEK	Human Embryony Kidney
HPLC	High Performance Liquid Chromatography
IC_{50}	Concentration at which half inhibitory response occurs
ICI 118, 551	(-)-1-[2,3-(Dihydro-7-methyl-1H-inden-4-yl)oxy]-3-[(1- methylethyl)amino]-2-butanol
IMAC	Immobilised Metal Affinity Chromatography
IPTG	Isopropyl β-d-1-thiogalactopyranoside
K_d	Equilibrium dissociation constant (concentrations at which half the receptors are occupied)
K_{obs}	Observed rate of association
K_{on}	Association rate constant
K_{off}	Dissociation rate constant
NECA	5'-*N*-Ethylcarboxamidoadenosine
Noradrenaline	4-[(1*R*)-2-amino-1-hydroxyethyl]benzene-1,2-diol
NTPs	Nucleotide Triphosphates
PBS	Phosphate buffered saline
PCR	Polymerase Chain Reaction
PDL	Poly D-lysine
PEI	Polyethylenimine
PEN/Strep	Penicillin Streptomycin
SEC	Size Exclusion Chromatography
SMA	Styrene Maleic Acid
SMALP	Styrene Maleic Acid Lipid Particles

Table of Contents

Chapter 1 ..... *1*

Introduction *1*

1.1 GPCRs **2**

1.2 The therapeutic potential of GPCRs **3**

1.3 The β_2-adrenoceptor **3**

1.4 Heterotrimeric G proteins **6**

1.4.1 Gα subunits and their activation at the structural level 6

1.4.2 Downstream signalling by heterotrimeric G proteins 7

1.5 GPCR pharmacology **10**

1.5.1 Drug receptor theory 10

1.5.2 The extended ternary complex model 11

1.5.3 Agonists and antagonists 13

1.6 Current understanding of molecular basis of efficacy at GPCRs **14**

1.6.1 Contribution of structural studies to understanding the molecular basis of efficacy 15

1.6.2 Contribution of biophysical studies to understanding the molecular basis of efficacy 17

1.6.3 Evidence for the role of kinetics in the molecular basis of efficacy 18

1.7 Evidence for a role of ligand binding kinetics in the molecular basis of efficacy **19**

1.8 GPCR molecular pharmacology in the cellular environment **19**

1.8.1 Modulation of GPCR dynamics by the cell membrane 20

1.8.2 Modulation of GPCR signalling by cellular regulation 20

1.9 Methods to extract proteins from the plasma membrane **21**

1.10 Mini-G_s proteins: sensors for active GPCRs **24**

1.11 Aims and Objectives **27**

Chapter 2 ..... *28*

Materials and methods *28*

2.1 Materials **29**

2.1.1 Mammalian cell culture reagents: 29

2.1.2 Molecular biology reagents: 29

2.1.3 Protein purification materials: 30

2.1.4 Compounds: 30

2.2 Methods **32**

2.2.1 Molecular biology 32

2.2.2 Mammalian cell culture 39

2.2.3 NanoBRET 43

2.2.4 Venus-mini-G_s recruitment BRET assays in HEK293T/17 cells 43

2.2.5 CASE-G_s activations BRET assays 44

2.2.6 Production of TS-SNAP-β_2AR from mammalian cells 45

2.2.7 Fluorescence Size Exclusion Chromatography (FSEC) 47

2.2.8 Bacterial cell culture 48

2.2.9 Production of purified mini-G_s proteins 49

2.2.10 SDS-page electrophoresis 50

2.2.11 TR-FRET 51

2.2.12 TR-FRET Ligand binding studies 53

2.2.13 TR-FRET thermostability assays 54

2.2.14 In solution intermolecular nanoBRET assays 55
2.2.15 Venus mini-G_s nanoBRET recruitment assays 56
2.2.16 Venus mini-G_s nanoBRET kinetic assays 56
2.2.18 Data analysis 58

Chapter 3 65

Solubilisation of the functional β_2AR using Diisobutylene Maleic acid (DIBMA) 65

3.1 Introduction 66
3.1.1 Methods previously employed to solubilize the β_2AR 66
3.1.2 Applicability of using polymers to solubilize the β_2AR 67
3.1.3 Methods to characterise membrane protein stability 68
3.1.4 Methods to characterise membrane protein functionality 70

3.2 Methods 72
3.2.1 Mammalian cell culture 72
3.2.2 Solubilisation of TS-SNAP-β_2AR or TS-SNAP-A_{2A} using DDM or DIBMA. 72
3.2.3 TR-FRET thermostability assays 72
3.2.4 TR-FRET ligand binding assays 72
3.2.5 Halo-mini-G_s shift assay 73

3.3 Results 74
3.3.1 Solubilisation of the TS-SNAP-β_2AR from the mammalian membrane 74
3.3.2 Saturation ligand binding studies on TS-SNAP-β_2AR in membranes, DDM micelles and DIBMALPs 78
3.3.3 Competition ligand binding studies on TS-SNAP-β_2AR in membranes, DDM micelles and DIBMALPs: 81
3.3.4 TR-FRET thermostability studies on TS-SNAP-β_2AR in membranes, DDM micelles and DIBMALPs 84
3.3.5 TR-FRET ligand binding shift studies to investigate the ability of DIBMALP-β_2AR to couple Halo-mini-G_s 90
3.3.6 TR-FRET ligand binding shift studies to investigate the ability of DIBMALP-A_{2A} to couple Halo-mini-G_s 94

3.4. Discussion 97
3.4.1 DIBMA can extract β_2AR from the mammalian cell membrane 97
3.4.2 DIBMALP-β_2AR retains ligand binding capabilities 97
3.4.3 DIBMALP-β_2AR retains native pharmacology and conformational landscape 98
3.4.4 DIBMALP-β_2AR shows improved thermostability 99
3.4.5 DIBMALP-β_2AR cannot couple Halo-mini-G_s 100
3.4.6 Conclusion 101

Chapter 4 102

Pharmacological characterisation of eight agonists for the β_2AR 102

4.1 Introduction 103
4.1.1 The eight β_2AR agonists chosen for this study 103
4.1.2 Use of TR-FRET to measure ligand binding kinetics 106
4.1.3 Defining efficacy using a G_s protein activation assay 107
4.1.4 Aims: 109

4.2 Methods 110
4.2.1 TR-FRET ligand binding assays 110
4.2.2 CASE-G_s activation assays 110

4.3 Results 112
4.3.1 Development of a TR-FRET ligand binding kinetics assay 112
..... 114

4.3.2 Measurement of the ligand binding kinetics of eight β_2AR agonists..... 120
4.3.3 Equilibrium competition binding of eight β_2AR agonist..... 123
4.3.4: Assessment of the relative time to reach equilibrium of eight β_2AR agonists..... 127
4.3.5 Development of CASE G_s activation assay..... 128
4.3.6 Quantifying the efficacy of eight β_2AR agonists using the CASE G_s activation assay..... 137
..... 139

4.4 Discussion..... 141
4.4.1 The development and limitations of a TR-FRET kinetic ligand binding assay..... 141
4.4.2 The ligand binding kinetics of eight β_2AR agonists binding the DDM-TS-SNAP-β_2AR..... 142
4.4.3 The relative K_{off} values of eight β_2AR agonists can be ranked by time to equilibrium..... 143
4.4.4 The CASE G_s activation assay required the development of the clone A5 144
4.4.5 Comparison of the CASE G_s activation data to published studies 145
4.4.6 Quantification of efficacy of eight β_2AR agonists efficacy using CASE G_s activation 146
4.4.7 There is no correlation between ligand residence time and efficacy for these β_2AR agonists..... 148
4.4.8 Conclusion 150

Chapter 5..... 151

Investigating the role of G_s protein binding kinetics in the molecular basis of efficacy 151

5.1 Introduction..... 152
5.1.1 Use of mini-G_s proteins as tools to investigate β_2AR activation 152
5.1.2 Use of nanoBRET to investigate β_2AR-mini-G_s binding 153
5.1.3 Aims: 154

5.2 Methods 155
5.2.1 Production of mini-G_s proteins..... 155
5.2.2 Production of TS-SNAP-β_2ARnLuc 155
5.2.3 In-solution intermolecular BRET assays to investigate TS-SNAP-β_2ARnLuc: venus-mini-G_s pharmacology 155
5.2.4 Venus-mini-G_s recruitment assays in cells..... 156

5.3 Results 157
5.3.1 Production of mini-G_s proteins from *E*. coli..... 157
5.3.2 Characterisation of mini-G_s protein preparations binding the TS-SNAP-β_2ARnLuc 159
5.3.3 Characterisation of venus-mini-G_s association and dissociation from the DDM-TS-SNAP-β_2ARnLuc..... 164
5.3.4 Investigation of purified venus-mini-G_s binding kinetics at DDM- TS-SNAP-β_2ARnLuc in complex with eight β_2AR agonists..... 176
5.4.1 Mini-G_s proteins produced in this study bound TS-SNAP-β_2AR in response to agonists stimulation..... 187
5.4.2 N terminal fusion tags decreased mini-G_s affinity for TS-SNAP-β_2ARnLuc 188
5.4.3 Venus-mini-G_s association to TS-SNAP-β_2ARnLuc is biphasic and dissociation is incomplete 189
5.4.4 Full agonists increased the affinity of DDM-TS-SNAP-β_2ARnLuc for the venus-mini-G_s protein..... 191

Chapter 6 ..... *193*

General discussion *193*

6.1 General discussion **194**

6.1.1 DIBMALPs but not detergent affected β_2AR function 194

6.1.2 Demonstration of novel methods to characterise membrane protein preparations 196

6.1.3 Agonist residence time did not correlate with efficacy at the β_2AR 197

6.1.4 Agonist efficacy correlated with likelihood to recruit mini-G_s at the β_2AR 197

6.1.5 Future work 202

6.2 General conclusion **203**

Chapter 7 ..... *204*

Appendices and references *204*

7.1 Supplementary data **205**

7.1.1 Vector maps 205

7.1.3 Monte carlo simulations of TR-FRET ligand binding assays 209

7.1.4 Analysis of percentage of fast reversible and slow irreversible components of venus- mini-G_s binding to the DDM-TS-SNAP-β_2ARnLuc 213

Chapter 1
Introduction

1.1 GPCRs

G protein-coupled receptors (GPCRs) are seven transmembrane receptors that regulate a broad range of physiological processes. This includes the detection and transmembrane transduction of signals mediated by hormones, chemokines in the immune system, neurotransmitters, and even light from the retina. In addition to their seven transmembrane helices, GPCRs are defined by their ability to couple to heterotrimeric guanine nucleotide binding proteins (G proteins), although it is now understood that GPCRs can signal through other proteins and signalling cascades, for example arrestins.

This superfamily of receptors accounts for 2% of the human genome and are therefore the largest family of transmembrane receptors (Schiöth & Fredriksson, 2005) (Venter et al., 2001). Phylogenetic analysis of human GPCRs has subdivided GPCRs into the five classes of the GRAF classification system, which is based primarily on sequence homology; namely Rhodpsin-Like (class A), secretin receptor family (class B), glutamate receptor family (class C), adhesion receptor family and frizzled receptor family (Schiöth & Fredriksson, 2005). These sub families show functional and structural differences. The β_2-adrenoceptor is a class A or rhodopsin-like GPCR. The majority of class A GPCRs contain a NsxxNPxxY motif in transmembrane domain 7 (TM7), a DRY motif between TM3 and intracellular loop (IL2) and generally have shorter N termini then other classes of GPCR (Figure **1.1**). The DRY motif forms a salt bridge with TM6, known as the ionic lock, which stabilises the receptor in its inactive conformation and is broken upon receptor activation. Similarly, the NsxxNPxxY motif stabilises the active state via a hydrogen bond between $Y^{7.53}$ and $Y^{5.58}$ (Ballesteros & Weinstein, 1995). The ligands of class A GPCRs generally bind between the TM regions as opposed to the larger N termini as is the cases in other classes of GPCR.

1.2 The therapeutic potential of GPCRs

GPCRs are easily accessible membrane receptors, which generally have modulatory roles in physiology. GPCRs therefore represent an opportunity to target a large range of diseases. Indeed, GPCRs currently represent 34% of all US food and drug administration (FDA) approved drugs, with 475 drugs targeting over 100 diverse receptors. Moreover, a further 321 agents aimed at over 60 novel GPCR targets are in clinical trials (Hauser et al., 2017), implying that the therapeutic potential of GPCRs is still underexploited.

1.3 The β_2-adrenoceptor

The β_2AR is a member of the adrenoceptor sub family within the class A GPCR family. Adrenoceptors respond to neurotransmitters adrenaline and noradrenaline to form the interface between the sympathetic nervous system and the cardiovascular system (Triposkiadis et al., 2009), therefore contributing to the modulation of the 'fight or flight' response. As such adrenoceptors are expressed in most tissues and organ systems.

There are nine different adrenoceptors in total, including three α_1, three α_2 and three β receptors (Alexander et al. 2021). α-adrenoceptors are concerned with regulation of smooth muscle and vascular tone whilst α_2-adrenoceptors are also involved in regulation of neurotransmitter release (Philipp et al., 2002). Understanding of the precise role of α-adrenoceptor subtypes remains incomplete (Philipp et al., 2002). Conversely, the specific physiological roles of the β-adrenoceptors are much better characterised. The β_1-adrenoceptor (β_1AR) is expressed primarily in the heart and its stimulation is well-established in increasing the rate and contractility of the heart. The β_3-adrenoceptor is also involved in modulation of heart contractility and in lipolysis and thermogenesis of adipose tissues (Schena & Caplan, 2019).

The β_2 adrenoceptor (β_2AR) (Figure **1.1**) is expressed primarily in the lungs, heart, peripheral vasculature, gastrointestinal (GI) tract, adipose tissue, skeletal muscle, and female reproductive system. The β_2AR signals primarily via the G_s protein although it has also been showed to couple G_i in the heart (Hill and Baker, 2003). The β_2-adrenoceptor is a well-established target for asthma whereby β_2 agonists are used to relax the constricted lung smooth muscle via G_s protein activation and adenylyl cyclase signalling (Cazzola, et al., 2011). As such, a large range of agonists of varying potencies and selectivity's for β_2AR compared to the other adrenoceptors have been developed. These ligands are discussed in more detail in **sec 4.1.**

The clinical importance of β_2AR in combination with it being one of the first GPCRs to be cloned (Dixon et al., 1986), has led to β_2AR becoming one of the most studied GPCRs over the years and therefore a prototypical GPCR to study. Indeed, there are now 38 structures of the β_2AR (Berman et al., 2000). These include β_2AR in complex with an inverse agonist (Rasmussen et al., 2007) (Wacker et al., 2010), partial agonist (Masureel et al., 2018), full agonist (Zhang et al. 2020), antagonist (Wacker et al., 2010) and in complex with the full length G_s protein (Rasmussen et al., 2011b). Moreover, there have also been several in-depth biophysical studies into its dynamics and activation of the heterotrimeric G_s protein in response to different ligands (Du et al., 2019) (Gregorio et al., 2017) (Nygaard, et al. 2013) (Manglik et al., 2015). These structural and biophysical studies are discussed in more detail in **sec 1.5**. The clinical importance of the β_2AR have led to the development of a range of agonists and more advanced understanding of its molecular mechanism compared to other GPCRs, this makes β_2AR an sensible choice to study the molecular basis of efficacy at class A GPCRs.

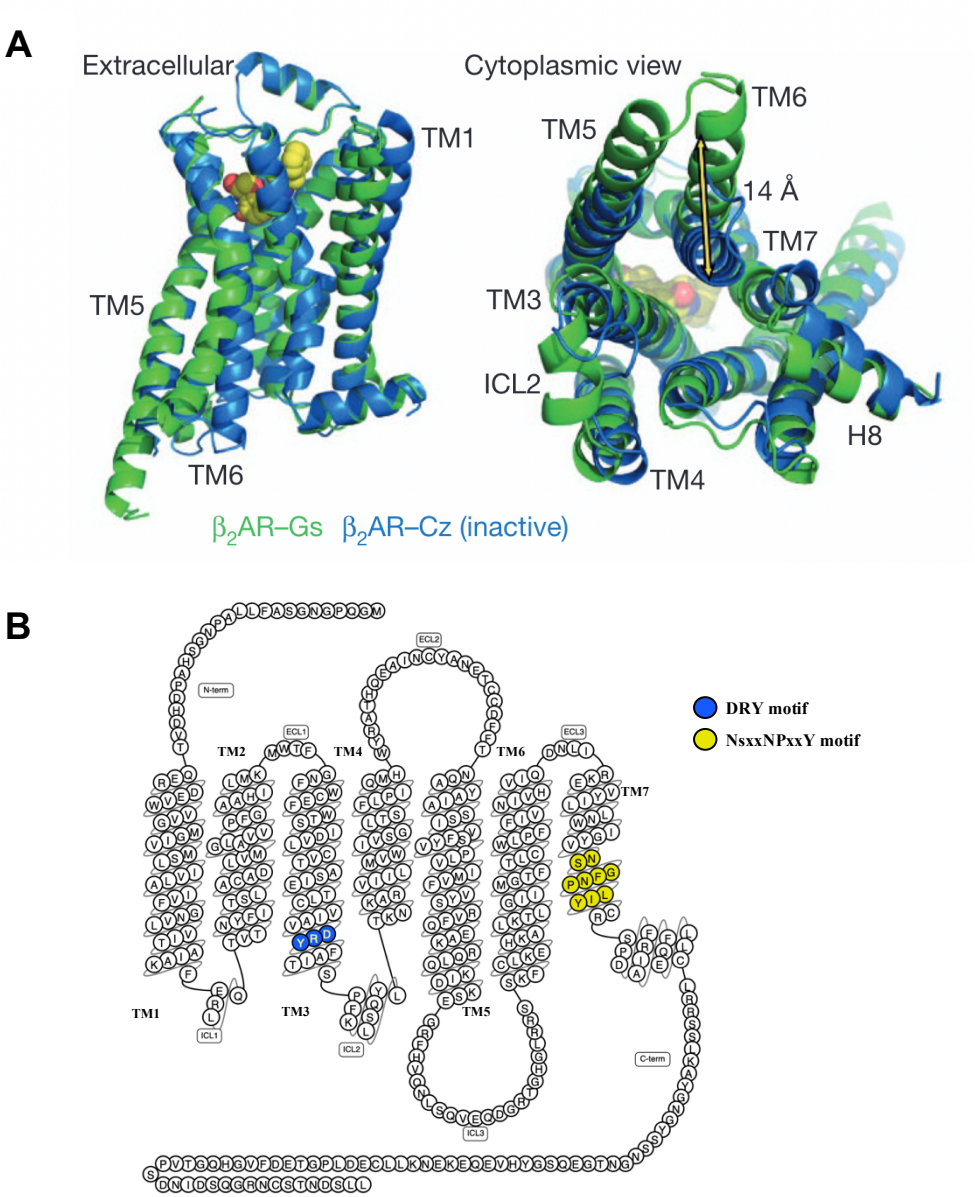

Figure 1.1: The β_2-adrenoceptor A) Comparison of the active (green) and inactive (blue) structures of the β_2AR, showing outward movement of TM5 and 6 to accommodate G_s protein coupling (Rasmussen et al. 2011b), **B)** Primary sequence of the human β_2AR showing DRY and NPY motifs**,** snake plot adapted from www.gpcrdb.org (Pándy-Szekeres et al., 2018)

1.4 Heterotrimeric G proteins

GPCRs signal primarily through coupling heterotrimeric guanine nucleotide binding proteins (G proteins). Heterotrimeric G proteins consist of an α, β, and γ subunit. Although G protein subunits are far from as numerous as their receptors there are 16 Gα subunits, 5 Gβ subunits, and 11 Gγ subunits (Downes & Gautam, 1999). α subunits are classified into four main classes (α_s, α_i, α_q and $\alpha_{12/13}$) according to their sequence homology. This allows for numerous heterotrimer combinations, indeed except for β5, all possible βγ combinations have been shown to form dimers and to heterotrimerise with α_{i1} and α_{sL} in insect cells (Hillenbrand et al., 2015). This is the largest characterisation study to date, however the functional and physiological relevance of these different heterotrimer combinations remains poorly characterised. Although a GPCR is generally able to couple multiple G proteins not every GPCR is necessarily able to couple all heterotrimer combinations of the Gα subunit, (Hillenbrand et al., 2015) and different ligands have been shown to differentially effect heterotrimer coupling of a GPCR. This is true for both synthetic (Mukhopadhyay, 2005) and endogenous ligands (McLaughlin et al., 2005). G protein subunit expression has been shown to vary across the body (Syrovatkina et al. 2016), suggesting G protein subunit combinations to be a physiological mechanism for modulating signalling. Overall, different heterotrimer combinations, expression and ligands allow for a diverse range of GPCR-G protein signalling responses.

1.4.1 Gα subunits and their activation at the structural level

Although knowledge of the physiological relevance of different G β and γ subunits remains limited, knowledge of Gα signalling and the structural mechanism of activation is much better understood. Gα proteins consist of a GTPase domain and α helical domain, which close around the nucleotide binding pocket. The GTPase domain has intrinsic GTPase activity, whilst the helical domain forms a lid over the nucleotide binding pocket preventing nucleotide dissociation. Upon activation of the G protein the helical domain rotates out from the GTPase domain and

structural changes in the nucleotide binding pocket allow GDP dissociation and GTP association (Rasmussen et al., 2011b). The full structure of the heterotrimeric G protein is shown in figure **1.5**. The β_2AR is understood primarily to signal through the stimulatory G protein $G\alpha_s$. Structural studies of agonist-β_2AR-$G\alpha_s$ (Rasmussen et al., 2011b) (Zhang et al., 2020) complexes show that outward displacement of the TM6 of β_2AR allows binding of the G_s heterotrimer via the $G\alpha_s$ GTPase domain. The C terminus of the activated $G\alpha_s$ projects into the transmembrane core of the receptor and appears to displace the α5 helix which propagates structural changes to disrupt the nucleotide binding pocket, leading to the displacement of GDP. Cytoplasmic GTP then associates activating the heterotrimeric G protein so that the α and βγ subunits dissociate.

1.4.2 Downstream signalling by heterotrimeric G proteins

Both α and βγ subunits may activate further signalling molecules for example $G\alpha_s$ commonly activates adenylyl cyclases (AC) (Tang et al., 2016), which then goes on to activate the conversion of ATP into cyclic 3',5'- adenosine monophosphate (cAMP). βγ subunits has been shown to independently directly activate inward rectifying potassium channels (GIRKs) (Logothetis et al. 1987), various isoforms of phospholipase C (PLC) (Kresge, et al 1992) and SNAP-25 (Blackmer et al., 2005) which is directly involved in neurotransmitter release. G protein signalling is terminated when GTP is hydrolysed to GDP through the intrinsic GTPase activity of the α subunit**.** The G protein activation cycle is summarised in figure **1.2.**

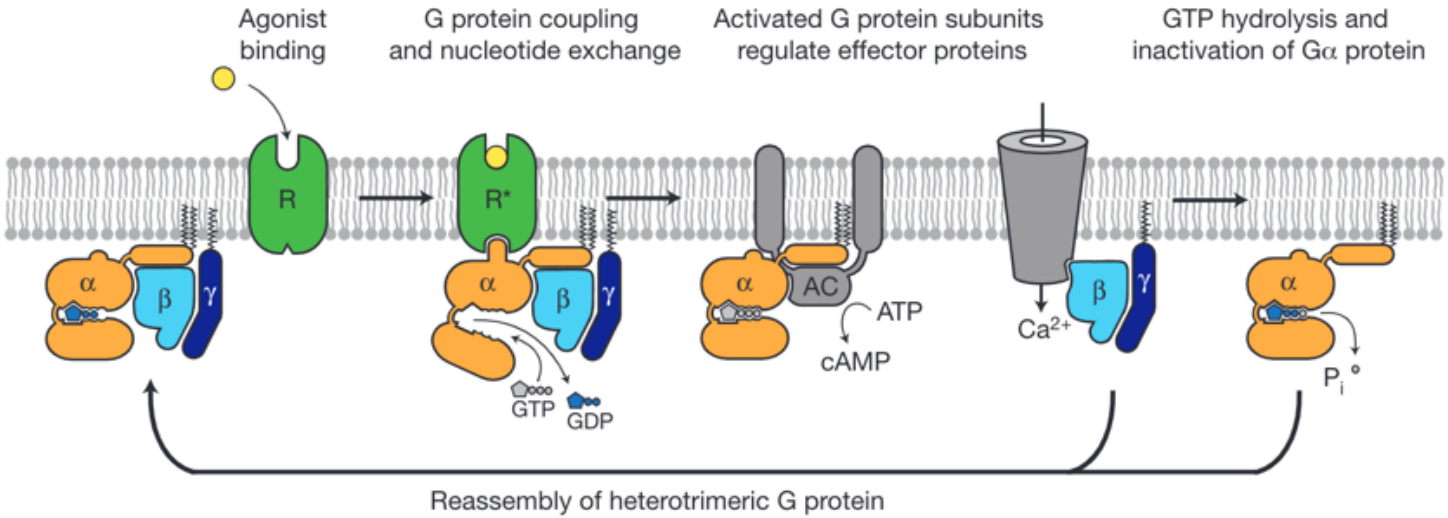

Figure 1.2: Ligand induced G protein activation by the β_2AR: GPCRs can signal through G proteins whereby GPCR- G protein coupling activates the G protein through nucleotide exchange releasing Gα and Gβγ subunits which go on to initiate downstream signalling. β_2AR activates $G\alpha_s$ which couples AC whilst *G*βγ subunits can initiate several responses including the direct activation of ion channels. Adapted from (Rasmussen et al. 2011).

1.5 GPCR pharmacology

1.5.1 Drug receptor theory

Naturally, to affect the activity of any receptor a ligand must firstly bind to that receptor. Ligand binding can be described by the law of mass action as shown in equation **1.1.**

$$Ligand + Receptor \underset{K_{on}}{\overset{K_{off}}{\leftrightharpoons}} Ligand.Receptor.$$

Equation 1.1: Lligand binding can be described by the law of mass action, whereby ligand binds with the receptor to give the ligand-receptor complex.

The affinity of a ligand for a receptor can be described by the equilibrium dissociation constant K_d which is the ratio of K_{off}/K_{on}. K_d can be measured in equilibrium binding conditions as the concentration at which 50% of the maximal binding of the ligand at the receptor is achieved. Whilst optimising the affinity of ligand for receptor has always been considered essential in drug development, more recently the kinetic properties of the ligand are becoming increasingly recognised in pharmacodynamics (Sykes et al. 2019).

Equation **1.1** shows that the rate of association of the ligand-receptor complex is described by the k_{on} and the rate of dissociation of the complex by the k_{off} (Kenakin, 2016). The K_{on} is a second order reaction as it describes the rate at which two molecules (ligand and receptor) bind. The K_{on} is diffusion limited as this is clearly the maximum rate at which two molecules can move through aqueous solution to collide. Therefore, K_{on} cannot be greater than K_{on} $1x10^9$ M^{-1} s^{-1} (D'ans et al., 1952). As K_{off} describes the dissociation of the ligand-receptor complex this a first order reaction, which is independent of the ligand

concentration and entirely dependent on the specific interactions of the ligand and receptor. A ligands' residence time at the receptor is the reciprocal of K_{off}.

1.5.2 The extended ternary complex model

The ternary complex model (De Lean et al., 1980) (Figure **1.3**) describes how a ligand must bind the GPCR and then in turn form an active complex with a G protein to bring about a response. The original ternary complex model evolved from the observation that guanine nucleotides affect the affinity of agonists binding to the GPCR therefore showing the co-operativity of agonists and G protein binding (De Lean, 1980). This model was then developed into the extended ternary complex model following the observation that constitutively active GPCRs could also couple G proteins in the absence of an agonist (Samamasb et al., 1993). As such, the extended ternary complex model describes how GPCR signalling through G protein coupling is subject to a number of rate-limiting steps, namely the association and dissociation rates of both the agonist and the G protein. These rates have rarely been characterised when considering agonist efficacy. However, both this model and these rates with will form the basis of our study.

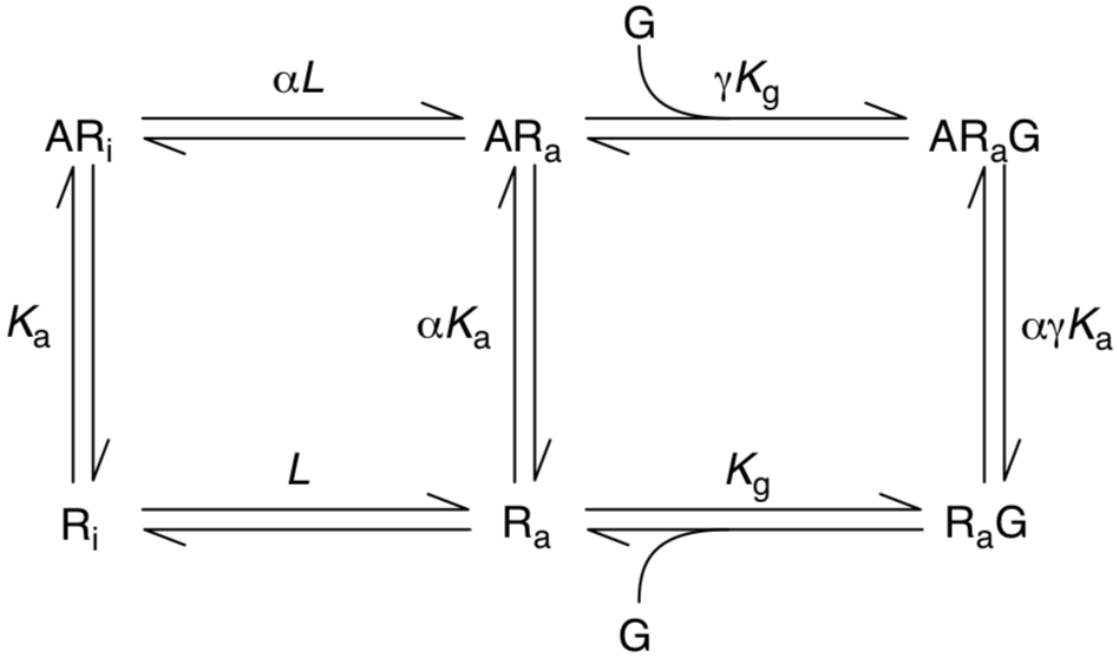

Figure 1.3: The extended ternary complex model describes how G protein coupling to ligand bound GPCR is a two-step process, whereby agonist binding precedes G protein binding: A = agonist, R = receptor, G = G protein, R_I = inactive receptor, R_a= active receptor, α and γ describe efficacy (Kenakin 2017).

1.5.3 Agonists and antagonists

Once a ligand has bound to a receptor it can be classified by the type of effect it brings about. An agonist can be defined as a ligand that binds to a receptor and causes a response. The ability of an agonist to bring about a response will depend on both its affinity for the receptor and its intrinsic efficacy, that is the efficiency of the ligand to bring about the response. Agonists can be broadly categorised into three types: full, partial, and inverse. These are summarised in figure **1.4**. A full agonist can be defined as a ligand which causes the maximal possible response for the receptor in the system in question, and a partial agonist can be defined as a ligand which causes a response that is less than that of the maximal response of the receptor in the system in question. An inverse agonist is a ligand which decreases the constitutive or basal activity of a receptor. A neutral antagonist is a ligand which blocks the activity of a ligand at a receptor but does not decrease the constitutive activity of that receptor. Furthermore, it is now appreciated that a GPCR may signal through multiple pathways, and that different ligands may differentially modulate the signalling down each of these pathways. This phenomenon is known as ligand bias.

As GPCRs are important therapeutic targets for a broad range of diseases it would be advantageous to better understand agonism at the molecular level. As such we currently have very little understanding of what distinguishes a partial agonist from a full agonist or leads to biased signalling at the molecular level. A better understanding of the molecular basis of agonism may allow the design of more therapeutically useful drugs.

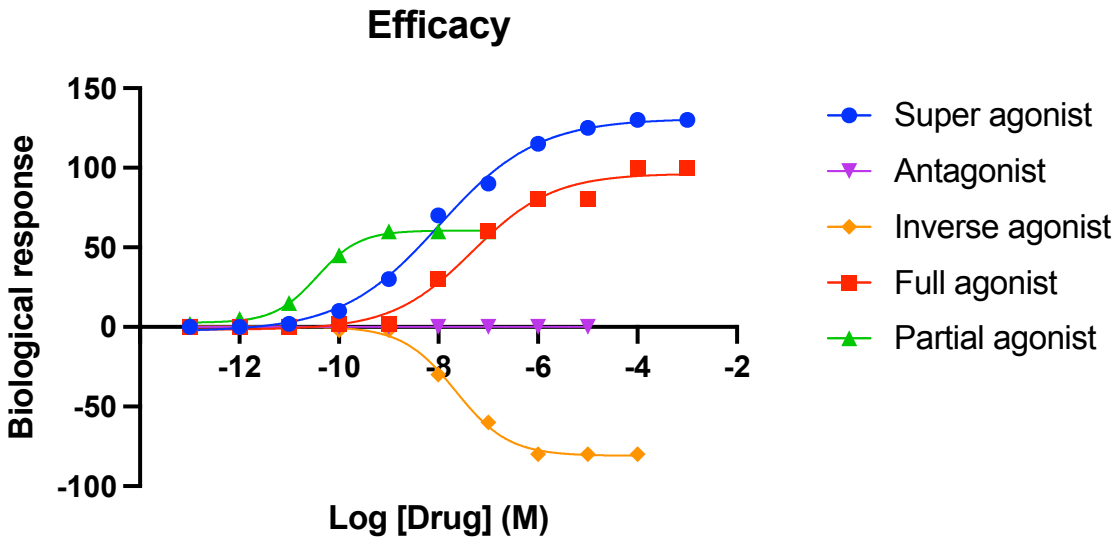

Figure 1.4: Classification of ligands according to their biological response.

1.6 Current understanding of molecular basis of efficacy at GPCRs

Whilst the molecular basis of efficacy is far from understood, it is now well-established that GPCRs are highly flexible and dynamic proteins which rapidly convert between different conformations, as such any population will exist in a number of populations at any one time (Mary et al., 2012). Biophysical studies into the effect of agonists binding to populations of GPCRs show that an agonist will affect the equilibrium of receptor conformations in a population, stabilising the receptor in a number of energetically favourable conformations (Deupi & Kobilka, 2011) (Nygaard et al. 2013) (Mary et al. 2012). This may occur by

conformational selection, or conformational induction or a combination of both (Zhao & Furness, 2019). This has led to the paradigm that the efficacy of an agonist to cause the receptor to couple its intracellular signalling molecule depends upon the conformations preferentially stabilised by that agonist. As such it has been hypothesized that structural studies may reveal the conformations of GPCRs responsible for different transduction efficiencies by different ligands.

1.6.1 Contribution of structural studies to understanding the molecular basis of efficacy

There has been a great deal of focus on obtaining x-ray crystallography and cryo-electron microscopy (cryo-EM) structures of GPCRs in complex with agonists, partial agonists, antagonists and intracellular signalling proteins (Masureel et al., 2018) (Rasmussen, Devree, et al., 2011b) (Wacker et al., 2010). These studies show a conserved mechanism for GPCR activation whereby agonist binding causes the outward movement of TM6 to allow G protein coupling. Comparison of these structures may give some insight into the molecular basis of efficacy. β_2AR structural studies show substantial differences in the binding poses of different β_2AR agonists, namely formoterol, adrenaline, salmeterol and BI-167-107, (Masureel et al., 2018)(Zhang et al., 2020) and variations in the extracellular domain of the receptor but little difference in the intracellular proportion. Zhang and colleagues (Zhang et al. 2020) show significant differences in the engagement and conformational rearrangement of the G_s protein when in complex with the formoterol- β_2AR, compared to BI-167-107-β_2AR. These differences may be important in the increased potency of BI-167-107 compared to formoterol (Rasmussen et al., 2011b) (Zhang et al., 2020).

Similar comparisons of structures supposed to represent conformations of different efficacies have been made for other GPCRs. For example, Warne and colleagues (Warne et al., 2011) use x-ray crystallography to compare structures of the β_1-adrenoceptor (β_1) in complex with two partial and two full agonists. Although the thermostabilising mutations used in this study decrease the likelihood that these structures show the active state of the β_1AR, this study shows several differences in the initial binding and ligand-residue interactions. Warne and colleagues suggest that differences in contraction of the orthosteric ligand binding pocket, and interaction with helix 5 underlie the difference in efficacy of the full Vs partial agonists.

Furthermore, Liang and colleagues (Liang et al., 2018) use cryo-EM to investigate differences in the active structure of the GLP-1 receptor, a class B GPCR, when bound to GLP-1 and the G_s biased peptide exendin-5 (Zhang et al. 2015) in complex with G_s. Similarly, to the above structural studies on β_2AR, this study shows differences in the transmembrane domain structure of GLP-1 receptor and resulting differences in the conformation and angle of engagement of the G protein for GLP-1 and exendin-5.

Whilst these structural differences could be important in the molecular basis of efficacy, structural studies can only ever provide snapshots of the receptor conformation in its lowest energy state when bound to the ligand. Such a state is the most likely and average active receptor state, not all the states which will exist within the dynamic and heterogeneous population. Whilst these states are therefore important to understanding the active conformation, they cannot provide the entire explanation for the molecular basis of efficacy. Moreover, technical limitations of structural biology mean that structures of the agonist-GPCR state prior to G protein binding, i.e the GPCR state most likely to recruit

a G protein, cannot be obtained. Moreover, the agonist-GPCR-G-protein state cannot inform on the number or rate of productive complexes.

1.6.2 Contribution of biophysical studies to understanding the molecular basis of efficacy

Biophysical studies into GPCR conformational dynamics have also furthered our understanding into the molecular basis of efficacy at GPCRs. Whilst it is understood that the unliganded GPCRs exist in a dynamic landscape of numerous conformations (Mary et al., 2012) Manglik and colleagues (Manglik et al 2015) used NMR to show that even in complex with agonists the β_2AR remain highly dynamic and continues to interconvert between different conformations. The role of these other different conformations, intermediates in signalling and the kinetics of conversion between these states in signalling remains unknown.

NMR studies have also allowed the investigation into the agonist-GPCR state prior to G protein coupling, a state which has not been possible to obtain structurally. Such studies (Manglik et al. 2015) (Nygaard et al 2013,) show that agonist binding alone is not enough to fully stabilise the active state of a GPCR and that a G protein mimetic nanobody is required to fully stabilise the active state. Moreover, Liu and colleagues (Liu et al., 2013) investigated the conformational states of β_2AR bound to agonists of a range of efficacies and show efficacy dependant differences in the agonist-β_2AR conformational state. Taken together, these studies suggest that distinct conformational states of the GPCRs are induced by different agonists with differing activity towards transducer coupling. As discussed, it has not been possible to obtain structures of agonist-GPCR complexes in the absence of a G protein or

G protein mimetic although the above studies suggest the pre-coupled state to be important in transducer coupling.

1.6.3 Evidence for the role of kinetics in the molecular basis of efficacy

Several studies have investigated a role of kinetics in both receptor activation and in agonist bound GPCR to G protein complex formation in the molecular basis of efficacy. For example, Nikoleav and colleagues (Nikolaev et al., 2006) use FRET to show a correlation between the rate of α_{2A}-receptor activation, G_i protein activation and ligand efficacy, suggesting faster GPCR-G protein kinetics to play a role in the molecular basis of efficacy. Moreover, Gregorio and colleagues (Gregorio et al., 2017) show that full agonists at the β_2AR show increased GTP turnover compared to partial agonists, suggesting an increased number of G proteins being activated. Similarly, this study also showed that the rate and/or amplitude of receptor TM6 movement, and complex stability also correlated with ligand efficacy. This suggests that differences in efficacy may result from an increased rate of G protein activation as a result of either increased TM6 displacement of increase rate or TM6 movement. Furthermore, Furness and colleagues (George et al. 2016) investigated the rate of G protein and GTP turnover by the human calcitonin (CT) receptor and show that these are increased in response to the higher efficacy human calcitonin peptide (hCT) compared to the lower efficacy salmon calcitonin peptide (sCT). Collectively, these studies suggest agonists of higher efficacy increase the rate of GPCR activation by the GPCR through conformational differences in the receptor.

Overall, our understanding of the molecular basis of GPCR activation and GPCR ligand efficacy remains limited. Whilst structural studies have shown some insight into the conformations of different signalling

complexes, we have not been able to characterise the dynamic conformational landscapes of ligand-GPCR complexes or of the kinetic relationships between these, ligands and signalling proteins. Whether or not all G proteins recruited to a GPCR undergo productive nucleotide exchange also remains to be elucidated.

1.7 Evidence for a role of ligand binding kinetics in the molecular basis of efficacy

Aside from GPCR-G protein complex kinetics several studies have shown correlations between ligand residency time and drug efficacy. For example, a positive correlation has been shown between the efficacy of seven agonists at the M3 muscarinic receptor, and ten agonists at the A_{2A} receptor and their ligand residence time (Sykes, et al. 2009) (Guo et al., 2012). Conversely, no correlation between efficacy and residency time was shown for the Adenosine A_1 receptor (Louvel et al., 2014). The molecular basis for these differences in ligand residency time nor how this related to differences in efficacy is not understood. It was not possible to find any studies addressing how ligand and G protein kinetics correlate.

1.8 GPCR molecular pharmacology in the cellular environment

It is also understood that, aside from the ability of the ligand to stabilise the active complex there are many regulatory mechanisms in both the cell and the cell membrane which will modulate the ability of the ligand-receptor complex to couple intracellular signalling molecules.

1.8.1 Modulation of GPCR dynamics by the cell membrane

Firstly, it has been shown that membrane composition can influence receptor function, in the context of both ligand binding and signalling. For example, cholesterol has been shown to affect ligand-GPCR binding both allosterically to Cannabinoid receptor 1 (CB1) in rat glioma (Bari et al., 2005) and orthosterically to the Adenosine-2A receptor (A_{2A}) (Guixà-González et al., 2017). Indeed, in the context of the β_2AR, cholesterol has been shown to associate with the receptor in structural studies (Cherezov et al., 2007) and to greatly improve β_2AR stability (Zocher et al., 2012). Moreover, cholesterol depletion has been shown to increase β-adrenoceptor signalling in cardiac myocytes (Paila et al., 2011). Additionally, Strohman and colleagues (Strohman et al., 2018) showed that modification to the lipid content of detergent/lipid micelles affected β_2AR to G_{i3} coupling and G_{i3}-mediated Ca^{2+} signalling. Taken together these studies, suggest that local membrane composition is specifically important in regulating β_2AR pharmacology, and therefore that cell type or the method of β_2AR solubilisation is an important consideration for a physiologically relevant study.

1.8.2 Modulation of GPCR signalling by cellular regulation

The ability of the protein to signal intracellularly will also depend upon the local concentration of downstream signalling molecules relative to receptor concentration. Clearly, both receptor and signalling molecule need to be present for the signalling response in question to take place. Both receptor and G protein expression varies across the body and even across different locations in the cell (Dick et al., 2010), therefore affecting the ability of the GPCR to signal. Moreover, it is well established that increased receptor expression levels allow a ligand to induce a more efficacious response (Zhao and Furness 2019). Additionally Halls and colleagues showed how differential organisation of the μ opioid receptor

on the plasma membrane is linked to differential spatiotemporal signalling responses intracellularly by the agonists morphine and DAMGO, (Halls et al., 2016).

Overall, cellular regulation of GPCRs and their signalling transducers play an important role in modulating pharmacology and are important considerations for experimental design and understanding the molecular basis of efficacy.

1.9 Methods to extract proteins from the plasma membrane

Considering the complexity of receptor pharmacology in the cellular environment this study chose to study β_2AR in isolation. To study membrane proteins in the absence of the cellular regulation the membrane protein must be extracted from the plasma membrane. Finding conditions that mimic the membrane protein's native environment and allow the membrane protein in question to remain active and folded has generally proven a difficult task for biochemists.

Most often, detergents are used to extract membrane proteins from the plasma membranes. Detergents can be defined as any agent that consists of a polar hydrophobic head group and nonpolar hydrophilic tail. Whilst soluble in aqueous solution detergent molecules will aggregate into micelles, this process is known as micellization. These properties, and those of the plasma membrane, mean that the detergent molecules are able to incorporate into the plasma membrane via the lipophilic tail and therefore extract membrane proteins within a detergent micelle. The detergent micelle serves to mimic the hydrophobic environment of the cell membrane whilst hydrophilic head groups mean that the protein containing micelle remains soluble in aqueous solution.

The ability of the detergent to disrupt the plasma membrane and its contents depends on the net charge of the head group. As such ionic detergents such as sodium dodecyl sulphate (SDS) are the harshest types of detergents. Such detergents disrupt protein-lipid interactions and inter- and intramolecular protein-protein interactions and are therefore most often denaturing to the protein. Non-ionic detergents such as maltosides (e.g n-dodecyl β-D-maltoside) will disrupt only lipid-protein interactions and are therefore useful for extraction of functional membrane proteins from the lipid bilayer.

Whilst detergents have classically been used to extract proteins from the plasma membrane it is generally accepted that the detergent micelle far from fully recapitulates the plasma membrane environment. Use of detergents often results in poor protein stability and inactivity. Multiple studies have improved protein stability by reconstitution of the detergent solubilised receptor in synthetic nanodiscs (Skrzypek et al., 2018). Such nanodiscs are typically 8-16nm in diameter and consist of a phospholipid bilayer encircled by a helical ‘membrane scaffold protein’ (MSPs). Whilst synthetic nanodiscs are clearly advantageous over detergents, their use still has the disadvantages of still requiring detergents to initially extract the membrane protein from the lipid bilayer, which may irreversibly have damaged the protein. Furthermore, the lipids within the synthetic nanodisc are not identical to the plasma membrane and are clearly different from the specific native phospholipids of the isolated protein. The precise content of the phospholipid bilayer has been shown to modulate the function of many membrane proteins (Strohman et al., 2018) and is therefore clearly important in the study of the native receptor.

Recently, it was realised that styrene maleic acid copolymer (SMA) will incorporate into biological membranes and self-assemble into

nanoparticles known as Styrene Maleic Acid Lipid Particles (SMALPs) (Knowles et al., 2009) (Stroud, et al., 2018). This provides a novel mechanism for isolating a membrane protein within its native phospholipids whilst avoiding use of detergents at any stage. SMALPs have already been used to isolate a range of membrane proteins (Dörr et al., 2014) (Sun et al., 2018) (Gulati et al., 2014) including GPCRs (Bada Juarez et al., 2020) (Jamshad et al., 2015). Although the mechanism by which SMA polymer disrupts the plasma membrane and self-assembles into nanodiscs is not completely understood, coarse grain molecular dynamic simulations have given some insight. These simulations show that styrene moiety of the SMA copolymer binds to the membrane, inserting into the core of the membrane, underneath the phosphate headgroups via hydrophobic interactions. As polymers disrupt the membrane, they cause the membrane to bend, and the polymer creates pores in the membrane to grow until all of the membrane has self-assembled into nanodiscs. These simulations showed just one polymer chain per nanodiscs.

Whilst use of SMALPs has significant advantages, they also bring a number of limitations. Firstly, SMALPs are disrupted by divalent cations, which hinders biophysical study of any process where cations are required as a cofactor, for example ATP hydrolysis. Furthermore, SMALPs also precipitate out of solution when exposed to a pH below 7 and the high UV absorbance of the SMA polymer makes optical spectroscopic studies of membrane proteins that are encapsulated within SMALPs challenging (Oluwole et al., 2017a). Additionally, there is evidence that the conformational flexibility of GPCRs within SMALPs is restricted, (Mosslehy et al., 2019) (Routledge et al., 2020) and therefore that the conformational dynamics of the SMALP encapsulated protein may differ from that of the native protein.

The copolymer Diisobutylene maleic acid (DIBMA), was developed specifically for the extraction of membrane proteins from the intact bilayer (Oluwole et al., 2017b). Compared to SMALPs, DIBMALPs are believed to have only a mild effect on lipid packing, be compatible with optical spectroscopy in the far UV range and tolerate low millimolar concentrations of divalent cations (Oluwole, et al., 2017a). This makes DIBMA far more amenable for functional biophysical studies. Although the disk size of SMALPs is believed to vary with different ratios of styrene to maleic acid, DIBMALPs are generally thought to have a larger hydrodynamic radius. The diameter of SMALPS and DIBMALPs have been characterised at 13nm and 29nm respectively (Oluwole et al., 2017a).

1.10 Mini-G_s proteins: sensors for active GPCRs

As described above G proteins are heterotrimeric, consisting of α, β and γ subunits with the G_α subunits consist of the helical domain and GTPase domain. As such full-length heterotrimeric G proteins are dynamic complexes that are difficult to isolate. To overcome this, this study chose to utilise mini-G proteins as tools to study the dynamics of β_2AR activation. Mini-G proteins were developed by the Tate lab, Cambridge as a method of stabilising the active state of the GPCRs for structural studies (Carpenter & Tate, 2016) and successfully used to obtain an active structure of the A_{2A}R. The mini-G_s protein is the isolated GTPase domain of the G_α subunit which has been engineered with several thermostabilising mutations.

In the most used mini-G_s, mini-G_s-393, modifications from the wild-type GTPase domain include truncation of the N terminus and switch III region, and 7 thermostabilising mutations. Thermostabilising mutations are in switch II, the nucleotide binding pocket and the α5 helix

as summarised in figure **1.5.** Biophysical characterisation of mini-G_s-393 compared to other mini-G_s proteins and the full length G_s protein reveal that the L272D mutation prevents the mini-G_s-393 coupling the βγ subunits and that the I273A mutation prevents nucleotide exchange. The thermostabilising mutations in mini-G_s proteins make them rigid proteins, locked in the active state of the G_α protein as shown in the agonist bound A_{2A}R-mini-G_s structure (Carpenter et al., 2016) It is therefore, important to view mini-G_s proteins as conformational sensors for all active states of the GPCR as opposed to 'miniature G proteins.'

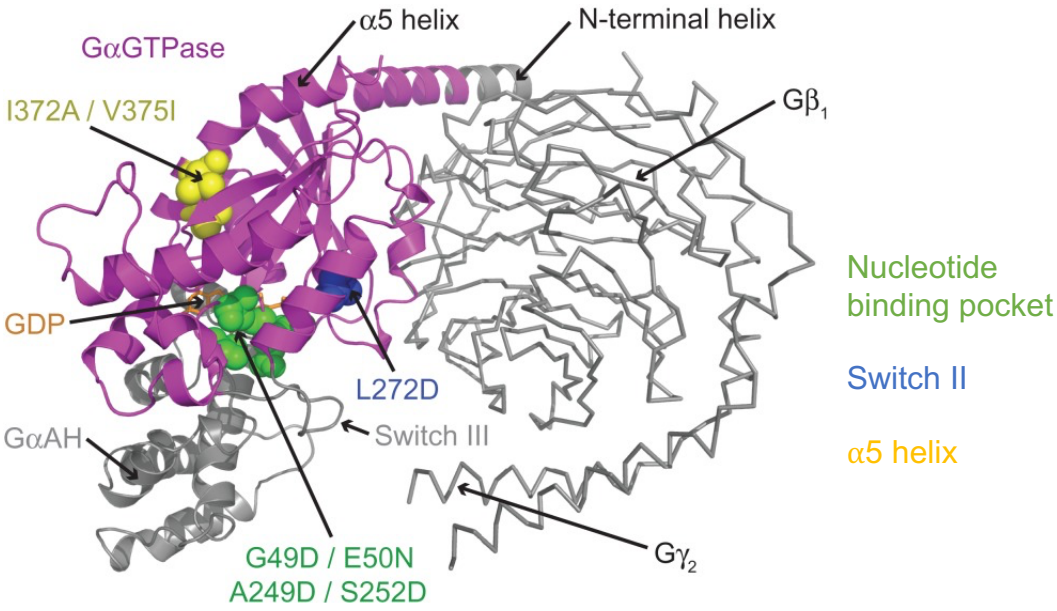

Figure 1.5: A summary of the structure of the mini-G_s-393 protein compared to the full length heterotrimeric G_s protein: the mini-G_s-393 structure is shown in magenta and is superimposed against the full length G_s protein. Grey areas show deletions. Adapted from (Carpenter and Tate 2016).

Moreover, although mini-G proteins were initially developed as tools for stabilising GPCRs in the active state for structural studies, they have more recently been used as biosensors to detect the GPCR active state in living cells. This approach was first adopted and validated by Wan and colleagues (Wan, et al., 2018) who fused the venus fluorophore to the N terminus of several mini-G proteins and show that mini-G protein binding upon agonist stimulation is reversible and recapitulates the pharmacology and coupling specificity of a G protein for a range of GPCRs in mammalian cells. Furthermore, Carpenter and colleagues (Carpenter & Tate, 2016) also show that, unlike full length G proteins, mini-G proteins can be expressed and purified from *E*. *coli* in large yields, making their production easy and cheap. Based on this literature mini-G_s proteins were chosen for this study, as tools to investigate the kinetics of G protein recruitment to the β_2AR in response to agonists of different efficacies and kinetics.

1.11 Aims and Objectives

Considering the limited understanding of the molecular basis of efficacy, this study aimed to further our understanding by investigating a role for kinetics. The hypothesis underlying this study was that ligand residence time effects β_2AR receptor conformational dynamics to affect G_s protein activation efficacy. For example, a ligand of longer or shorter residence time could allow more G proteins to be activated. The overarching aim of this study was to investigate the correlations between agonist kinetics, β_2AR conformational dynamics and agonist ability to induce G_s activation at the β_2AR. Studying this in a purified protein system allows the molecular dynamics of the receptor itself to be investigated in isolation from the complex cellular and subcellular regulation discussed above. The main objectives were:

1. To investigate the applicability of the polymer DIBMA to extract the β_2AR from mammalian cells in a functional state.

2. To characterise the ligand binding and G_s protein activation efficacy of eight partial and full β_2AR agonists.

3. To investigate mini-G_s binding kinetics to β_2AR in the presence of these eight agonists.

Chapter 2
Materials and methods

2.1 Materials

2.1.1 Mammalian cell culture reagents:

The T-REx™-293 cell line was obtained from Invitrogen (CA, U.S.A). HEK293T/17 cells were obtained from American Tissue Culture Collection (ATCC) (VA, U.S.A.). T75 and T175 mammalian cell culture flasks were purchased from Fisher scientific (Loughborough, UK). All cell culture reagents, including Phosphate Buffered Saline (PBS) and Fetal Calf Serum (FCS) were purchased from Sigma Aldrich (Gillingham, UK), except for blastocidin which was obtained from Gibco™ (MA, U.S.A) and zeocin™ and sheared salmon sperm from Invitrogen (MA, U.S.A). SNAP labelling reagents (SNAP-surface Alexa Fluor-488 and SNAP-surface Alexa Fluor-647) were purchased from New England Biolabs (NEB) (Hitchen, U.K.). Tag-lite SNAP-Lumi4-Tb labelling reagent and LabMed buffer was purchased from Cisbio (Codolet, France). Polyethylenimine (PEI) (25kDa) was obtained from Polysciences Inc (PA, U.S.A), and CellStar® 96 well tissue culture plates from Greiner Bio-One (Kremsmünster, Austria).

2.1.2 Molecular biology reagents:

Phusion® high fidelity PCR Master mix, Beta-NAD^+, Taq DNA Ligase, T5 exonuclease and chemically competent *E. coli* cells were obtained from NEB (Hitchen, U.K). Gelpilot loading dye, Qiagen MiniElute reaction clean up kit, QIAprep spin miniprep kit were obtained from Qiagen (Hilgen, Germany). NTPs were obtained from Promega (WI, U.S.A), Phusion polymerase from Thermoscientific (MA, U.S.A). SYBER safe and Generuler 1kb DNA ladder were from Thermofisher (MA, U.S.A).

2.1.3 Protein purification materials:

DIBMA and DDM were obtained from Anatrace (OH, U.S.A). 5% Magstrep 'type3' XT magnetic bead suspension was obtained from IBA Lifesciences (Göttingen, Germany). Yarra 1.8µm SEC-x300 2.5mL column was obtained from Phenomenex, (CA, U.S.A). cOmplete™ Protease inhibitor cocktail was obtained from Roche (Basel, Switzerland). HisTrap FF crude 5mL columns were obtained from GE Healthcare (IL, U.S.A). Vivaspins® protein concentrators were obtained from Sartorious (Göttingen, Germany). Slide-a-Lyzer™ dialysis cassettes, Nupage™ LDS sample buffer, Nupage™ 4-12% Bis-Tris 15 x 1.0mm well gels, Nupage™ MOPs SDS running buffer, Pageruler™ pre-stained protein ladder and BODIPY™ F-L-cystine dye were all obtained from Thermofisher (MA, U.S.A).

2.1.4 Compounds:

β_2AR antagonist [(S)-propranolol-green] (CA200693), (S)-propranolol-red (CA200689) and fluorescent XAC (CA200634) were all from CellAura, UK, and supplied by Hello Bio, (Bristol, U.K) (s)-(-)-Propranolol hydrochloride, cyanopindolol hemifumerate and salmeterol were obtained from Tocris, (Bristol, U.K). ICI 118, 551 hydrochloride was obtained from Selleckchem, (Munich, Germany), Formoterol hemifurate from APExBIO (TX, U.S.A), and BI-167-107 from Boehringer Ingelheim (Ingelheim, Germany). (±)-epinephrine hydrochloride, noradrenaline, salbutamol hemisulfate and isoprenaline hydrochloride were purchased from Sigma Aldrich (Gillingham, UK). C26 was a gift from Professor Steven Charlton.

Nano-Glo® luciferase substrate was obtained from Promega (WI, U.S.A). All other chemicals were purchased from Sigma Aldrich (Gillingham, UK).

2.2 Methods

2.2.1 Molecular biology

The constructs used in this study:

This study required the production of both GPCRs and mini-G proteins. The GPCRs β_2AR, and A_{2A}R were expressed in mammalian cells using the plasmid pcDNA4TO with a Twin-strep and SNAP tag on the N terminus of the GPCR. These constructs were made by Franziska Heydrenreich and Brad Hoare respectively according to the methods below. The construct pcDNA4TO-TS-SNAP-β_2ARnLuc was also made by Brad Hoare and the construct pcDNA3-A_{2A}nLuc by Mark Soave.

Venus and Halo-tagged as well as unlabelled mini-G_s constructs were expressed in bacteria in the vector PJ411(Kan) (appendix **7.1.4**). These mini-G_s sequences were a kind gift from Nevin Lambert which were then recloned into the PJ411 vector containing MKK_HIS10_TEV (Flock et al., 2016) to give the constructs MKK_HIS10_TEV_Halo_mini-G_s, MKK_HIS10_TEV_venus_mini-G_s, and MKK_HIS10_TEV-mini-G_s, according to the methods below. This cloning strategy is summarised in figure **2.1**. MKK is a tag that is often used to improve the expression levels of bacterially expressed recombinant proteins. Its DNA encoding sequence (ATGAAAAAA) improves flexibility of the RNA and therefore ribosome priming. His10 is a purification tag consisting of 10 Histidine residues which has a high affinity for nickel and hence acted as an affinity purification tag for the protein. TEV refers to the sequence Glu-Asn-Leu-Tyr-Phe-Gln-Gly-Gly-Ser which can be cleaved specifically at the Gly/Ser junction by the cysteine protease Tobacco Etch Virus (TEV). This enables removal of the MKK_HIS10 post purification. Mini-G_s constructs were optimised for bacterial expression as this was the preferred expression system for cost, protein yield and ease.

Mini-G_s proteins and the biosensor CASE-G_s were also expressed in mammalian HEK cells. The mammalian mini-G_s constructs were a gift from Nevin Lambert (Wan, et al., 2018). CASE G_s constructs were generated by Hannes Schihada and colleagues (Schihada et al., 2021) and were obtained from Addgene. Full vector maps of all constructs can be found in the appendix's sec (**7.1.1**).

Polymerase chain reaction

The polymerase chain reaction (PCR) is a procedure used to amplify a single strand of DNA as dictated by the designed primers. To generate the mini-G_s constructs PCR was used to amplify the Halo-mini-G_s, venus-mini-G_s and mini-G_s DNA sequence and the PJ411_ MKK_HIS10_TEV vector. These primers are summarised in table **2.1.** Primers were designed using 'PCRcloning' software, a part of the AAScan suite (Sun et al., 2013). Which optimised the melting temperature (T_m) to 65^{o}C and ensured a CG clamp. For this project, overhangs were added to mini-G_s inserts only for simplicity so that the same vector DNA fragments could be used for each assembly reaction.

PCR reactions were set up in 0.2mL PCR tubes and in a total volume of 20µL with a final concentration of 0.5ng/µL template, 500nM forward and reverse primers, 3% DMSO and x1 Phusion master mix in HF buffer. All dilutions were made in MilliQ deionised water. PCR reactions used a touch down protocol. A DNA denaturing temperature of 98^{o}C was used followed by cycling down to 55°C decreasing 0.5°C at a time, for 2 x 20 cycles, this allowed primer annealing to DNA sequences. A final extension phase took place at 72°C, 2 min was used for extension phase of vector and 30 secs for mini-G_s inserts due to the difference in length of these DNA sequences.

To check success of PCR reactions 2µL PCR fragments were run on a 1% agarose gel containing SYBER safe diluted 20,000 times. This allowed assessment to of correctly sized fragments and purity. Gels were run for 50 min at 100V in Tris-acetate-EDTA (TAE) running buffer, with samples loaded in Gelpilot loading dye. GeneRuler 1kb DNA ladder was used to calibrate molecular weights of fragments. The remaining PCR reaction products were incubated with *Dnp1* for 3 hours at 37°C, to digest remaining template. Fragments were then purified using Qiagen MinElute Reaction Cleanup Kit according to manufacturer's instructions.

PCR Fragment	Forward primer	Reverse primer
PJ411_MKK_His 10_TEV	TAACCCCCTAGCAT AACCCCTTGGGGC CTC	GGATCCACCCTGGAAGT ACAGGTTTTC
Halo-mini-G_s insert	TTCCAGGGTGGATC CATGGCAGAAATCG GTACTGGCTTTCCA TTC	TATGCTAGGGGGTTATC TAGCAAATTCCGGGAAG TAGTCCTCAATC
Venus-mini-G_s insert	TTCCAGGGTGGATC CGTGAGCAAGGGC GAGGAGCTG	TATGCTAGGGGGTTATC TAGCAAATTCCGGGAAG TAGTCCTCAATC
Mini-G_s insert	TTCCAGGGTGGATC CATCGAGAAACAAT TGCAGAAAGACAAA CAGGTC	TATGCTAGGGGGTTATC TAGCAAATTCCGGGAAG TAGTCCTCAATC

Table 2.1 A summary of the primers used to clone Halo and Venus-tagged and untagged miniG_s protein into the PJ411_MKK_His10_TEV vector

Gibson assembly reactions

Gibson assembly (Gibson et al., 2009) is a method for the assembly of multiple fragments of DNA. In short, DNA fragments are designed with overlapping ends and produced by PCR. The Gibson assembly reaction then uses T5 exonuclease to chew back overlapping ends of single stranded DNA from the 5' end so that complementary

regions of DNA fragments will anneal to each other. A polymerase then closes any gaps in the DNA, before a DNA ligase covalently links the DNA fragments together.

In these Gibson assembly reactions insert and vector PCR fragments were incubated for 1 hour at 50°C in a molar ratio of 1:3 (vector:insert), where 50ng of DNA was used for the vector. Assembly reactions took place in 10uL. Where 2.5µL consisted of DNA 50ng and 7.5µL consisted of home-made Gibson assembly master mix. Assembly master mixture was prepared by combining 320µL 5xisothermal reaction buffer, 0.64µL of 10U/µL^{-1} T5 exonuclease, 20 µL of 2U/µL^{-1} Phusion DNA polymerase, 160µL of 40U/µL^{-1} Taq DNA ligase and water up to a final volume of 1.2 mL. Frozen 50µL assembly mixture aliquots were thawed and then kept on ice until ready to be used. 6mL of 5 × isothermal reaction buffer had been prepared by combining 3mL of 1M Tris-HCl pH 7.5,150µL of 2M $MgCl_2$, 60µL of 100mM dGTP, 60µL of 100mM dATP, 60µL of 100mM dTTP, 60µL of 100 mM dCTP, 300µL of 1M DTT, 1.5 g PEG-8000 and 300µL of 100mM NAD. Where assembly reactions were unsuccessful, assembly reactions were repeated using NEB DNA assembly master mix E2621L.

Transformation of competent cells

Chemically competent Turbo *E. coli* cells were thawed on ice for approximately 20min. 50µL of these competent cells were transferred to a fresh, sterile 0.5mL eppendorf microcentrifuge tube and used for each transformation. 2µL assembly reaction was added to competent cells in proximity to a Bunsen burner to create sterile conditions and incubated for 20min on ice. This allowed the DNA to associate with the outer membrane of the competent cells. Cells were then heat shocked for 1 min at 42^{o}C using a heat block and then placed back on ice. Heat

shocking allowed the plasmid to pass through the cell membrane and into the cell cytoplasm. Cells were then incubated at 37°C and 225RPM in 500 µL Lennox's Broth (LB). in a shaking incubator. This allowed the cells to recover and begin replicating and expressing the plasmid. Cells were then spun out (14,000xg for 5min) of LB and plated onto room temperature LB agar plates containing 50µg/mL kanamycin. Again, this was done in close proximity to a Bunsen burner to maintain sterility. The plates were then incubated at 37 °C overnight (approximately 15h) upside down so that condensation did not interfere with bacterial colony development. Only colonies that had taken up the PJ411 plasmid were resistant to kanamycin. Using a sterile pipette tip colonies were removed to a 15mL U-bottomed tube containing 5mL LB with 50µg/mL kanamycin and left at 4°C for approximately 8h.

Minipreps of DNA

5mL cultures (as described above) were incubated overnight at 37°C and 225RPM overnight. This allowed the bacteria containing the plasmid to reproduce, therefore amplifying the DNA. The following morning bacteria were pelleted at 4122*xg* and DNA isolated using the QIAprep spin miniprep kit used according to manufacturer instructions.

This miniprep system extracts DNA using a spin column system. Firstly, cells were lysed under alkaline conditions which allowed selective denaturation of chromosomal DNA, but not the covalently closed circular DNA plasmid of interest. This solution was then neutralised which simultaneously aggregated chromosonal DNA and bacterial plasmids (Birnboim & Doly, 1979) so that these contaminates could be removed through centrifugation. Neutralisation (N3) buffer also contained a high concentration of salts therefore allowing nucleic acids to bind to the silica spin column. Therefore, contaminants such as RNA and other cellular metabolites could be removed in the column flow through via

centrifugation before circular DNA was eluted from the spin column using the low salt containing (EB) buffer.

DNA sequencing

All DNA sequencing was performed by Genewiz UK. Generally, 50-100ng DNA was sent for sequencing. To confirm successful cloning of the MKK-His10-mini-G_s constructs minipreps were sequenced with T7 forward primer (5'TAATACGACTCACTATAGGG) and a primer specifically designed to bind just downstream of the mini-G_s stop codon (5'GGTTGGGGTTATGCTAGGG) which was called PJ411_R

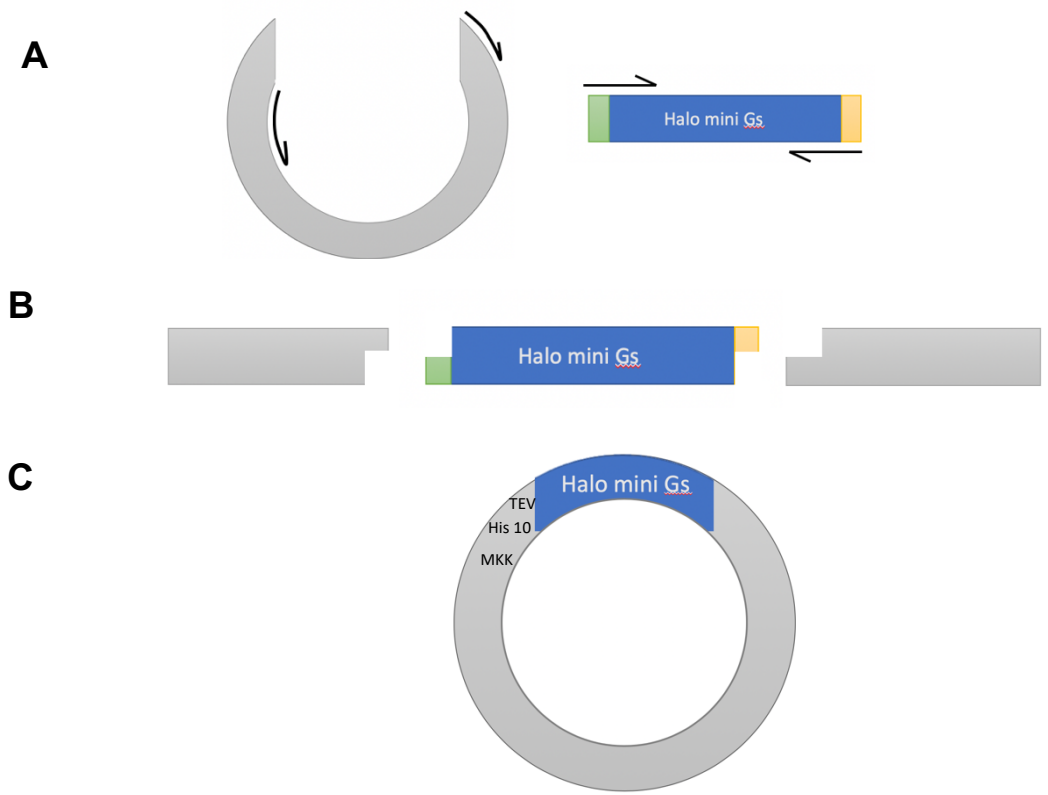

Figure 2.1: Schematic of cloning strategy for mini-G_s constructs by PCR and Gibson assembly: A) PJ411 vector containing MKK His10 and TEV (PJ411_MKK_His 10_TEV) and relevant mini-G_s insert were amplified by PCR **B),** these PCR fragments were then assembled by Gibson assembly to give the resulting construct PJ411_MKK_His 10_TEV_halo-mini-G_s shown in **C)**

2.2.2 Mammalian cell culture

The T-REx™-293 cell line is a Human Embryonic Kidney 293 (HEK293) line which has been stably transfected with pcDNA6™/TR. This vector expresses a high level of a tetracycline repressor (tetR) under the control of the human cytomegalovirus immediate early (CMV) promotor. T-REx™-293 cells were co-transfected with pcDNA4TO containing the protein of interest under the control of the CMV promoter containing a tet-Operator. Expression of the protein of interest could then be induced with tetracycline which inhibits tetR repression of the protein of interest. This system was first described in (Yao et al., 1998). This system was chosen to obtain high protein expression and used for all small-scale protein production throughout this thesis.

HEK 293T/17 cells were used for all transient transfections. HEK 293T cells are HEK293 cells which contain the SV40 large T antigen, which enables then to produce recombinant proteins under the control of the SV40 promotor. HEK 293T/17 cells descend from clone 17 of these cells which was showed high transfectability.

T-REx™-293 cells were maintained in high glucose Dulbecco's modified Eagle's medium with 10% FCS, 5µg/µL blastocidin and 20µg/µL zeocin (growth medium). Blasticidin and zeocin are used in T-REx™-293 stable cell line culture to maintain pcDNA6™/TR and pcDNA4TO expression respectively. HEK 293T/17 cells were maintained in DMEM with 10% FCS. Cells were grown in cell culture incubators at 37°C and 5% CO_2 in a humified atmosphere.

Passaging of cells

Adherent T-REx™-293 cells and HEK 293T/17 cells were generally maintained in 75cm^2 or 175cm^2 tissue culture flasks until 90% confluent. When passaging was required, media was aspirated from the flasks and flasks were washed with 10mL PBS prior to detachment with 2mL trypsin-EDTA for 2min at 37°C. Detached cells were washed off

flasks, and trypsin deactivated with 10mL growth medium. Cells were then pelleted by centrifugation at 362*xg* for 5min. Supernatant was aspirated and cells were resuspended in growth medium before transfer to a new tissue culture flask. All cell culture was performed in a class II tissue culture hood and using sterile technique.

Induction of protein expression in T-REx^{TM}-293 cell

Protein expression was generally induced in T-REx^{TM}-293 cells when cells were 70% confluent in T175 tissue culture flasks using 1µg/mL tetracycline. Cells were allowed to express for a further 50 h before experimentation. Expressing cells were detached as above but using non-enzymatic cell dissociation solution instead of trypsin and washing with PBS. This was so that membrane proteins were not internalised in response to trypsin. Pelleted cells were immediately frozen at -80^{o}C until further use.

Cryopreservation of mammalian cells

For long term storage cells were stored in liquid nitrogen or its vapour. For cryopreservation 80% confluent cells were detached as above but resuspended in cell freezing media consisting of 10% DMSO and 90% FBS after centrifugation. Cells were resuspended in freezing media at a density of one T175 flask of cells per 10mL freezing media and stored in 1mL aliquots in 2mL cryovials. Cryovials were then transferred to a CoolCell freezing system container and cooled to -80^{o}C at a rate of 1 ^{o}C/min. Cells were transferred from the -80^{o}C freezer to a dewar containing liquid nitrogen for long term storage.

Recovery of cryopreserved mammalian cells

To recover cells from liquid nitrogen vials were thawed rapidly at 37^{o}C in a water bath and diluted ten-fold into growth medium. Cells were pelleted by centrifugation at 362*xg* for 5min and then resuspended in growth medium before transfer to tissue culture flasks. Cells were

allowed to adhere for 24h before growth media was changed to removed cell debris from cryopreservation.

Generation of stable cells lines

Four T-REx™ -293 stable cell lines were used in this study expressing either pcDNATO-TS-SNAP-A_{2A}, pcDNA4TO-TS-SNAP-β_2AR, pcDNA4TO-TS-SNAP-β_2ARnLuc or pcDNA4TO-TS-SNAP-β_2AR and Clontech-style N1-CASE G_s. For generation of these cells lines T-REx™ -293 cells were transfected with 5μg DNA using PEI in a ratio of 1:3 DNA:PEI in Opti-MEM™ media, in T75 flasks when cells were 70% confluent. Cells were incubated with DNA for 24h at 37°C and 5% CO_2. After 48h media was changed for selection media, which was normal growth media with 20μg/mL zeocin for T-REx™ -293 cells and 500μg/mL G418 for CASE G_s cells. Cells were incubated with selection media until all cells in a corresponding untransfected flask died.

Fluorescence-Activated Cell sorting (FACS)

T-REx™-293 pcDNA4TO-TS-SNAP-β_2AR CASE G_s stable cell line was sorted into mixed populations and single cells based on both TS-SNAP-β_2AR and CASE G_s expression levels. The CASE G_s expression was detected using the venus fluorophore on the Gγ subunit and TS-SNAP-β_2AR via SNAP Surface Alexa-Fluor®647 labelling. Cells were labelled as described in sec **2.3.** Untransfected T-REx™-293 cells were used as a negative control and a T-REx™-293 cell line stable expressing SNAP-Cannabinoid receptor 1 (CB1) and β-arrestin-2-venus was used as the positive control. Protein expression had been induced for 48h with 1μg/mL tetracycline prior to detachment for FACS. Cells were detached from T75 flasks using non-enzymatic cell dissociation solution according to Section **2.2.** Cells were resuspended in DMEM with 10% FBS, 100 U/mL penicillin and 100μg/mL Streptomycin and diluted to 100,000 cells/mL. T-REx™-293 pcDNA4TO-TS-SNAP-β_2AR CASE G_s cells were sorted in the University of Nottingham Flow Cytometry Facility using Coulter Astrios EQ sterile cell sorter. FACS was conducted at room

temperature and thresholds fluorescence set against untransfected cells. Gating took place using venus and Alexa-Fluor®647 fluorescent intensity. Mixed populations were placed in T75 flasks and single cells into 96 well cell culture plates. Media was replaced regularly. When single cells formed colonies, they were expanded to T25 flasks before passaging to T75 flasks.

Transient transfection

For all pcDNA4TO-TS-SNAP-β_2AR, pcDNA4TO-TS-SNAP-A_{2A}R CASE G_s or venus-mini-G_s transient transfections HEK293T/17 or occasionally T-REx^{TM}-293 cells were transfected in suspension. Cells were detached from flasks when 60-70% confluent using trypsin. Transfections took place using 0.8μg/mL DNA at a 3:1 ratio with PEI in OptiMEM^{TM} media. Sheared salmon sperm was used to normalise DNA to 0.8μg/mL, where less than 0.8μg/mL receptor or biosensor was used. Transfection mixtures were vortexed thoroughly and incubated at room temperature for 20 min before addition to cells suspensions in growth media. Cell suspensions containing transfection mixtures were plated onto PDL coated white 96-well cell culture plates and incubated for 48h at 37^{o}C and 5% CO_2.

2.2.3 NanoBRET

Bioluminescence Resonance Energy Transfer (BRET) occurs when the emission spectra of a donor luciferase overlap with the excitation spectra of an acceptor fluorophore, such that the nonradiative transfer of energy can occur and cause the acceptor to be excited and emit light of a longer wavelength. BRET will occur only when the acceptor and donor are in proximity (<10nm), as such BRET is well suited to studying protein-protein interactions in real time.

NanoBRET refers to BRET which utilises the Nanoluc (nLuc) luciferase, which an engineered luciferase subunit from the deep-sea shrimp *Oplophorus gracilirostris* (Hall et al., 2012). NanoLuc represents an improved luciferase in comparison to previously development renilla luciferase (RLuc) or firefly luciferase (FLuc) which is around 150 times brighter, has a narrower bioluminescent spectrum and is half the size (19kDa). NLuc therefore increases the sensitivity of BRET, range of acceptor fluorophores that can be utilised and is less likely to affect the function of the protein of interest (Machleidt et al., 2015). Moreover, in parallel, Hall and colleagues, (Hall et al., 2012) developed the improved nLuc substrate furimazine, which, when paired with nLuc in mammalian cells is 2.5 million-fold brighter relative to the native *Oplophorus gracilirostris* enzyme subunit Oluc-19 with the conventional substrate coelenterazine. The development of nLuc and furimazine, have therefore increased the sensitivity and therefore application of BRET, providing an improved method for investigating the protein-protein interactions in our study.

2.2.4 Venus-mini-G_s recruitment BRET assays in HEK293T/17 cells

For venus-mini-G_s recruitment assays HEK293T/17 cells were plated at a density of 30,000 cells/well in 100μL. 48h later media was aspirated from 96 well plates containing HEK293T/17 cells transiently transfected with pcDNA4TO-TS-SNAP-β_2ARnLuc or pcDNA3.1-A_{2A}RnLuc and venus-mini-G_s in a ratio of 1:9, receptor to venus-mini-G_s.

Plates were washed twice with 100μL /well HBSS, to remove excess media. 80μL/well assay buffer (HBSS + 0.1% BSA) was added to plates. 10μL of x10 furimazine diluted in assay buffer was added to each well and plates were incubated at 37ºC and 5% CO_2 for 20min. A white back seal was placed on underside of plate and luminescence was read on PHERAstar FSX using 450-80/550LP module. Online PHERAstar injectors were used to add 10μL of x10 ligand dilutions to the plate. Saturating concentrations of Isoprenline (100μM), ICI 118, 551 (100μM), NECA (10μM) and ZM241385 (1μM) were used.

2.2.5 CASE-G_s activations BRET assays

For CASE-G_s activation assays HEK293T/17 cells transiently transfected with pcDNA4TO-TS-SNAP-β_2ARnLuc and CASE-G_s at various transfection ratios and plated at a density of 50,000 cells/well in 100μL. Alternatively, T-REx^{TM}-293 pcDNA4TO-TS-SNAP-β_2ARnLuc + 500ng or 1000ng CASE-G_s stable cell line were plated at 50,000 cells/well in 100μL and induced for 48h with 1μg/mL tetracycline. Plates were prepared for BRET assays as described for venus-mini-G_s recruitment assays, and then read on PHERAstar FSX using 450-80/550LP module for 3 min to establish a basline BRET signal. The plate reader was then paused and 10μL of x10 ligand dilutions were added to plate offline.

2.2.6 Production of TS-SNAP-β_2AR from mammalian cells

SNAP labelling of A_{2A} or β_2AR receptors with various fluorophores

For all TR-FRET experiments SNAP tag technology was used to label the A_{2A}R or β_2AR with Lumi4-terbium (terbium cryptate). The SNAP tag is a 19.6kDa peptide tag and a mutant of the O^6-alkylguanine-DNA alkyltransferase. The SNAP tag reacts rapidly and specifically with benzylguanine derivatives. Attachment of benzylguanine to terbium cryptate or other fluorophores, such as the AlexaFluor 488 used in FSEC experiments, allows specific and covalent attachment these labels to the SNAP tagged protein of interest. This is summarised in **figure 2.2**

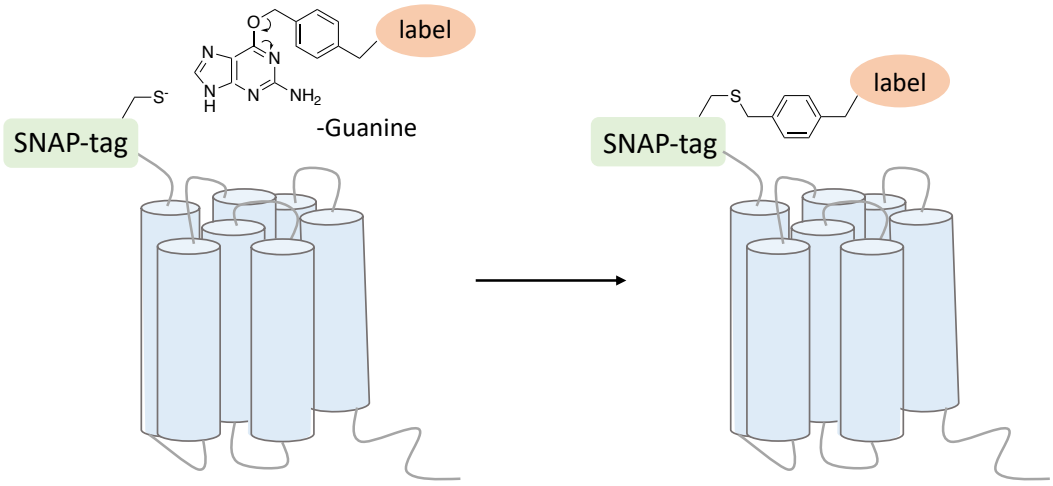

Figure 2.2: Various fluorophore labels were added to GPCR via N terminus SNAP tag

TS-SNAP-β_2AR membrane preparation

Membrane preparations were made from terbium labelled TS-SNAP-β_2AR T-REx™-293 cells. Cells were cultured, induced and detached as described above (Sec **2.2**). Cell pellets were then thawed on ice and resuspended in 20mL buffer B (10mM HEPES and 10mM EDTA, pH 7.4). Suspensions were homogenised using 6 x 1 sec pulses of a Polytron tissue homogeniser (Werke, Ultra-Turrax). Suspensions were spun at 48,000x*g* and 4°C for 30min, supernatant was removed and resuspended and centrifuged again as above. Resulting pellets were resuspended in buffer C (10mM HEPEs and 0.1mM EDTA, pH 7.4) aliquoted and frozen at -80°C.

Solubilisation of TS-SNAP-β_2AR using DDM or DIBMA

TS-SNAP-β_2AR was extracted from membranes by incubating membranes with 3% DIBMA (w/v) in 20mM HEPEs, 10% (v/v) glycerol, and 150mM NaCl, pH 8 at room temperature or 1% DDM (w/v), 20mM HEPEs, 10% (v/v) glycerol, and 150mM NaCl, pH 8 at 4°C for 2-3h. Samples were clarified by ultracentrifugation at 100,000*xg* for 1h at 4°C for ligand binding assays and 16900*xg* for thermostability assays.

Small scale affinity purification of DDM or DIBMALP-TS-SNAP-β_2AR

Solubilised DDM-β_2AR and DIBMALP-β_2AR samples were purified using 20µL of 5% MagStrep “type3” XT magnetic beads suspension. These beads bind to the twin-strep tag on the N-terminus of the receptor.

The strep tag is an 8 amino acid peptide sequence (WSHPQFEK) which binds to biotin and streptavidin as well as the engineered streptavidins such as streptactin® and streptactin® XT. The twin-strep tag contains the strep tag repeated twice, separated by a flexible linker so that it can bind two streptavidin protomers in a tetramer. The twin-strep tag system was chosen for affinity purification from mammalian cells because it has very high affinity for streptactin® resulting in high

yields. Moreover, the binding reactions between the twin strep tag and streptactin® is very specific and generally results in fewer impurities in samples from mammalian cells compared to use of other affinity tags such as the His tag system.

Beads were prepared by removal of supernatant using a magnetic rack and 2x 200µL washes in solubilisation buffer before resuspension. Samples were incubated with beads for 2h at 80RPM on a roller at 4°C in a cold room. Supernatant was then removed from beads using the magnetic rack and beads were washed twice with wash buffer (20mM HEPES, 10% glycerol, 150mM NaCl, pH 7.5 with 0.1% DDM for DDM sample only), before resuspension in 50µL elution buffer. Elution buffer consisted of 1-part 10X buffer BXT (IBA), which contains biotin and 9 parts wash buffers. Elution took place for 2 hours at 80RPM on a roller in cold room. Sample were then separated from beads using magnetic rack.

2.2.7 Fluorescence Size Exclusion Chromatography (FSEC)

Size exclusion chromatography (SEC), also known as gel filtration, is technique used to separate molecules based on their size. SEC columns consists of a porous matrix of inert beads of decreasing size such that molecules of decreasing size will elute further down the column. FSEC employs a fluorescence detector in-built to a HPLC system to analyse SEC column output.

For FSEC on samples of Alexa488 labelled DDM-β_2AR or DIBMALP-β_2AR, 30µL crude lysate was run through a Yarra 1.8µm SEC-x300 2.5mL column using a Shimadzu prominence HPLC system. Running buffer consisted of 20mM HEPEs, 150mM NaCl, 5% glycerol, and 0.03% DDM (for DDM-β_2AR sample only). FSEC took place at a flow rate of 0.2mL/min and 0.2mL fractions were collected. Samples were excited at 488nm, and emission collected at 520nm. GE HMW calibration kit was use as a standard to characterise the elution volume of the column.

2.2.8 Bacterial cell culture

Mini-G_s proteins were expressed in either B384(DE3) or Nico21 (DE3) strains of *E. coli.* B834 (DE3) is the parent strain of BCL21, which are methionine auxotrophs and protease deficient. These were used to decrease proteolytic cleavage. DE3 refers to the strain containing the λDE3 lysogen which carries the gene for T7 RNA polymerase under the control of the lacUV5 promotor. This therefore allows use of the T7-lac promotor. Nico21 (DE3) are derived from the BL21 strain commonly used for protein expression which is deficient in *lon* and *ompT* proteases. Nico21 cells differ from BCL21 in that the protein and common IMAC impurity GlmS is mutated to prevent its binding the nickel column.

PJ411_MKK_HIS10_TEV_Halo_mini-G_s was transformed into *E. coli* and then a single colony was picked and used to inoculate 5mL LB. After overnight incubation, 2.5mL of this 5mL culture was used to inoculate 1L of Terrific broth (TB) in a 2L conical flask. TB is a nutrient enriched phosphate buffered medium containing, yeast extract (24g/L), casein peptone (12g/L) and glycerol (4% (v/v). These higher levels of nutrients compared to other broths such as 2YT and LB allow greater densities of *E. coli* to be sustained and therefore protein yield is increased.

1L cultures were grown at 37°C and 225RPM until optical density (OD) of the culture reached 0.6. At this point protein expression was induced with 1mM Isopropyl β-D-1-thiogalactopyranoside (IPTG), which is a mimic of allolactose which binds to the Lac repressor, releasing it from the lac operators and therefore allowing transcription of the protein of interest. Following induction, cultures were incubated for 24h at 20°C. The temperature was dropped for expression in order to prevent degradation of the protein of interest. Cultures were then transferred to 1L centrifuge buckets and cells pelleted via centrifugation at 4122*xg* for 20min at 4°C. Cells were resuspended in PBS and transferred to 50mL Falcon tubes, before being pelleted again as above and frozen at -80 °C.

2.2.9 Production of purified mini-G_s proteins

Bacterial cell pellets expressing His-TEV-venus-mini-G_s, His-TEV-halo-mini-G_s or His-TEV-mini-G_s were thawed on ice. Cell pellets from 1L culture were resuspended in 50mL lysis buffer consisting of 20mM HEPEs, 500mM NaCl, 40mM imidazole, 10% glycerol, 8mM β-mercaptoethanol (BME), 1μM GDP, cOmplete protease inhibitors (Roche), DNAase I and lysozyme pH 7.5 using a douse. Bacterial cells were lysed by 5 x 10 second pulses of sonication on ice at 30 second intervals. Unlysed and larger components of the cells were removed using ultracentrifugation at 25,000*xg* at 4°C for 45 min. Lysate was filtered through a 0.45μm membrane using a syringe and loaded onto HisTrap™ FF crude 5mL column, to capture His-tagged protein of interest, using ÄKTA™ start protein purification system at a flow rate of 5mL/min. System and column had been equilibrated with 10 column volumes (CV) buffer A (20mM HEPEs, 500mM NaCl, 40mM imidazole, 10% glycerol, 8mM BME, 1μM guanosine diphosphate GDP). Unbound protein was washed out with 10 column volume (CV) buffer A. Bound protein was then eluted over an 8CV gradient of 0-100% buffer A to B at a flow rate of 5mL/min. Buffer B consisted of 20mM HEPEs, 500mM NaCl, 400mM imidazole, 10% glycerol, 8mM BME and 1μM GDP. Fractionation took place in 5mL volumes. Presence of the protein of interest was confirmed by gel electrophoresis and staining for protein as described in sec **2.2.10**. Pooled elution fractions were concentrated using 10,000 or 30,000 molecular weight cut off (MWCO) Vivaspin protein concentrators by centrifugation at 3000*xg* and 4°C for 15 min intervals for an average of 2-3 hours. Protein prep was exchanged into assay buffer using slide-A-lyzer™ 10,000 or 30,000 MWCO dialysis cassettes for tagged and untagged mini-G_s protein samples, respectively. Dialysis took place overnight in cold room and under constant stirring. Assay buffer consisted of 20mM HEPEs, 150mM NaCl, 10% glycerol, 8mM BME and 1μM GDP. Purified mini-G_s proteins were flash frozen using liquid nitrogen and stored at -80°C.

2.2.10 SDS-page electrophoresis

To check for the presence of the protein of interest and the purity of the sample, sodium dodecyl sulphate-polyacrylamide gel electrophoresis (SDS-page) electrophoresis was used to separate proteins by mass. This system uses SDS to denature the tertiary structure of the proteins and coat protein samples with an overall negative charge so that they migrate along the gel to the positive anode based of their molecular weight only. A protein marker is used to identify the size of proteins on the gel.

For SDS-PAGE gels 15µL sample was diluted in 5µL NuPAGE™ LDS sample buffer. Samples were not boiled prior to electrophoresis. Sample were then run on NuPage™ 4-12% Bis-Tris 15 x 1.0mm well gel using NuPage™ MOPs SDS running buffer. Gels were run for 50 min at 200V and Pageruler prestained protein ladder was used to estimate molecular weights.

For in-gel fluorescence, gels were scanned on an Amersham Typhoon imaging system (GE Healthcare Life Sciences, Pittsburgh, PA) using Fluorostage and Cy5 670BP300 filter sets with the PMT set to auto and pixel size to 200µm. After fluorescence was measured, protein was stained using InstantBlue® protein stain. Gels were removed from cassette and washed twice in deionised water, stained overnight on a rocker, and then imaged using a standard smart phone camera.

2.2.11 TR-FRET

Fluorescence Resonance Energy Transfer (FRET) (Figure **2.2**) is the non-radiative transfer of energy from an excited donor fluorophore to a ground state acceptor fluorophore. Energy transfer will only occur when the fluorescence emission spectrum of the donor overlaps with the excitation spectrum of the acceptor fluorophore, and these fluorophores are within ~10nm of each other, and dipoles are in the parallel orientation. Most fluorophores have short lived emission lasting nanoseconds (ns), in contrast the lanthanide metals have much longer half times (~1ms). Time resolved FRET (TR-FRET) uses this property to increase the signal to noise ratio of the FRET. TR-FRET uses a fluorophore of longer half time and measures FRET at time delay of approximately 50μs after excitation therefore separating the FRET between the molecules of interest and background auto-fluorescence. In these experiments, terbium cryptate is used as the acceptor fluorophore.

TS-SNAP-A_{2A} or TS-SNAP-β_2AR receptors were expressed in T-REx^{TM} cells as described above (sec **2.2**). Receptors were labelled in adherent whole cells. Media was aspirated from T175 flasks and adherent cells washed twice at room temperature with Phosphate Buffered Saline (PBS). Adherent cells were labelled with 100nM SNAP-Lumi4-Tb labelling reagent in Labmed buffer for 1 h at 37°C and 5% CO_2. Cells were washed twice more with PBS and detached with 5mL non enzymatic cell dissociation solution (Sigma, UK). Cells were pelleted by centrifugation for 10 min at 1000*xg*, supernatant was removed, and cell pellets frozen at -80°C.

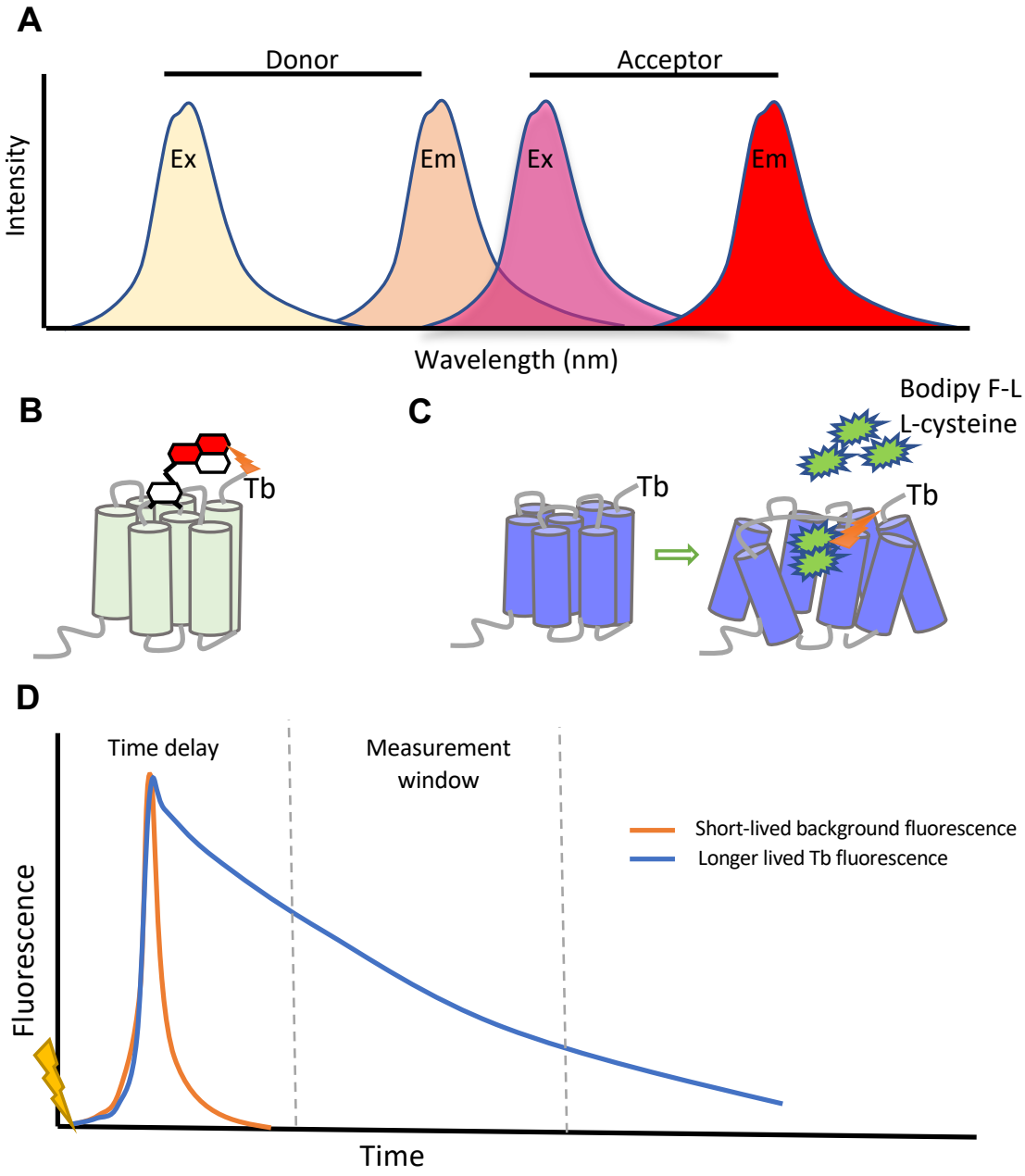

Figure 2.3: A summary of the TR-FRET methods used in this study ***A)*** FRET occurs when the emission of spectra of an excited donor fluorophore overlaps with the excitation spectra of an acceptor fluorophore hence energy is transferred **B*)*** TR-FRET between terbium on the N terminus of the GPCR and F-propranolol was used to measure ligand binding **C)** TR-FRET between terbium on the N terminus of the GPCR and BODIPY F-L-cysteine, which bound to the core of the GPCR during unfolding, was used to measure protein thermostability **D)** TR-FRET shows improved signal to noise over conventional FRET as the

long fluorescence lifetime of the donor allows the FRET signal of interest to be measured after background FRET is emitted.

2.2.12 TR-FRET Ligand binding studies

For TR-FRET ligand binding experiments membranes of Lumi4-Tb labelled TS-SNAP-A_{2A} or TS-SNAP-β_2AR receptors were solubilised as described in **Sec 2.3.** TR-FRET between the donor Lumi4-Tb and the fluorescent acceptors CA200689 (s)-propranolol-red (F-propranolol) was measured by exciting the sample at 337nm and quantifying emission at 665nm and 620nm using a PheraStar FSX (BMG Labtech) and HTRF 337 665/620 module (BMG Labtech). Assay buffer consisted of 20mM HEPEs, 5% glycerol, 150mM NaCl, and 0.5% BSA and 0.1% ascorbic acid, pH 8 and, for DDM samples only, 0.1% DDM was used. All binding assays used a final concentration of 1% dimethyl sulfoxide (DMSO), assay volume of 30µL, and 3µM cyanopindolol was used for non-specific binding (NSB). For equilibrium binding experiments solubilised receptors were added to plates last, and the plates were incubated at room temperature for 45min prior to reading. For equilibrium competition binding assays 100nM of CA200689 (s)-propranolol-red (F-propranolol) was used for membrane and DDM samples and 200nM CA200689 (s)-propranolol-red (F-propranolol) for DIBMA samples. For A_{2A} the fluorescent adenosine antagonist XAC CA200634 (F-XAC) was used as the tracer. For kinetic binding experiments DDM solubilised receptors were added last to plates using PHERAstar FSX in built injectors. CA200693 (s)-propranolol-green was used as the tracer and 3µM alprenolol as the NSB.

2.2.13 TR-FRET thermostability assays

For TR-FRET thermostability assays membranes of Lumi4-Tb labelled TS-SNAP-A_{2A} or TS-SNAP-β_2AR receptors and solubilsation of these proteins took place as described above **section 2.2.6.** Solubilised β2AR was incubated with 100nM BODIPY™ FL L-Cystine dye with or without 200nM F-propranolol or 100μM cyanopindolol, for 15min on ice in 20mM HEPES, 150mM NaCl, 5% glycerol, 0.5% BSA, pH8 and for DDM samples 0.1% DDM was used. 20μL samples were added to each well of a 96 well plate and incubated for 30min over a temperature gradient of 20-78°C across the plate. Samples were transferred to 384 well proxiplate and TR-FRET between BODIPY™ FL L-Cystine dye and Lumi4-Tb was read by exciting at 337nm and reading emission at 620nm and 520nm using Pherstar FSX and 337 520/620 module (BMG Labtech). F-propranolol and fluorescent XAC (F-XAC) (CellAura, UK) binding was measured using HTRF 337 665/620 module as above.

2.2.14 In solution intermolecular nanoBRET assays

For all solution BRET assays, membranes were made from cells expressing TS-SNAP-A_{2A}-nLuc or TS-SNAP-β_2AR-nLuc receptors and solubilisation of these proteins took place as described above (**sec 2.3**). 20mM HEPEs, 150mM NaCl, 10% glycerol, 1µM GDP, 8mM BME, 0.5% BSA and 0.1% ascorbic acid pH 7.4 was used as the assay buffer in all in solution nanoBRET assays. For all in solution nanoBRET assays luminescence at 450-80nm was quantified for nanoLuc and from 550nm and higher for venus mini-Gs using 450-80/550LP module and Pherastar FSX.

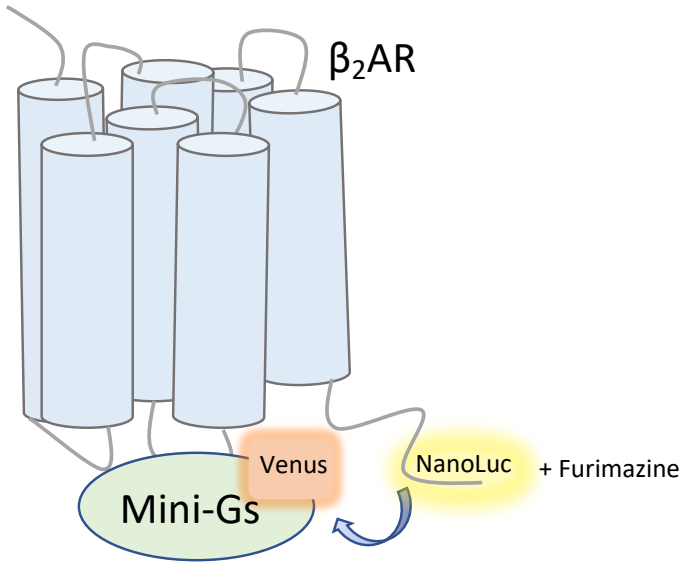

Figure 2.4: mini-G_s recruitment to the β_2AR was quantified by fusing nanoLuc to the C terminus of the β_2AR and venus to the N terminus of the mini-G_s and measuring BRET between nanoLuc and venus.

2.2.15 Venus mini-G_s nanoBRET recruitment assays

Solution-based recruitment assays in which varying concentrations of β_2AR agonists were used to recruitment an excess (1μM) of venus mini-G_s were run in 20μL volumes in white 384 well proxiplates. 25μM unlabelled mini-G_s was used to define specific binding of the venus mini-G_s to the TS-SNAP-β_2AR-nLuc receptors. Receptor, ligand and mini-G_s proteins were added to plate and incubated for 80 min at room temperature, 8μM furimazine was added to plate and incubated for a further 10 min before the plate was read on PHERAstar FSX as described above.

2.2.16 Venus mini-G_s nanoBRET kinetic assays

For in solution kinetic nanoBRET assays in which the affinity of venus-mini-G_s for the agonist bound TS-SNAP-β_2ARnLuc receptors was measured over time, assays were run in 20μL volumes in white 384 well proxiplates. Varying concentrations (3000-1.4nM) of venus mini-G_s were added to plates with either buffer or 30μM mini-G_s to define total and non-specific binding, respectively. DDM solubilised receptors were incubated with saturating concentration of selected β_2AR agonists for 40min, and X4 (32μM) furimazine for 10 min, prior to addition to plate. Receptor was added to plate offline, mixed up and down rapidly with a matrix pipette and read immediately on PHERAstar FSX as described above. After reading for 20min to allow for association of venus-mini-G_s to TS-SNAP-β_2AR-nLuc receptors reader was paused and 2μL of 333μM mini-G_s added to total wells to dissociate, plate was read for a further 20min. Buffer was added to NSB wells. The saturating concentrations of each agonist used in these studies was defined by the in-solution venus-mini-G_s recruitment assays (chapter **5**) and are summarised in table **2.2.**

Ligand	Saturating concentration used
Formoterol	5μM
Isoprenaline	100μM
Adrenaline	500μM
Noradrenaline	1mM
C26	100nM
BI-167-107	100nM
Salmeterol	50nM
Salbutamol	60μM

Table 2.2: A summary of the saturating concentrations of β_2AR agonists used in section 3.02.

2.2.18 Data analysis

All non-linear regression fits were performed in GraphPad Prism 9.0 (Ca, U.S) using a least-squares fitting method.

TR-FRET equilibrium ligand binding data

Total and NSB for F-propranolol binding to the β_2AR was fitted to one-site models according to equations **2.1** and **2.2**.

$$Total\ binding = \left[\frac{Bmax * X}{(K_d + X)}\right] + [NS * X + background]$$

Equation **2.1**

Where:

NS = slope of linear nonspecific binding

Background = Y when X is 0

Bmax = the maximum specific binding

K_d = the equilibrium dissociation constant

X= concentration of tracer

Equilibrium specific binding of F-propranolol to the β_2AR and venus-mini-G_s binding the β_2ARnLuc was fitted to a one site specific binding model according to equation **2.2.** Final K_d values were taken as an average of K_d values from individual specific curve fits.

$$\boldsymbol{Y} = \frac{Bmax * X}{(K_d + X)}$$

Equation **2.2**

Where:

Y = specific binding

K_d = the equilibrium dissociation constant of the labelled ligand

Equilibrium competition binding data was fitted to the One site Fit K_i model according to equation **2.3.** K_i values were calculated from resulting IC_{50} values according to equation **2.4.** Final K_i values were taken as an mean of individual experiments.

$$Y = \frac{(Top - Bottom)}{(1 + 10^{(x - LogIC_{50})}) + Bottom}$$

Equation **2.3**

Where:

Y = binding of tracer

IC_{50} = the concentration of competing ligand which displaces 50% of radioligand specific binding.

$$K_i = \frac{IC_{50}}{1 + \left(\frac{[L]}{K_d}\right)}$$

Equation **2.4**

Where:

K_i = the inhibition constant of the unlabelled ligand

[L] = concentration of labelled ligand

K_d = the equilibrium dissociation constant of the labelled ligand.

TR-FRET kinetic ligand binding data

Specific binding of the kinetics of association of F-propranolol binding to DDM-β_2AR was fitted globally to simultaneously fit $K_{on,}$ and K_{off} using equation **2.5.**

$$K_{obs} = [Fluorescent - propranolol] * K_{on} + K_{off}$$

$$Y = Y_{max} * (1 - exp(-1 * K_{obs} * X)) \qquad \text{Equation } \mathbf{2.5}$$

Where:
K_{obs} = the observed rate of association
K_{on} = the association rate constant
K_{off} = the dissociation rate constant
Y = fluorescent propranolol binding

Specific binding for the competition association kinetics of the unlabelled ligands, formoterol, isoprenaline, adrenaline, noradrenaline, salmeterol, salbutamol, C26 and BI-167-107 binding to the DDM-β_2AR was fitted to the Motulsky Mahan competition kinetics model (Motulsky & Mahan, 1984) to calculate $K_{on,}$ and K_{off} of the unlabelled ligand according to equation **2.6.**

$$K_A = K_1[L] + K_2$$

$$K_B = K_3[I] + K_4$$

$$S = \sqrt{((K_A - K_{B)})^2 + 4 \cdot K_1 \cdot K_3 \cdot L \cdot I \cdot 10^{-18})}$$

$$K_F = 0.5 * (K_A + K_B + S)$$

$$K_s = 0.5 * (K_A + K_B - S)$$

$$Q = \frac{B_{max} * K_1 * L * 10^{-9}}{K_F - K_s}$$

$$Y = Q \cdot \left(\frac{K_4 \cdot (K_F - K_s)}{K_F \cdot K_s} + \frac{K_4 - K_F}{K_F} \exp^{(-k_F \cdot x)} - \frac{K_4 \ K_s}{K_s} \exp^{(-K_s \cdot x)}\right)$$

Equation **2.6**

Where:

Y= specific binding

K_1 = K_{on} of fluorescent propranolol

K_2 = K_{off} of fluorescent propranolol

K_3 = K_{on} of the unlabelled ligand

K_4 = K_{off} of the unlabelled ligand

[L] = [fluorescent propranolol]

[I] = [unlabelled ligand]

Thermostability curves

All thermostability data from each experiment was fitted to a Boltzmann sigmoidal curve according to equation **2.7** to obtain a melting temperature (Tm) value. Final T_m values were taken as an average of T_m values from individual curve fits.

$$Y = Bottom + \frac{(Top - Bottom)}{1 + \exp\left(\frac{Tm - X}{Slope}\right)}$$

Equation **2.7**

Where:

Y = the relative concentration of proteins in the unfolded state

X = Temperature (^oC)

T_m = The temperature at which half the protein of interest is unfolded

NanoBRET mini-G_s binding kinetics

Specific binding data for the association of venus-mini-G_s binding to the agonist bound DDM-β_2AR was fitted to a two-site exponential association model described in equation **2.8.** Where Y = specific binding.

$$Y = Y_{max1} \cdot (1 - e^{-K_1 - X}) + Y_{max2} \cdot (1 - e^{-K_2 - X})$$

Equation **2.8**

K_{obs} plots for K_{fast} values obtained from equation 2.8 were fitted to a simple linear regression model according to equation 2.9 to obtain the K_{on} of $K_{fast.}$

$$Y = mx + c$$

Equation **2.9**

Where:
m = slope or K_{on}
c = intercept or K_{off}

For the analysis the intercept was fixed to K_{off} values measured experimentally and obtained via equation 2.10.

Specific binding data for the dissociation of venus-mini-G_s from the agonist bound DDM-β_2AR complex was fitted to a one phase exponential decay model, according to equation **2.10.** Where Y = specific binding.

$$Y = Span \cdot e^{-k \cdot x} + Plateau$$

Equation **2.10**

NanoBRET concentration-response curves

Concentration response curves obtained for in-solution venus-mini-G_s recruitment to β_2AR and for CASE-G_s activation by the eight β_2AR agonists used in this study were fitted to a three-parameter logistic curve using equation 2.11.

$$\boldsymbol{Response} = \frac{(\boldsymbol{E_{max}} * [\boldsymbol{A}])}{([\boldsymbol{A}] + \boldsymbol{EC_{50}})}$$

Equation **2.11**

Where:

[A] = concentration of agonist

EC_{50} = concentration of agonist required to induce half the maximal response

E_{max} = the maximal response of the agonist

To obtain efficacy values (τ) for the eight β_2AR agonists to activate the CASE G_s protein concentration response curves were fitted to the operational model (equation **2.13**).

$$\boldsymbol{E} = \frac{\boldsymbol{E_{max}}\,\boldsymbol{\tau}\,[\boldsymbol{A}]}{\boldsymbol{K_A} + [\boldsymbol{A}](\mathbf{1} + \boldsymbol{\tau})}$$

$$\tau = \frac{R_T}{K_E}$$

Equation **2.13**

Where:

τ = the transducer ratio

K_A = the equilibrium association constant of the agonist

[A] = concentration of agonist

R_T = total receptor concentration

K_E = the concentration of agonist-receptor complex required for half maximal response

E_{max} = the maximal response of the agonist

Statistical analysis

Comparison of T_m, K_d, K_i, K_{off}, K_{on}, EC_{50} and τ values was made using a one-way Analysis Of Variance (ANOVA) test and Tukey's post hoc multiple comparison test. Statistical comparison of T_m values obtained with F-propranolol Vs BODIPY™ FL L-Cystine dye was made using an unpaired t test. A Pearson's correlation coefficient was used to investigate correlations between CASE-G_s activation, τ values and relative time to reach equilibrium (IC_{50}1min/IC_{50}End) and between CASE-G_s activation τ values and mini-G_s binding K_{on} and K_{off} values. All statistical analysis was completed in GraphPad Prism 9 and $p<0.05$ was considered statistically significant.

Chapter 3

Solubilisation of the functional β_2AR using Diisobutylene Maleic acid (DIBMA)

3.1 Introduction

This study aimed to investigate the kinetics of ligand-β_2AR and β_2AR-mini-G_s interactions in isolation from the cellular environment. As such, a prerequisite was extraction of the β_2AR from its cellular environment, such a biophysical study requires only small amounts of β_2AR, and benefits from maintaining the β_2AR in as physiological environment as possible to avoid compromising protein stability and native activity.

3.1.1 Methods previously employed to solubilize the β_2AR

Classically, extraction of the β_2AR has involved the use of detergents, often in the case of the β_2AR and other GPCRs (Munk et al., 2019), *n*-dodecyl-β-D-maltopyranoside (DDM) is used. It is however, well established that whilst the hydrophobic head groups of detergent molecules are designed to mimic the cell membrane, they far from recapitulate this complex environment of lipids and phospholipids. As such, protein stability and activity is compromised in the detergent micelle. More detail about the types of detergents used for solubilisation of membrane proteins and the mechanism for this is given in section **1.9.**

Clearly, optimal protein stability and activity is essential for accurate biophysical studies. One method to further stabilise membrane proteins is the introduction of thermostabilising mutations. This method has been employed to stabilise the DDM solubilized β_2AR (Serrano-Vega & Tate, 2009a) (Roth et al., 2009). Serrano-Vega and colleagues transferred 6 stabilizing mutations from the thermostabilized turkey β_1AR to the human β_2AR (m23-hβ_2AR) and showed that this improved the stability of the m23-hβ_2AR by an 11^{o}C increase in its T_m. Moreover, Roth and colleagues (Roth et al., 2009) substituted glutamic acid 122 (E122) for tryptohan to give a 9.3-fold increase in stability and an increase in membrane expression. Whilst thermostabilizing mutations undoubtedly improve the viability of membrane proteins for structural studies and the resolution of these studies, thermostabilizing mutations may affect

protein function. For example, E122W β_2AR showed a 2-fold loss in ligand binding affinity compared to the wild type (WT) (Roth et al., 2009), and ligand binding studies on m23-hβ_2AR showed a preference for the antagonist bound conformation. Therefore, whilst thermostabilizing mutations may be used to improve β_2AR stability for structural studies such methods are problematic for functional biophysical studies.

Another method to improve membrane protein stability has been use of synthetic nanodiscs, which better mimic the native membrane environment. More detail on the components of synthetic nanodiscs is given in **sec 1.9**. Leitz and colleagues (Leitz et al., 2006) first showed the reconstitution of functional β_2AR in a synthetic nanodisc. Whorton and colleagues (Whorton et al., 2007) also showed that β_2AR remained functional in monomers when reconstituted in high density lipoproteins (rHDL). Neither of these studies investigated the thermostability of the β_2AR in these environments. The main disadvantage of this method is that detergents are still required for extraction of the β_2AR from the membrane and detergents have been showed to irreversibly damage membrane proteins.

3.1.2 Applicability of using polymers to solubilize the β_2AR

Alternatively, SMA and DIBMA polymers have recently been employed as a novel method for extracting protein from the plasma membrane. These polymers incorporate into the membrane, disrupt the membrane, and self-assemble into lipid nanoparticles containing the membrane protein along with its' native phospholipids. This method has clear advantages over use of detergents which often denature the protein and are only a poor mimic of the membrane protein's native phospholipids.

The concept that membrane lipids and phospholipids modulate membrane protein functions is well established. Moreover, several studies point to a direct role for allosteric modulation by membrane lipids and phospholipids specifically in β_2AR function. Dawaliby and

colleagues, (Dawaliby et al., 2016) systematically characterized the effect of different phospholipids on purified β_2AR activation and ligand binding. This study showed that phosphatidylglycerol increased the proportion of the population of the receptor in the active state whereas phosphatidylethanolamine increased the proportion of the population of the receptor in the inactive state. Moreover, cholesterol has also been shown to modulate β_2AR signaling. Studies in HEK293 cells showed than cAMP signaling is increased when cholesterol is depleted from the cell membrane (Pontier et al., 2008), and Paila and colleagues showed that β-adrenoceptor signalling in response to isoprenaline is similarly affected in rat cardiomyocytes (Paila et al., 2011), suggesting that cholesterol modulation of β_2AR is physiologically relevant. Furthermore, Zocher and colleagues (Zocher et al., 2012) used single molecule force spectroscopy to show that presence of cholesterol increases the intramolecular interactions within the human β_2AR and therefore its stability. These studies provide direct evidence that native membrane composition is vital for native β_2AR activity and stability therefore supporting the use of native nanodiscs for these biophysical studies.

3.1.3 Methods to characterise membrane protein stability

Protein stability is the net balance of intramolecular forces within a protein that determine whether a protein will exist in its native or a denatured state. As such to measure protein stability the equilibrium between the native and denatured states must be assessed. The intramolecular forces that stabilize the folded structure of a protein include hydrophobic, electrostatic, hydrogen bonds, van der Waals and disulphide interactions. The denatured and unfolded state of a protein is characterized by disorder. The equilibrium between the natured (N) and denatured (D) states of a protein can be described by a two-step model (equation **3.1**) (Shirdel & Khalifeh, 2019).

$$N \rightleftharpoons D$$ Equation **3.1.**

Any chemical reaction is driven by a change in Gibb's free energy (ΔG), which will favour one direction of a reaction. In the case of protein unfolding the natured state will have a higher free energy than the denatured state hence the more positive ΔG the more stable the protein and the more negative ΔG the more protein will denature. Therefore, an increase in temperature causes an increase in enthalpy and so decrease in ΔG and therefore an increase in protein denaturing. This is summarised in equation **3.2**.

$$\Delta G = -R \cdot T \cdot ln\,(K) \qquad \text{Equation } \mathbf{3.2}$$

Where R = gas constant, T = temperature and K=the equilibrium constant of the reaction.

Hence measuring protein unfolding over an increasing temperature range will provide relative measurements of protein stability. Measurements of proteins stability are generally summarised by their melting temperature (T_m) values. T_m values are the point at which 50% of the protein is in the unfolded state. It is important to note that the T_m value of a protein is highly dependent upon pH and buffer conditions, as these will influence molecular interactions of the protein and therefore effect ΔG, therefore T_m values cannot be absolute (Gao et al., 2020).

Many techniques have been employed to measure protein unfolding in response to temperature during thermostability studies. Such methods include exposing the protein to increased temperatures, removing protein aggregates via ultracentrifugation and then measuring the relative amounts of protein remaining, for example FSEC or in gel fluorescence. The above methods are very labour intensive (Miljus et al., 2020). Other techniques allow for a direct measurement of protein unfolding. Differential scanning fluorometry (DSF) has become a popular method as it is both high throughput and economically viable. DSF generally uses a fluorescent dye such as SYPRO orange or 7-

Diethylamino-3-(4'-Maleimidylphenyl)-4-Methylcoumarin (CPM) which are quenched in aqueous solution but show a significant increase in quantum yield when bound to hydrophobic regions of an unfolded protein (Gao et al., 2020) (Huynh, 2016). A drawback of DSF assays is that they require the protein to be purified as there is otherwise nothing to distinguish one protein from another. Protein purification is very labour intensive and often takes multiple optimisation steps.

This study uses a novel TR-FRET based thermostability assay described in section (**2.2.13**). This method works on a similar premise to the DSF assay. The dye BODIPY™ FL L-cystine binds to cysteine residues within the core of the GPCR which are only exposed when the GPCR unfolds, and this acts as a FRET acceptor for a terbium label on the N terminus of the GPCR. The advantage of this method over other DSF methods is that the terbium tag means that the protein of interest does not need to be purified for the assay, whilst the assay is still high throughput.

3.1.4 Methods to characterise membrane protein functionality

One method to elucidate if a protein remains folded and active once extracted from the plasma membrane is to investigate if it retains ligand binding ability. Classically, pharmacologists have used radioligands to detect ligand binding to a receptor of interest. However, due to the safety concerns associated with radioactivity and therefore the cost of their licensing and disposal use of fluorescence ligands has become more prominent. The TR-FRET ligand binding assay used in this study detects FRET been a terbium label on the GPCR N terminus and fluorescently labelled propranolol, as described in section **2.2.12**. In addition to safety and economic concerns TR-FRET ligand binding has the advantage of showing a more specific signal than radioligand binding as only ligand bound to the receptor produces a FRET signal and not that which is non-specifically bound to the membrane.

The aim of this chapter was to examine the use of the polymer DIBMA as an improved method to extract the β_2AR from mammalian cell membranes. To this end, this study aimed to investigate:

1. The ability of DIBMA to extract β_2AR from T-REx^{TM}-293 cell membranes.
2. If DIBMALP-β_2AR retained the native β_2AR activity.
3. If DIBMALP-β_2AR retained the native β_2AR conformational landscape.
4. The stability of the β_2AR inside the DIBMALP compared to conventional methods
5. The ability of the DIBMALP-β_2AR to couple to the mini-G_s protein

3.2 Methods

3.2.1 Mammalian cell culture

T-REx™ cell lines expressing either stably expressing TS-SNAP-β_2AR or TS-SNAP-A_{2A} were used in this chapter. These cell lines were cultured and induced as described in **sec 2.2.2.**

3.2.2 Solubilisation of TS-SNAP-β_2AR or TS-SNAP-A_{2A} using DDM or DIBMA

Small scale solubilisation trials took place on TS-SNAP- β_2AR or TS-SNAP-A_{2A} expressing membranes. Membranes were generated from terbium-cryptate labelled TS-SNAP- β_2AR or TS-SNAP-A_{2A} expressing T-REx™ cell lines as described in **sec 2.2.5.** Receptors were extracted from membranes in either 1% DDM or 3% DIBMA as described in **sec 2.2.6.** Unsolubilised material was removed via ultracentrifugation.

3.2.3 TR-FRET thermostability assays

Protein unfolding was driven by incubation of the sample over an increasing temperature range. Protein unfolding was measured by an increase in FRET signal between Lumi-4-terbium on the N terminus of the GPCR and BODIPY™ FL L-Cystine dye which bound to cysteine in the now exposed core of the receptor. TR-FRET signal was measured using PHERAstar FSX plate reader at room temperature using 520/620 TRF module. This assay is described in **sec 2.2.12.**

3.2.4 TR-FRET ligand binding assays

The affinity of F-propranolol for the TS-SNAP-β_2AR in the membrane, DDM micelle and DIBMALP environments was measured by TR-FRET between Lumi4-Tb and CA200689 (s)-propranolol-red (F-propranolol) using PHERAstar FSX plate reader at room temperature using HTRF module. This method is described in **sec 2.2.13.** 100nM (for membrane or DDM samples) or 200nM (for DIBMA samples) F-propranolol was used as the tracer for competition binding studies with propranolol, isoprenaline and ICI 118, 551.

3.2.5 Halo-mini-G_s shift assay

The ability of Halo-mini-G_s to couple TS-SNAP-β_2AR in membranes, DDM or DIBMALPs was measured by performing the above TR-FRET isoprenaline competition binding experiments in the absence and presence of 25μM Halo mini-G_s. Binding of Halo-mini-G_s to the TS-SNAP-β_2AR would be expected to increase the affinity of TS-SNAP-β_2AR for isoprenaline and hence shift the ligand binding curve. Halo-mini-G_s proteins were made as described in chapter **2** and discussed in chapter **5**.

3.3 Results

3.3.1 Solubilisation of the TS-SNAP-β_2AR from the mammalian membrane

The first aim of this study was to investigate if the polymer DIBMA was able to extract the TS-SNAP-β_2AR from the mammalian cell membrane. To investigate this the TS-SNAP-β_2AR was labelled with AlexaFluor488 in whole adherent T-REx^{TM} cells. Membranes were then prepared from these cells and incubated with 3% DIBMA for 3h at room temperature. Extraction with 1% DDM was used as the positive control. Following the removal of unsolubilised material using ultra centrifugation the TS-SNAP-β_2AR was quantified using the Pherastar FSX plate reader and AlexaFluor 488. A high fluorescent emission at 520nm would indicate a high efficiency for DIBMA to extract the TS-SNAP-β_2AR from the mammalian cell membrane whilst no increase in the 520nm signal compared to background would indicate that the polymer DIBMA was unable to extract TS-SNAP-β_2AR from the mammalian cell membrane. Figure **3.3.1B** shows 3% of the polymer DIBMA was able to extract 32±7% of the TS-SNAP-β_2AR from the T-REx^{TM} cell membrane whilst 1% DDM extracted 90±11%. Figure **3.3.1A** shows in gel fluorescence of purified AlexaFluor-647 labelled TS-SNAP-β_2AR confirming presence of this protein at 75kDa.

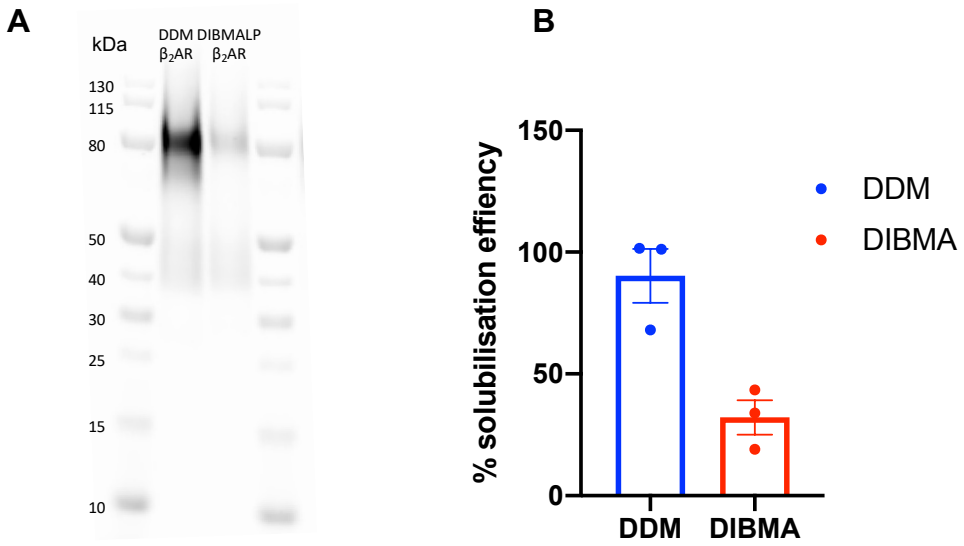

Figure 3.3.1: Solubilisation of TS-SNAP-β_2AR from the membrane of T-REx^{TM}-293 cells stably expressing TS-SNAP-β_2AR using 1% DDM and 3% DIBMA A) In gel fluorescence SDS-PAGE gel of AlexaFluor-647 labelled affinity purified TS-SNAP-β_2AR read on Amersham Typhoon using Cy5 filter set, representative of n=2, **B)** Solubilisation efficiency of DDM Vs DIBMA to extract the Alexa488 labelled TS-SNAP-β_2AR from T-REx^{TM}-293-TS-SNAP-β_2AR cells, where 520nm fluorescence intensity of samples was quantified on PHERAstar FSX using 520nm FI module and percentage of membrane sample used for receptor extraction calculated (n=3 ± SEM).

In addition to confirming DIBMA could be used to extract the TS-SNAP-β_2AR and quantifying its solubilization efficiency, Fluorescent Size Exclusion Chromatography (FSEC) was used to characterize the quality of DDM and DIBMA solubilized TS-SNAP-β_2AR. Figure **3.3.2A** shows mean (n=3) FSEC traces for DDM and DIBMA solubilized TS-SNAP-β_2AR. These traces peak at 1.6-1.8mL, roughly 75kDa which corresponds to DDM-β_2AR or DIBMALP-β_2AR. Additionally, there was a higher molecular weight peak for the DIBMALP-β_2AR and two higher molecular weight peaks for DDM-β_2AR. The higher molecular weight peaks are presumed to correspond to protein aggregates. Whilst the achieved resolution does not show a difference in size between the two preparations it is evident that a lesser proportion of the DIBMALP-β_2AR is aggregated compared to the DDM-β_2AR.

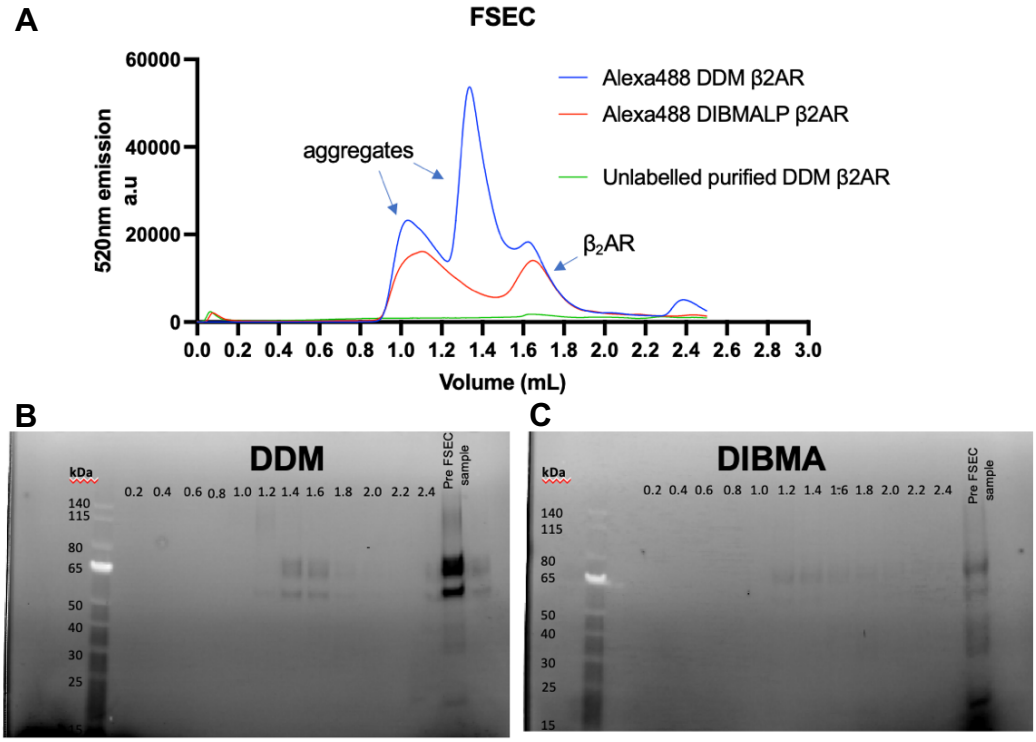

Figure 3.3.2: Characterisation of Alexa488 labelled DDM and DIBMALP TS-SNAP-β_2AR using FSEC A) FSEC analysis of DDM-TS-SNAP-β_2AR and DIBMA-TS-SNAP-β_2AR samples using Yarra X300 column and Shimadzu HPLC system to measure 520nm emission (Mean of n=3). **B-C)** Confirmation of FSEC fractions by representative in gel fluorescence, of SDS-PAGE gel, columns show elution volume (mL) read on Amersham Typhoon using Cy2 filter set

3.3.2 Saturation ligand binding studies on TS-SNAP-β_2AR in membranes, DDM micelles and DIBMALPs

The next aim was to investigate whether the TS-SNAP-β_2AR remained functional when extracted from the mammalian cell membrane using DIBMA. This was assessed using a TR-FRET ligand binding assay. Ligand binding was indicated by TR-FRET between the fluorescent antagonist CA200689 (s)-propranolol-red (F-propranolol) and Lumi4-Tb on the TS-SNAP-β_2AR N-terminus. Figure **3.3.3** shows saturation ligand binding experiments for F-propranolol binding membrane-β_2AR, DDM-β_2AR and DIBMALP-β_2AR. As indicated, ligand binding capacity was retained when TS-SNAP-β_2AR was extracted from the membrane using the conventional detergent DDM and the polymer DIBMA. These data also showed similar mean pK_d values (±SEM) for F-propranolol binding membranes (7.50±0.05), DDM (7.10±0.08) and DIBMA (7.00±0.13), although with slightly reduced affinity in DIBMALPs compared to membranes (P=0.02, one-way ANOVA and Tukey's multiple comparison). The maximal binding signal obtained for F-propranolol binding to the TS-SNAP-β_2AR was 3-fold lower for DIBMALP-β_2AR than its binding to β_2AR in membranes.

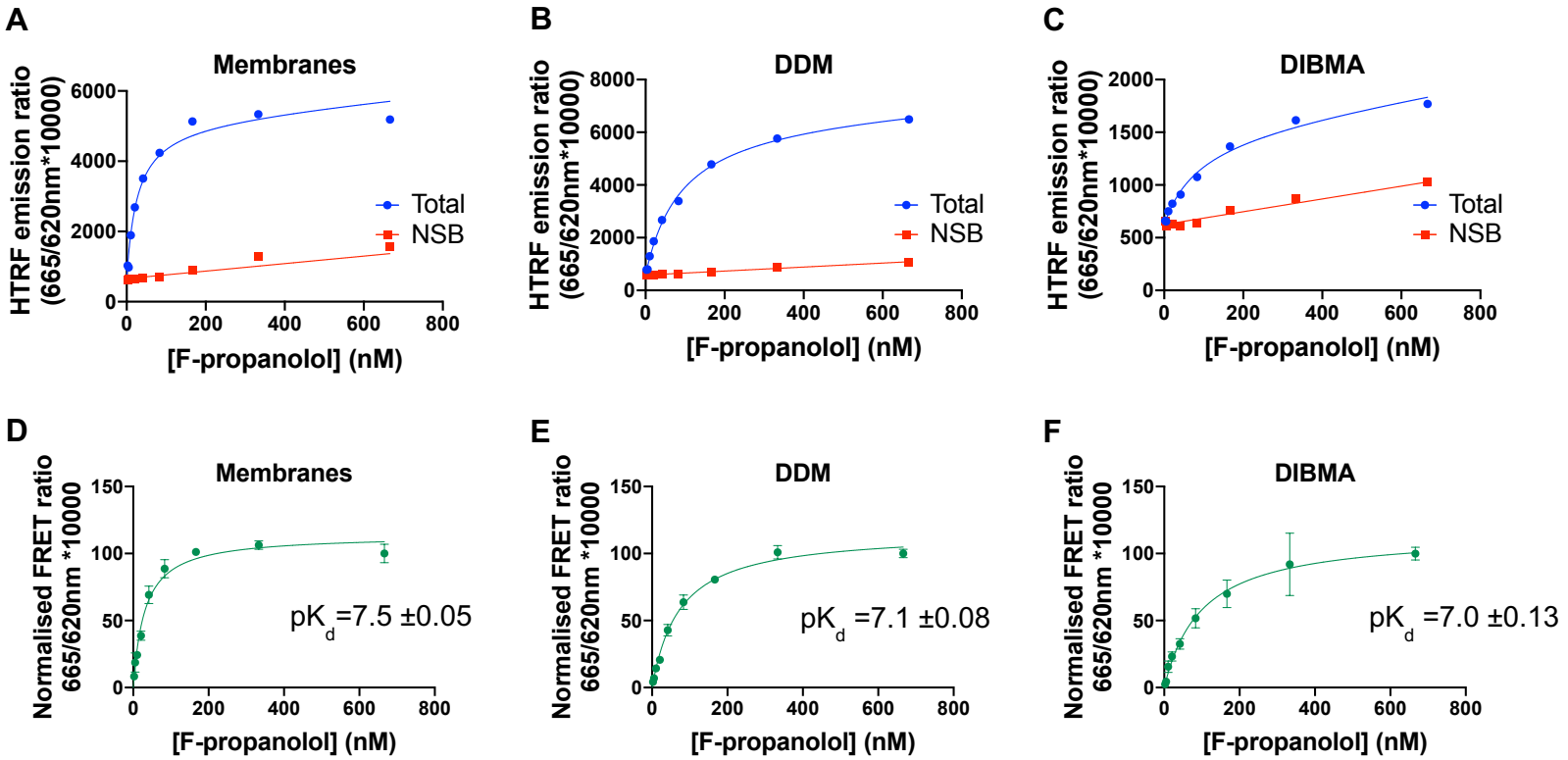

Figure 3.3.3: A comparison of F-propranolol binding to TS-SNAP-β_2AR in membranes, DDM and DIBMALPs A-C) Representative F-propranolol (2-666nM) saturation plots showing total and non-specific binding to the β_2AR in **A)** TS-SNAP-β_2AR T-REx^{TM}-293 cell membranes, **B)** DDM and **C)** DIBMALPs. **D-F)** Saturation binding curves showing specific binding and associated affinity (pK_d) values for F-propranolol binding to the β_2AR in **D)** HEK cell membranes, **E)** DDM and **F)** DIBMALPs, curves show combined data normalised to maxium signal of each preparation, data points show mean ± SEM, n=3. TR-FRET between Lumi4-Tb and F-propranolol was read on PHERAstar FSX using HT

3.3.3 Competition ligand binding studies on TS-SNAP-β_2AR in membranes, DDM micelles and DIBMALPs:

The next aim was to investigate if the conformational landscape of the TS-SNAP-β_2AR was restricted by the DIBMALP. To ascertain this, the ability of DIBMALP-TS-SNAP-β_2AR to bind the agonist isoprenaline, the inverse agonist ICI 118, 551 and the antagonist propranolol was investigated using a TR-FRET equilibrium competition binding assay with F-propranolol as the tracer. As agonists, inverse agonists and antagonists respectively, these ligands will bind different receptor conformations and a difference in affinity between DIBMALP-β_2AR and membrane-β_2AR would indicate that the conformational landscape of TS-SNAP-β_2AR differed from its native conformational landscape. Figure **3.3.4** shows that increasing concentrations of each ligand produced a reduction in the specific binding of F-propranolol bound to the TS-SNAP-β_2AR in membranes, DDM and DIBMALPs with largely comparable pK_i values (Table **3.3.1**). The only statistically significant difference was between isoprenaline binding to the TS-SNAP-β_2AR found in membranes versus the DDM solubilised β_2AR ($p=0.03$) (one-way ANOVA and Tukey's post hoc).

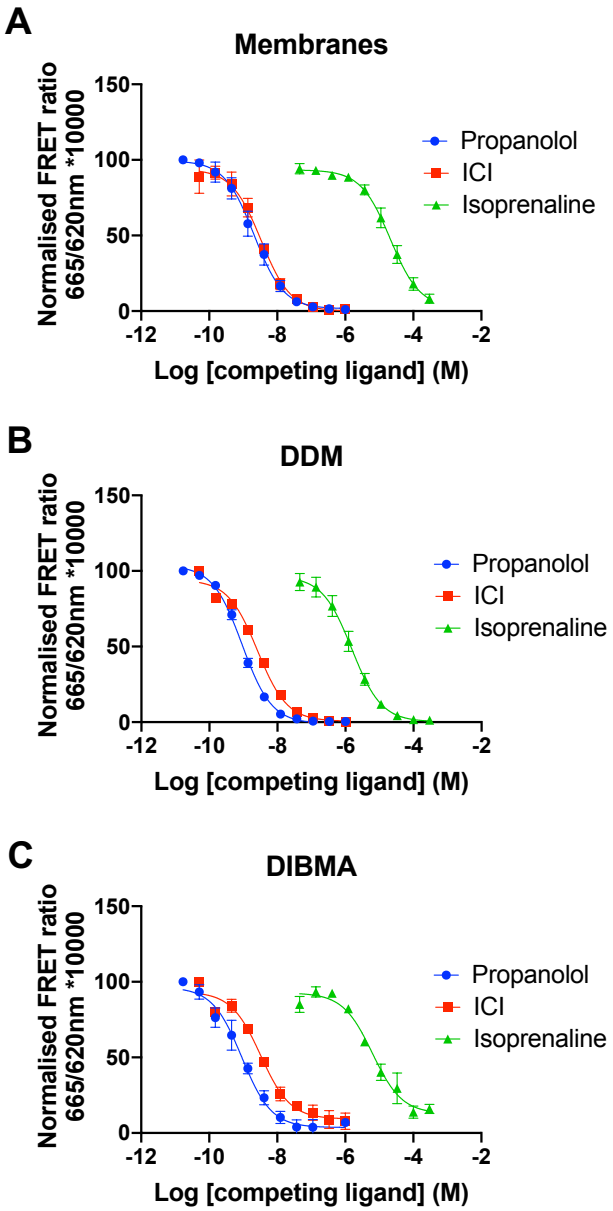

Figure 3.3.4: Competition TR-FRET ligand binding studies using F-propranolol as a tracer and unlabelled propranolol, ICI 118, 551 and isoprenaline as competitors in A) β_2AR membranes, **B)** DDM-β_2AR **C)** DIBMALP- β_2AR, curves show normalized combined data of n=3, error bars show SEM. TR-FRET between Lumi4-Tb and F-propranolol was read on PHERAstar FSX using HTRF module.

	Membranes			DDM			DIBMA		
	pIC_{50}	**pK_i**	**Slope**	**pIC_{50}**	**pK_i**	**Slope**	**pIC_{50}**	**pK_i**	**Slope**
Propranolol	8.7 ±0.13	9.5 ±0.03	1.0 ±0.02	9.0 ±0.04	9.5 ±0.03	1.2 ±0.04	9.1 ±0.10	9.6 ±0.10	0.8 ±0.30
ICI 118, 551	8.5 ±0.10	9.3 ±0.15	1.1 ±0.22	8.5 ±0.02	8.9 ±0.10	1.0 ±0.06	8.3 ±0.15	9.1 ±0.06	1.3 ±0.23
Isoprenaline	4.7 ±0.12	5.5 ±0.20	1.1 ±0.11	5.8 ±0.06	6.3 ±0.13	1.1 ±0.09	5.1 ±0.18	5.8 ±0.10	1.1 ±0.15

Table 3.3.1: A summary of pIC_{50}, pK_i and Hill slope values for propranolol, ICI 118,551, and isoprenaline obtained through TR-FRET competition binding assays Values show mean of n=3 individually fitted curves ±SEM, TR-FRET between Lumi4-Tb and F-propranolol was read on PHERAstar FSX using HTRF module.

3.3.4 TR-FRET thermostability studies on TS-SNAP-β_2AR in membranes, DDM micelles and DIBMALPs

We then investigated the thermostability of the DIBMALP-β_2AR compared to the conventionally used DDM solubilised β_2AR. This was first investigated using a novel ThermoFRET assay (Tippett et al., 2020). As with the TR-FRET ligand binding assay a SNAP tag on the N terminus of the TS-SNAP-β_2AR was labelled with Lumi4-Tb and the preparation was then heated over an increasing temperature range, in the presence of BODIPY™ FL L-Cystine dye. BODIPY™ FL L-Cystine covalently reacts with cysteines on the receptor which become exposed as the receptor unfolds. β_2AR unfolding was then measured by quantifying TR-FRET between Lumi4-Tb and BODIPY™ FL L-Cystine. This allowed thermostability to be investigated without purifying the receptor.

Figure **3.3.5B** shows thermostability curves for DDM-β_2AR in the absence and presence of the high affinity antagonist cyanopindolol. These data show DDM-β_2AR alone has a T_m of 35.2±2.4^{o}C, which is increased by the presence of cyanopindolol (41.9±0.1^{o}C, p=0.04) and F-propranolol T_m=37.8±0.4^{o}C, p>0.05 (one-way ANOVA and Tukey's multiple comparison test). Figure **3.3.5A** shows thermostability curves for TS-SNAP-β_2AR in the cell membrane in the absence and presence of cyanopindolol and F-propranolol. These data give a T_m of 62.4±0.2^{o}C for membrane-β_2AR alone and showed no shift in thermostability when measured in the presence of cynopindolol and F-propranolol. This suggests the unfolding of the receptor itself is not directly measurable and perhaps that these data show the disintegration of the membrane itself. ThermoFRET data for the DIBMALP-β_2AR did not fit a Boltzmann sigmoidal curve as the top end of the temperature range did not plateau (Figure **3.3.5C)**. No effect on any part of the DIBMALP-β_2AR thermostability curve was observed when measured in the presence of cyanopindolol or F-propranolol.

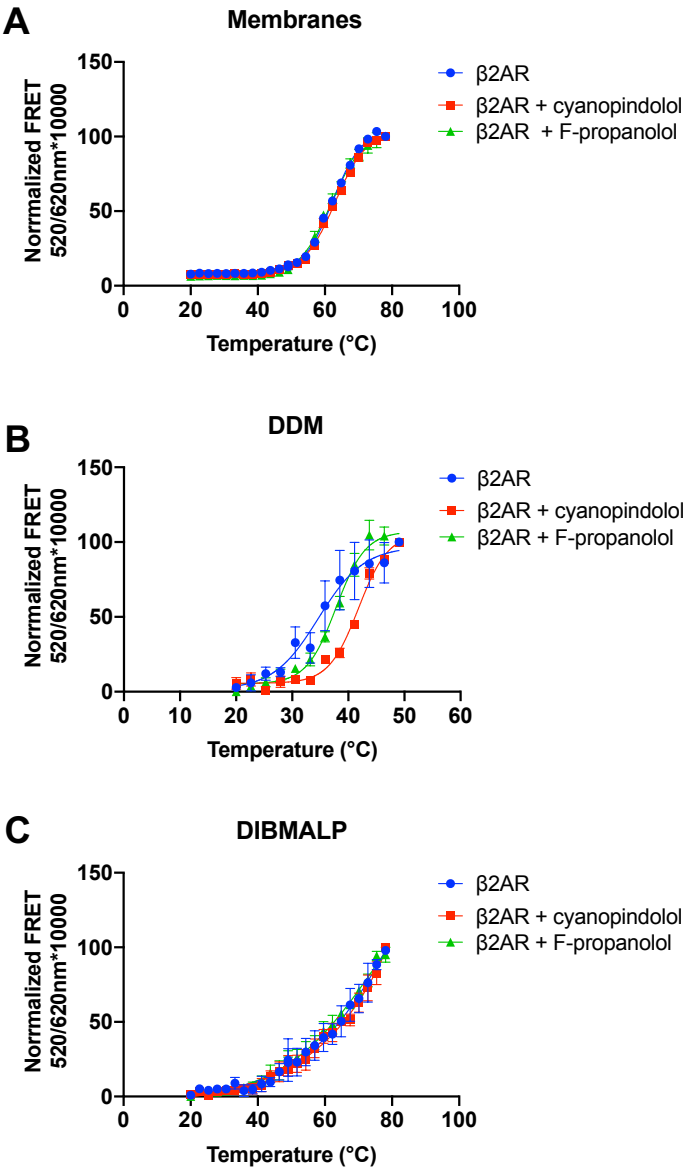

Figure 3.3.5: TR-FRET thermostability measurements using terbium cryptate and BODIPY™ FL L-Cystine dye in A) β_2AR membranes **B)** DDM solubilised β_2AR **C)** DIBMALP-β_2AR in the presence and absence of cyanopindolol (100nM) and F-propranolol (200nM). All curves show normalized combined data, mean ± SEM, for n=3. TR-FRET between Lumi4-Tb and BODIPY™ FL L-Cystine dye was measured on PHERAstar FSX at room temperature using 520/620 TRF module.

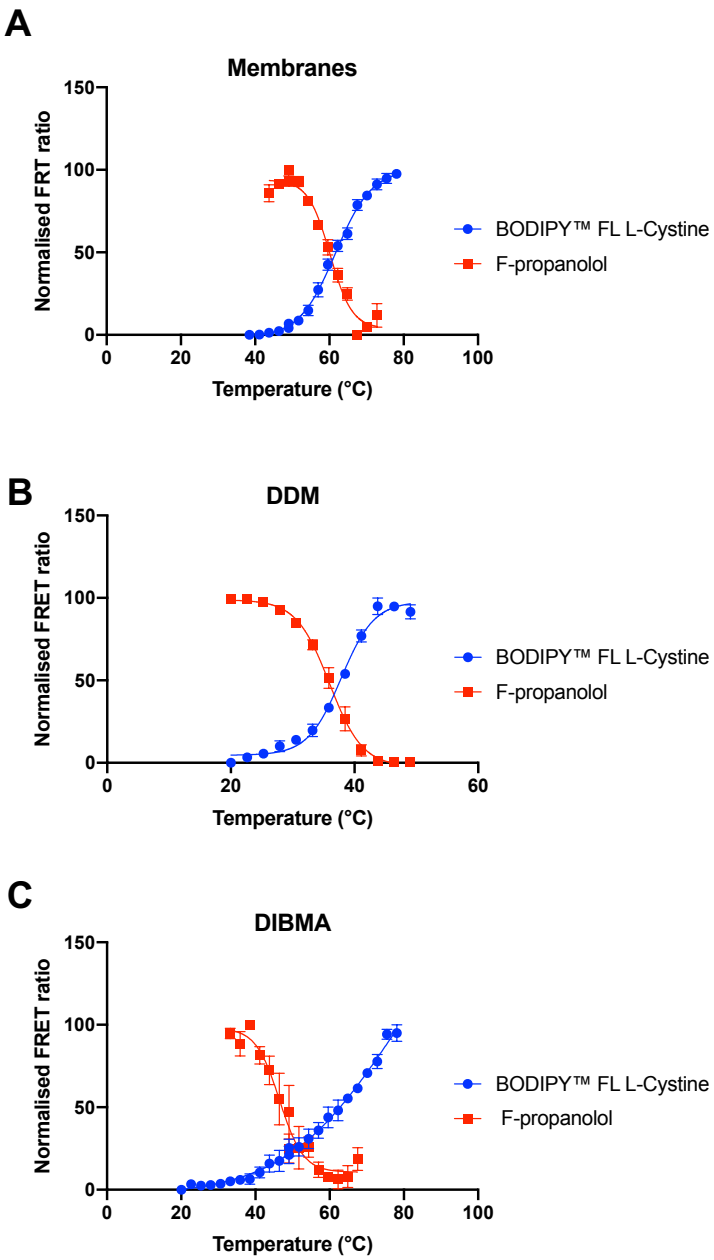

Figure 3.3.6: A comparison of TR-FRET thermostability curves obtained for β_2AR A) membranes, **B)** DDM and **C)** DIBMA using BODIPY™ FL L-Cystine dye or F-propranolol. All curves show normalized combined data, mean ± SEM, for n=3. TR-FRET between Lumi4-Tb and BODIPY™ FL L-Cystine dye was measured on PHERAstar FSX at room temperature using 520/620 TRF module, and for TR-FRET between Lumi4-Tb and F-propranolol using HTRF module.

As the ThermoFRET data for DIBMALP-β_2AR did not fit a Boltzmann sigmoidal curve we then investigated thermostability using F-propranolol as a probe rather than BODIPY™ FL L-Cystine dye. An increase in temperature would be expected to cause a decrease in ligand binding as the β_2AR unfolds. Figure **3.3.6** compares thermostability data for membrane-β_2AR, DDM-β_2AR and DIBMALP-β_2AR in the presence of F-propranolol obtained by measuring either TR-FRET between Lumi4-Tb and BODIPY™ FL L-Cystine dye or between Lumi4-Tb and F-propranolol. The resulting data showed similar T_m values determined for the membrane-β_2AR (60.1±0.6^{o}C) and DDM-β_2AR (36.0±0.6^{o}C) using F-propranolol as those obtained using BODIPY™ FL L-Cystine dye. Unpaired two-tailed t tests showed no statistically significant differences between membrane-β_2AR and DDM-β_2AR T_m values obtained with F-propranolol measured using either TR-FRET method. Thermostability curves for DIBMALP-β_2AR measured by quantifying TR-FRET between F-propranolol and Lumi4-Tb could be fitted to a Boltzmann sigmoidal curve with a corresponding T_m value of 46.8 ± 2.1^{o}C. This T_m value is statistically significant from that of membrane-β_2AR ($p=0.0002$) and DDM-β_2AR ($p=0.0009$) obtained by the same method (one-way ANOVA and Tukey's multiple comparison test). Therefore, the DIBMALP-β_2AR shows approximately 10^{o}C improved stability over the conventional DDM-β_2AR. The slope of DIBMALP-β_2AR also differed from that of DDM-β_2AR, these were -3.2 and -2.7 respectively.

In addition to investigating the thermostability of the β_2AR in these different environments, the thermostability of of another rhodopsin-like GPCR, the adenosine 2A receptor (A_{2A}R) in a DIBMALP was measured using a fluorescent adenosine receptor antagonist (F-XAC) (Hello Bio, UK). Measuring the reduction in F-XAC bound to A_{2A}R over an increased temperature range gave a T_m value of 44.8±0.7^{o}C, which was not statistically significantly different from that of the DIBMALP-β_2AR (Figure **3.3.7**).

T_m values for membrane-β_2AR, DDM-β_2AR, DIBMALP-β_2AR and DIBMALP-A_{2A} obtained measuring TR-FRET between Lumi4-Tb and BODIPY™ FL L-Cystine dye, and between Lumi4-Tb and F-propranolol or F-XAC are summarized in table **3.3.2.**

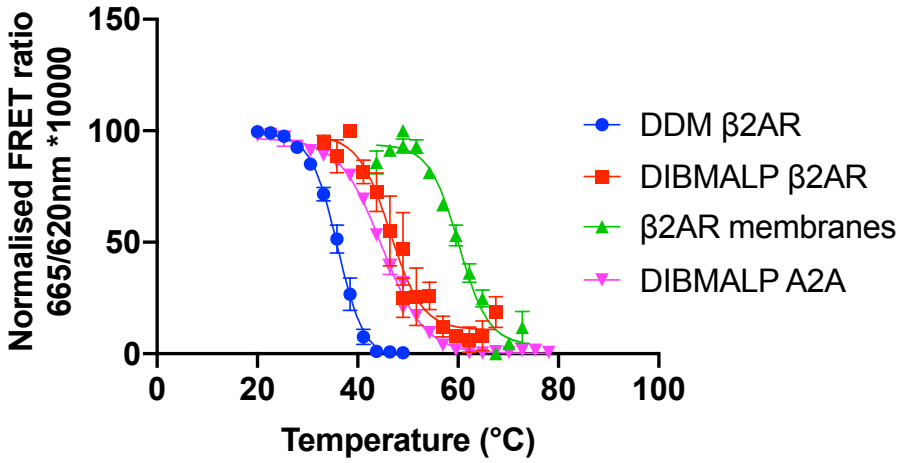

Figure 3.3.7: A summary of thermostability curves obtained by TR-FRET ligand binding. β_2AR and A_2AR thermostability measurements were made using F-propranolol (200nM) and F-XAC (200nM) respectively. All curves show normalized combined data, mean ± SEM, for n=3. TR-FRET between Lumi4-Tb and F-ligands was measured on PHERAstar FSX at room temperature using HTRF module.

	T_m (ºC) BODIPY™ FL L-Cystine	T_m(ºC) F-propranolol
Membrane β_2AR	62.4±0.2	-
Membrane β_2AR + F-propranolol	61.6±0.4	60.1±0.6
Membrane β_2AR + cyanopindolol	63.0±0.4	-
DDM β_2AR	35.2±2.4	-
DDM β_2AR + F-propranolol	37.8 ±0.4	36.0 ±0.6
DDM β_2AR + cyanopindolol	41.9 ±0.1	-
DIBMALP β_2AR	-	46.8 ±2.1
DIBMALP A_{2A}	-	44.8 ±0.7

Table 3.3.2: A summary of mean T_m values ± SEM for TS-SNAP-β_2AR and TS-SNAP-A_{2A}R in mammalian cell membranes, DDM detergent micelles or DIBMALPs with or without F-propranolol or cyanopindolol, using either BODIPY™ FL L-Cystine or F-propranolol or F-XAC. T_m values were a mean of n=3 experiments individually fitted to a Boltzmann sigmoidal curve.

3.3.5 TR-FRET ligand binding shift studies to investigate the ability of DIBMALP-β_2AR to couple Halo-mini-G_s

Finally, to investigate whether the DIBMALP-β_2AR retained its ability to couple its G protein, isoprenaline TR-FRET competition ligand binding assays were performed in the absence and presence of saturating concentrations (25μM) of Halo-mini-G_s. Saturating concentrations were defined by the experiments in chapter 5. If the DIBMALP-β_2AR affinity for the agonist isoprenaline increased in the presence of saturating concentrations of Halo-mini-G_s this implies that the β_2AR has bound the mini-G_s. An agonist such as isoprenaline will have higher affinity for β_2AR in an active or G protein coupled state.

Figure **3.3.8A-C** shows the effect of 25μM Halo-mini-G_s on the antagonist F-propranolol binding to the TS-SNAP-β_2AR in membranes, DDM, and DIBMALPs. It was necessary to assess the effect of Halo mini-G_s on binding of the tracer F-propranolol to the β_2AR so that isoprenaline competition binding data could be accurately fitted. F-propranolol pK_d values were 6.9±0.07, 7.3±0.01 and 7.1±0.22 for membrane-β_2AR, DDM-β_2AR and DIBMALP-β_2AR respectively in the absence of mini-G_s. There was no statistically significant difference between these pK_d values and those obtained for F-propranolol in the presence of saturating concentrations of Halo-mini-G_s, these were 7.0±0.06 (p=0.89), 7.3±0.10 (p=0.86) and 7.3±0.14 (p=0.47) for membrane-β_2AR + 25μM Halo-mini-G_s, DDM-β_2AR + 25μM Halo-mini-G_s and DIBMALP-β_2AR + 25μM Halo-mini-G_s respectively. Statistical comparison between pK_d values in the absence and presence of 25μM Halo-mini-G_s were made using unpaired two-tailed T-tests.

Figure **3.3.8D-F** shows competition binding studies to investigate the effect of saturating concentrations of Halo-mini-G_s on binding of the agonist isoprenaline to the TS-SNAP-β_2AR in membranes, DDM or DIBMALPs. These data showed statistically significant shifts of in the

affinity of membrane-β_2AR and DDM-β_2AR for isoprenaline in the presence of 25μM Halo-mini-G_s. The presence of 25μM Halo-mini-G_s decreased the pK_d value of isoprenaline binding membrane-β_2AR from 5.3 to 7.4 ($p=0.0002$, unpaired t-test) and from 6.4 to 8.5 ($p=0.0058$, unpaired t-test) for DDM-β_2AR. This indicates Halo-mini-G_s binding to these β_2AR preparations. There was no effect of the presence of 25μM Halo-mini-G_s on the affinity of isoprenaline for DIBMALP-β_2AR ($p=0.84$, unpaired t-test). pK_d values for isoprenaline binding DIBMALP-β_2AR were 6.0 ±0.21 in the absence of Halo-mini-G_s and 6.1±0.24 in the presence of 25μM Halo-mini-G_s.

	pK_d F-propranolol	pK_i isoprenaline
Membranes- β_2AR	6.9±0.07	5.3±0.11
Membranes-β_2AR + 25μM Halo-miniG_s	7.0±0.06	7.4±0.27
DDM- β_2AR	7.3±0.01	6.4±0.02
DDM-β_2AR + 25μM Halo-miniG_s	7.3±0.10	8.5±0.38
DIBMALP- β_2AR	7.1±0.22	6.0±0.21
DIBMALP- β_2AR + 25μM Halo-miniG_s	7.3±0.14	6.1±0.24

Table 3.3.3: A summary of the mean pK_d and pK_i values ± SEM for F-propranolol and isoprenaline binding TS-SNAP-β_2AR in mammalian cell membranes, DDM detergent micelles or DIBMALPs in the absence and presence of 25μM Halo-mini-G_s. TR-FRET between Lumi4-Tb and F-propranolol was measured on PHERAstar FSX at room temperature using HTRF module, values are mean of n=3 experiments individually fitted to a one-site specific binding model for F-propranolol, or One-site competition binding for isoprenaline.

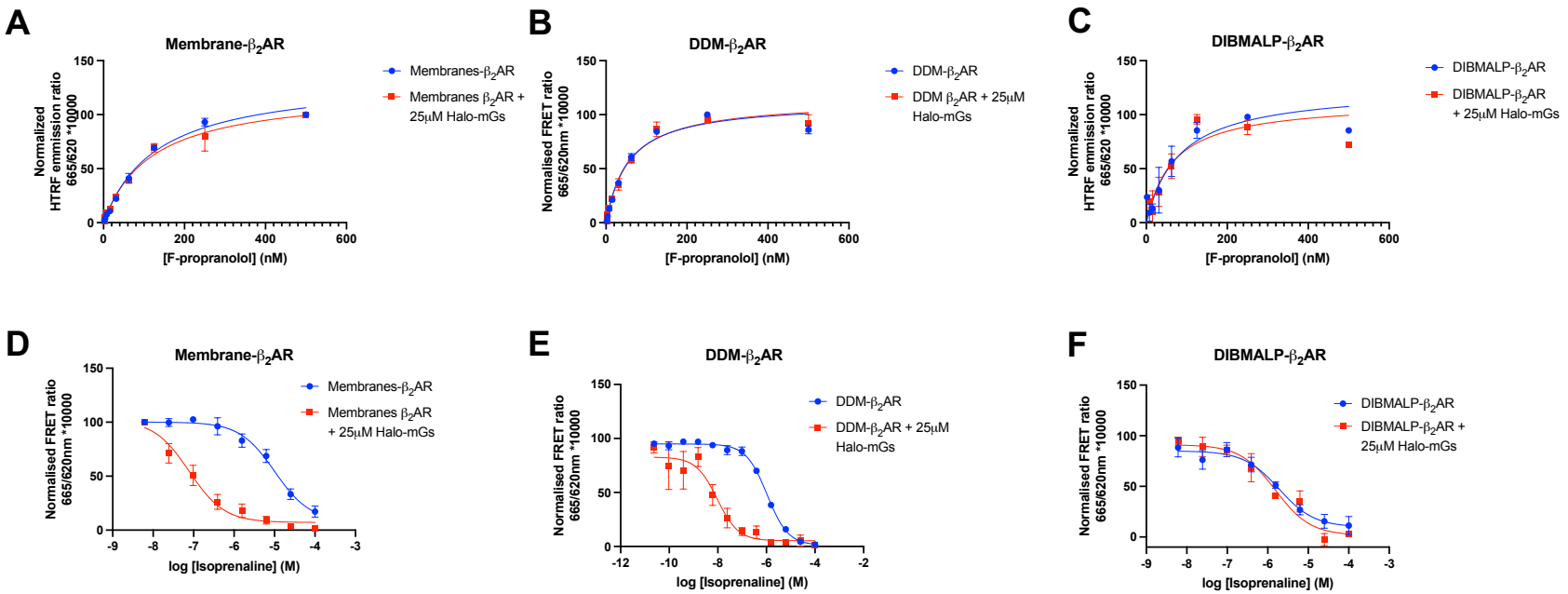

Figure 3.3.8: TR-FRET ligand binding shift studies to investigate the effect the presence of Halo-min-G_s on F-propranolol binding to A) membranes-β_2AR **B)** DDM-β_2AR **C)** DIBMALP-β_2AR and Isoprenaline binding to **D)** Membranes-β_2AR **E)** DDM-β_2AR **F)** DIBMALP-β_2AR**.** All curves show normalized combined data, mean ± SEM, for n=3-4. TR-FRET between Lumi4-Tb and F-propranolol was measured on PHERAstar FSX at room temperature using HTRF module.

3.3.6 TR-FRET ligand binding shift studies to investigate the ability of DIBMALP- A_{2A} to couple Halo-mini-G_s

Following the observation that Halo-mini-G_s bound to membrane-β_2AR and DDM-β_2AR but not DIBMALP-β_2AR, it was possible that this was a specific problem with β_2AR when in the DIBMALP, or a more general effect for class A GPCRs in DIBMALPs or a problem with the assay conditions. To further understand the reason that DIBMALP-β_2AR did not bind Halo-mini-G_s we investigated if DIBMALP-A_{2A} could bind Halo-mini-G_s. To this end F-XAC was used as a tracer to detect binding of the full agonist NECA to membrane-A_{2A} and DIBMALP-$A_{2A.}$ Figure **3.3.9A** shows that, as with F-propranolol binding β_2AR, there was no statistically significant effect of 25μM Halo-mini-Gs protein on F-XAC binding to membrane-A_{2A} or DIBMALP-A_{2A}. The resulting pK_d values are summarised in table **3.3.4.** The pK_d value obtained for F-XAC binding membranes-A_{2A} was 6.11±0.02 compared to 6.18±0.01 in the presence of 25μM Halo-mini-G_s (p=0.059, unpaired t-test).). Similarly, the pK_d value for F-XAC binding DIBMALP-A_{2A} was 6.03±0.06 compared to 6.08±0.02 in the presence of 25μM Halo-mini-G_s (p=0.056). Moreover, as with the β_2AR, the presence of 25μM Halo-mini-G_s caused a 0.5 log unit shift in the affinity of the full agonist NECA for membrane-A_{2A}. These pK_i values were 6.44±0.12 for membrane-A_{2A} and 6.99±0.10 for membrane- A_{2A}+25μM Halo-mini-G_s (p=0.03, unpaired t-test). There was no statistically significant effect of 25μM Halo-mini-G_s on the affinity of NECA for DIBMALP-A_{2A} again showing the Halo-mini-G_s could not bind the DIBMALP-$A_{2A.}$ pK_i values were 5.53±0.05 for DIBMALP-A_{2A} and 5.70±0.08 for DIBMALP-A_{2A} + 25μM Halo-mini-G_s (p=0.15, unpaired t-test).). The difference in affinity of NECA for membranes-A_{2A} (pK_i=6.44±0.12) and DIBMALP-A_{2A} (pK_i=5.53±0.05) was statistically significant 0=0.0038, (unpaired t-test).). This suggests a difference in the conformational landscape of A_{2A} compared to its native membrane state.

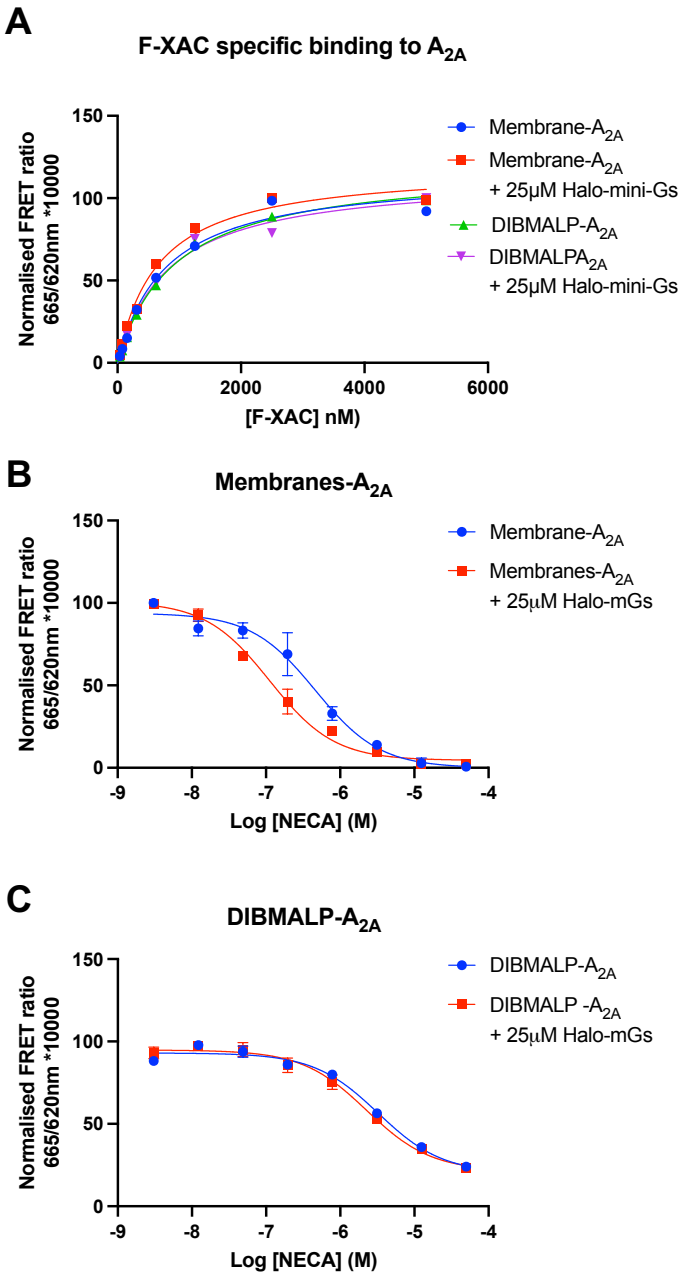

Figure 3.3.9: TR-FRET ligand binding shift studies to investigate Halo-min-G_s binding to membrane and DIBMALP A_{2A} A) F-XAC binding to membranes-A_{2A} and DIBMALP-A_{2A} in the absence and presence of 25μM Halo-mini-G_s **B)** NECA binding to membranes-A_{2A} in the absence and presence of 25μM Halo-mini-G_s, **C)** NECA binding to DIBMALP-A_{2A} in the absence and presence of 25μM Halo-mini-G_s. All curves show normalized combined data, mean ± SEM, for n=2 for F-XAC and n=3 for NECA, TR-FRET between Lumi4-Tb and F-XAC was measured on PHERAstar FSX at room temperature using HTRF module.

	pK_d F-XAC	pK_i NECA
Membranes- A_{2A}	6.11±0.02	6.44±0.12
Membranes-A_{2A} + 25μM Halo-miniG_s	6.18±0.01	6.99±0.10
DIBMALP- A_{2A}	6.03±0.06	5.53±0.05
DIBMALP- A_{2A} + 25μM Halo-miniG_s	6.08±0.02	5.70±0.08

Table 3.3.4 A summary of the mean pK_d and pK_i values ± SEM for F-XAC and NECA binding A_{2A} in mammalian cell membranes, or DIBMALPs in the absence and presence of 25μM Halo-mini-G_s. TR-FRET between Lumi4-Tb and F-XAC was measured on PHERAstar FSX at room temperature using TRF module, values are mean of n=3 experiments individually fitted to a one-site specific binding model for F-XAC, or One-site competition binding for NECA.

3.4. Discussion

The β_2AR has become the prototypical GPCR for studies into GPCR activation be it structural, functional, or biophysical studies (Bang & Choi, 2015)(Gregorio et al., 2017). Structural and biophysical studies all require the extraction of the β_2AR from the plasma membrane, as such the above studies have employed use of the detergent DDM. Detergents do not recapitulate the complexity of the native membrane environment and so the stability of membrane proteins within the detergent micelle is often compromised. Alternative approaches have included use of synthetic nanodiscs and thermostabilizing mutations. Here, the applicability of the polymer DIBMA to extract the β_2AR was investigated.

3.4.1 DIBMA can extract β_2AR from the mammalian cell membrane

This study showed it was possible to extract the β_2AR from mammalian cell membranes using DIBMA although solubilization efficiency for DIBMA (32±7%) was dramatically lower that of the conventional detergent DDM (90±11%). It was possible to find one other study examining solubilisation efficiency by DIBMA; Gulamhussein and colleagues (Gulamhussein et al., 2020) show a similar solubilisation efficiency of approximately 30% to extract the ABC transporter BmrA from *E. coli*. Additionally, they show it was possible to extract the A_{2A} receptor from yeast membranes using DIBMA, which supports the findings of this study. Whilst low solubilisation efficiency may decrease purification yields and make structural studies unfeasible this lower yield was not problematic for this study. Furthermore, FSEC analysis suggested that although DIBMA yield was lower a lesser proportion of it was aggregated than that of the DDM preparation.

3.4.2 DIBMALP-β_2AR retains ligand binding capabilities

To investigate if the β_2AR remained functional in the DIBMALP ligand binding ability was assessed using a TR-FRET ligand binding assay. Saturation TR-FRET binding data showed F-propranolol binding to DIBMALP-β_2AR, therefore indicating that the β_2AR was functional. The

pK_d value (7.0±0.13) for F-propranolol binding DIBMALP-β_2AR was comparable to that of membrane-β_2AR (7.5±0.05) and DDM- β_2AR (7.10 ± 0.08). Although the difference in pK_d values for F-propranolol binding DIBMALP-β_2AR was statistically different (p=0.02) from that of membranes-β_2AR this is only 3-fold which is not a large difference.

While the pK_d values for different preparations of the receptor were comparable, the signal amplitude obtained for F-propranolol binding DIBMALP-β_2AR in TR-FRET experiments was 3-fold lower than for membranes-β_2AR. This reduction in signal amplitude could be due to an effect of the DIBMA polymer on the TR-FRET, for example fluorescence quenching. Alternatively, it could reflect that a lower fraction of the β_2AR receptors have retained ligand binding capabilities.

However, it should be noted that the assay window for DDM-β_2AR was higher than that of membranes whilst it would be expected that less β_2AR is functional, suggesting that the solubilization environment can influence the observed signal amplitude. Whilst the concentration of β_2AR used in each experimental condition was quantified using 620nm emission of Lumi4-Tb, it was not possible to account for difference in Lumi4-Tb quantum yield in the membrane, DDM and DIBMALP environments.

3.4.3 DIBMALP-β_2AR retains native pharmacology and conformational landscape

Next, the conformational landscape of DIBMALP-β_2AR was investigated using an equilibrium TR-FRET competition binding assay. To ascertain the relative populations of active and inactive conformations of the β_2AR in the DDM, DIBMALP or membrane environment the affinity of the agonist isoprenaline, the antagonist propranolol and the inverse agonist ICI 118,551 was investigated. A dramatic increase or decrease in the affinity (pK_i) of any of these ligands for any of the β_2AR preparations would indicate a respective increase or decrease in the proportion of the population of receptors in the conformational state

stabilised by the relevant ligand and hence a difference in the conformational landscape of the β_2AR. There is evidence that the conformational flexibility of the rhodopsin and A_{2A}R within SMALPs is restricted (Mosslehy et al. 2019) (Routledge et al., 2020). Interestingly, this study also found that the affinity of DIBMALP-A_{2A} for the full agonist NECA was reduced compared to its native membrane state suggesting DIBMA restricts the conformational changes of the full active state of A_{2A} as Routledge and colleagues showed was the case of A_{2A} in SMALPs (Routledge et al., 2020).

Competition TR-FRET ligand binding studies showed comparable pK_i values for propranolol and ICI 118, 511 in membrane-β_2AR, DDM-β_2AR and DIBMALP-β_2AR, and for isoprenaline in membrane-β_2AR and DIBMALP-β_2AR. This suggests that the β_2AR remains in its native conformational state inside the DIBMALP. The difference in pK_i value between DDM-β_2AR (6.3±0.13) and membrane-β_2AR (5.5±0.2) for isoprenaline was statistically significant ($p=0.03$), this may indicate a change in the conformational state of β_2AR in the DDM micelle compared to its native conformational state. Propranolol, ICI 118, 551 and isoprenaline pK_i values obtained in this study are in line with the previous studies that investigate the affinity of these compounds for the β_2AR (Baker, 2005) (Sykes et al., 2014a). All ligand binding curves showed one phase binding and a slope of 1 indicating no co-operativity of ligand binding.

3.4.4 DIBMALP-β2AR shows improved thermostability

The next aim of this study was to investigate the thermostability of the DIBMALP-β_2AR. This was explored using novel TR-FRET thermostability assays. The key finding was that DIBMALP-β_2AR showed a 10^{o}C increase in thermostability compared to DDM-β_2AR. It was not possible to find any thermostability data for the β_2AR in synthetic nanodiscs; however, the only other method to show a similar (11^{o}C) increase in thermostability for β_2AR is that of thermostabilizing mutations

(Serrano-Vega & Tate, 2009b). Since these mutations also lead to a shift in the β_2AR's conformational landscape to the antagonist-bound and inactive form, the DIBMALP-β_2AR offers a clear advantage for study of β_2AR function.

This study also found that there was no ligand induced shifts in the ThermoFRET curve of DIBMALP-β_2AR suggesting the thermostability curve of DIBMALP-β_2AR and T_m of 46.8±2.1^{o}C corresponded to disruption of the protein-lipid-polymer particles as opposed to the β_2AR itself. This conclusion was also supported by the Tm value of 44.8±0.7^{o}C obtained for DIBMALP-A_{2A} not being statistically significantly different from that of the DIBMALP-β_2AR. We also noted a shallower slope for DIBMALP-β_2AR (-3.2) compared to DDM-β_2AR (-2.7), this broader transition may reflect the more heterogenous nature of DIBMALPs compared to the detergent micelle. The T_m values obtained for DIBMALP encapulsated β_2AR and A_{2A} in this study are similar to that of 51.4±0.8^{o}C obtained for DIBMALP encapulsated Rho by Grime and colleagues (Grime et al., 2021).

3.4.5 DIBMALP-β_2AR cannot couple Halo-mini-G_s

Lastly, this study investigated if the DIBMALP-β_2AR could couple the Halo-mini-G_s proteins produced in chapter 5 in response to agonist stimulation. Mini-G_s proteins are the engineered GTPase domain of the α subunit of the G protein, they act as conformational sensors for the active state of the GPCR. This study used the TR-FRET competition binding assay to detect Halo-mini-G_s binding by shifts in agonist affinity for the receptor. Using this method, we were able to detect halo-mini-G_s binding to the TS-SNAP-β_2AR in membranes and DDM but not DIBMALPs. Similarly, we were able to detect Halo-mini-G_s binding TS-SNAP-A_{2A} in membranes but not DIBMALPs. It is not known why it was not possible to detect Halo-mini-G_s binding to DIBMALP-β_2AR or DIBMALP-A_{2A} although clearly the assay was able to detect binding of halo-mini-G_s to the other preparations. It could be that both the A_{2A}R and β_2AR are conformationally restricted in DIBMALPs or the free polymer or

non-receptor containing DIBMALPs or something else interfere with the preparation interfere with the assay. However, removing the free polymer by dialysis did not affect the result. Moreover, it was not possible to purify enough DIBMALP-GPCR to complete the assay with purified material. It was not possible to find any other studies showing G protein or mini-G coupling to a GPCR encapsulated in a DIBMALP. However, Logez and colleagues (Logez et al., 2016) show arrestin and G protein recruitment to purified SMALP-MT1.

3.4.6 Conclusion

Overall, this study shows that the polymer DIBMA can be used to extract the human β_2AR from the plasma membrane. This study showed that this method offers improved stability over the use of the conventional detergent DDM. Moreover, this study shows both DDM-β_2AR and DIBMALP-β_2AR maintain their native pharmacology and conformational landscape however only DDM-β_2AR was shown to be able to couple mini-G_s. Based on these conclusions the conventional detergent DDM was chosen as the best method to extract the β_2AR. Future work would investigate why DIBMALP-β_2AR would not couple mini-G_s in this study.

Chapter 4
Pharmacological characterisation of eight agonists for the β_2AR

4.1 Introduction

The hypothesis underlying this study was that differences in the kinetics of agonist-β_2AR-G_s protein complex formation underly differences in agonist efficacy at the β_2AR. Investigation of this hypothesis required a range of fully pharmacologically characterised agonists of varying ligand binding and efficacy profiles. To this end this study chose eight β_2AR agonists from the literature based on their published ligand binding kinetics and efficacies and fully characterised their pharmacology in our own systems.

4.1.1 The eight β_2AR agonists chosen for this study

Table **4.1.1** summarises pharmacological properties of the eight β_2AR agonists from published literature chosen for this study. These data were taken from different studies (Baker, 2005)(Rasmussen, et al., 2011a) (Rosethorne et al., 2016) (Sykes et al., 2014) and systems.

Taken together these data predict these compounds to have a range of residence times at the β_2AR, for example isoprenaline, salbutamol, and formoterol, are predicted to have short residence times and C26 to have a very long residence time. These data also suggest salbutamol and salmeterol to be partial agonists, whilst formoterol, adrenaline and isoprenaline are full agonists and C26 is a super agonist. Overall, these synthetic ligands were chosen for this study because of their range of kinetic and efficacy values, adrenaline and noradrenaline were chosen based on this and being endogenous ligands for the β_2AR. Despite these published studies characterising these compounds, this study chose to characterise the ligand binding kinetics of these compounds so that these parameters could be obtained for all ligands in one data set and whilst the β_2AR was in the DDM micelle. The β_2AR was solubilised in DDM in this and other chapters in our study to isolate it from the regulation of the cell. Moreover, this study also specifically aimed to characterise the efficacy of these compounds to activate the heterotrimeric G_s protein, as opposed to cAMP. Efficacy of these

compounds to activate the heterotrimeric G_s protein is the most relevant system to compare to the mini-G_s kinetic data obtained in chapter **5.**

β_2AR agonist	pK_d	cAMP pEC$_{50}$	cAMP E_{max} (% of Isoprenaline)	K_{off} (Min^{-1})	K_{on} ($Mol^{-1}Min^{-1}$)
Adrenaline	6.13 ±0.05 (Baker, 2005)	7.93 ±0.07 (Baker, 2005)	101% (Baker, 2005)	-	-
Isoprenaline	6.64 ±0.09 (Baker, 2005)	8.22 ±0.11 (Baker, 2005)	100% (Baker, 2005)	3.06 ±1.53 (Sykes et al., 2014b)	2.47±1.39 X10^7 (Sykes et al., 2014b)
Salbutamol	6.01 ±0.01 (Baker, 2005)	7.72 ±0.07 (Baker, 2005)	95.8% (Baker, 2005)	4.06 ±1.19 (Sykes et al., 2014b)	2.05±1.03 X10^7 (Sykes et al., 2014b)
BI 167-107	9.07 (Rasmussen, et al., 2011b)	10.3 (Rasmussen, et al., 2011b)	100% (Rasmussen, et al., 2011b)	-	-
Noradrenaline	5.41 ±0.07 (Baker, 2005)	6.36 ±0.04 (Baker, 2005)	103% (Baker, 2005)	-	-
Formoterol	7.77 ±0.01 (Sykes et al., 2014b)	8.29 ±0.08 (Baker, 2005)	111% (Baker, 2005)	3.00 ±0.38 (Sykes et al., 2014b)	1.78±0.21 X10^8 (Sykes et al., 2014b)
Salmeterol	9.26 ±0.06 (Baker, 2005)	9.89 ±0.08 (Baker, 2005)	94% (Baker, 2005)	1.16 ±0.16 (Sykes et al., 2014b)	3.50±0.57 X10^9 (Sykes et al., 2014b)
C26	9.78 (Rosethorne et al., 2016)	10.2 ±0.07 (Rosethorne et al., 2016)	117% (Rosethorne et al., 2016)	0.02 ±0.003 (Rosethorne et al., 2016)	3.70±0.47 X10^8 (Rosethorne et al., 2016)

Table 4.1.1: A summary of ligand binding affinity, kinetics and potency values obtained from literature for the eight β_2AR agonists selected in this study.

4.1.2 Use of TR-FRET to measure ligand binding kinetics

Traditionally, radiolabelled ligands have been used to investigate ligand binding to a receptor of interest. Aside from the problems associated with cost and radiation disposal and exposure, the practicalities of radioligand binding do not allow for the kinetic resolution required to study the kinetics of many ligands. Radioligand binding assays require a separate sample for each time point as the assay is not homogenous and requires the separation of bound and free. Conversely, more recently developed, and homogenous, TR-FRET ligand binding assays can be continuously read from the same well for up to 5 second time cycles (Sykes et al., 2019). The principles of TR-FRET are discussed in more detail in sec **2.2.8**. Ease and greatly improved kinetic resolution were the main reasons for choosing TR-FRET technology as opposed to radioligand binding assays.

4.1.3 Defining efficacy using a G_s protein activation assay

Classically, radiolabelled GTPγS has been used to quantify G protein turnover by GPCRs in cell membranes. Although a sensitive method, this assay has high background and is difficult to apply in whole cells or measure kinetically.

More recently, FRET and BRET based biosensors for G protein activation have been developed. Such methods are much easier to apply kinetically and in live cell system. Moreover, since their initial use, a great deal of work into identification of optimal labelling sites has taken place to improve G protein biosensor sensitivity (Yu & Rasenick, 2002). BRET sensors are generally advantageous over FRET sensors due to their increased sensitivity and elimination of the photobleaching associated with FRET.

Generally, use of G protein biosensors in cellular assays involves the simultaneous transfection of the 3 G protein subunits (Galés et al., 2006). This approach can prove a difficult step in assay optimisation as multiple transfections can lead to variability in expression between cells, absence of all proteins in some cells will clearly decrease assay sensitivity. To overcome this, Schihada and colleagues (Schihada et al., 2021), recently generated multicistronic vectors for common G protein heterotrimer biosensors, therefore allowing the simultaneous expression of the three G protein subunits from a single vector. They show improved sensitivity compared to other G protein biosensors, and use of the heterotrimeric G_s protein biosensor (CASE G_s) to detect G_s protein activation by the β_2AR in response to isoprenaline. The CASE G_s protein biosensor is summarised in figure **4.1.1.** This study chose to use the CASE G_s protein biosensor to investigate and quantify G_s protein activation by the eight β_2AR agonists described in sec **4.1.1.**

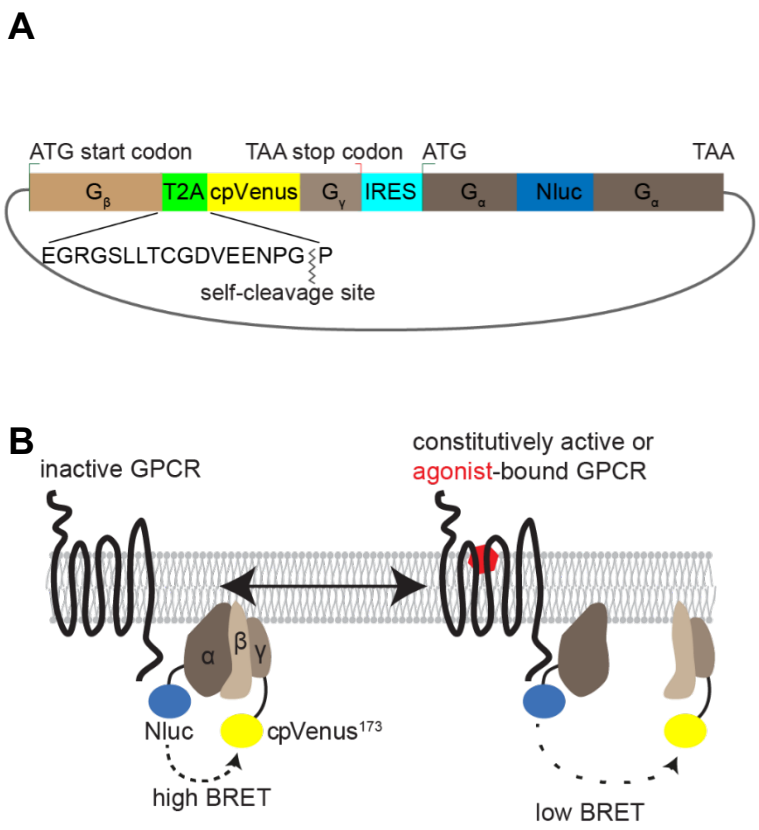

Figure 4.1.1: A summary of the CASE G_s biosensor used in this study A) A summary of the vectors design of CASE G_s: β1 and venus-γ1 were separated by a T2A element venus-γ1 from $G\alpha s_{short}$ by an IRES element, nLuc is inserted between N136 and V137 of $G\alpha s_{short}$. **B)** Activation of the CASE G_s biosensor is indicated by a decrease in BRET as venus-γ1 dissociates from $G\alpha s_{short}$nLuc following activation. Figure adapted from (Schihada et al., 2021).

4.1.4 Aims:

The purpose of this study was to characterise the pharmacology of eight agonists for the β_2AR, to this end this study aimed to:

1. To characterise the ligand binding kinetics and affinity of eight β_2AR agonists for the DDM solubilised β_2AR

2. To measure the ability of eight β_2AR agonists to activate the G_s protein

3. To investigate the correlation between ligand residence time and G_s protein activation efficacy.

4.2 Methods

4.2.1 TR-FRET ligand binding assays

Optimisation of the kinetic TR-FRET ligand binding assay was performed on Lumi4-Tb labelled TS-SNAP-β_2AR in membranes due to ease and COVID-19 time restrictions. TS-SNAP-β_2AR was labelled in mammalian T-REx^{TM}-293 cells and membranes prepared as described in sec **2.2.6**. For final competition kinetics studies of the eight cold agonist; adrenaline, noradrenaline, isoprenaline, formoterol, salbutamol, salmeterol, BI-167-107 and C26 the TS-SNAP-β_2AR was solubilised n the detergent DDM as described in sec **2.2.6.**

Kinetic ligand binding studies were run in white 384 well plates. CA200693 (S)-propranolol-green and unlabelled ligand dilutions were added to plate, and plate placed into PHERAstar FSX plate reader. TS-SNAP-β_2AR was added online using in-build PHERAstar FSX injectors. Binding between CA200693 (S)-propranolol-green and lumi4-Tb was read immediately using two laser flashes per cycle and 520/620 TRF module. 3μM alprenolol was used to define the non-specific binding. Kinetic ligand binding studies are fully described in sec **2.2.13.**

4.2.2 CASE-G_s activation assays

CASE-G_s activation assays to measure G_s protein activation were performed in HEK 293T/17 cells that had been transiently transfected, T-REx^{TM}-293 cells stably expressing TS-SNAP-β_2AR or T-REx^{TM}-293 cells stably expressing both TS-SNAP-β_2AR and CASE G_s. All cell lines were adherent in white 96 well plates, all cell culture and transfections took place as described in sec **2.2.2.** Various concentrations and induction times were used to control TS-SNAP-β_2AR expression as shown.

For CASE G_s BRET assays cells were incubated with furimazine for 20min prior to assay. BRET between Gαs-nLuc and γ-venus was read

using PHERAstar FSX using 550LP/450-60nm luminescence module. Plates were read for 3 min prior to addition of agonists, and then for a further 20min. CASE-G_s assays are fully described in **sec 2.2.4.**

4.3 Results

4.3.1 Development of a TR-FRET ligand binding kinetics assay

The first aim of this study was to measure the ligand binding affinities and kinetics of eight β_2AR agonists for the DDM-TS-SNAP-β_2AR. To this end, a TR-FRET ligand binding kinetic assay was developed on membranes from HEK cells expressing TS-SNAP-β_2AR which had been labelled with Lumi4-Tb. Firstly, it was necessary to assess the best fluorescently labelled antagonist to use as a tracer for these assays. Figure **4.3.1** shows the association (**4.3.1A-B**) and saturation binding plots (**4.1C**) of two different fluorescent variants of propranolol; CA200693(-S)-propranolol-green and CA200689(s)-propranolol-red to membranes expressing TS-SNAP-β_2AR labelled with Lumi4-Tb. Figure **4.3.1A-B** shows that, using 2 laser flashes per cycle, TR-FRET between Lumi4-Tb and CA200693 (-S)-propranolol-green and could be read for 30 min without a decrease in TR-FRET signal due to photobleaching (Figure **4.3.1A)**. In contrast CA200689 (s)-propranolol-red (Figure **4.3.1B**) showed photobleaching after 20min.

K_{on}, K_{off} and K_d values for these experiments are summarised in table **4.3.1**. The K_{on} value of 1.57 ± 0.92 x 10^7 Mol^{-1} Min^{-1} for CA200693(-S)-propranolol-green was not statistically significantly different to that of 5.69 ±3.4x 10^6 Mol^{-1} Min^{-1} obtained for CA200689 (s)-propranolol-red (p=0.28, unpaired t-test). Neither was there any statistically significant difference between pK_d obtained from kinetic association fits, these were 8.09 ±0.15 for CA200693(-S)-propranolol-green and 7.36±0.27 CA200689 (s)-propranolol-red (p=0.07, unpaired t-test). The K_{off} values for these compounds were also similar, these were 0.12 ±0.03 Min^{-1} and 0.22±0.01 Min^{-1} for CA200693(-S)-propranolol-green and CA200689 (s)-propranolol-red respectively (p=0.047, unpaired t-test).

Based on these experiments CA200693(-S)-propranolol-green was chosen as the best tracer for TR-FRET ligand binding kinetic

experiments as there was no significant differences in kinetics or affinity values between these two compounds but there was photobleaching of CA200689 (s)-propranolol-red over the time course relevant to these experiments.

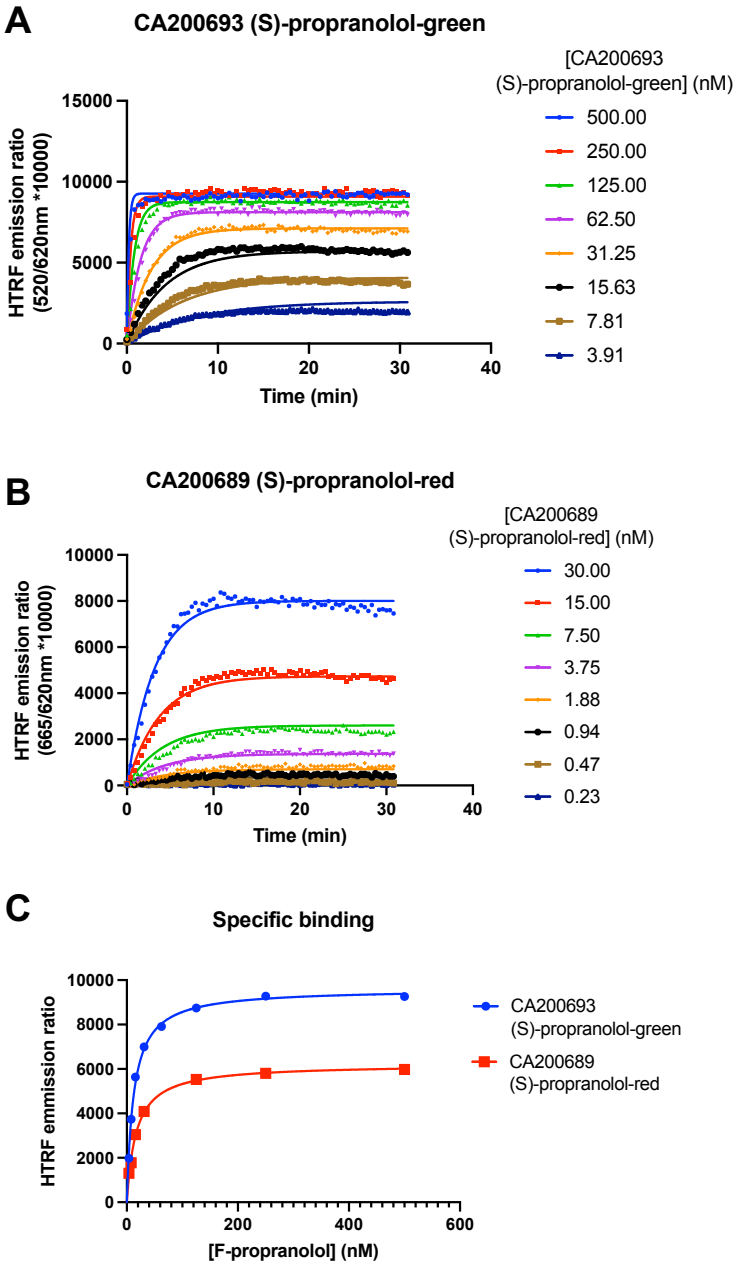

Figure 4.3.1: Characterisation of the ligand binding kinetics of commercially available fluorescent propranolol compounds in Lumi4-Tb labelled TS-SNAP-β_2AR membranes using TR-FRET. **A)** Specific binding for the association varying concentrations of CA200693 (S)-propranolol-green to Lumi4-Tb labelled TS-SNAP-β_2AR membranes **B)** Specific binding for the association of varying concentrations of CA200689-(s)-propranolol-red to Lumi4-Tb labelled TS-SNAP-β_2AR membranes **C)** Specific saturation binding for varying concentrations of CA200693 (S)-propranolol-green or CA200689 (s)-propranolol-red to Lumi4-Tb labelled TS-SNAP-β_2AR membranes at 30min time point. TR-FRET between Lumi4-Tb and CA200693 (S)-propranolol-green or

CA200689-(s)-propranolol-red was read on PHERAstar FSX using 2 laser flashes per cycle and 520/620 TRF or HTRF modules respectively. All graphs show representative data of n=2 experiments.

	K_{on} (Mol^{-1} Min^{-1})	K_{off} (Min^{-1})	Kinetic pK_d	Equilibrium pK_d
CA200693(-S)-propranolol-green	1.57 ± 0.92 x 10^7	0.12 ±0.03	8.09 ±0.15	8.03 ±0.16
CA200689(-S)-propranolol-red	5.69 ±3.4 x 10^6	0.22 ±0.01	7.36 ±0.27	7.66 ±0.16

Table 4.3.1: A summary of the mean K_{on}, K_{off} and K_d values for fluorescent propranolol variants CA200693(-S)-propranolol-green and CA200689(-S)-propranolol-red binding Lumi4-Tb labelled TS-SNAP-β_2AR membranes. TR-FRET between Lumi4-Tb and CA200693 (S)-propranolol-green or CA200689 (s)-propranolol-red was read on PHERAstar FSX using 2 laser flashes per cycle and 520/620 TRF or HTRF modules respectively**.** Values show mean of n=2 experiments ±SD.

Next, this study investigated the best concentration of the tracer CA200693 (S)-propranolol-green to use in kinetic competition assays with the eight unlabelled β_2AR ligands. An increased concentration of tracer will associate to the receptor faster, therefore affecting the kinetic resolution of the assay. 1x K_d, or 15nM, 3x K_d or 45nM, and 5x K_d or 75nM concentrations of CA200693 (S)-propranolol-green were trialled in kinetic competition assays with varying concentrations of formoterol and isoprenaline (Figure **4.3.2).** Formoterol and isoprenaline were chosen for these experiments because, based on literature they were expected to represent medium and fast K_{off} compounds. Kinetic competition binding data shown in figure **4.3.2** was fitted to the Motulsky-Mahan model and the ligand binding parameters obtained for each compound at each concentration of CA200693 (S)-propranolol-green are summarised in table **4.3.2.** These data show that although the Motulsky-Mahan model fitted well to both compounds at all tracer concentrations (Figure **4.3.2**), feasible K_{on} and K_{off} values could only be obtained for formoterol and not for isoprenaline (Table **4.3.2**). K_{on} and K_{off} values obtained for formoterol at 45nM ($2.8\pm1.6\times10^8$ Mol^{-1} Min^{-1} and 4.2 ± 2.9 Min^{-1} respectively) and 75nM ($3.1\pm1.8\times10^7$ Mol^{-1} Min^{-1} and 1.0 ± 0.4 Min^{-1} respectively) tracer were not statistically significantly different (unpaired t-test).

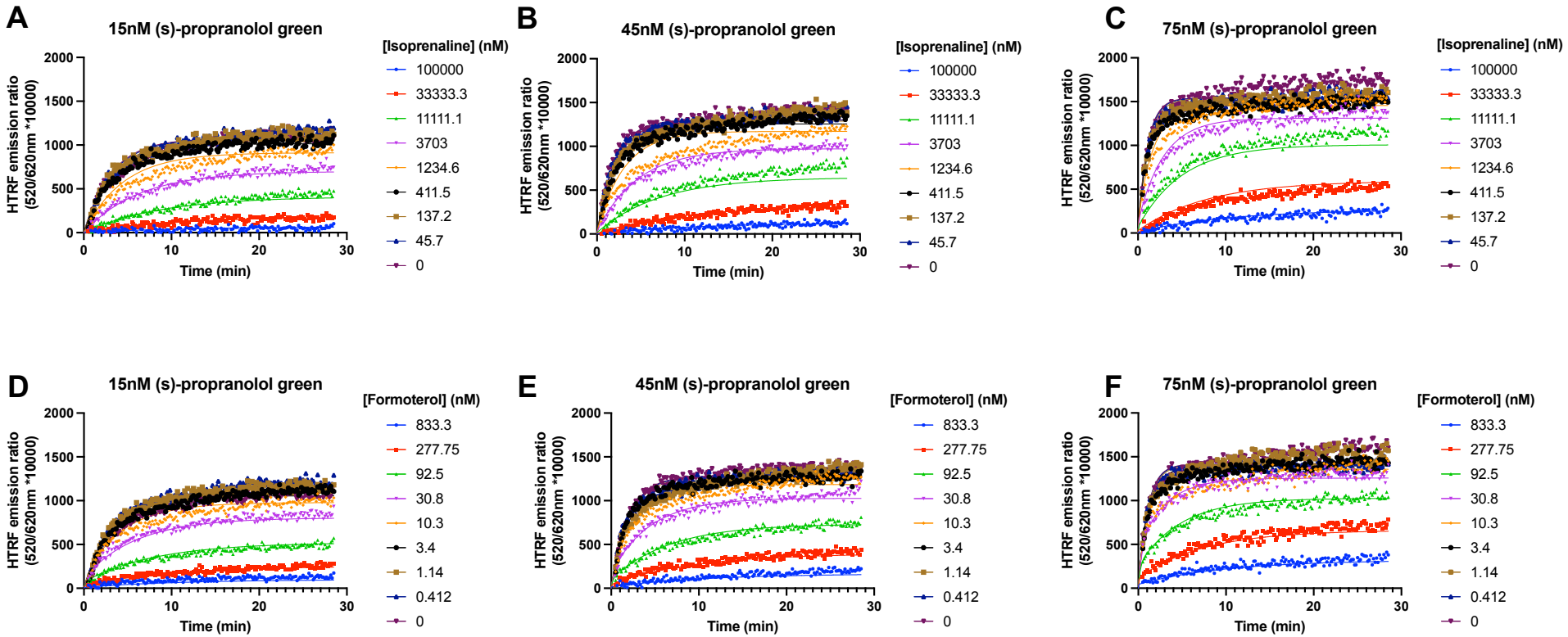

Figure 4.3.2: Trial and optimisation of CA200693-(S)-propranolol-green concentration for kinetic competition binding experiments: 15nM, 45nM and 75nM of CA200693-(S)-propranolol-green were trialled with varying concentrations of Isoprenaline **A-C)** or formoterol **D-F),** Lumi4-Tb labelled TS-SNAP-β_2AR membranes, TR-FRET between Lumi4-Tb and CA200693 (S)-propranolol-green PHERAstar FSX using 2 laser flashes per cycle and 520/620 TRF module, **A-F** shows representative data of n=2-3.

Ligand	CA200693(-S)-propranolol-green	K_{on} (Mol^{-1} Min^{-1})	K_{off} (Min^{-1})	Kinetic K_d
Isoprenaline	15nM	>6 x$10^{10\$}$	>6 x$10^{10\$}$	N/A
	45nM	>6 x10^{10}	>6 x10^{10}	N/A
	75nM	>6 x10^{10}	>6 x10^{10}	N/A
Formoterol	45nM	2.8±1.6 x10^{8}	4.2±2.9	7.8
	75nM	3.1±1.8 x10^{7}	1.0±0.4	7.5

Table 4.3.2: A summary of the kinetic ligand binding parameters obtained for isoprenaline and formoterol using 15nM, 45nM or 75nM CA200693 (S)-propranolol-green as the tracer for kinetic competition binding experiments on Lumi4-Tb labelled TS-SNAP-β_2AR in membranes. TR-FRET between Lumi4-Tb and CA200693 (S)-propranolol-green PHERAstar FSX using 2 laser flashes per cycle and 520/620 TRF module. Values are mean of n=3 ±SEM or $^{\$}$ denotes n=2.

4.3.2 Measurement of the ligand binding kinetics of eight β_2AR agonists

Following the optimisation of a TR-FRET kinetic ligand binding assay using Lumi4-Tb labelled TS-SNAP-β_2AR in membranes, this assay was used to investigate the ligand binding kinetics of formoterol, isoprenaline, adrenaline, noradrenaline, salmeterol, salbutamol, BI-167-107 and C26 binding DDM-TS-SNAP-β_2AR. Specific binding for a representative replicate of these experiments is shown in figure **4.3.3**. Using this assay and fitting the results to the Motulsky-Mahan model enabled k_{on} and k_{off} rates for formoterol, salmeterol, C26 and BI-167-107 to be obtained. These results (summarised in table **4.3.3)** show that salmeterol had the fastest K_{on} of the compounds measured, (1.35 ± 0.45 x10^8 Mol $^{-1}$ Min^{-1}) which was significantly faster than those obtained for formoterol (2.6 ± 0.43 x10^7 Mol $^{-1}$ Min^{-1}), C26 (1.06 ± 0.05 x10^7 Mol $^{-1}$ Min^{-1}) and BI-167-107 (2.6 3± 0.15 x10^6 Mol $^{-1}$ Min^{-1}) (P=0.021, One-way ANOVA and tukey's posthoc). There were no other statistically significant differences in the K_{on} values of these four compounds. Table **4.3.3** also shows that formoterol had the fastest K_{off} at 0.47 ± 0.08 Min^{-1}. This was statistically significantly faster than that of salmeterol (0.13±0.03 Min^{-1}), C26 (0.005±0.001 Min^{-1}) and BI-167-107 (0.0021±0.001 Min^{-1}) (One-way ANOVA and tukey's posthoc). There were no other statistically significant differences in the K_{off} values of these four compounds.

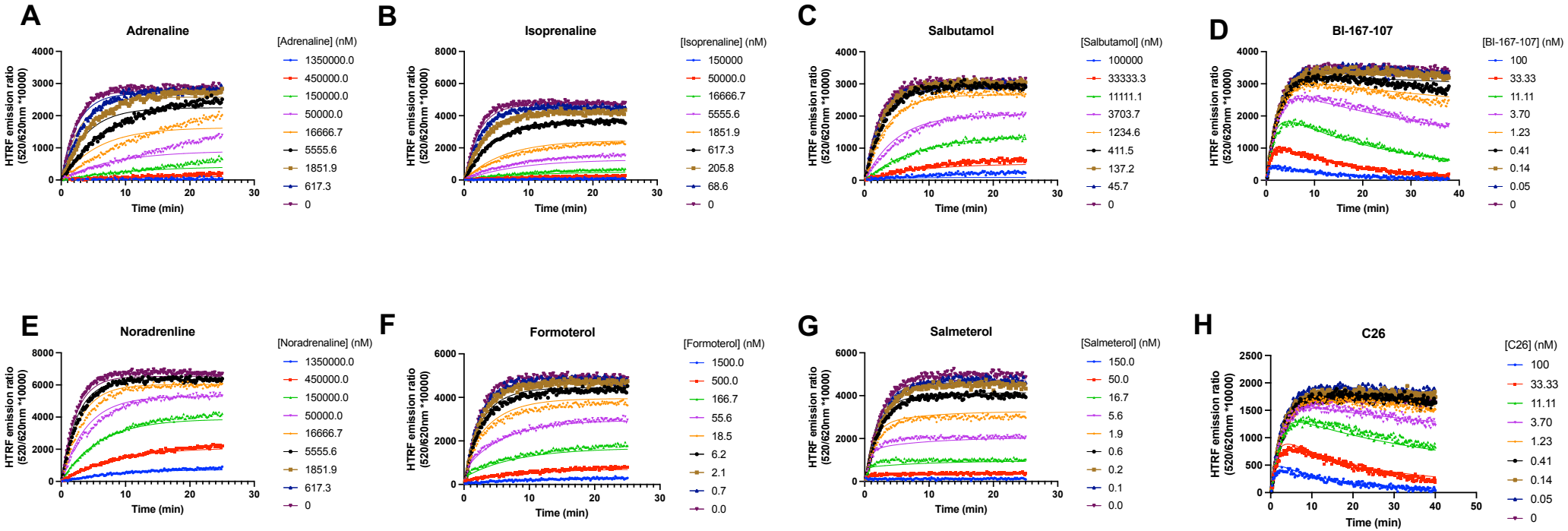

4.3.3: TR-FRET competition kinetic binding studies for A) Adrenaline B) Isoprenaline C) Salbutamol, D) BI-167-107, E) Noradrenaline, F) Formoterol G) Salmeterol, H) C26 on DDM-TS-SNAP-β_2AR using 75nM CA200693 (S)-propranolol-green. TR-FRET between Lumi4-Tb and CA200693 (S)-propranolol-green PHERAstar FSX using 2 laser flashes per cycle and 520/620 TRF module. Data are representative of n=3, fitted to Motulsky-Mahan model for kinetic competition binding.

	K_{on} (Mol^{-1} Min^{-1})	K_{off} (Min^{-1})	Residence time (Min)	pK_d (From k_{off}/k_{on})
CA200693(-S)-propranolol-green	4.09±0.9 x10^6	0.08 ± 0.009	12.2	7.7 ± 0.04
Formoterol	2.6 ± 0.43 x10^7	0.47 ±0.08	2.1	7.8 ±0.05
Salmeterol	1.35 ± 0.45 x10^8	0.13 ± 0.03	7.89	9.0 ±0.0005
C26	1.06 ± 0.05 x10^7	0.005 ± 0.001	189	9.3 ±0.13
BI-167-107	2.6 3± 0.15 x10^6	0.0021 ± 0.001	480	10.3 ±0.27

Table 4.3.3: A summary of the kinetics ligand binding parameters obtained from TR-FRET ligand binding studies of formoterol, salmeterol, C26 and BI-167-107 on Lumi4-Tb labelled DDM-TS-SNAP-β_2AR using 75nM CA200693 (S)-propranolol-green. TR-FRET between Lumi4-Tb and CA200693 (S)-propranolol-green PHERAstar FSX using 2 laser flashes per cycle and 520/620 TRF module. Data show mean of n=3 experiments ±SEM.

4.3.3 Equilibrium competition binding of eight β_2AR agonist

To obtain equilibrium pK_i values for the eight β_2AR agonists at DDM TS-SNAP-β_2AR, specific competition binding curves were fitted to a one-site model at the 40 min time point for C26 and BI-167-107 and 20 min for all other compounds (Figure **4.3.4).** Mean pK_i values are summarised in table **4.3.4.** pK_i affinity values ranged from 4.4±0.09 for noradrenaline to 9.2±0.08 for BI-167-107.

pK_i values obtained from equilibrium competition curve fits for the four compounds for which K_{on} and K_{off} values were obtained were generally similar to the pK_d values calculated from K_{off} and K_{on} (Table **4.3.3**). These were pK_i=7.8±0.07 Vs pK_d 7.8±0.05 (p=0.49) for formoterol, pK_i =8.7 ± 0.03 Vs pK_d 9.3 ± 0.13 (p=0.01) for C26, pK_i = 9.2 ±0.08 Vs pK_d 10.3± 0.27 (p=0.02) for BI-167-107 and pK_i = 9.1±0.08 Vs pK_d =9.0 ±0.0005 (p=0.04) for salmeterol. Statistical comparison of pK_i Vs pK_d values for each compound was made using an unpaired t-test.

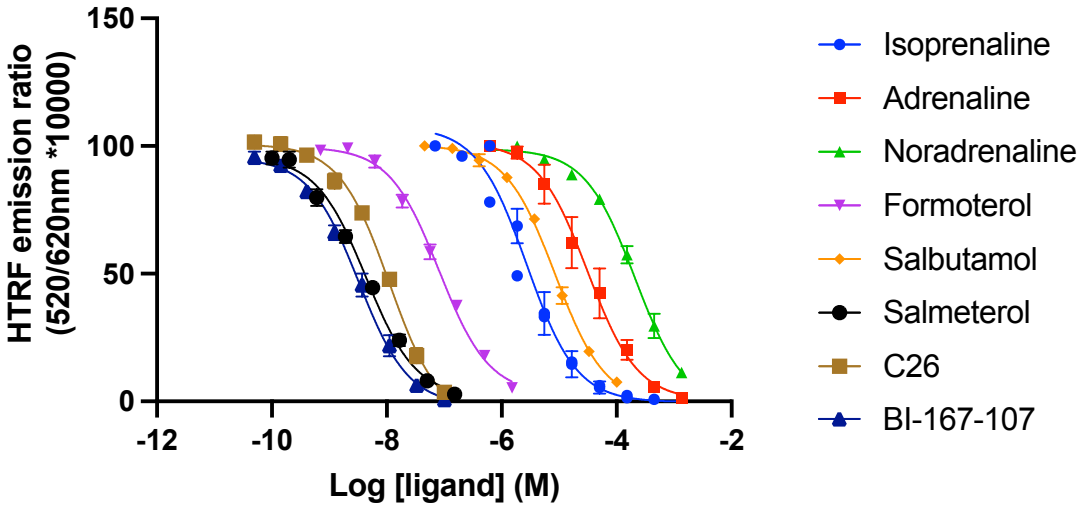

Figure 4.3.4: Equilibrium competition binding studies for isoprenaline, adrenaline, noradrenaline, formoterol, salbutamol, salmeterol, C26, BI-167-107 binding Lumi4-Tb labelled DDM-TS-SNAP-β_2AR, using 75nM CA200693 (S)-propranolol-green. Equilibrium measure measurements were read at 20 min post DDM-TS-SNAP-β_2AR addition for all compounds except C26 and BI-167-107 which were read at 40 min. TR-FRET between Lumi4-Tb and CA200693 (S)-propranolol-green PHERAstar FSX using 2 laser flashes per cycle and 520/620 TRF module. Data points show mean of n=3 experiments normalised to 0% inhibition for each compound, ±SEM

	pK_i ± SEM
Isoprenaline	6.4 ± 0.12
Adrenaline	5.2 ± 0.25
Noradrenaline	4.4 ± 0.09
Formoterol	7.8 ± 0.07
Salbutamol	5.8 ± 0.06
Salmeterol	9.1 ± 0.02
C26	8.7± 0.03
BI-167-107	9.2 ±0.08

Table 4.3.4: A summary of pK_i values for Isoprenaline, adrenaline, noradrenaline, formoterol, salbutamol, salmeterol, C26 and BI-167-107 binding DDM-TS-SNAP-β_2AR obtained from equilibrium competition binding. TR-FRET between Lumi4-Tb and CA200693 (S)-propranolol-green PHERAstar FSX using 2 laser flashes per cycle and 520/620 TRF module. Values are mean of n=3 experiments ±SEM.

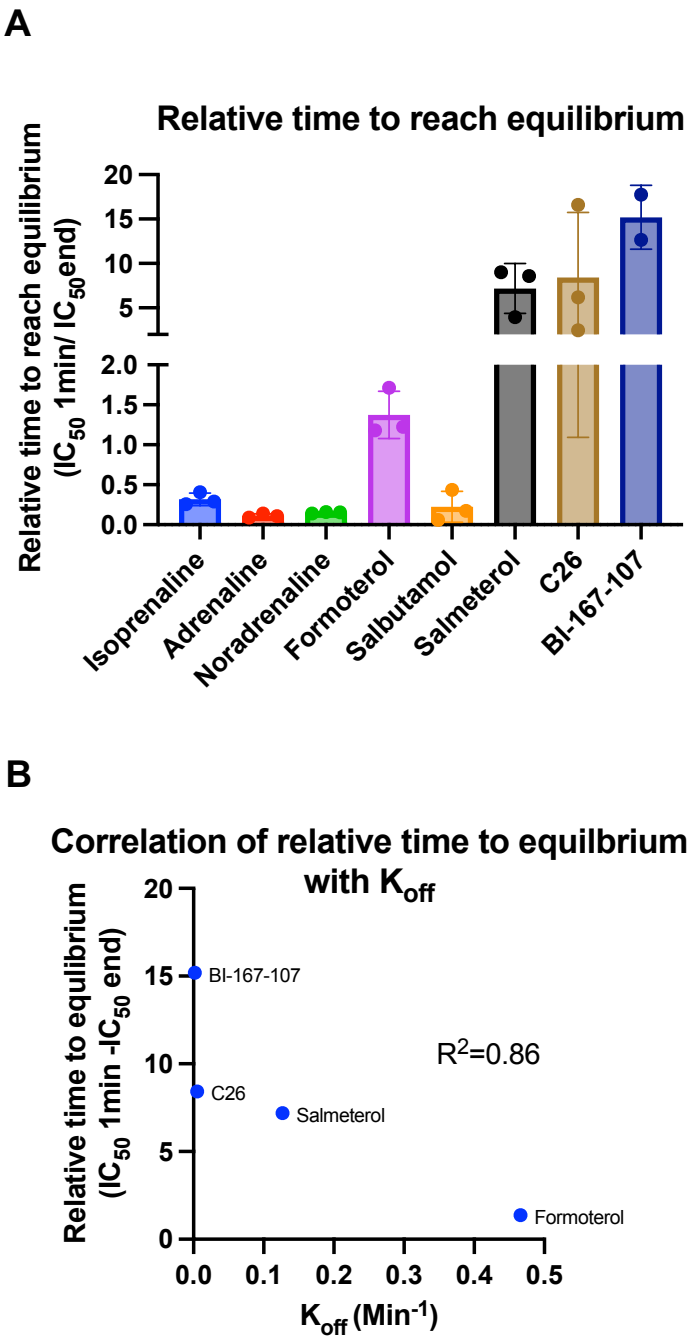

Figure 4.3.5: A summary of the relative time to reach equilibrium for isoprenaline, adrenaline, noradrenaline, formoterol, salbutamol, salmeterol, C26, BI-167-107 binding to the DDM-TS-SNAP-β_2AR A) relative time to reach equilibrium (IC_{50} 1min/IC_{50}end) as measured by TR-FRET for all eight compounds, bars show mean of n=3 individually plotted, error bars show SEM, **B)** Correlation plot for relative time to reach equilibrium (IC_{50} 1min/(IC_{50}end) for BI-167-107, C26, salmeterol and formoterol and their obtained K_{off} values using Pearsons' correlation.

4.3.4: Assessment of the relative time to reach equilibrium of eight β_2AR agonists

Having been unable to obtain K_{on} and K_{off} values for isoprenaline, adrenaline, noradrenaline and salbutamol binding the DDM-TS-SNAP-β_2AR, this study calculated the relative time for each compound to reach equilibrium by the fold difference in the IC_{50} at 1 minute Vs at the final measurement time, either 40min for C26 and BI-167-107 or 20min for all other compounds (Figure **4.3.5A).** This analysis should indicate a rank order of K_{off} values, and therefore residence time for all eight compounds. This analysis showed the rank order of K_{off} values for these compounds to be adrenaline (0.11 ±0.01), < noradrenaline (0.15 ±0.01), < salbutamol (0.22 ±0.11), < isoprenaline (0.32±0.05), < formoterol (1.37 ± 0.17). < salmeterol (7.19 ±1.63), < C26 (8.42 ± 4.23), < BI-167-107 (15.20 ± 3.6).

Figure **4.3.5B** shows a Pearsons' correlation for experimentally obtained K_{off} values (table **4.3.3**) and relative time to reach equilibrium for the four β_2AR agonist for which K_{off} values were obtained. These data show a strong (R^2=0.86) correlation between relative time to reach equilibrium (IC_{50} 1 min/ IC_{50} end) for these four compounds (BI-167-107, C26, salmeterol and formoterol) and K_{off}.

4.3.5 Development of CASE G_s activation assay

The second aim of this study was to quantify the efficacy of the eight β_2AR agonists to activate the G_s protein. To this end, this study initially tried to establish the CASE G_s assay in HEK293T/17 cells transiently transfected with β_2AR and CASE G_s biosensor. The full agonist formoterol was used to stimulate β_2AR mediated CASE G_s activation (Figure **4.3.6)**. Figure **4.3.6A** shows that TS-SNAP-β_2AR expression could be detected by SNAP488 labelling 48h after HEK293T/17 cells had been transiently transfected with 100ng pcDNA4TO-TS-SNAP-β_2AR using PEI. Likewise, figure **4.3.6B** shows that addition of furimazine resulted in luminescence at 450-80nm, indicating nanoLuc expression and therefore expression of the CASE G_s biosensor. Despite confirming expression of both TS-SNAP-β_2AR and CASE G_s figure **4.3.6C** shows that no decrease in BRET ratio was detected when a saturating concentration (10μM) of formoterol was added to these HEK293T/17 expressing TS-SNAP-β_2AR and CASE G_s.

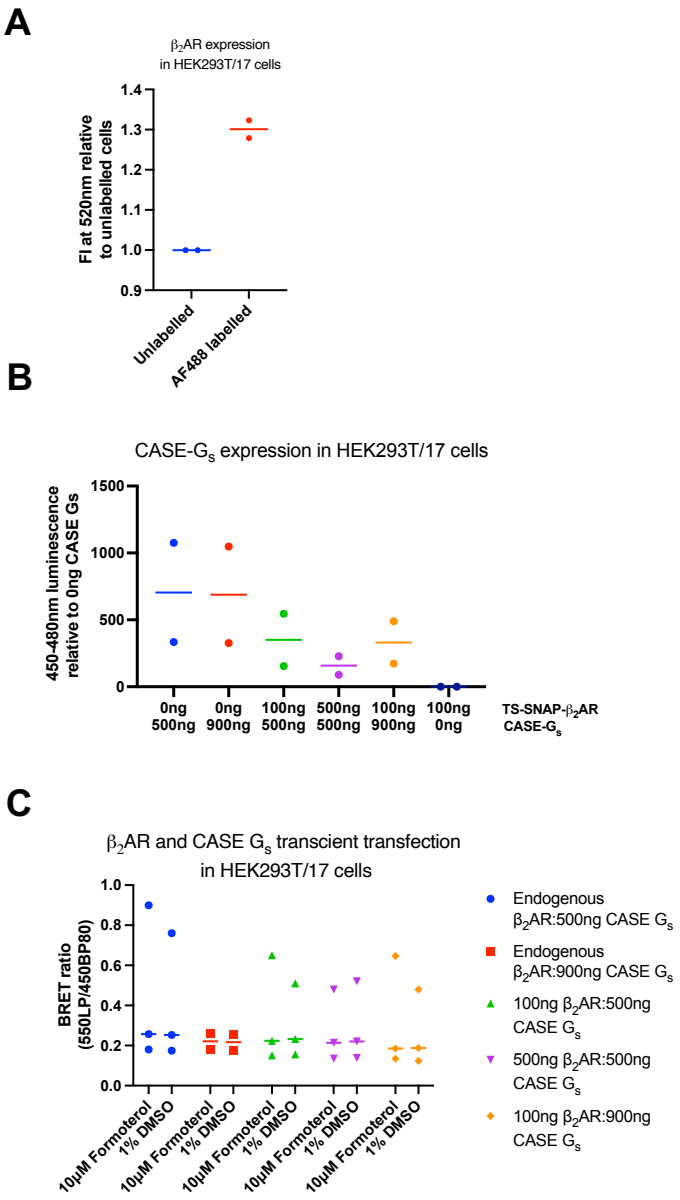

Figure 4.3.6: Trial of the CASE G_s activation assay using transient transfection of TS-SNAP-β_2AR and CASE G_s into HEK293T/17 cells **A)** investigation of TS-SNAP-β_2AR expression following 48h transient transfection of 100ng pcDNA4TO-TS-SNAP-β_2AR using PEI and SNAP-488 labelling, data points show n=2 **B)** Investigation of CASE G_s expression following varying 48h transcient transfections using PEI and 8μM furimazine, points show raw data of n=2 **C)** trial of CASE G_s activation assay at various 48h transfection ratios using 10μM formoterol to stimulate CASE G_s activation, data points show raw data from n=3

independent experiments. Fluorescence intensity and luminescence were read on PHERAstar FSX.

Following the observation that CASE G_s activation could not be detected with transient transfection of TS-SNAP-β_2AR and CASE G_s in HEK293T/17 cells, we investigated if CASE G_s activation could be detected when either 500ng or 1000ng CASE G_s was transiently transfected into T-REx^{TM}-293 cells stably expressing TS-SNAP-β_2AR (Figure **4.3.7**). Figure **4.3.7A** shows a time course for TS-SNAP-β_2AR expression over time since the initiation of induction. Figure **4.3.7A** shows that TS-SNAP-β_2AR expresses in this cell line and that there is approximately a 20% increase in TS-SNAP-β_2AR expression at 48h compared to 24h. Induction at the 24h and 48h time point was used to modulate TS-SNAP-β_2AR expression in CASE G_s activation assays in T-REx^{TM}-293 cells stably expressing TS-SNAP-β_2AR (Figure **4.3.7B**). Simular to results obtain with transcient transfection of receptor and biosensor, figure **4.3.7B** shows that there was no decrease in BRET ratio was detected when formoterol was added to T-REx^{TM}-293 cells stably expressing TS-SNAP-β_2AR and transciently transfected with CASE G_s.

In light of these results, we generated a double stable cell line of TS-SNAP-β_2AR and CASE G_s by stably transfecting CASE G_s into the T-REx^{TM}-293 cells TS-SNAP-β_2AR stable cell line (Figures **4.3.7A-C).** A mixed population of this cell line was tested for CASE G_s activation as shown in figure **4.3.7D.** Again, these data show no decrease in BRET when these cells were stimulated with 10μM formoterol, indicating that CASE G_s activation was not detectable. Figure **4.3.7C** shows that TS-SNAP-β_2AR expression can be modulated by different concentrations of tetracycline added at the same time point. Based on this, varying concentrations of tetracycline was used to modulate TS-SNAP-β_2AR expression in figure **4.3.8D**.

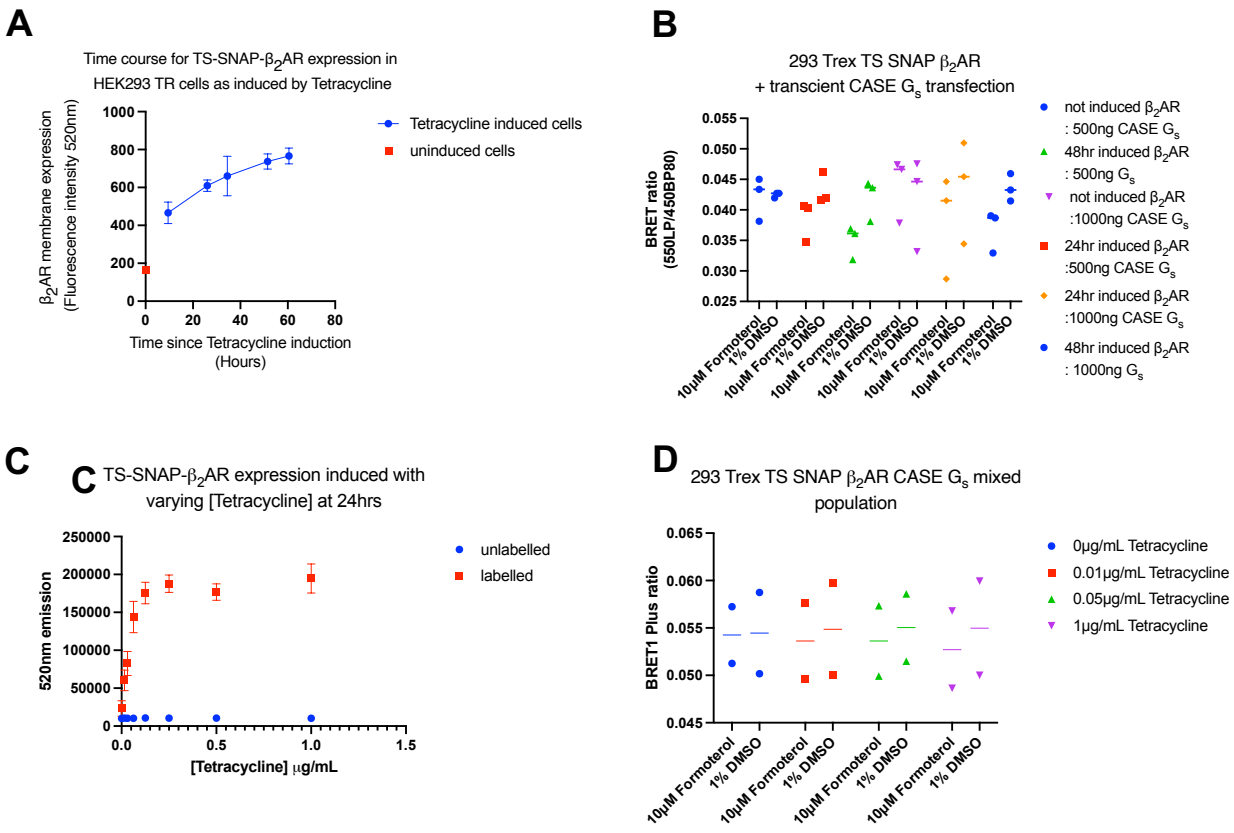

Figure 4.3.7 Trial of the CASE G_s assay in T-REx™-293 cells stably expressing TS-SNAP-β_2AR with transient CASE G_s expression or T-**REx™-293 cells stably expressing TS-SNAP-β_2AR and CASE G_s A)** investigation of TS-SNAP-β_2AR expression in T-REx™-293 cells stably expressing TS-SNAP-β_2AR over time since induction with 1μg/mL tetracycline (n=1) **B)** trial of CASE G_s activation assay in T-REx™-293 cells stably expressing TS-SNAP-β_2AR with 48h transient transfection of 500ng or 1000ng CASE G_s, using 10μM formoterol to stimulate CASE G_s activation, data points show raw data from n=3 independent experiments, **C)** investigation of TS-SNAP-β_2AR expression in T-Rex™-293 cells stably expressing TS-SNAP-β_2AR induced with varying concentrations of tetracycline for 48h, n=3±SEM **D)** Trial of CASE G_s activation assay in T-REx™-293 cells stably expressing TS-SNAP-β_2AR and CASE G_s, using 10μM formoterol to stimulate CASE G_s activation, data points show raw data from n=2 independent experiments. Fluorescence intensity and luminescence were read on PHERAstar FSX.

Finally, the mixed population T-REx^{TM}-293 cells TS-SNAP-β_2AR + CASE G_s stable cell line was FACS sorted into single cell populations with varying TS-SNAP-β_2AR and CASE G_s expression levels. Figure **4.3.8** shows the FACS plot and assignment of the mixed population T-REx^{TM}-293 cells TS-SNAP-β_2AR + CASE G_s stable cell line to quadrants. A single cell was picked from each quadrant and expanded to a single clone population that could be tested for CASE G_s expression and activation. The colonies corresponding from each quadrant are summarised in table **4.3.5.** All clones except A2 and A4 showed 450-80nm luminescence following the addition of furimazine therefore indicating CASE G_s expression. Clones A1, A3, A5 and A6 were screened for CASE G_s upon stimulation with formoterol and salbutamol (Figure **4.3.9**). No clear CASE G_s activation response in the clones A1, A3 and A6, however a clear CASE G_s activation concentration response curve was observed for the clone A5 (Figure **4.3.9C**). Figure **4.3.9C** shows distinct EC_{50} and differences in the E_{max} for the full agonist formoterol and partial agonist salbutamol. These data indicate the clone A5 to be a viable system to characterise the efficacy of the eight β_2AR agonists. A screen of the clones A1, A3, A5 and A6 took place at varying tetracycline concentrations to assess the optimal receptor level for the assay. Figure **4.3.10** shows that for the clone A5 the highest concentration of tetracycline (1μg/mL) was required for CASE G_s activation.

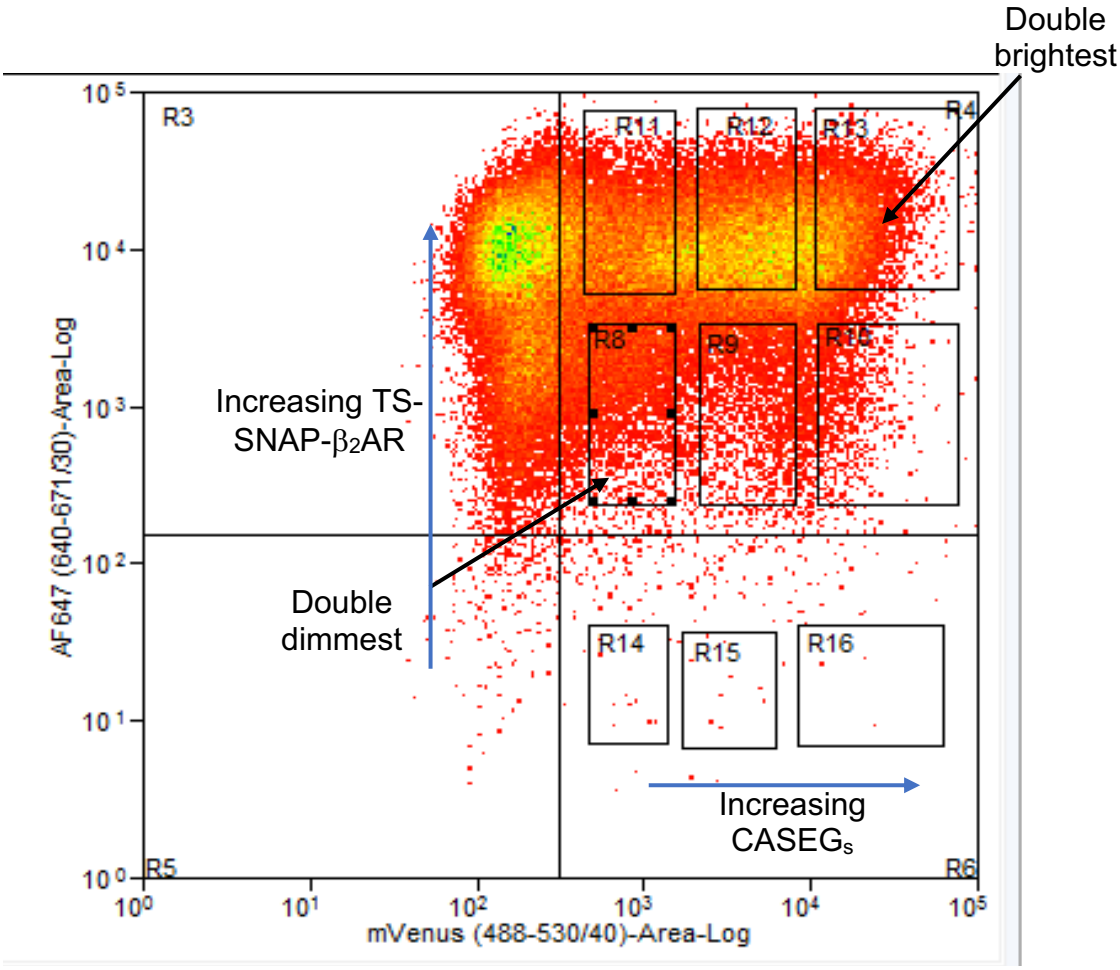

Figure 4.3.8: FACS plot of T-REx™-293 cells TS-SNAP-β_2AR and CASE G_s mixed population sorting and resulting quadrants

Clone	FACS quadrant
A1	R13
A2	R10
A3	R12
A4	R9
A5	R8
A6	R11

Table 4.3.5: A summary of the T-REx^{TM}-293 cells TS-SNAP-β_2AR and CASE G_s clones picked from each quadrant of the FACS analysis.

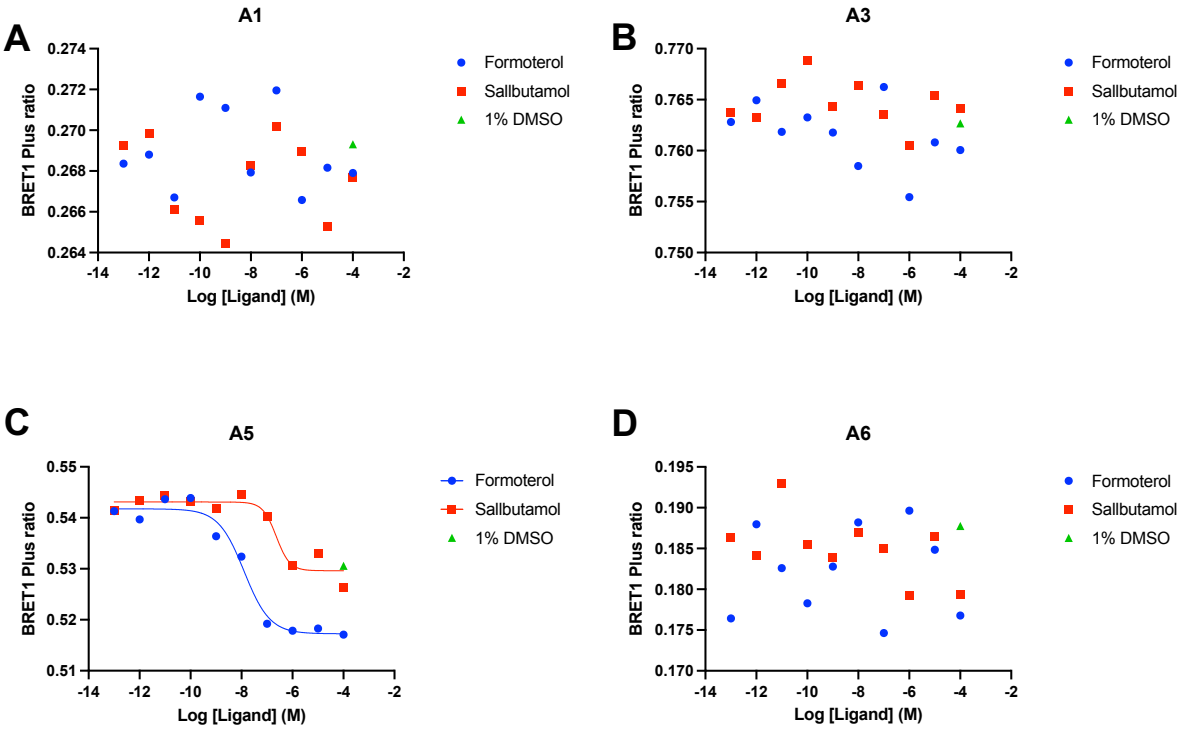

Figure 4.3.9: Trial of CASE G_s activation assay in T-REx^{TM}-293 TS-SNAP-β_2AR and CASE G_s clones A1, A3 A5 and A6: Cells were induced with 1μg/mL tetracycline for 48h at time of plating, adherent cells in 96 well were stimulated with varying concentrations of formoterol and salbutamol, BRET was read at 10min using 550LP/450-80nm Luminescence module and PHERAstar FSX. Data are a representative replicate of single wells of n=3.

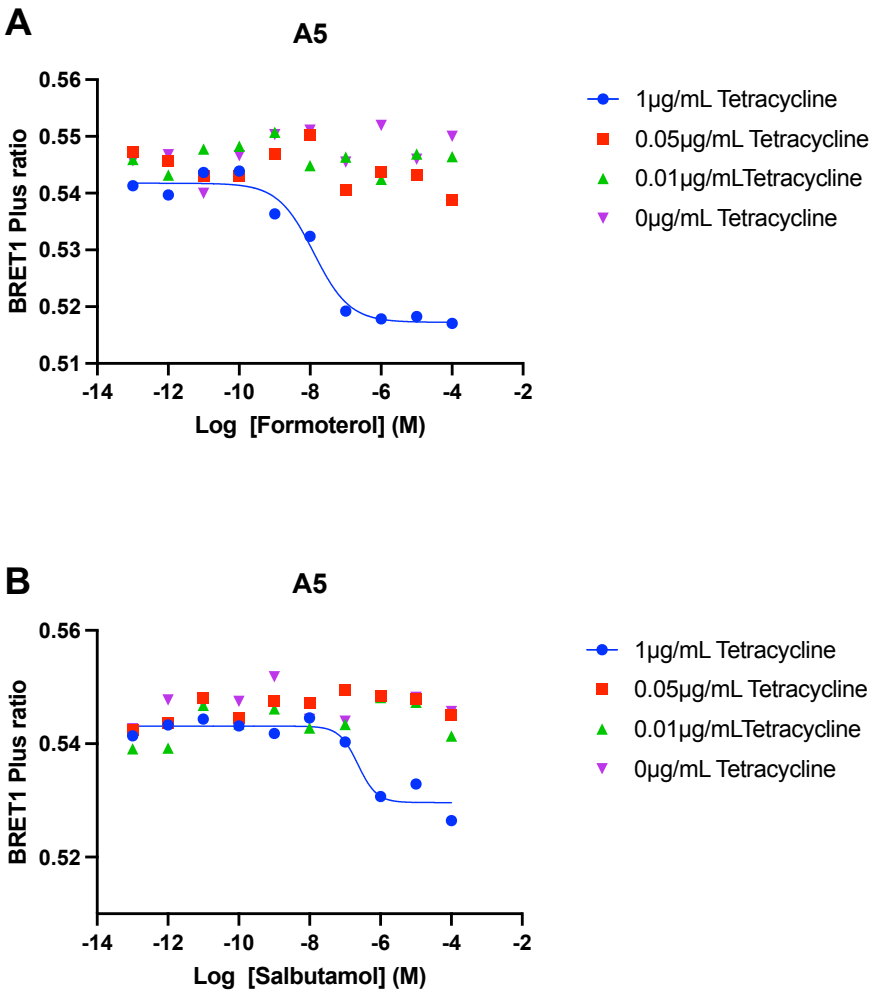

Figure 4.3.10: Trial of CASE G_s activation assay in T-REx™-293 - SNAP-β_2AR and CASE G_s clone A5 using varying concentrations (0-1µg/mL) of tetracycline to induce varying levels of β_2AR expression: Cells were induced with tetracycline for 48h, adherent cells were stimulated with varying concentrations of **A)** formoterol and **B)** salbutamol, BRET was read at 10min using 550LP/450-80nm Luminescence module and PHERAstar FSX Data are a representative replicate of n=3.

4.3.6 Quantifying the efficacy of eight β_2AR agonists using the CASE G_s activation assay

The T-REx^{TM}-293 cells TS-SNAP-β_2AR and CASE G_s clone A5 was consequentially used to screen the efficacy of the β_2AR agonists isoprenaline, adrenaline, noradrenaline, formoterol, salbutamol, salmeterol, C26 and BI-167-107. These data are fitted to a sigmoidal concentration response curve in figure **4.3.11**. Corresponding pEC_{50}, and E_{max} values are summarised in table **4.3.6.** These data showed the most potent compounds to be BI-167-107 and formoterol with a pEC_{50} values of 8.8±0.62 and 8.7±0.18 respectively. The least potent compound was noradrenaline with a pEC_{50} value of 5.6±0.33. There was no statistically significant difference between the E_{max} of the eight β_2AR agonists (p=0.47, One-way ANOVA) (Figure **4.3.11)**

These data were also fitted to the operational model using the pK_i values obtained in table **4.3.4** to obtain log τ values for efficacy. A representative example of fitting of these data to the operational model is shown in figure **4.3.12.** Data for all compounds except C26 fitted well to the operational model, for this reason C26 was excluded from the analysis. Mean log τ values ranged from 0.05±0.05 for salmeterol to 1.26±0.84 for adrenaline and 1.6±0.96 for isoprenaline (p=0.37 One-way ANOVA).

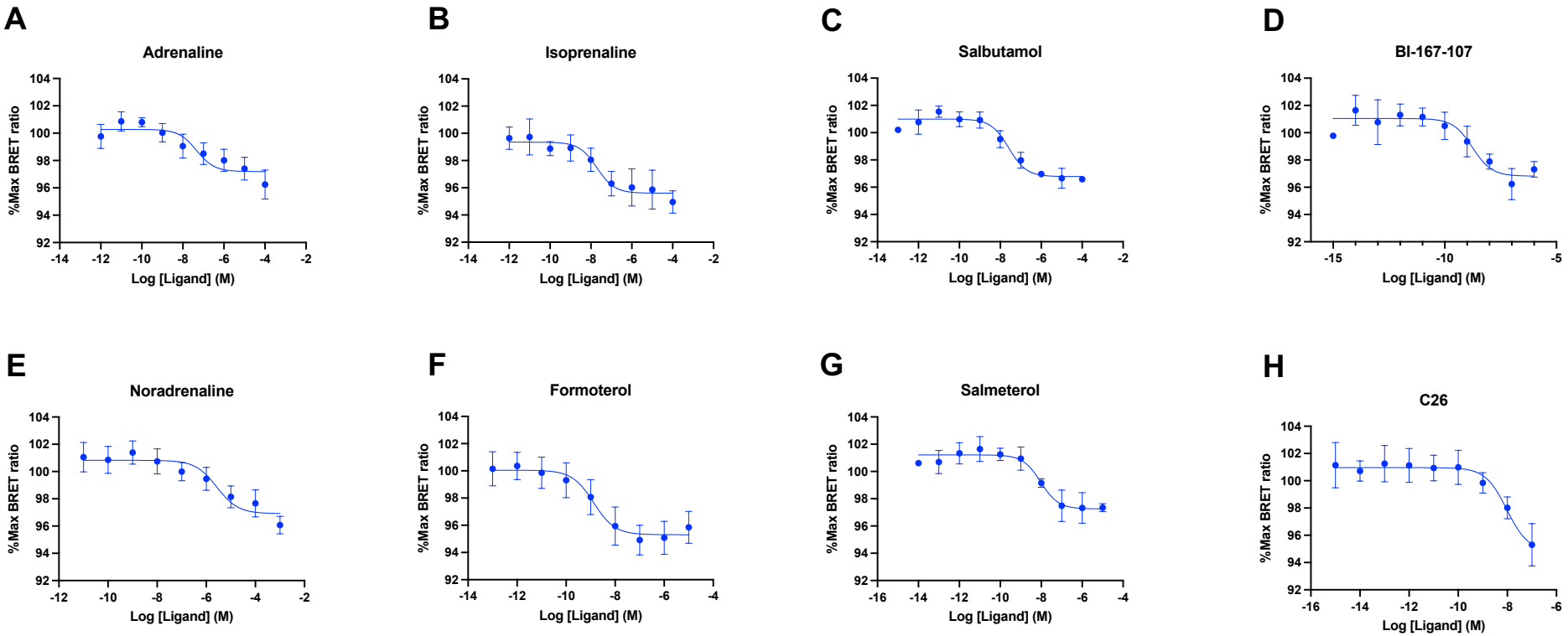

Figure 4.3.11: CASE G_s activation studies on A) Adrenaline, **B)** Isoprenaline, **C)** Salbutamol, **D)** BI-167-107, **E)** Noradrenaline, **F)** Formoterol, **G)** Salmeterol, **H)** C26 in the T-REx^{TM}-293 -SNAP-β_2AR and CASE G_s clone A5 which had been induced with 1μg/mL tetracycline for 48h. Duplicate wells of adherent cells were stimulated with varying concentrations of ligand and BRET was read at 15min post ligand addition using 550LP/450-80nm luminescence module and PHERAstar FSX. Data points are mean of 3 independent experiments normalised to 1% DMSO control, error bars show SEM.

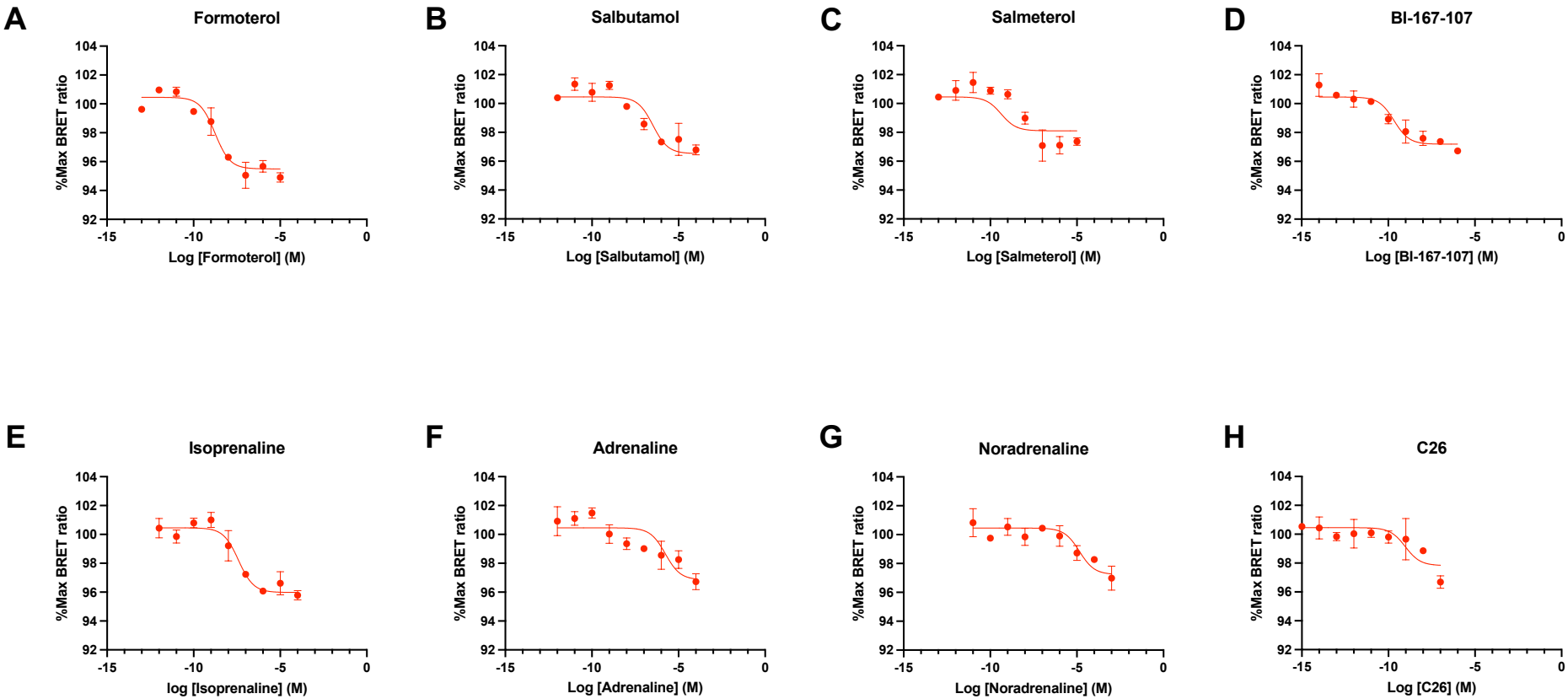

Figure 4.3.12: Example of fitting CASE G_s activation in response to A) formoterol, B) salbutamol, C) salmeterol, D) BI-167-107, E) isoprenaline, F) adrenaline, G) noradrenaline and H) C26 to the operational model: Formoterol was used as the reference ligand and K_A values fixed to experimentally obtained K_i values. CASE G_s activation was obtained in the T-REx^{TM}-293 - SNAP-β_2AR and CASE G_s clone A5 which had been induced with 1μg/mL tetracycline for 48h. Duplicate wells of adherent cells were stimulated with varying concentrations of ligand and BRET was read at 15min post ligand addition using 550LP/450-80nm luminescence module and PHERAstar FSX, Data points show mean of duplicate wells from a single experiment, error bars show SD.

Ligand	pEC_{50}	E_{max}	Log τ	pEC_{50}-pK_i
Adrenaline	7.2 ± 0.5	97.2%	1.26 ±0.84	2.0
Isoprenaline	7.5 ±0.23	95.6%	1.64 ±0.96	1.7
Salbutamol	7.5 ±0.19	96.8%	0.40 ±0.09	1.6
BI-167-107	8.8 ±0.62	96.8%	0.36 ±0.04	-0.4
Noradrenaline	5.6 ±0.33	96.9%	0.52 ±0.45	1.2
Formoterol	8.7 ±0.18	95.31%	-	0.9
Salmeterol	8.0 ±0.18	97.3%	0.05 ±0.05	-1.1
C26	7.9 ±0.21	-	-	-

Table 4.3.6: A summary of efficacy and potency values obtained for CASE-G_s activation by adrenaline, isoprenaline, salbutamol, BI-167-107, noradrenaline, formoterol, salmeterol and C26 in the T-REx™-293 -SNAP-β_2AR and CASE G_s clone A5 which had been induced with 1μg/mL tetracycline for 48h, pEC_{50} values are mean of n=3 individually experiments individually fitted to a sigmoidal curve, E_{max} values were obtained from sigmoidal curve fits in figure 4.3.11, log τ values are mean of n=3 individually experiments individually fitted to the operational model with K_A values fixed to experimentally obtained K_i values, All error bars show SEM. pEC_{50}-pK_i values correspond to the pEC_{50} value above minus pK_i values in table **4.4.**

4.4 Discussion

The aim of this study was to characterise the pharmacology of eight β_2AR agonists so that they could be used at tools to investigate the role of kinetics in the molecular basis of efficacy. To this end, this chapter shows the development of a kinetic TR-FRET ligand binding assay and the BRET based CASE G_s activation assay to investigate the ligand binding kinetics and G_s protein activation efficacy of these eight β_2AR agonists, and the correlations between them.

4.4.1 The development and limitations of a TR-FRET kinetic ligand binding assay

This study chose the fluorescent propranolol tracer CA200693(-S)-propranolol-green as, although it has similar ligand binding kinetics to CA200689(-S)-propranolol-red, it did not photo bleach. This study then used CA200693(-S)-propranolol-green as a tracer in kinetic competition binding studies to investigate the ligand binding kinetics of eight β_2AR agonists. Using this approach, this study was able to obtain k_{on} and K_{off} values for BI-167-107, C26, formoterol and salmeterol by fitting specific kinetic competition binding data to the Motulsky-Mahan model. It was not possible to obtain k_{on} and K_{off} for adrenaline, noradrenaline, isoprenaline and salbutamol. According to literature values (Sykes & Charlton, 2012) these compounds all have faster K_{off} values than the compounds which this study was able to obtain kinetic parameters for. Moreover, the tracer compound used by Sykes and colleagues had a much faster K_{off} of 0.23±0.02 compared to the tracer used in this study which had a K_{off} of 0.08±0.009. It therefore seems likely that the tracer used in this study did not have a fast enough K_{off} value to measure the kinetics of adrenaline, noradrenaline, isoprenaline and salbutamol. Indeed, Monte Carlo simulations (appendix **7.1.3**) of the tracer and time cycles used in our assay and a hypothetically cold compound with a K_{off} of 0.1min^{-1}, 1 min^{-1}, 3 min^{-1} and 10 min^{-1} showed that the tracer and time cycles used in this study could correctly calculate k_{on} and K_{off} values for a cold ligand

with a K_{off} of up to 3min^{-1} using the Motulsky-Mahan model. This modelling and comparison to Sykes and colleagues' study validates that the limitation of the TR-FRET kinetic ligand binding assay was the slow kinetics of the tracer and that a tracer with a faster K_{off} would be required to obtain the k_{on} and K_{off} values for adrenaline, noradrenaline, isoprenaline and salbutamol.

4.4.2 The ligand binding kinetics of eight β_2AR agonists binding the DDM-TS-SNAP-β_2AR

To our knowledge, this was the first study to examine the ligand binding kinetics of these eight β_2AR agonists binding to the β_2AR in the DDM micelle. Of the four ligands that k_{on} and K_{off} values were obtained three had published k_{on} and K_{off} values (table **4.3.1**). Published k_{on} values for salmeterol (3.50±0.57 x10^9 Mol^{-1} Min^{-1}) (Sykes et al., 2014b), C26 (3.70±0.47 x10^8 Mol^{-1} Min^{-1}) (Rosethorne et al., 2016), and formoterol (1.78±0.21 x10^8 Mol^{-1} Min^{-1}) (Sykes et al., 2014b) differed substantially from the values obtained in this study although they followed a similar rank order. The rank order of k_{on} values obtained in this study was salmeterol (1.35±0.45 x10^8 Mol^{-1} Min^{-1}) > formoterol (2.6±0.43 x10^7 Mol^{-1} Min^{-1}), >C26 (1.06 ±0.05x10^7) Mol^{-1} Min^{-1} > BI-167-107 (2.63±0.15x10^6 Mol^{-1} Min^{-1}). Moreover, published K_{off} values followed the same rank order as those obtained in this study although they differed substantially from the absolute values. These were formoterol (0.47±0.008 Vs 3.00±0.38 Min^{-1} (Sykes et al., 2014b)) > salmeterol (0.13±0.03 Vs 1.16±0.16 Min^{-1} (Sykes et al., 2014))>C26 (0.005±0.001 Vs 0.02±0.003 Min^{-1} (Rosethorne et al., 2016)). In general, these values from the literature were all much faster than those obtained in this study, and this is explained by the higher temperature of 37^{o}C used compared to 20^{o}C used in our study. The similar rank order of k_{on} and K_{off} values and similarity in the kinetic K_d and equilibrium K_i values obtained in this study give confidence in this kinetic data set.

Comparison of the pK_i values obtained in this study (table **4.3.4**) and those from the literature also show generally very similar results. This is except for adrenaline (6.1±0.05 Vs 5.2±0.25), noradrenaline (5.4±0.07 Vs 4.4±0.09) and C26 (10.2±0.07 Vs 8.7±0.03). The reason for these differences is not clear, it could be that ligand affinity is lost when β_2AR is in the DDM micelle as opposed to the cell membrane, however adrenaline and noradrenaline also very easily oxidise. C26 also appears to have decreased efficacy compared to the literature in this study, therefore it is also possible that these compounds had slightly reduced activity at the time of the experiment due to long storage.

4.4.3 The relative K_{off} values of eight β_2AR agonists can be ranked by time to equilibrium

As it was not possible to quantify the K_{off} rates and corresponding ligand residence time of adrenaline, isoprenaline, noradrenaline and salbutamol, this study used the K_i ratio method of Heise and colleagues (Heise et al., 2007) to provide a relative measure of K_{off} values for all eight of the β_2AR agonists (Figure **4.3.5A)**. Heise and colleagues show that the fold change in K_i over time correlates with the K_{off} rate of the ligand, thus providing a relative measure of K_{off}. **4.3.5B** shows a strong correlation for the K_i ratios and experimentally obtained K_{off} values for salmeterol, formoterol, C26 and BI-167-107 in this study, therefore validating the applicability of this method to the data in this study. This method gave a rank order of K_{off} values as adrenaline > noradrenaline > salbutamol > isoprenaline > formoterol > salmeterol > C26 > BI-167-107. This also correlates well with the rank order of salbutamol >isoprenaline > formoterol > salmeterol K_{off} values obtained by Sykes and colleagues (Sykes et al., 2014b) therefore further validating this approach.

4.4.4 The CASE G_s activation assay required the development of the clone A5

To establish a CASE G_s activation assay, this study initially transiently transfected TS-SNAP-β_2AR and CASE G_s into HEK293T/17 cells as demonstrated by Schihada and colleagues (Schihada et al., 2021). In contrast to this study, these data showed that all though TS-SNAP-β_2AR and CASE G_s expressed, there was no CASE G_s response in these assays. This was hypothesised to be due to a low transfection efficiency meaning that TS-SNAP-β_2AR and CASE G_s expression levels were low or not often expressed in the same cell therefore making changes in BRET difficult to detect.

Consequentially, this study trialled transiently transfecting CASE G_s into a T-REx^{TM}-293 cell line stably expressing TS-SNAP-β_2AR. The advantage of using this approach is that TS-SNAP-β_2AR should be expressed in all cells which the CASE G_s is successful transiently transfected. However, this approach did not prove successful, hypothesising that this was due to low transfection efficiency of CASE G_s, this study generated a T-REx^{TM}-293 TS-SNAP-β_2AR + CASE G_s stable cell line. Again, the CASE G_s assay was not successful in the mixed population of this cell line. This data suggested that either the CASE G_s was not an effective biosensor, or it was difficult to detect differences in CASE G_s activation from a mixed population of cells all expressing CASE G_s to different extents.

Finally, this study FACS sorted the T-REx^{TM}-293 TS-SNAP-β_2AR + CASE G_s stable cell line into single clone populations with varying expression levels of TS-SNAP-β_2AR and CASE G_s. Of these clones, the clone A5 was the only clone to show a CASE G_s response. The CASE G_s response by A5 was only observed at the highest concentration of tetracycline (1μg/mL). Therefore, the clone A5 was used to investigate the efficacy of the eight β_2AR agonists following induction with 1μg/mL

tetracycline. It was not clear why the clone A5 was the only clone in which the CASE G_s was successful. The clone A5 was the lowest expressor of TS-SNAP-β_2AR and CASE G_s of the selected clones.

4.4.5 Comparison of the CASE G_s activation data to published studies

The pEC_{50} values obtained in CASE G_s activation studies were generally left shifted from literature pEC_{50} values for cAMP accumulation assays shown in table **4.1.1.** This is to be expected considering that cAMP is downstream of G_s signalling and therefore its signal will be further amplified. Moreover, the pEC_{50} value of 7.5±0.23 obtained for isoprenaline in this study is very similar to that of 7.2±0.37 obtained by Schihada and colleagues using the CASE G_s (Schihada et al., 2021), giving confidence to our data.

Although not statistically significant there was a slight reduction in the E_{max} of the partial agonist's salbutamol and salmeterol in the CASE G_s activation studies compared to the other agonists. This is in line with cAMP data (Baker, 2005) which shows salbutamol and salmeterol to be partial agonists with a reduced E_{max} compared to full agonists. Conversely, C26 has been shown to produce an E_{max} that is 117% of that of isoprenaline in a cAMP accumulation assays (Rosethorne et al., 2016). It was not possible to obtain a realistic E_{max} value in this assay due to not having a high enough concentration of C26.

4.4.6 Quantification of efficacy of eight β_2AR agonists efficacy using CASE G_s activation

As the aim of this study was to investigate the role of ligand and effector coupling kinetics in the molecular basis of efficacy, it was essential to quantify the efficacy of our eight β_2AR agonists in the CASE G_s activation assay. There is no perfect way to quantify efficacy, as such this study considers several methods of analysis. Firstly, this study considered the difference between pK_i and pEC_{50} values as a measure of efficacy (table **4.3.4).** This method gave the rank order of efficacy as adrenaline > isoprenaline > salbutamol > noradrenaline > formoterol > BI-167-107> salmeterol. These results do not match discussed literature cAMP values (table **4.1.1**) or G protein activation data (Gregorio et al., 2017) for these compounds which generally indicate, for example, that formoterol is a full agonist and salbutamol a partial agonist. Moreover, some of the values shown for this method (table **4.3.4**) show negative values which is not to be expected. This may suggest that this method is in appropriate in an assay with very little amplification. Moreover, a caveat of this method is that it does not consider the E_{max}.

Classically, efficacy has been quantified using the operational model (Black & Leff, 1983). The operational model considers the E_{max} of the system, and a ratio of agonist functional potency (EC_{50}) to the equilibrium dissociation constant of the agonist for the active state of the receptor (K_A) to produce the measure of efficacy τ. τ is the fractional occupancy of receptors required to give half the maximal effect. As both E_{max} and EC_{50} are system dependent so is τ. As such, an advantage of using this method over the EC_{50}-pK_i method is consideration of the E_{max}. As there were some differences in the E_{max} values in our data set considering the E_{max} seemed appropriate in our study. However, one problem with fitting the operational model is that the parameters K_A, E_{max} and τ are all inter-dependent. To overcome this, it has been shown that fixing K_A to experimentally obtained K_i values reduces error (Jakubík et al., 2019), despite K_i values being for the inactive state of the receptor.

As this study had obtained pK_i values we chose to adopt this approach in our study. The resulting log τ values are shown in table **4.3.4**.

These log τ values gave a rank order of efficacy of isoprenaline > adrenaline > noradrenaline > salbutamol >BI-167-107 >salmeterol. Which differed from the order of efficacy given by pK_i -$pEC_{5o.}$ However, Gregorio and colleagues (Gregorio et al., 2017) use a GTP turnover assay to define the G_s protein activation efficacy of the majority of these compounds at the purified β_2AR. Gregorio and colleagues define efficacy by the effectiveness to generate G_s (GTP) from G_s (GDP) (ε). This gave the rank order of efficacy as isoprenaline > adrenaline > BI-167-107 > salbutamol > salmeterol. The similarity of these results from our study to that of Gregorio and colleagues gives confidence in our data set and use of the operational model.

4.4.7 There is no correlation between ligand residence time and efficacy for these β_2AR agonists

The hypothesis underlying this study was that ligand residence time effects β_2AR receptor dynamics to affect G_s protein activation efficacy. As such the aim of this chapter was to characterise the ligand binding and efficacies of these eight β_2AR agonists and to investigate if there was a correlation between ligand residence time and efficacy. A positive correlation has been shown between the efficacy of seven agonists at the M3 muscarinic receptor, and ten agonists at the A_{2A} receptor and their ligand residence time (Sykes, et al. 2009) (Guo et al., 2012). Conversely, no correlation between efficacy and residency time was shown for the Adenosine A_3 receptor (Louvel et al., 2014).

As discussed above, this study was only able to quantify the K_{on} and K_{off} values of four of the eight β_2AR agonists however, this study was able to rank the relative order of K_{off} values via their time to reach equilibrium (Figure **4.3.5**) (Heise et al., 2007). This study was also able to quantify the efficacy of these eight β_2AR agonists to activate the G_s protein using the CASE G_s activation assay and the methods to quantify efficacy discussed in sec **4.4.6.** Using this data this study investigated the correlation between relative K_{off} values and efficacy using a Pearsons' correlation (Figure **4.4.1)**. This analysis showed no correlation between IC_{50} 1min/ IC_{50} end values and log τ values (R^2=0.26, p=0.29) and a statistically significant moderately positive correlation between IC_{50} 1min/ IC_{50} end values and pEC_{50}-pK_i values (R^2=0.64. p=0.03). Since this study considered log τ the most appropriate way to quantify efficacy, this study concludes that there is not a correlation between K_{off} values, or ligand residence time and efficacy for these eight β_2AR agonists.

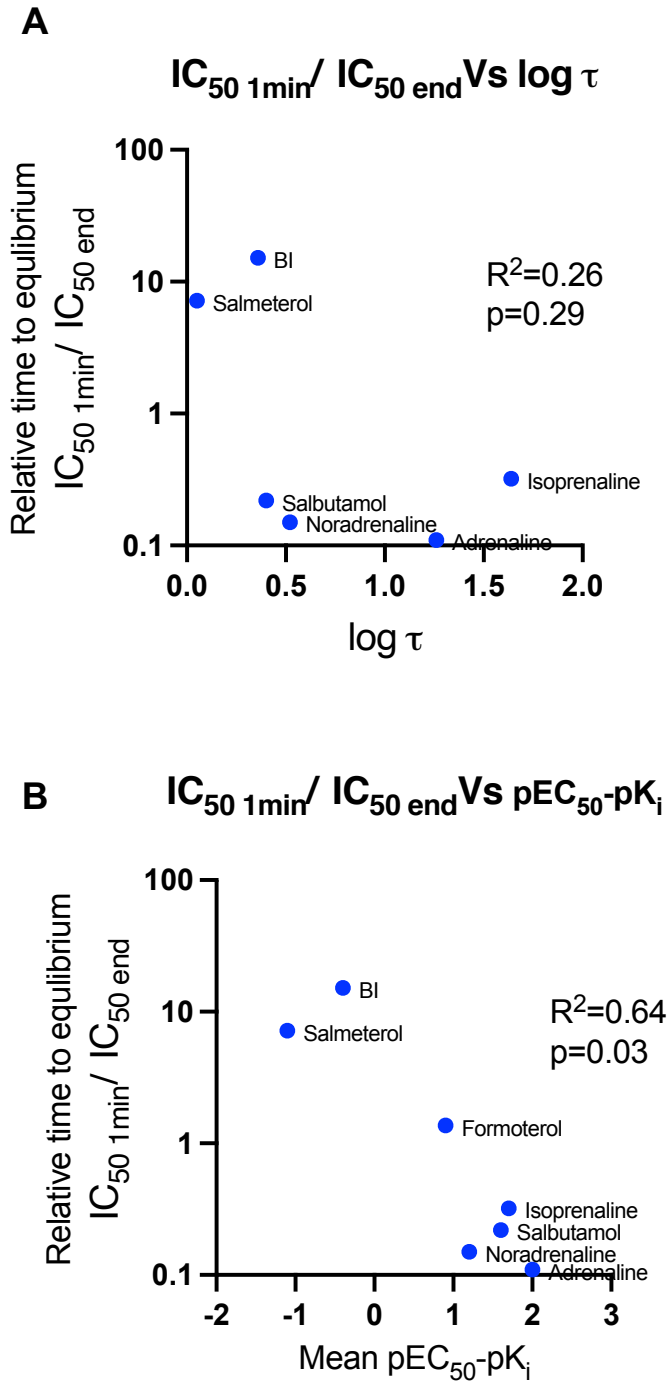

Figure 4.4.1: Correlation plot for relative time to reach equilibrium (IC_{50} 1min/IC_{50}end) for salmeterol, BI-167-107, salbutamol, noradrenaline, adrenaline and isoprenaline binding the DDM-TS-SNAP-β_2AR and **A)** log τ values or **B)** pEC_{50}-pK_i values for CASE G_s activation using Pearsons' correlation.

4.4.8 Conclusion

In summary, this chapter shows the development of a TR-FRET kinetics binding assay to investigate the ligand binding parameters of eight agonists binding to the DDM-TS-SNAP-β_2AR and its limitations. We also show the development of a BRET based assay to study G_s protein activation efficacy by these eight agonists. This study was able to accurately obtain K_{on} and K_{off} values of four of the eight β_2AR agonists and rank the relative order of K_{off} values for all eight. This study was then able to quantify the efficacy of the eight β_2AR agonists to activate the G_s protein and concluded that there is no correlation between ligand residence time and efficacy for these eight agonists at the β_2AR. These findings do not support a role for ligand binding kinetics in the molecular basis of efficacy at the β_2AR.

Chapter 5

Investigating the role of G_s protein binding kinetics in the molecular basis of efficacy

5.1 Introduction

The hypothesis underlying this study was that differences in the kinetics of agonist-β_2AR-G_s protein complex formation underly differences in agonist efficacy at the β_2AR. Evidence for this hypothesis came from Lamichhane and colleagues who use single molecule FRET to show that agonists prolong the time the β_2AR spends in the active conformation (Lamichhane et al., 2020). Moreover, Gregorio and colleagues show that full agonists at the β_2AR increased GTP turnover compared to partial agonists, suggesting an increased number of G proteins being activated (**sec 1.6**). However, neither study has investigated the kinetics of G protein binding and receptor dynamics in response to a larger range of agonists of different efficacies and kinetic profiles. Having characterised the pharmacological properties of eight β_2AR agonists in chapter **4**, this chapter aimed to investigate the kinetics of mini-G_s binding to β_2AR in response to these agonists. To this end, this chapter generated purified mini-G_s proteins with fluorescent labels as probes to directly investigate mini-G_s interaction with β_2ARnLuc in response to agonists of different efficacy using nanoBRET.

5.1.1 Use of mini-G_s proteins as tools to investigate β_2AR activation

As discussed in **sec 1.8,** mini-G_s proteins are the engineered GTPase domain of the Gα subunit of the heterotrimeric G_s protein (Carpenter & Tate, 2016). The thermostabilising mutations of the mini-G_s restrict it to the active and nucleotide free conformation (García-Nafría, et al. 2018), ensuring that mini-G proteins do not undergo nucleotide exchange. It is important to note that this active nucleotide-free state of the G protein would usually have dissociated from the GPCR. This makes mini-G proteins a sensor for G protein-activating conformations of the GPCR, as opposed to truly mimicking the G protein and its activation process. The use of mini-G proteins as tools for sensing the active states of a GPCR was validated by (Wan et al., 2018), who fused the venus fluorescent protein to the N terminus of a range of mini-G proteins and

showed that mini-G protein binding upon agonist stimulation is reversible and recapitulates the pharmacology and coupling specificity to a range of GPCRs in mammalian cells. With this in mind, this study generated constructs for the expression of these fusion mini-G proteins in *E*. coli and purified these proteins with the aim of establishing an in-solution nanoBRET assay with which the kinetics of these proteins binding the β_2AR could be directly measured.

5.1.2 Use of nanoBRET to investigate β_2AR-mini-G_s binding

To date, several studies have used BRET to investigate binding or protein-protein interactions at GPCRs. Such studies have included G protein (Galés et al., 2005), arrestin (Angers et al., 2000) and mini-G_s (Wan, et al., 2018) recruitment to β_2AR as well as G_s protein activation by β_2AR in mammalian cells. Moreover, NanoBRET has also been applied to probe ligand binding at the β_2AR (Stoddart, et al., 2015) and has been demonstrated to accurately measure ligand binding kinetics at the adenosine A_3 receptor (Bouzo-Lorenzo et al., 2019), in live cells. Taken together, these studies show that nanoBRET is a feasible method to measure mini-G_s recruitment specifically to β_2AR and that it yields adequate temporal resolution to study kinetics. Therefore, strongly supporting the applicability of NanoBRET to study the kinetics of purified mini-G_s proteins binding the β_2AR, although, the above studies were all performed in live mammalian cells, and, to our knowledge this is one of the first studies to investigate protein-protein interactions in-solution using NanoBRET.

The most used alternative technique to study the kinetics of ligand-protein or protein-protein kinetics in real time is Surface Plasmon Resonance (SPR). SPR occurs when light is shone on a metal surface at such an angle that the light photons oscillate along the surface (resonance). SPR can be used to detect protein-protein interactions as the binding of a freely diffusing protein to a protein that has been immobilised on this metal surface will interfere with this resonance

(Nguyen et al., 2015). The main advantage of SPR over BRET is that it is a label free technique, as such there is not the risk of the fusion proteins required for BRET interfering with the function of the protein of interest. Conversely, BRET is a higher throughput technique and offers a much more specific signal avoiding the problems of non-specific binding associated with SPR.

5.1.3 Aims:

The purpose of this Chapter was to use in-solution NanoBRET to investigate the kinetics of mini-G_s proteins binding the β_2AR when in complex with the agonists characterised in chapter **4**. This study therefore aimed to:

1. Purify fluorescently tagged and unlabelled mini-G_s proteins.
2. Characterise the affinity, association and dissociation of fluorescently tagged and unlabelled mini-G_s proteins binding to the TS-SNAP-β_2ARnLuc using NanoBRET.
3. Use the fully characterised TS-SNAP-β_2ARnLuc-mini-G_s NanoBRET system to investigate mini-G_s interaction with β_2ARnLuc in response to agonists of different efficacy.

5.2 Methods

5.2.1 Production of mini-G_s proteins

Labelled and unlabelled mini-G_s proteins used in this study were produced from *E.* coli using immobilised metal affinity chromatography (IMAC) as described in **sec 2.2.10.**

5.2.2 Production of TS-SNAP-β_2ARnLuc

TS-SNAP-β_2ARnLuc expression took place in stably transfected HEK T-REx^{TM} cells. TS-SNAP-β_2ARnLuc membranes were produced as described in **sec 2.2.6.** TS-SNAP-β_2ARnLuc were extracted from membranes in 1% DDM as described in **sec 2.2.6.** Unsolubilised material was removed via ultracentrifugation at 600,000*xg* for 1h.

5.2.3 In-solution intermolecular BRET assays to investigate TS-SNAP-β_2ARnLuc: venus-mini-G_s pharmacology

BRET was used to investigate the interactions between membrane or DDM TS-SNAP-β_2ARnLuc and venus-mini-G_s, as described in **sec 2.2.3.** Serial dilutions of venus mini-G_s, with 30μM unlabelled mini-G_s for NSB wells only were added to 384 well plates. Saturating concentrations of agonists were pre-incubated with membrane or DDM TS-SNAP-β_2AR-nLuc and (x4 or 32μM furimazine). TS-SNAP-β_2AR-nLuc complexes were added to plates containing mini-G_s proteins and luminescence at 450-80nm and >550nm was quantified immediately using 550LP/450-80nm LUM module and PHERAstar FSX plate reader. Or, for end point reads plates were incubated for 90min at room temperature before reading. Characterisation and optimisation of the TS-SNAP-β_2AR-nLuc:venus-mini-G_s NanoBRET system took place using TS-SNAP-β_2AR-nLuc in membranes due to ease and COVID-19 time restrictions. Final experiments took place in using DDM solubilised TS-SNAP-β_2AR-nLuc.

5.2.4 Venus-mini-G_s recruitment assays in cells

Cellular A_{2A}RnLuc or TS-SNAP-β_2ARnLuc:venus-mini-G_s assays were performed in HEK293T/17 cells that had been transiently transfected with receptor and biosensor. All cell lines were adherent in white 96 well plates, all cell culture and transfections took place as described in sec **2.2.** Cells were incubated with furimazine for 20min prior to assay. Plates were read for 3 min using 550LP/450-60nm luminescence module, prior to addition of agonists using in-built PHERAstar FSX injectors, and then for a further 20min.

5.3 Results

5.3.1 Production of mini-G_s proteins from *E*. coli

The first aim of this study was to produce fluorescently labelled mini-G_s proteins. To this end, N terminally labelled venus, halo and unlabelled mini-G_s protein DNA was inserted into the PJ411 vector containing His10-TEV sites to give the constructs PJ411-MKK-His10-label-mini-G_s as described in section **2.2.9**. Mini-G_s proteins were expressed in *E. coli*, which were then lysed and mini-G_s proteins purified via the His10 tag on their N terminus which has affinity for a nickel column. Analysis of mini-G_s protein preparations by SDS-PAGE gel (Figure **5.3.1**) showed His10-TEV-Halo-mini-G_s (63kDa), His10-TEV-Venus-mini-G_s (55kDa) and His10-TEV-mini-G_s (28kDa) at their respective molecular weights. Figure **5.3.1** also shows some impurities for each protein preparation of both higher and lower molecular weights than the protein of interest.

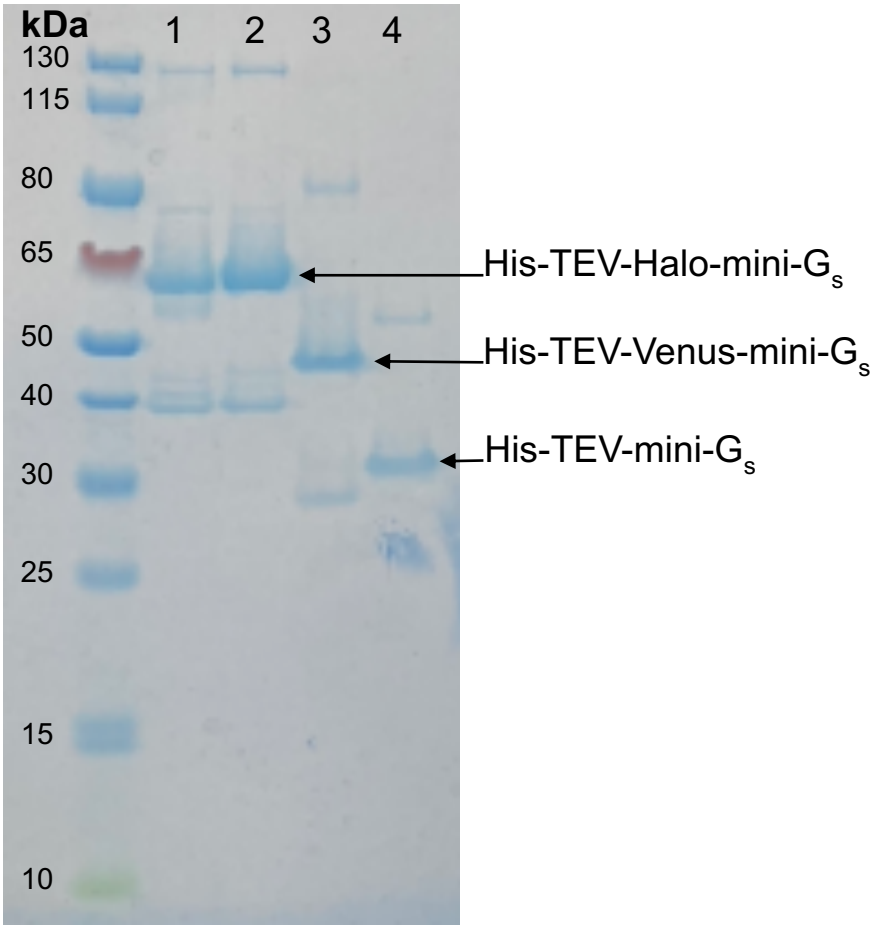

Figure 5.3.1: Production of mini-G_s proteins from *E.* coli: SDS PAGE gel stained for protein with InstantBlue® showing production and purity of His10-Halo-mini-G_s (lanes 1-2), His10-venus-mini-G_s (lane 3) and His10-mini-G_s proteins (lane 4). Representative gel of n=4 protein preps for His10-Halo-mini-G_s and His10-mini-G_s proteins and n=1 for His10-venus-mini-G_s.

5.3.2 Characterisation of mini-G_s protein preparations binding the TS-SNAP-β_2ARnLuc

Next this study investigated if the venus-mini-G_s and unlabelled proteins produced in figure **5.3.1** were functional, by interrogation of their ability to couple the TS-SNAP-β_2ARnLuc. Figure **5.3.2B** shows venus-mini-G_s proteins produced in this study were recruited to TS-SNAP-β_2ARnLuc in membranes, in response to increasing concentrations of isoprenaline, with a pEC_{50} value of 7.1±0.2 (n=3) and that this could be blocked by presence of an excess of unlabelled mini-G_s protein. This suggests both venus and unlabelled mini-G_s protein preparations were functional. The equivalent experiment in HEK293T/17 cells expressing TS-SNAP-β_2ARnLuc and venus-mini-G_s (Figure **5.3.2A**) gave a pEC_{50} value of 6.7±0.6 (n=3) which was not statistically significantly different from that of 7.1±0.2 obtained in the purified system (p=0.59, unpaired Student's t-test).

The affinity of the labelled and unlabelled mini-G_s proteins for the TS-SNAP-β_2ARnLuc were subsequently determined. Knowledge of the affinity of the labelled and unlabelled mini-G_s proteins is essential for designing kinetic experiment (section **5.3.4**), as unlabelled mini-G_s proteins would be used to displace the venus-mini-G_s protein. Figure **5.3.2C** shows saturation binding curves for venus-mini-G_s binding to TS-SNAP-β_2ARnLuc in the absence and presence of the saturating concentrations of an agonist isoprenaline. Figure **5.3.2C** shows venus-mini-G_s only binds TS-SNAP-β_2ARnLuc in the presence of the agonist. In the presence of saturating concentrations of isoprenaline venus-mini-G_s bound TS-SNAP-β_2ARnLuc with a pK_d of 7.65 ±0.11.

Next, the venus-mini-G_s was used as a tracer in competition binding experiments to examine the affinities of the halo or unlabelled mini-G_s proteins for TS-SNAP-β_2ARnLuc in the presence of saturating concentrations of isoprenaline. Figure **5.3.3A** shows that 20μM of unlabelled mini-G_s protein can be used to define the non-specific binding

of venus-mini-G_s to TS-SNAP-β_2ARnLuc. This allowed the pK_d of 7.65±0.11 for venus-mini-G_s binding TS-SNAP-β_2ARnLuc to be obtained from its specific saturation binding curve. Based on this 30nM venus-mini-G_s was used as the tracer for competition binding experiments.

Figure **5.3.3C-D** shows a competition binding curve for unlabelled mini-G_s and Halo-mini-G_s displacing venus-mini-G_s from TS-SNAP-β_2ARnLuc, with a pK_i values of 8.33±0.14, and 7.28±0.15, respectively. These data show that venus-mini-G_s and Halo-mini-G_s have statistically significantly lower affinity for the receptor than unlabelled mini-G_s ($p=0.028$ and $p=0.003$ respectively, One-way ANOVA and Tukey's multiple comparison test)

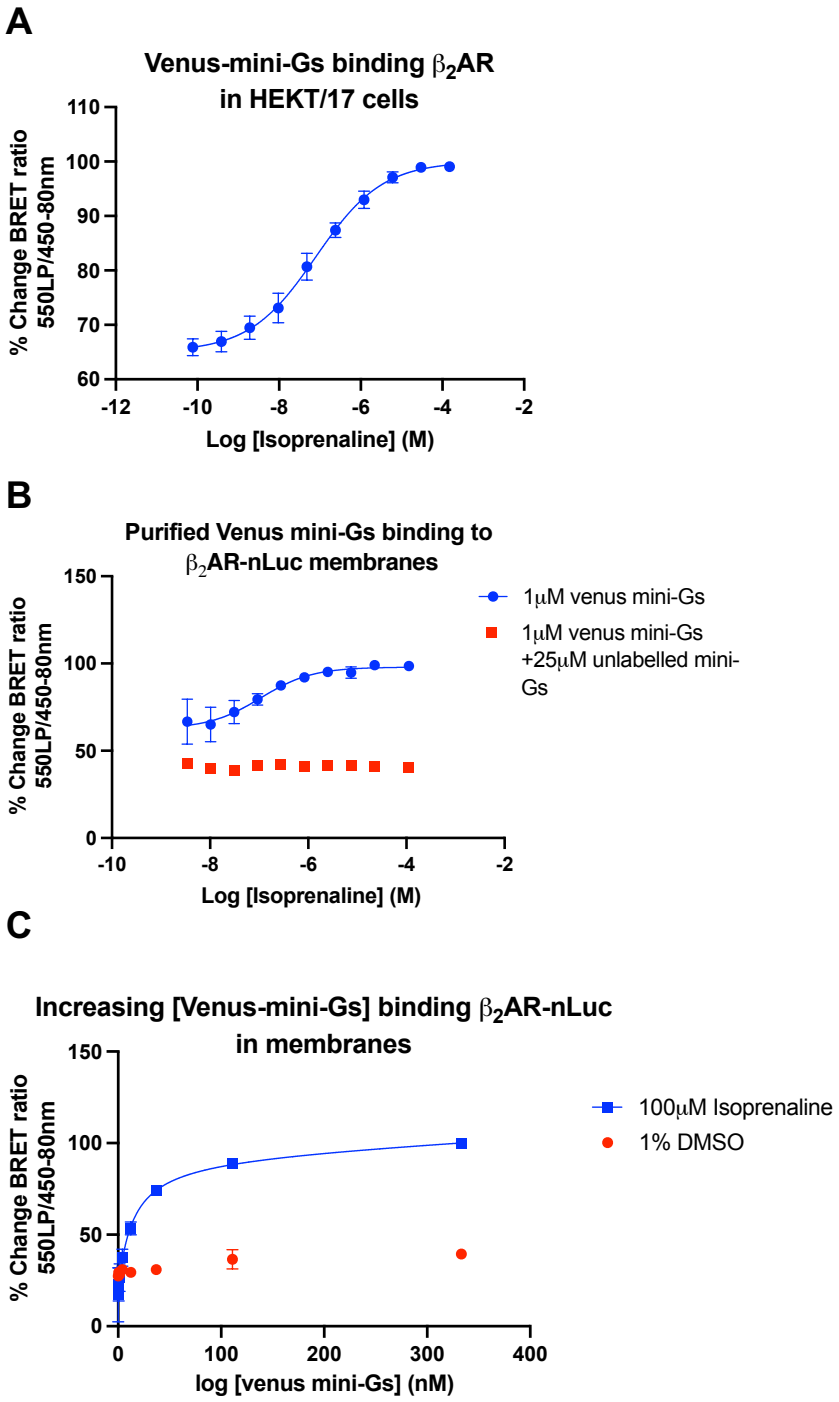

Figure 5.3.2: Venus and unlabelled mini-G_s proteins produced bind TS-SNAP-β_2ARnLuc. A) Recruitment of venus-mini-G_s to TS-SNAP-β_2ARnLuc in transciently transfected HEK293T/17 cells in response to varying concentrations of isoprenline **B)** Recruitment of purified venus mini-G_s to membranes expressing TS-SNAP-β_2ARnLuc in response to varying concentrations of isoprenaline **C)** Saturation binding curves for varying concentrations of purified venus-mini-G_s binding to TS-SNAP-β_2ARnLuc membranes in the absence and presence of 100μM

Isoprenaline. nanoBRET between TS-SNAP-β_2ARnluc and venus-mini-G_s was read on PHERAstar FSX using LUM 550LP/450-80nm module. All curves show combined normalised data of n=3, error bars show ±SEM.

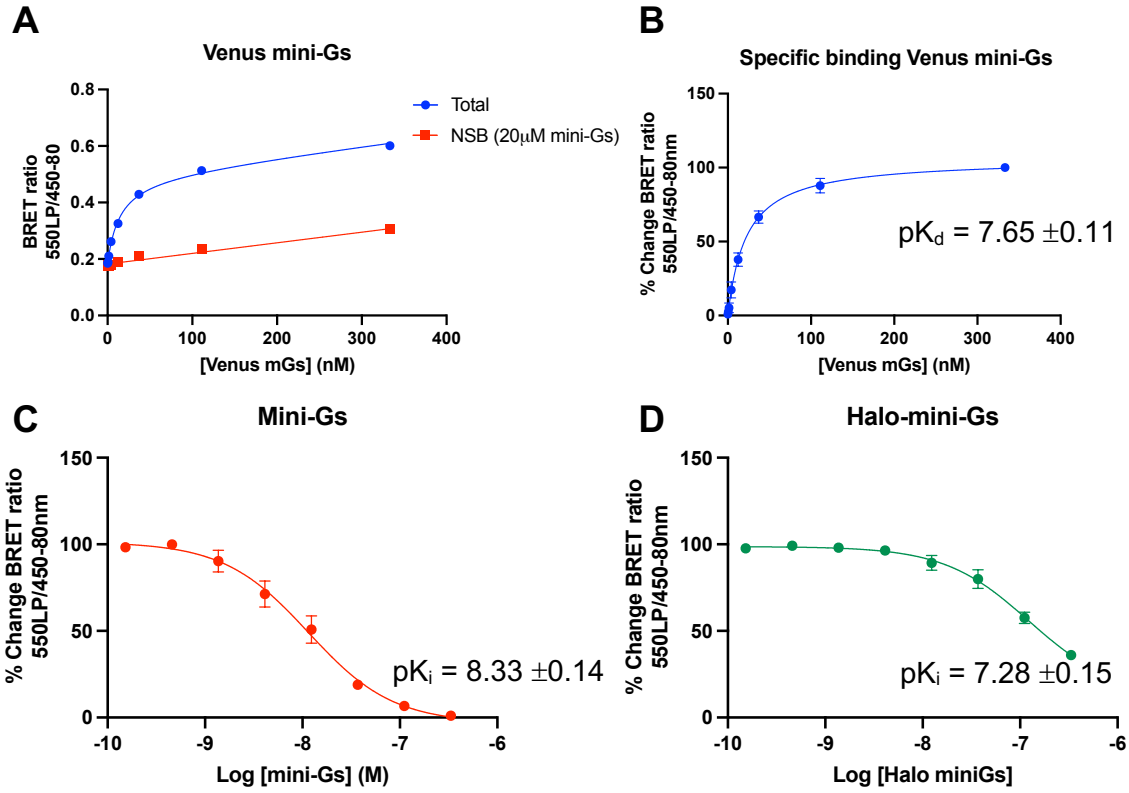

Figure 5.3.3 Characterising the affinity of mini-G_s proteins for the isoprenaline bound TS-SNAP-β_2ARnLuc in membranes A) Representative total and NSB plot for increasing concentrations of purified venus-mini-G_s binding the isoprenaline bound TS-SNAP-β_2ARnLuc in membranes, **B)** Specific saturation binding for purified venus-mini-G_s, data points show mean±SEM, from 3 independant experiments **C)** Competition binding between 30nM purified venus-mini-G_s and varying concentrations of purified mini-G_s, data points show n=3± SEM, **D)** Competition binding between varying concentrations of Halo-mini-G_s, and 30nM of purified venus-mini-G_s, data points show n=3± SEM. BRET between TS-SNAP-β_2ARnLuc and venus-mini- G_s was read on PHERAstar FSX using LUM 550LP/450-80nm module. pK_d values are mean of n=2±SD or 3±SEM individual experiments.

5.3.3 Characterisation of venus-mini-G_s association and dissociation from the DDM-TS-SNAP-β_2ARnLuc

Having defined the affinities of the labelled and unlabelled mini-G_s proteins for the TS-SNAP-β_2ARnLuc in membranes, this study began setting up venus-mini-G_s kinetic studies with the DDM-TS-SNAP-β_2ARnLuc, using unlabelled mini-G_s to define the NSB and measure dissociation of the DDM-TS-SNAP-β_2ARnLuc:venus-mini-G_s complex . Specific binding for the association of venus-mini-G_s to isoprenaline bound TS-SNAP-β_2ARnLuc and its dissociation using 33.3μM mini-G_s is shown in figure **5.3.4.** Figure **5.3.4** shows that the association of venus-mini-G_s to DDM-TS-SNAP-β_2ARnLuc best fitted a two-phase association model. The dissociation was incomplete and did not revert to the baseline. Whilst the percentage of the association that could be attributed to the fast component was concentration dependent, the percentages of complexes that could be dissociated was consistent across concentrations. A summary of the percentage of fast and slow association and percentage dissociated is shown in table **5.3.1**. The percentage of the association that could be attributed to the fast phase increased from 23% at 111nM venus-mini-G_s to 71.4% at 3000nM venus-mini-G_s, whilst the percentage of complexes dissociated was always 70-74% (Table **5.3.1**).

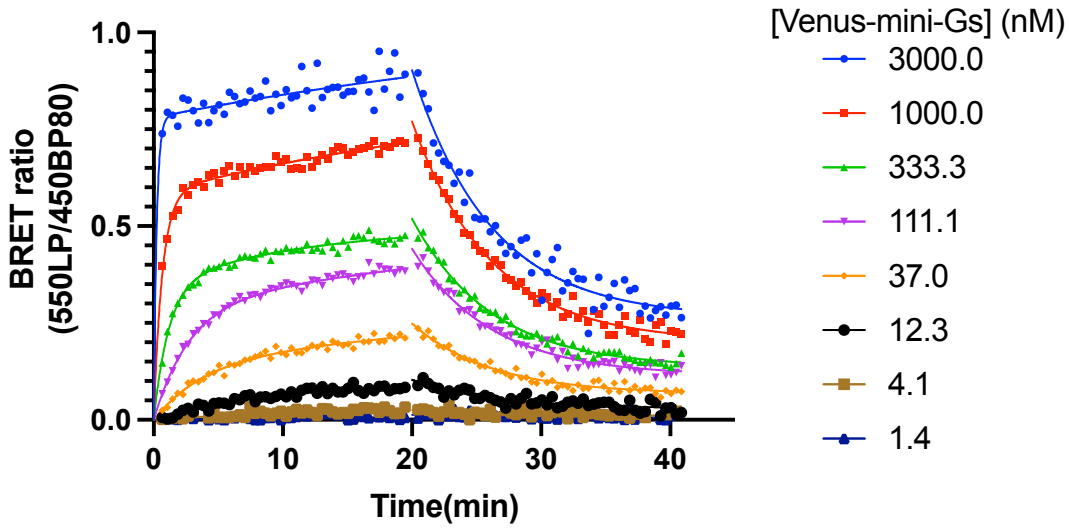

Figure 5.3.4 Characterising the association and dissociation of purified venus-mini-G_s binding to the isoprenaline bound DDM-TS-SNAP-β_2AR-nLuc using nanoBRET: DDM-TS-SNAP-β_2ARnLuc was incubated with saturating concentration of isoprenaline for 20min before addition to plate containing varying concentrations of venus-mini-G_s. BRET between TS-SNAP-β_2ARnLuc and venus-mini-G_s was immediately read on PHERAstar FSX using LUM 550LP/450-80nm module. 30μM unlabelled mini-G_s was used to define the NSB and 33μM to dissociate the venus-mini-G_s. Representative data of n=3, showing specific binding.

	% Fast association	% Slow association	% Dissociated
3000nM	71.4±3.0	39.9±12.1	72.1±1.2
1000nM	63.6±6.5	46.5±10.8	70.7±4.3
333nM	49.9±11.5	58.4±17.6	73.0±4.1
111nM	23.0±9.0	77.3±11	74.3±2.7

Table 5.3.1: A summary of the phases of the association and dissociation of varying (3000-111nM) concentrations of venus-mini-G_s to the isoprenaline bound DDM-TS-SNAP-β_2AR: % fast and slow association was calculated from two site fits and % dissociated was calculated from the differences in the top and bottom of the dissociation curve. Data show mean of 3-4 individual experiments ± SEM.

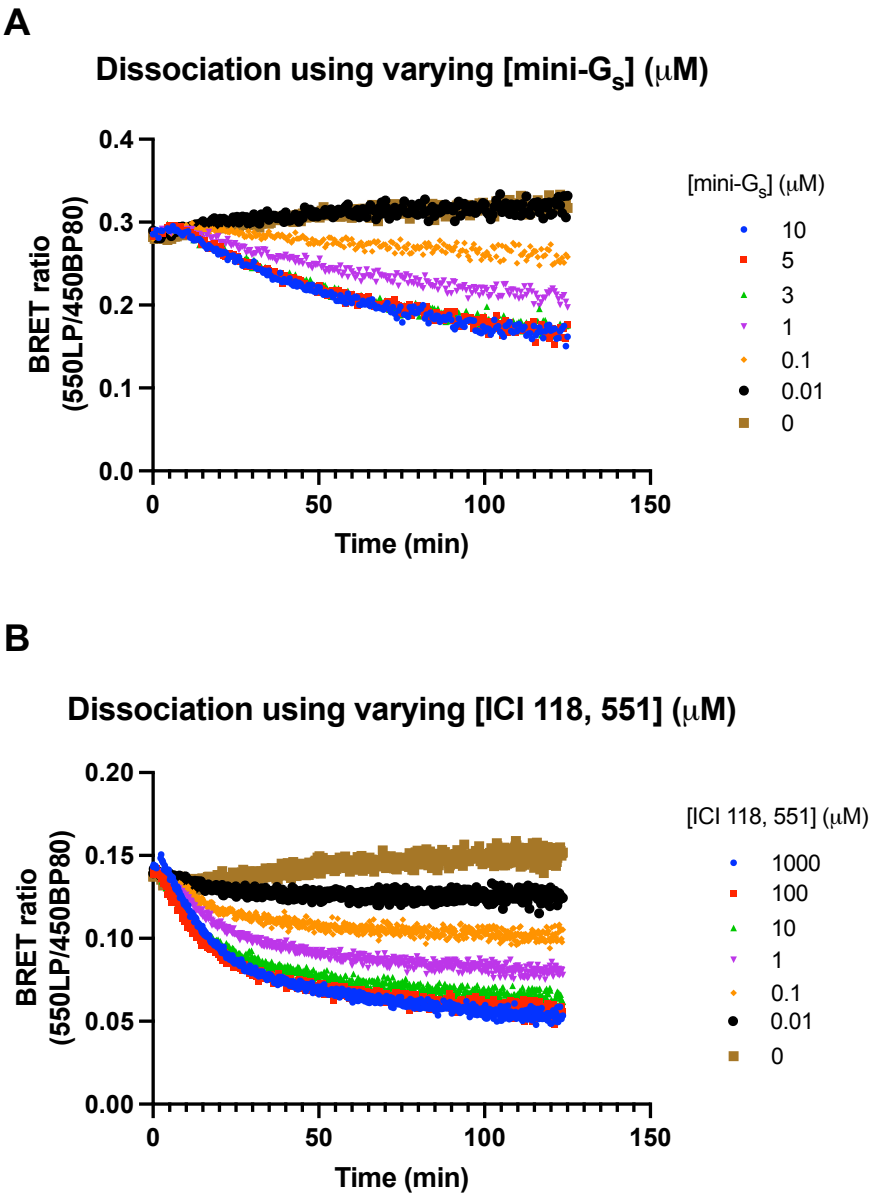

Figure 5.3.5: Validation of the concentration of disociator required to dissociate the membrane-TS-SNAP-β_2ARnLuc complex: membrane-TS-SNAP-β_2ARnLuc was preincubated with saturating concentration of isoprenaline and 333nM venus-mini-G_s before nanoBRET between TS-SNAP-β_2ARnLuc and venus-mini-G_s read on PHERAstar FSX, at room temperature, using LUM 550LP/450-80nm module for 3 min before addition of varying concentrations of **A)** mini-G_s or **B)** the inverse agonist ICI 118, 551 to dissociate the membrane-TS-SNAP-β_2ARnLuc complex, and read for a further 2h, specific binding data, where unlabelled mini-G_s was used to define NSB, representative data of n=3.

In order to confirm that the incomplete dissociation of the TS-SNAP--β_2ARnLuc:venus-mini-G_s complex was real and not caused by an inadequate concentration of unlabelled mini-G_s being used to dissociate, this study then investigated dissociation of the TS-SNAP-β_2ARnLuc:venus-mini-G_s complex by varying concentrations of either the unlabelled mini-G_s protein or by the inverse agonist ICI 118, 551 (Figure **5.3.5**). Figure **5.3.5A** confirms that a high enough concentration of mini-G_s was being using to dissociate the TS-SNAP-β_2ARnLuc:venus-mini-G_s complex**.** Moreover **5.3.5B** shows that dissociation of this protein complex is also incomplete using the antagonist ICI 118, 551 as the dissociator.

Next, this study sought to validate the findings of the two-phase association and incomplete dissociation of the TS-SNAP-β_2ARnLuc and venus-mini-G_s in a physiological setting. Consequently, TS-SNAP-β_2ARnLuc and venus-mini-G_s were transiently transfected into HEK293T/17 cells and the association and dissociation of venus-mini-G_s to the TS-SNAP-β_2ARnLuc in response to agonist stimulation or antagonist displacement investigated in both this, and the purified protein system (Figure **5.3.5A-B)** using nanoBRET. Figure **5.3.6B** shows that in the case of the TS-SNAP-β_2ARnLuc, agonist induced stimulation of venus-mini-G_s still appeared biphasic in HEK293T/17 cells and dissociation of the complex by the antagonist ICI 118, 551 was incomplete. Figure **5.3.6B** also shows an increase in nanoBRET when saturating concentrations of isoprenaline and ICI 118, 551 are added simultaneously. Figure **5.3.6A** shows identical results for TS-SNAP-β_2ARnLuc and purified venus-mini-G_s. To investigate if the biphasic association and incomplete dissociation was unique to β_2AR or universal to other GPCR-mini-G_s interactions, this study also investigated the association and dissociation of the venus-mini-G_s to A_{2A}nLuc in HEK293T/17 cells using saturating concentrations of the agonist NECA to stimulate mini-G_s recruitment and saturating concentrations of the antagonist ZM241385 to displace this.

Figure **5.3.6C** shows the association of venus-mini-G_s to A_{2A}nLuc in HEK293T/17 cells using 10μM NECA followed a one phase association and the A_{2A}nLuc:venus-mini-G_s complex was then completely dissociated by saturating concentrations of the antagonist ZM241385.

In the above experiments, saturating concentrations of the agonist and antagonists were added simultaneously as a control to confirm that the antagonist concentration was high enough to displace the agonist. Whilst an increase in nanoBRET between TS-SNAP-β_2ARnLuc and venus-mini-G_s was observed when isoprenaline and ICI 118, 551 were added simultaneously, no increase in BRET between A_{2A}nLuc and venus-mini-G_s was observed when NECA and ZM241365 were added simultaneously (Figure **5.3.6B-C**). Considering that, the binding of venus-mini-G_s to TS-SNAP-β_2ARnLuc was partially irreversible and the association of isoprenaline to TS-SNAP-β_2ARnLuc was faster than ICI 188, 551, it was realised that the simultaneous addition of isoprenaline and ICI 118, 551 would likely still show and increase in BRET despite isoprenaline being displaced by ICI 118, 551. This study therefore repeated this experiment with antagonist preincubation, instead of simultaneous addition (Figure **5.3.7A-B**). For both TS-SNAP-β_2ARnLuc and A_{2A}nLuc preincubation with the respective antagonist shows complete block of venus-mini-G_s recruitment by the agonist (Figure **5.3.7A-B**). These data therefore support the finding that venus-mini-G_s binding is displaceable for A_{2A}nLuc but not TS-SNAP-β_2ARnLuc.

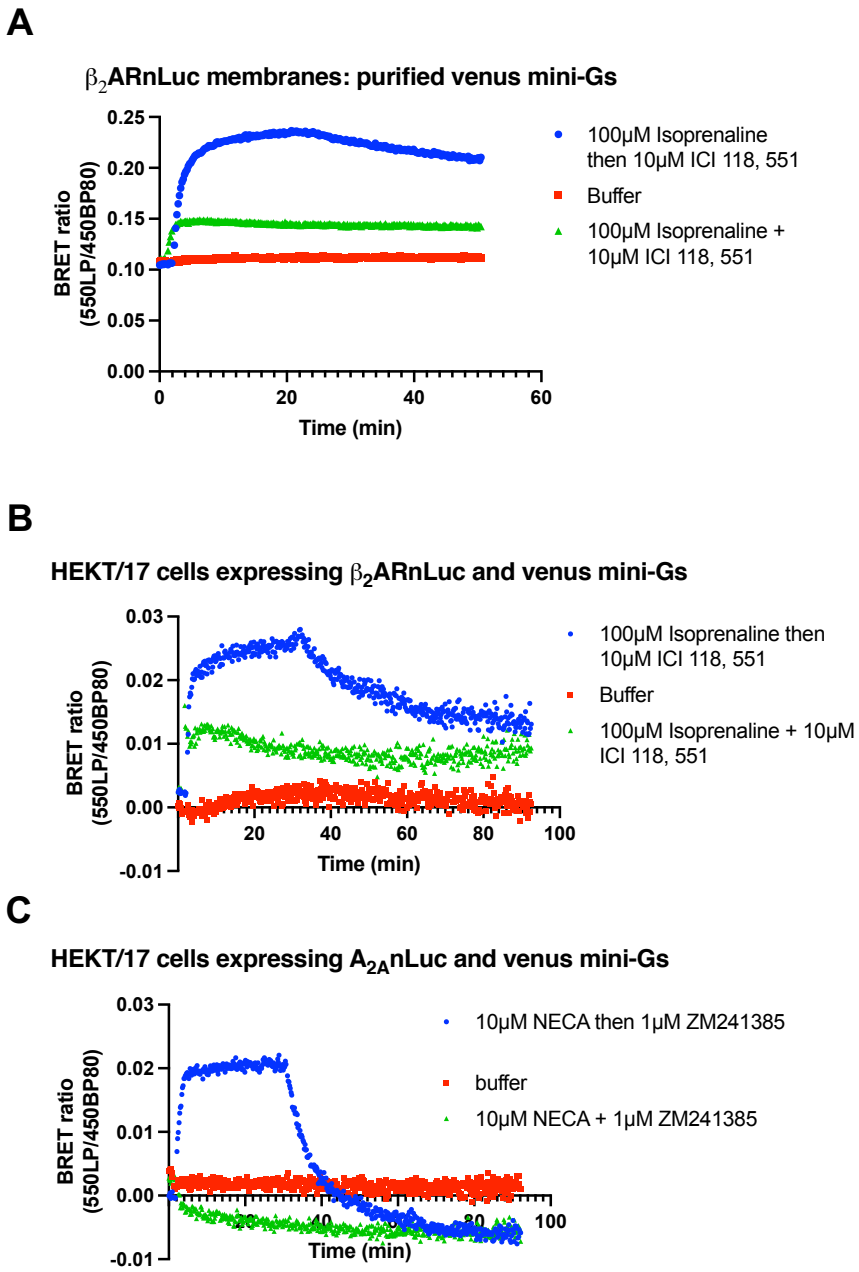

Figure 5.3.6: Characterising the association and dissociation of venus-mini-G_s binding to A_{2A}nLuc and TS-SNAP-β_2ARnLuc in HEK293T/17 cells using nanoBRET, A) Association of purified venus-mini-G_s to TS-SNAP-β_2ARnLuc membranes using 100μM isoprenaline added using injectors at 3 min and dissociation using 10μM antagonist ICI 118, 551 at 20min **B)** Association of venus-mini-G_s to TS-SNAP-β_2ARnLuc in HEK293T/17 cells using 100μM isoprenaline added using injectors at 3 min and dissociation using 10μM antagonist ICI 118, 551

at 20min **C)** Association of venus-mini-G_s to A_{2A}nLuc in HEK293T/17 cells using 10μM NECA and dissociation using 10μM ZM241385. NanoBRET between venus-mini-G_s and TS-SNAP-β_2ARnLuc or A_{2A}nLuc was read on PHERAstar FSX, at room temperature, using LUM 550LP/450-80nm module All figures show representative raw data from duplicate wells, of n=3.

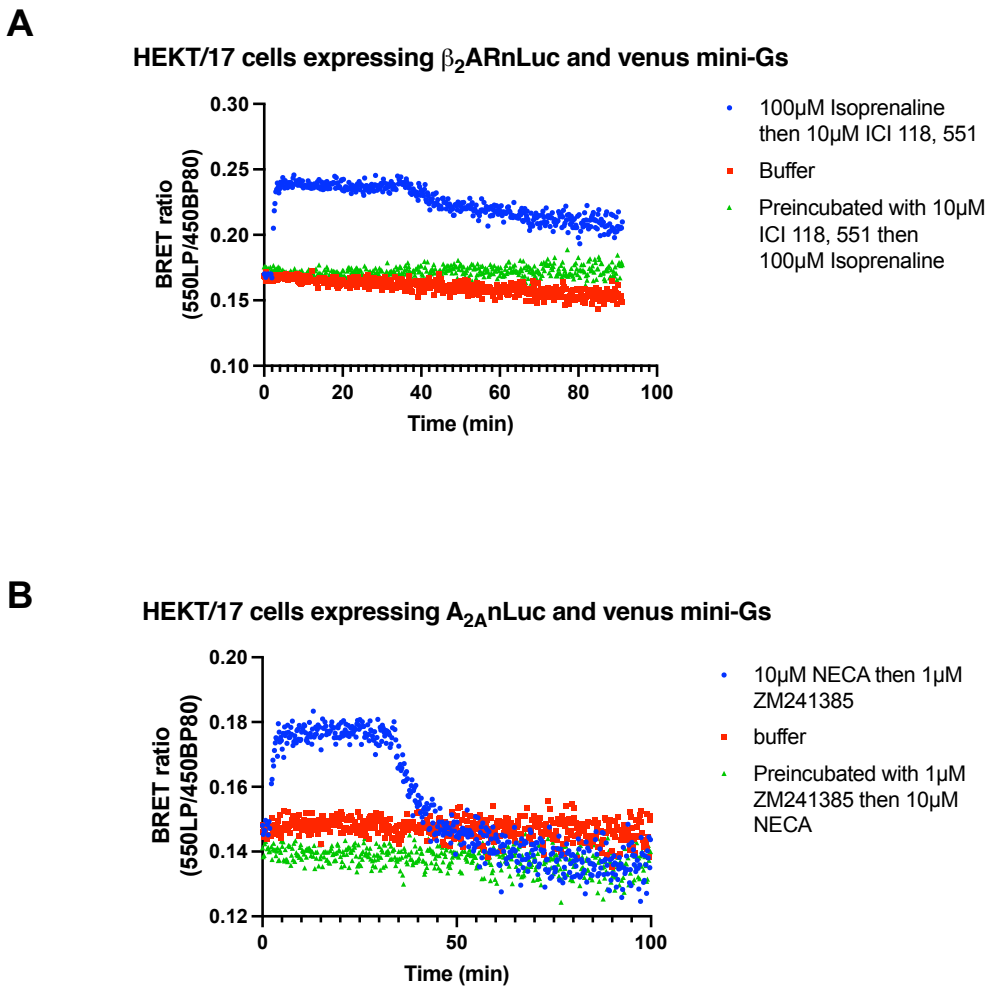

Figure 5.3.7 Investigating agonist induced recruitment of venus mini-G_s following antagonist 20min preincubation to A) Association of venus-mini-G_s to TS-SNAP-β_2ARnLuc in HEK293T/17 cells using 100μM isoprenaline added using injectors at 3 min and dissociation using 10μM antagonist ICI 118, 551 at 20min **B)** Association of venus-mini-G_s to A_{2A}nLuc in HEK293T/17 cells using 10μM NECA and dissociation using 10μM ZM241385. NanoBRET between venus-mini-G_s and TS-SNAP-β_2ARnLuc or A_{2A}nLuc was read on PHERAstar FSX, at room temperature, using LUM 550LP/450-80nm module All figures show representative raw data from duplicate wells, of n=3.

Following the validation that the biphasic association and incomplete dissociation of venus-mini-G_s from TS-SNAP-β_2ARnLuc observed in the in-solution system was recapitulated in HEK293T/17 cells, this study investigated if the proportion of non-dissociating complexes changed over time. Figure **5.3.8A** shows the association of venus-mini-G_s to isoprenaline bound TS-SNAP-β_2ARnLuc membranes and then dissociation of the TS-SNAP-β_2ARnLuc:venus-mini-G_s complex using 33μM mini-G_s at varying time points since the start of the association. Figure **5.3.8B** shows a comparison of the dissociation at each time point normalised to its peak. Figure **5.3.8B** shows that there was no difference in the percentage of TS-SNAP-β_2ARnLuc:venus-mini-G_s complexes dissociated at varying time points up to 20 min after the association began. The proportion of TS-SNAP-β_2ARnLuc:venus-mini-G_s complexes dissociated at 30min was always similar to 60%, and there no statistically significant difference between the exact percentage dissociated when 33μM mini-G_s was added at 5, 10 or 20min ($p=0.09$, One-way ANOVA and Tukey's post-hoc comparison). The percentage TS-SNAP-β_2ARnLuc:venus-mini-G_s complexes dissociated when dissociation was initiated at 5, 10 or 20min is summarised in table **5.3.2.**

Initiation of dissociation	% of TS-SNAP-β_2ARnLuc:venus-mini-G_s complexes dissociated
5 min	64.1 ± 2.7
10 min	57.2 ± 0.5
20 min	56.2 ± 2.8

Table 5.3.2: A summary of the percentage of TS-SNAP-β_2ARnLuc:venus-mini-G_s complexes dissociated at 30 min when dissociation was initiated at 5, 10 or 20min post the initiation of complex association. NanoBRET between 333nM venus-mini-G_s and TS-SNAP-β_2ARnLuc membranes was read on PHERAstar FSX, at room temperature, using LUM 550LP/450-80nm module, Data show of n=3 ±SEM.

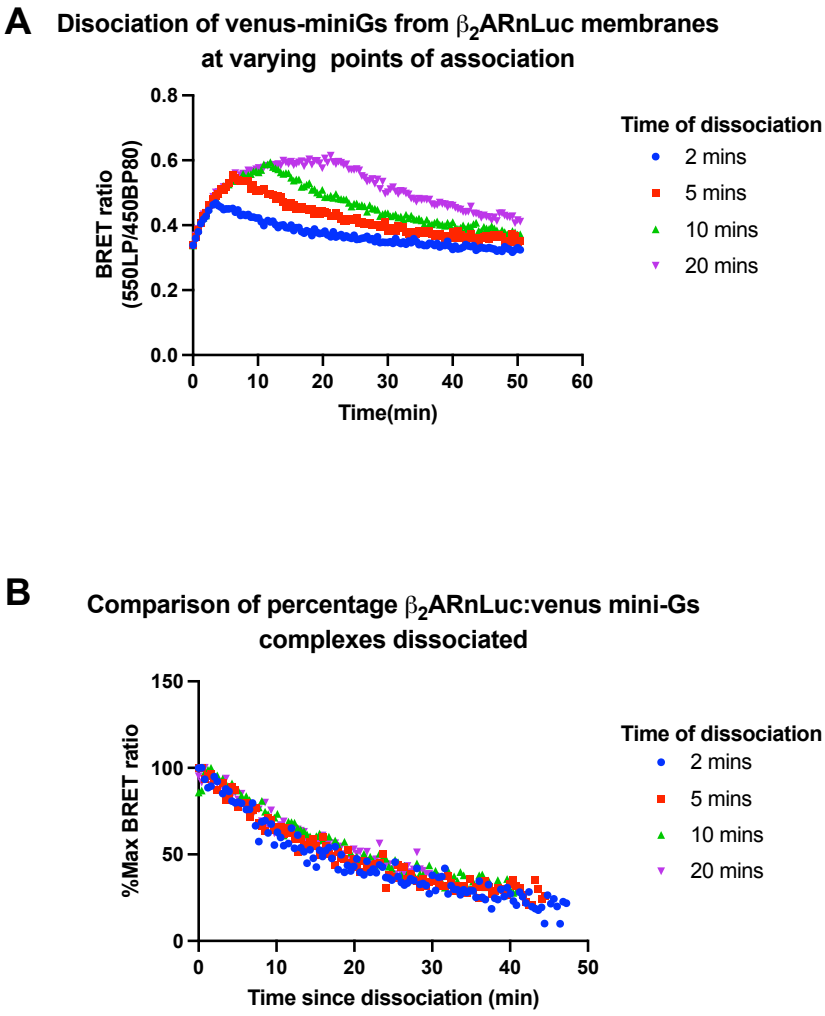

Figure 5.3.8 Investigating dissociation of the TS-SNAP-β2ARnLuc:Venus-mini-Gs complex after various association times, A) Total binding of venus-mini-Gs association to isoprenaline bound TS-SNAP-β2ARnLuc and dissociation at varying time points using mini-Gs, **B)** Comparison of dissociation of venus-mini-Gs from TS-SNAP-β2ARnLuc at varying time points show in 5.3.8A, each time point is normalized to the point of dissociation, All figures show representative raw data of n=3.

5.3.4 Investigation of purified venus-mini-G_s binding kinetics at DDM-TS-SNAP-β_2ARnLuc in complex with eight β_2AR agonists

Following the completion of the pharmacological and biophysical characterisation of venus-mini-G_s binding TS-SNAP-β_2ARnLuc, this study then aimed to investigate the kinetics of purified venus-mini-G_s binding to DDM solubilised TS-SNAP-β_2ARnLuc in response to agonists of different efficacies and kinetic profiles. To this end the ability of the eight β_2AR agonists characterized in chapter **4** to recruit venus-mini-G_s to DDM-TS-SNAP-β_2ARnLuc was investigated. Figure **5.3.9** shows all eight β_2AR agonists were able to recruit venus-mini-G_s to the DDM-TS-SNAP-β_2ARnLuc in rank order of their ligand binding affinities (chapter **4**). Indeed, for the agonists adrenaline (pki = 5.2±0.25 Vs pEC_{50} =5.8 ±0.4), noradrenaline (pki = 4.4± 0.09Vs pEC_{50} = 4.5±0.3), formoterol (pki = 7.8±0.07 Vs pEC_{50} = 8.0±0.2), isoprenaline (p*k*i = 6.4 ±0.12 Vs pEC_{50} =7.9 ±0.4), salbutamol (pki = 5.8±0.06 Vs pEC_{50} = 6.2±0.4), and salmeterol (pki =9.1 ±0.02 Vs pEC_{50} = 8.7±0.2), there was no difference between the pEC_{50} value obtained for venus-mini-G_s recruitment and ligand binding affinity values determined in chapter **4** (all P>0.05, unpaired t-test). In contrast, the agonists C26 (pki = 8.7±0.03 Vs pEC_{50} = 9.2±0.1, p=0.004) and BI-167107 (pki = 9.2±0.08 Vs pEC_{50} =8.6±0.1p=0.01) showed statistically significant differences in pEC_{50} and pK_i values.

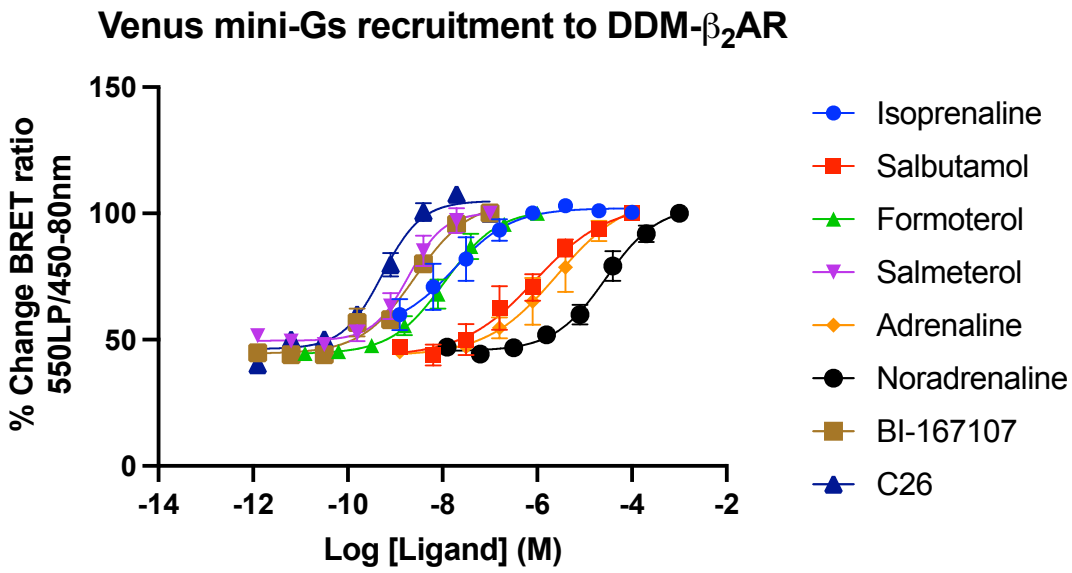

Figure 5.3.9: Venus-mini-G_s recruitment to DDM-TS-SNAP-β_2ARnLuc in response to increasing concentrations of eight β_2AR agonists: 1μM purified venus-mini-G_s was incubated with DDM-β_2ARnLuc and varying concentrations of isoprenaline, salbutamol, formoterol, salmeterol, adrenaline, noradrenaline, BI-167-107 or C26 at a final concentration 1% DMSO for 90min, before nanoBRET between TS-SNAP-β_2ARnLuc and venus-mini-G_s read on PHERAstar FSX, at room temperature, using LUM 550LP/450-80nm module. All curves show combined normalised data of n=3, error bars show ±SEM.

	pEC_{50}
Isoprenaline	7.9 ± 0.4
Salbutamol	6.2 ± 0.4
Formoterol	8.0 ± 0.2
Salmeterol	8.7 ± 0.2
Adrenaline	5.8 ± 0.4
Noradrenaline	4.5 ± 0.3
BI-167107	8.6 ± 0.1
C26	9.2 ± 0.1

Table 5.3.3: A summary of mean pEC_{50} values for purified venus-mini-G_s recruitment to DDM-TS-SNAP-β_2ARnLuc by various β_2AR agonists, nanoBRET between TS-SNAP-β_2ARnLuc and venus-mini-G_s read on PHERAstar FSX, at room temperature, using LUM 550LP/450-80nm module. pEC_{50} values show mean of n=3 individually fitted experiments ± SEM.

Finally, this study investigated the kinetics of venus-mini-G_s binding to the DDM-TS-SNAP-β_2ARnLuc bound to each of the eight β_2AR agonists. Saturating concentrations of each agonist, as defined by ligand binding studies (chapter **4**), were incubated with the DDM-TS-SNAP-β_2ARnLuc for 20-40min depending on the time ligand in question took to reach equilibrium (chapter **4**) at room temperature.

To investigate the rate of association of venus-mini-G_s to the agonist-DDM-TS-SNAP-β_2ARnLuc complex, the agonist-DDM-TS-SNAP-β_2ARnLuc complex was then added offline to a plate containing various concentrations of venus-mini-G_s proteins and nanoBRET measured immediately. As above unlabelled mini-G_s was used to define non-specific binding. After 20 min, a saturating concentration of 33μM mini-G_s was added to total wells, offline, to dissociate the DDM-TS-SNAP-β_2ARnLuc**:**venus-mini-G_s complex. For each experiment specific binding data was fitted to a two-site association and one phase dissociation (Figure **5.10)**. There was no difference in the percentage of the fast and slow phase of the association across the eight β_2AR agonist (appendix table **7.1.5**). For all compounds, the dissociation of the venus-mini-G_s from the agonist bound DDM-TS-SNAP-β_2ARnLuc was incomplete. The average percentage of complexes dissociated was very similar across the eight agonists, ranging from 72-80% (appendix table **7.1.6**). A one-way ANOVA test shown no statistically significant difference (p=0.47) between the percentage of complexes dissociated for the different agonists.

K_{obs} plots for K_{fast} and K_{slow} are shown in figures **5.3.11** and **5.3.12** respectively. K_{obs} plots for K_{slow} did not follow a linear relationship. K_{obs} plots for K_{fast} followed a linear relationship for the majority of plots and were used to calculate the K_{on} of $K_{fast.}$ Mean K_{on} of K_{fast} and K_{off} values were calculated from an average of n=3-4 experiments (Table **5.3.2)**. pK_d values for the venus-mini-G_s binding the agonist:DDM-TS-SNAP-β_2ARnLuc complex were obtained by fitting association data at 20 min to

a one-site saturation specific binding model as shown in figure **5.3.13.** Residence time was calculated as the reciprocal of K_{off}.

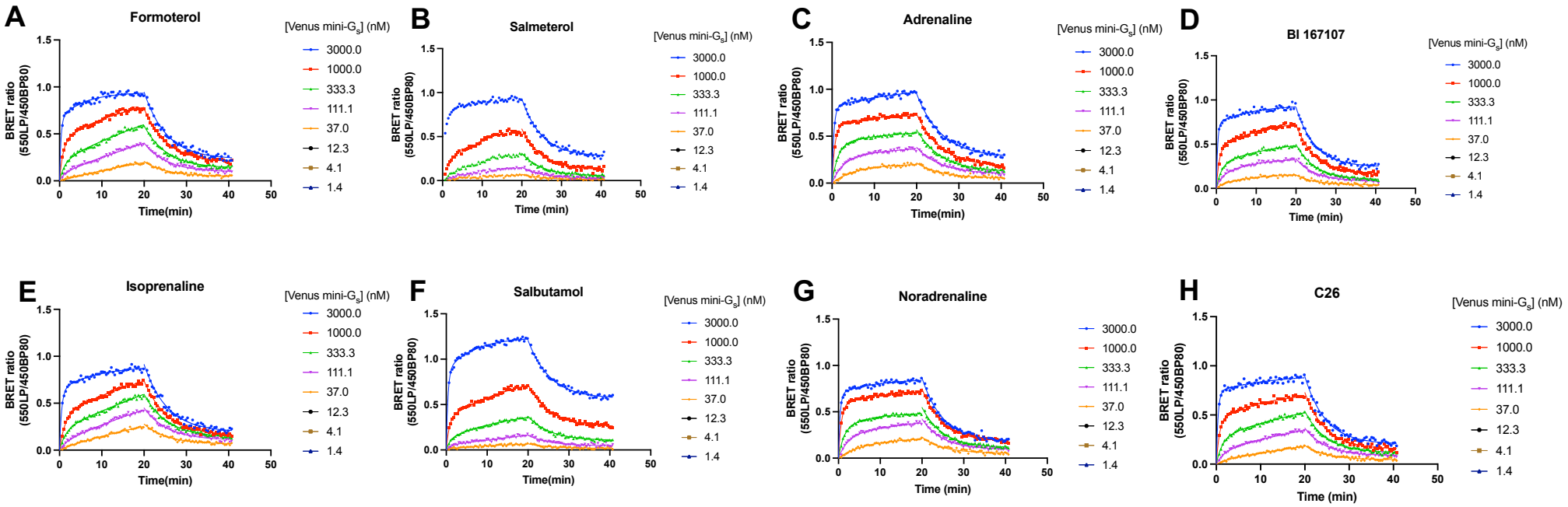

Figure 5.3.10: Investigation of the association and dissociation at 20min using 33μM mini-G_s, of venus-mini-G_s binding to DDM-TS-SNAP-β_2AR when preincubated with saturating concentration of A) Isoprenaline **B)** Formoterol **C)** Salbutamol **D)** Salmeterol **E)** Adrenaline **F)** Noradrenaline **G)** BI-167107 **H)** C26, using nanoBRET between DDM-TS-SNAP-β_2ARnLuc and venus-mini-G_s which was read on PHERAstar FSX, at room temperature, using LUM 550LP/450-80nm module. All figures show specific binding, where 30μM mini-G_s was used to define the NSB, representative raw data of n=3, fitted to a two-phase association and one phase dissociation.

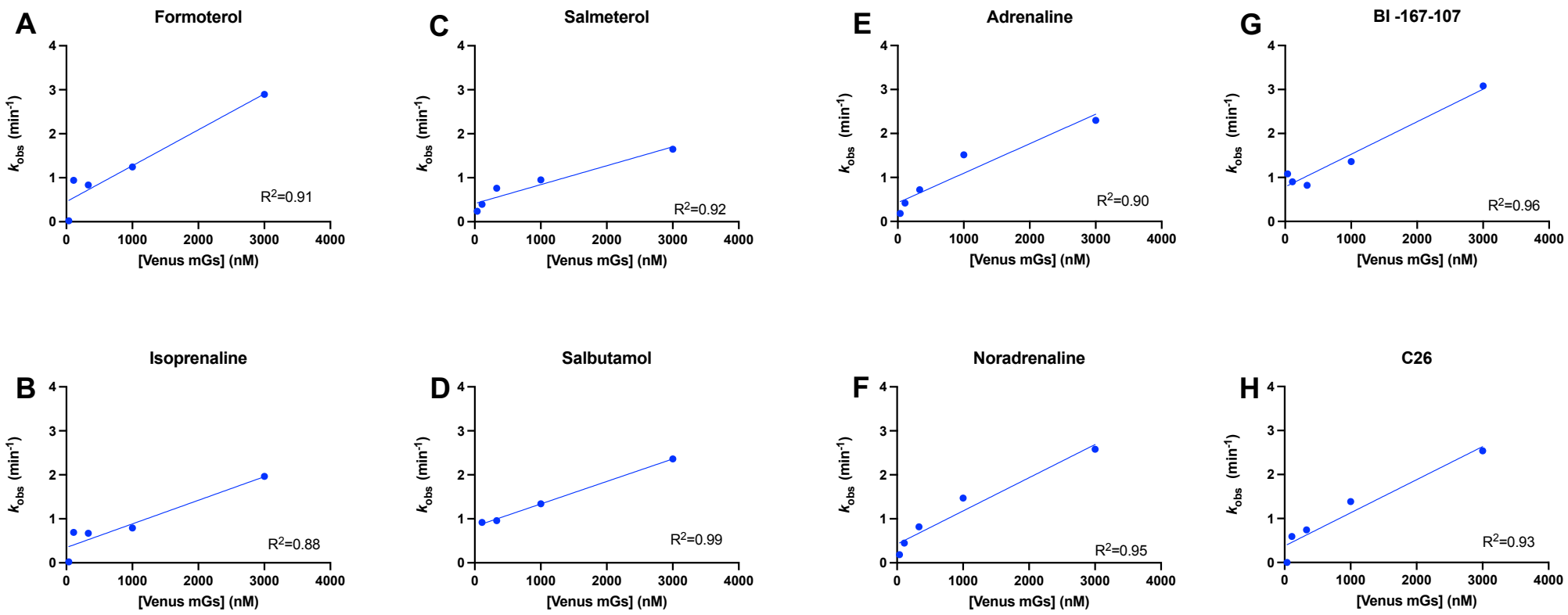

Figure 5.3.11: K_{obs} plots of K_{fast} for venus-mini-G_s association to DDM solubilised TS-SNAP-β_2AR bound to A) Isoprenaline **B)** Formoterol **C)** Salbutamol **D)** Salmeterol **E)** Adrenaline **F)** Noradrenaline **G)** BI-167107 **H)** C26, asscoication was read using nanoBRET between TS-SNAP-β_2ARnLuc and venus-mini-G_s which was read on PHERAstar FSX, at room temperature, using LUM 550LP/450-80nm module, K_{obs} of K_{fast} at each venus-mini-G_s concentration was obtained by fitting association to a two phase association model, All figures show representative raw data of n=3, fitted to a linear model.

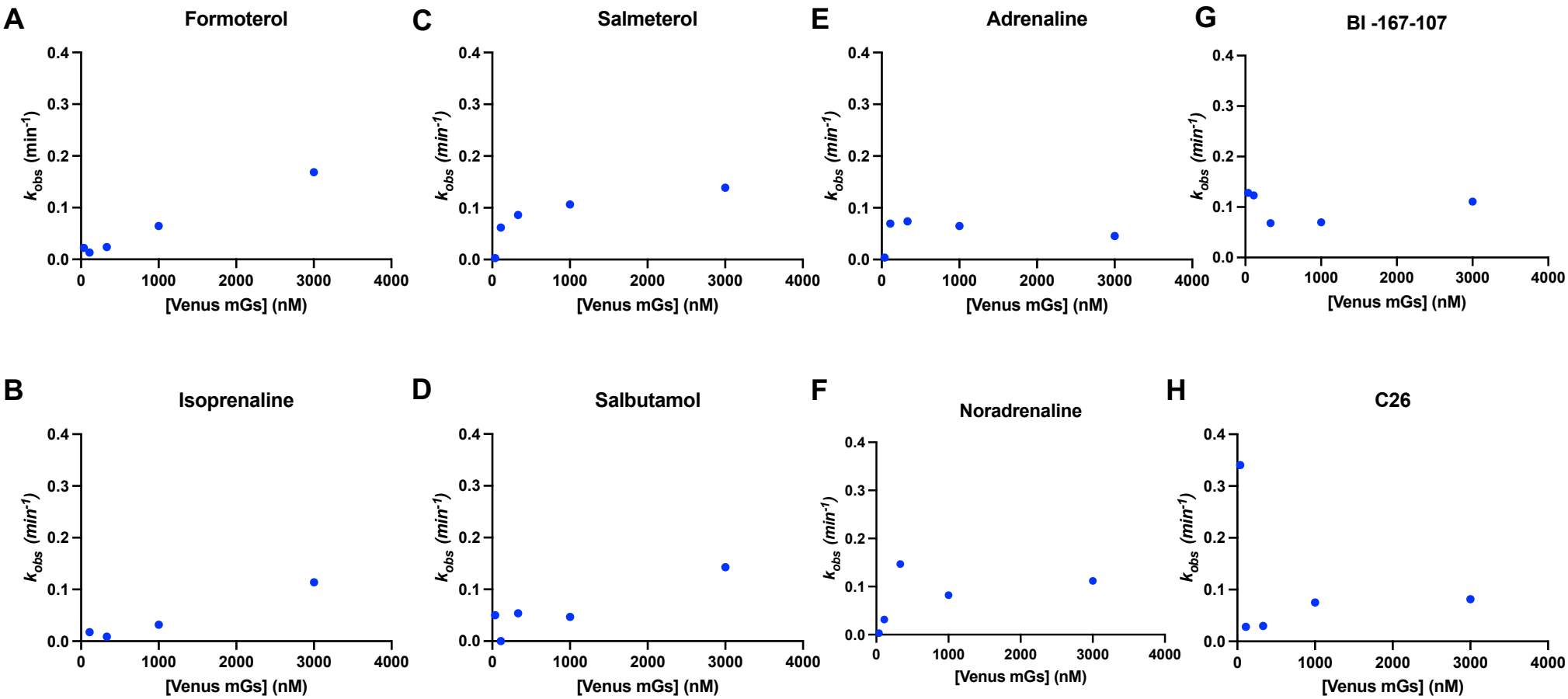

Figure 5.3.12: K_{obs} plots of K_{slow} for venus-mini-G_s association to DDM solubilised TS-SNAP-β_2ARnLuc bound to A) Isoprenaline **B)** Formoterol **C)** Salbutamol **D)** Salmeterol **E)** Adrenaline **F)** Noradrenaline **G)** BI-167-107 **H)** association was read using nanoBRET between TS-SNAP-β_2ARnLuc and venus-mini-G_s which was read on PHERAstar FSX, at room temperature, using LUM 550LP/450-80nm module, K_{obs} of K_{slow} at each venus-mini-G_s concentration was obtained by fitting association to a two phase association model, All figures show representative raw data of n=3.

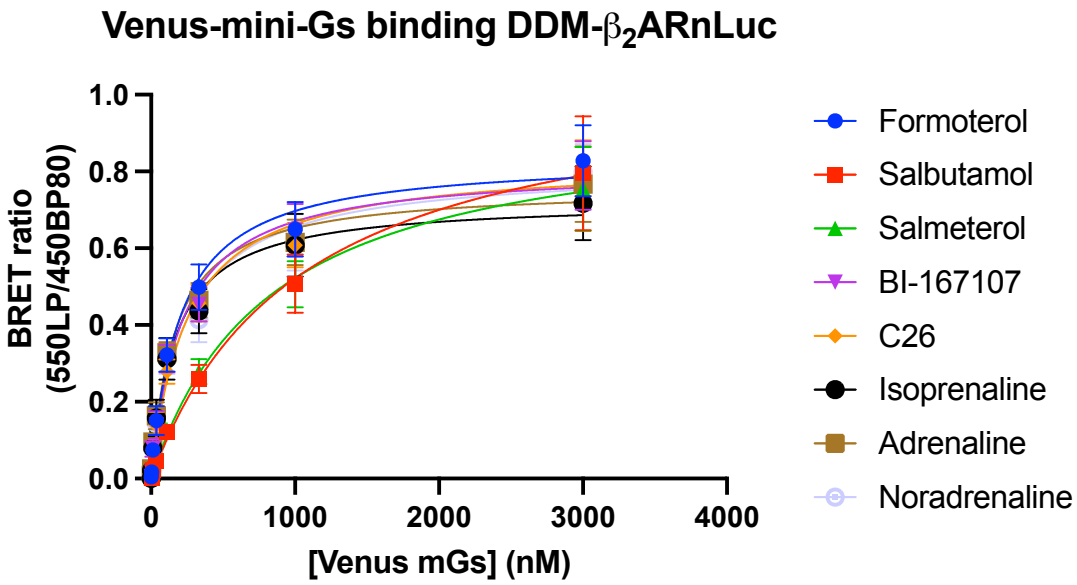

Figure 5.3.13: Specific saturation binding of increasing concentrations of purified venus-mini-G_s binding DDM-TS-SNAP-β_2ARnLuc in the presence of saturating concentrations of formoterol, salbutamol, salmeterol BI-167-107, C26, isoprenaline, adrenaline and noradrenaline. nanoBRET between TS-SNAP-β_2ARnLuc and venus-mini-G_s was read on PHERAstar FSX, at room temperature, using LUM 550LP/450-80nm module at 20min, Data is fitted to one-site specific binding model, Data points show mean of n=4 ± SEM.

Kinetic and affinity values for venus-mini-G_s binding agonist bound DDM-TS-SNAP-β_2ARnLuc nanoBRET assays are summarised in table **5.3.3.** pK_d values for venus-mini-G_s binding the DDM-TS-SNAP-β_2ARnLuc in response to all agonists were in the 100 nanomolar to micromolar range. However, there were 0.5-0.8 log units increased affinity for venus-mini-G_s binding the full agonist (adrenaline, noradrenaline, formoterol, isoprenaline, BI-167-107 and C26) bound DDM-TS-SNAP-β_2ARnLuc compared to the partial agonist (salbutamol and salmeterol) bound. These differences were statistically significant (one-way ANOVA and Tukey's post hoc). Agonist efficacy to activate the G_s protein is defined in chapter **4**. Table **5.3.3** shows K_{on} of K_{fast} values for venus-mini-G_s binding agonist bound DDM-TS-SNAP-β_2ARnLuc were in the range of 3.4±0.64 $x10^5$ Mol^{-1} Min^{-1} to 9.19± 0.26 $x10^5$ Mol^{-1} Min^{-1}.

A one-way ANOVA showed that this variation in range was statistically significant (p=0.03), but Tukey's multiple comparison test shown no statistically significant difference in pairwise comparisons. There was very little variation in K_{off} values for venus-mini-G_s dissociating from the agonist bound DDM-TS-SNAP-β_2ARnLuc, table **5.3.3** shows a range of 0.17 to 0.21 $min^{-1.}$ Subsequently residence times for the venus-mini-G_s were all approximately 5 minutes, (Table **5.3.3**).

	pK_d	K_{off} (Min^{-1})	K_{on} (of k_{fast}) (Mol^{-1} Min^{-1})	Residence time (Min)
%BI-167107	6.7 ±0.03	0.21 ±0.003	7.29 ± 2.16 x10^5	4.76
%C26	6.6 ±0.03	0.21 ±0.004	7.80 ± 2.32 x10^5	4.76
%Formoterol	6.7 ±0.05	0.20 ±0.011	4.59± 1.64 x10^5	5.00
%Isoprenaline	6.8 ±0.07	0.17 ±0.004	9.19± 0.42 x10^5	4.76
%Adrenaline	6.8 ±0.05	0.18 ±0.014	8.56± 0.13 x10^5	5.50
%Noradrenaline	6.6 ±0.08	0.19 ±0.007	7.92 ±0.56 x10^5	5.20
$Salbutamol	6.0 ±0.07	0.20 ±0.006	3.36±0.64 x10^5	5.00
$Salmeterol	6.1 ±0.09	0.21 ±0.006	4.18±1.2 x10^5	4.76

Table 5.3.3: A summary of the mean pK_d, K_{off} , K_{on} (of K_{fast}) and residence time values for venus-mini-G_s proteins binding the DDM solubilised TS-SNAP-β_2AR bound to the β_2AR agonists BI-167107, C26, formoterol, isoprenaline, adrenaline, noradrenaline, salbutamol and salmeterol, as measured by nanoBRET, values show mean of n=3-4 experiments ± SEM. %denotes full agonist and $partial agonist, as defined by CASE G_s activation assay (chapter **4**).

5.4 Discussion

The aim of this chapter was to produce purified fluorescently labelled mini-G_s proteins and investigate the kinetics of mini-G_s protein binding to β_2AR bound agonists different potencies and kinetics profiles. The pharmacology of these eight β_2AR agonists had been characterised in chapter **4.**

5.4.1 Mini-G_s proteins produced in this study bound TS-SNAP-β_2AR in response to agonists stimulation

This study produced semi-pure unlabelled, venus and halo N terminal tagged mini-G_s proteins from *E. coli* using IMAC. Commonly another purification step would be required to purify a protein to homogeneity. Although it was demonstrated that these proteins could be purified to homogeneity using secondary gel filtration step, this was not possible in this study due to COVID-19 restrictions. Consequentially, these semi-pure protein preparations were used in this study. This study demonstrated confirmed mini-G_s proteins produced in this study were functional as they bind the DDM-β_2AR in response to agonist stimulation and their interactions with the β_2AR was similar to that in mammalian cells, this supports use of these mini-G_s preparations in our study.

Saturation binding data for increasing concentrations of purified venus-mini-G_s binding TS-SNAP-β_2ARnLuc membranes in the absence and presence of the agonist isoprenaline showed no constitutive activity of the β_2AR. This was also the case in mammalian cells. Whilst our study showed no β_2AR constitutive activity, Lamichhane and colleagues (Lamichhane et al., 2015) use single molecule FRET to show that 31% of unbound β_2AR are in the active state when β_2AR are isolated in synthetic nanodiscs. However, differences in basal activity in different systems are often due to receptor number and expression. Indeed, Bond and colleagues (Bond et al.,) show that β_2AR overexpression increases β_2AR constitutive activity in rat atria. It therefore seems likely that, the

ratio of β_2AR to venus-mini-G_s is too low to see constitutive activity in our system.

Moreover, the ability of a series of eight β_2AR agonists (characterised in chapter **4**) to recruit purified venus-mini-G_s to the DDM solubilised TS-SNAP-β_2ARnLuc was investigated using nanoBRET. These compounds all recruited venus-mini-G_s with potencies that matched their affinity values. The pEC_{50} values obtained of 6.7±0.6 for isoprenaline was similar to that of 6.9 shown by (Wan et al., 2018). The similarity of pEC_{50} to pK_i values suggest a 1:1 relationship between ligand binding and venus-mini-G_s binding in this non-amplifying system.

5.4.2 N terminal fusion tags decreased mini-G_s affinity for TS-SNAP-β_2ARnLuc

Next, this study investigated the binding affinity of the venus-mini-G_s, mini-G_s and Halo-mini-G_s for the Isoprenaline bound TS-SNAP-β_2AR, using nanoBRET. To our knowledge this was the first study to investigate the affinity of a mini-G protein for a GPCR, this study showed that mini-G_s binds isoprenaline bound TS-SNAP-β_2AR with a pK_d of 8.33±0.14. It was not possible to find any literature investigating the affinity of the full length G_s protein for the β_2AR or agonist bound β_2AR.

Moreover, this study showed pK_d values of 7.65±0.11 and 7.28±0.15 for venus-mini-G_s and halo-mini-G_s respectively binding the isoprenaline bound TS-SNAP-β_2AR. This decrease in affinity was consistent across protein preparations and so is most likely due to the addition of the N terminal tags to the mini-G_s. Considering the proximity of the mini-G_s N terminus to the GPCR coupling interface it seems likely that addition of an N terminal fusion protein would have this affect. This difference in affinity was accounted for in the design of kinetics studies, where 33μM mini-G_s was calculated to be adequate to displace 3μM venus-mini-G_s considering its increased affinity.

5.4.3 Venus-mini-G_s association to TS-SNAP-β_2ARnLuc is biphasic and dissociation is incomplete

This study characterised the association and dissociation of the purified venus-mini-G_s proteins from the agonist bound DDM-TS-SNAP-β_2ARnLuc (Figure **5.3.4**). This study showed a biphasic association and incomplete dissociation of this complex both in this purified protein system and mammalian cells. Similarly, Wan and colleagues (Wan et al. 2018) also use ICI 118, 551 show to incomplete dissociation of the venus-mini-G_s protein from the agonist bound β_2AR-cerulean in HEK cells after 3 minutes. Although Wan and colleagues state that this complex dissociated after 15 minutes this data is not shown and so this study largely supports the findings that dissociation of venus-mini-G_s from TS-SNAP-β_2ARnLuc was incomplete. Moreover, Wan and colleagues showed rapid (<3 min) and complete dissociation of venus-mini-G_{si} and venus-mini-G_{sq} from muscarinic acetylcholine receptor 4 (M4) and muscarinic acetylcholine receptor (M3) receptors respectively. This, in combination with the fact that venus-mini-G_s could be fully dissociated from the A_{2A}R in our study suggests that this incomplete dissociation is specific to the β_2AR-venus-mini-G_s complex (Figure **5.3.6**).

Following the finding that association of the venus-mini-G_s to the β_2AR is biphasic and dissociation is incomplete, this study sought to further understand the mechanism behind this. Analysis of these data showed that ~70% of the association could be accounted to the fast phase, and likewise ~70% of complexes could be dissociated. Suggesting that the fast-binding phase binds reversibly and the slow irreversibly. Figure **5.3.8** shows that the percentage of TS-SNAP-β_2ARnLuc-venus-mini-G_s complexes that are dissociable is not time dependent, this suggests that the two components occur simultaneously. This observation that the slow component is irreversible is furthered by the finding that the K_{obs} plots corresponding to the slow component are not linear.

The identity of these two components not understood, whilst the fast and reversible state was expected, the slow and irreversible state could correspond to a very high affinity or stable complex. Chapter **4** shows that the high affinity state of DDM-TS-SNAP-β_2AR can be induced in this system and under these buffer conditions, which include 150mM NaCl by Halo-mini-G_s binding, despite it being generally stipulated that the physiological sodium concentration used prevents the high affinity state (Zarzycka et al., 2019). The physiological mechanism for there being two different states in this system remains to be elucidated.

Moreover, Galés and colleagues (Galés et al., 2005) used a similar BRET assay to investigate full length G_s protein dissociation from isoprenaline bound β_2AR-RLuc in response to the antagonist ICI 118, 551 in HEK293T cells and show dissociation of the G_s protein occurs completely and in the order of seconds. Considering this, with the findings of this study, it seems likely that the interaction of mini-G_s with the β_2AR differs from that of the full length G_s protein because of its modification from the wild type G_s alpha protein, for example forming a more stable complex. Whilst the mechanism of agonist-β_2AR-mini-G_s complex formation is not fully understood the fast and reversible component of its binding seemed most relevant and relatable to β_2AR-G_s protein interactions and so this study chose to study this component in relation to β_2AR-G_s protein kinetics in response to agonist of differing efficacies. However, a major limitation of this study is the incomplete understanding of the two phase β_2AR-mini-G_s interaction in our system.

5.4.4 Full agonists increased the affinity of DDM-TS-SNAP-β_2ARnLuc for the venus-mini-G_s protein

Finally, this study investigated the kinetics and affinity of venus-mini-G_s binding to the DDM-TS-SNAP-β_2ARnLuc when bound to the eight β_2AR agonists above (Table **5.3.3)**. These data showed no difference in the K_{off} or corresponding residence time of the venus-mini-G_s for the receptor when bound to the different agonists. There were statistically significant differences in the affinity of the venus-mini-G_s for the full agonist bound DDM-TS-SNAP-β_2ARnLuc compared to the partial agonist bound DDM-TS-SNAP-β_2ARnLuc. These differences appeared to be driven by an increase in the K_{on} of K_{fast}, although these were only small differences. This data, does not, therefore suggest a role for kinetics in the molecular basis of efficacy but suggests a model whereby full agonist stabilise a conformation of the receptors which is more likely to recruit the venus-mini-G_s protein, but once bound to the receptor there is no conformational difference in the agonist-DDM-TS-SNAP-β_2ARnLuc-venus-mini-G_s complex. As mini-G proteins sense the active states of the GPCR, an agonist-receptor complex being more likely to recruit a mini-G protein suggests that the agonist-receptor complex is more likely to be in the active state.

These data provide no evidence for a role of kinetics in the molecular basis of efficacy. This conformational model is supported by data from hydrogen/deuterium exchange mass spectrometry (HDMS) and hydroxy radical foot printing mass spectrometry (HDX) (Du et al., 2019), whereby the conformational changes involved in β_2AR to full length G_s protein complex formation are investigated. This study showed that the conformation of the initial β_2AR-G_s structure differs from that of the full formed nucleotide free β_2AR-G_s complex. Furthermore, nuclear magnetic resonance (NMR) studies (Manglik et al., 2015; Nygaardet al., 2013), show that the agonist BI-167-107 alone is not enough to fully

stabilise β_2AR in the active state and the nanobody 80 is required to fully stabilise the active state. These data support our findings that the conformation of the agonist-β_2AR complex differs from that of the agonist-β_2AR-mini-G_s although it was not possible to find any biophysical studies examining differences in the conformation of the β_2AR bound to such a range of agonists.

Naturally, structural studies of the agonist bound β_2AR or other class A GPCRs have only been possible in the presence of a G protein mimetics (Rasmussen et al., 2011a). Only small differences in the conformations of these active structures have been observed and these do not seem to explain differences in efficacy (Katritch et al., 2009) and so support our finding that there was no difference in the agonist-β_2AR-mini-G_s conformation.

Conclusion:

In summary, this study generated purified fluorescently labelled mini-G_s proteins and investigated the kinetics and affinity of their binding to the DDM-TS-SNAP-β_2ARnLuc when bound to agonists of different efficacies and binding kinetics. These studies showed small differences in the affinity of full agonist-β_2AR complexes for venus-mini-G_s compared to partial agonist-β_2AR complexes driven by an increased K_{on} supporting a model for different agonist-β_2AR conformations in the molecular basis of efficacy.

Chapter 6
General discussion

6.1 General discussion

The β_2AR is a prototypical class A GPCR and an essential therapeutic target in asthma, whereby β_2AR agonists cause smooth muscle relaxation. As such, a large range of agonists have been developed for the β_2AR of differing kinetic and efficacious properties (Baker, 2005) (Rosethorne et al., 2016) (Sykes & Charlton, 2012) . Moreover, the β_2AR, has become one of the most well studied GPCRs with many structural (Masureel et al., 2018) (Rasmussen, Devree, et al., 2011b) (Wacker et al., 2010) and biophysical studies (Gregorio et al., 2017) (Liu et al., 2013) into its mechanism of activation. Despite these studies, and the broadly recognised therapeutic importance of GPCRs, the molecular basis of efficacy at the β_2AR and other GPCRs is far from understood. The hypothesis underlying this study was that ligand residence time effects β_2AR receptor conformational dynamics to affect G_s protein activation efficacy. As such, the aim of this thesis was to investigate the correlations between agonist binding kinetics, β_2AR conformational dynamics and agonist ability to induce G_s activation at the β_2AR. An increased understanding into the molecular basis of efficacy at the β_2AR and GPCRs could aid more rational drug design at the molecular level. This thesis shows the development of novel methods to investigate this and concludes that there is no role for kinetics in the molecular basis of efficacy at the β_2AR.

6.1.1 DIBMALPs but not detergent affected β_2AR function

(Zhao & Furness, 2019)(Zhao & Furness, 2019) It's appreciated that receptor signalling is greatly influenced by cellular context. For example, components of the cell membrane (Paila et al., 2011) (Strohman et al., 2018), protein expression levels (Zhao & Furness, 2019), and spatio-temporal regulation (Halls et al., 2016) can all influence receptor pharmacology and signalling. Consequentially, this study chose to consider β_2AR pharmacology in isolation from the cell to investigate β_2AR function exclusively at the molecular level. Classically, isolation of

membrane protein has employed detergents, which poorly recapitulate the plasma membrane and compromise protein function and stability. The first aim of this study was therefore to investigate the applicability of the polymer DIBMA to extract the β_2AR from mammalian cells. Polymers, such as DIBMA incorporate into the cell membranes and self-assemble into lipid particles containing the membrane proteins along with their native phospholipids. As such the native environment and stability of the membrane is maintained

The first chapter (**Ch. 3**) of this study shows that the polymer DIBMA can be used to extract the β_2AR from the mammalian cell membrane and that the β_2AR retains its ligand binding capability and native conformational landscape in the DIBMALP. Moreover, **Chapter 3** also shows improved thermostability of DIBMALP-β_2AR compared to use of the conventional detergent DDM. However, for reasons not understood, when inside the DIBMALP, β_2AR did not couple to the Halo-mini-G_s protein. This study therefore employed the detergent DDM to extract the β_2AR for ligand and mini-G_s binding experiments.

Whilst use of detergents over a more physiologically relevant nanodiscs could be a criticism of this study, **chapter 3** carefully validates how pharmacology and function is affected for DIBMALP-β_2AR but not DDM-β_2AR. This study therefore furthers our understanding of how receptor environment can affect pharmacology. Indeed, whilst several studies have shown how the conformational dynamics of SMALP encapsulated protein may differ from that of the native protein (Mosslehy et al., 2019) (Routledge et al., 2020), few studies have been able to show intracellular coupling of GPCRs to signalling proteins in native nanodiscs. To our knowledge, this is the first study to directly compare a GPCR coupling to its intracellular transducer in different solubilisation environments and show that intracellular coupling is affected in native nanodiscs. The reason for the DIBMALP-β_2AR not coupling to the Halo-mini-G_s protein is not understood, although it could be due to

conformational restriction of the β_2AR inside the DIBMALP or perhaps other steric hinderance. Overall, this study furthers our understanding of how difference solubilisation methods, particularly native nanodiscs, can affect receptor function.

6.1.2 Demonstration of novel methods to characterise membrane protein preparations

Moreover, characterisation of membrane protein preparations has traditionally used methods and techniques that are low-throughput and require protein purification (Miljus et al., 2020). For example, in-gel fluorescence based thermostability assays or DSF as discussed in sec **3.1.** This has greatly hindered advances in membrane protein preparation. This study has demonstrated a novel approach to characterising solubilised, but not purified GPCRs by specifically labelling the N-terminus of the receptor with the TR-FRET donor Lumi4-Tb and employing TR-FRET technology to investigate stability and functionality. As well as eliminating the requirement for protein purification this approach is also much higher throughput, utilising 96 or 384 well plate formats, therefore greatly decreasing the labour involved in a single preparation and increasing the number of conditions that can be screened at once. This thesis therefore demonstrates advances in the approaches and technologies involved in membrane proteins preparations. It is hoped that more widespread application of these ideas and techniques within the GPCR field and beyond will improve the membrane protein preparation and therefore the ability to perform biophysical studies on isolated membrane proteins.

6.1.3 Agonist residence time did not correlate with efficacy at the β_2AR

Chapter **4** shows the pharmacological characterisation of eight agonists of the β_2AR. We determined their ligand binding kinetics and efficacy to activate the heterotrimeric G_s protein and concluded that for these eight agonists there was no correlation between ligand residence time and efficacy at the β_2AR. This finding is in agreement with Louvel and colleagues (Louvel et al., 2014) who show that there is no correlation between ligand residence time and efficacy at the A_3 receptor. However, a positive correlation has been shown between the efficacy of seven agonists at the M3 muscarinic receptor, and ten agonists at the A_{2A} receptor and their ligand residence time (Sykes, et al. 2009) (Guo et al., 2012). Taken together, these studies suggest that ligand residence time could be an important determinant of efficacy for some ligands and receptors but not the only determinant. Therefore, implying that there may not be a general mechanism for efficacy.

6.1.4 Agonist efficacy correlated with likelihood to recruit mini-G_s at the β_2AR

Once the efficacies of the eight β_2AR agonists had been fully characterised, this study investigated the kinetics of venus-mini-G_s binding to the β_2AR following preincubation with saturating concentrations of each ligand (**Ch. 5**). These data showed small differences in K_{on} (of K_{fast}) and pK_d values for venus-mini-G_s binding the β_2AR bound to different agonists, but no difference in $K_{off.}$ This suggests differences in the likelihood of different agonist-β_2AR complexes to recruit the venus-mini-G_s, but that once the agonist-β_2AR-venus-mini-G_s complex is assembled there is no difference in the β_2AR conformation. Comparison of these K_{on} (of K_{fast}) and pK_d values for venus-mini-G_s binding β_2AR with efficacy values from the operational model for G_s activation for each of the eight β_2AR agonists (Figure **6.1**) showed a moderate correlation between ligand efficacy (τ) and mini-G_s K_{on} of K_{fast} (R^2=0.58, p=0.07) and a moderate correlation between ligand efficacy (τ) and mini-G_s K_{on} (R^2=0.50, p=0.11). Therefore, suggesting that the

differences in agonist-β_2AR complexes to recruit the venus-mini-G_s could be explained by differences in agonist efficacy.

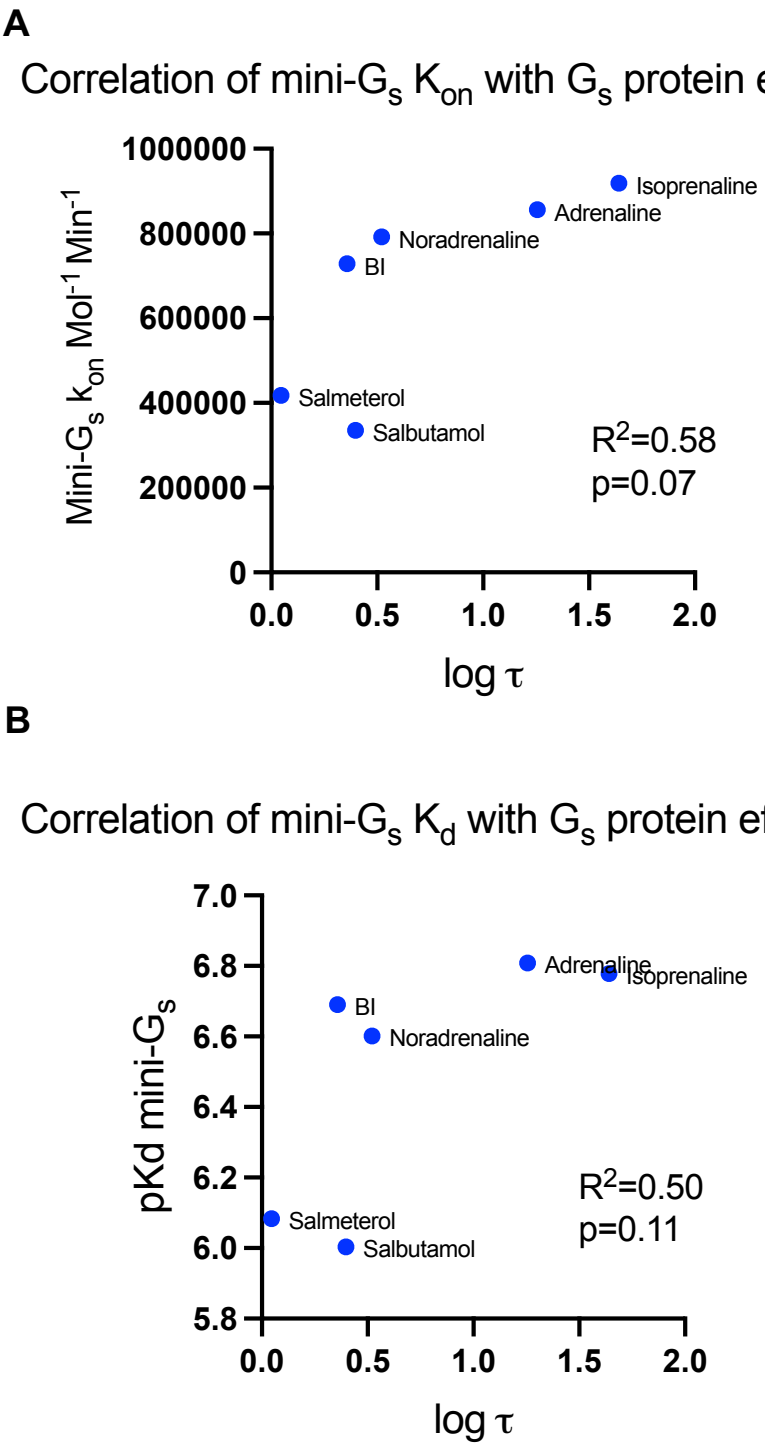

Figure 6.1: Correlation of CASE G_s activation efficacy τ with A) mini-G_s pK_d and B) mini-G_s $K_{on(fast)}$, τ values were obtained from fitting the operational model on individual data sets with fixed K_A values, correlations were made using Pearson's correlation coefficient, on replicates from n=3-4 experiments for pK_d, $K_{on(fast)}$ and τ values.

These data therefore support a model (Figure **6.2**) in which ligands of higher efficacy stabilise a conformation of the β_2AR that is more likely to recruit the G_s protein, but once bound there are no differences in the conformation of β_2AR in the agonist-β_2AR-mini-G_s complex. These data, therefore, supports an argument for differing receptor conformations in the molecular basis of efficacy, as opposed to receptor, ligand or G_s protein binding kinetics.

This conformational model is supported by Du and colleagues (Du et al., 2019), who investigated the conformational changes involved in β_2AR to full length G_s protein complex formation. They show that the conformation of the initial β_2AR-G_s structure differs from that of the full formed nucleotide free β_2AR-G_s complex. Furthermore, nuclear magnetic resonance (NMR) studies (Manglik et al., 2015) (Nygaard et al., 2013), show that the agonist BI-167-107 alone is not enough to fully stabilise β_2AR in the active state and the nanobody 80 is required to fully stabilise the active state.

Conversely, several studies (Gregorio et al. 2017) (Nikolaev et al., 2006) have implicated a role for kinetics in the molecular basis of efficacy. These studies show correlations between ligand efficacy, rate or extent of receptor activation and GTP turnover at the α_{2A} or β_2AR. Whilst these studies led to the hypothesis underpinning this study, these studies could also be interpreted as supporting the conformational model of efficacy suggested by our study. These studies both use FRET to investigate receptor dynamics and differences in intermolecular FRET could be caused by either a difference in the rate of receptor activation or in conformational differences.

Moreover, structural studies of the agonist bound β_2AR or other class A GPCRs have only been possible in the presence of a G protein mimetics (Rasmussen et al., 2011a). Only small differences in the conformations of these active structures have been observed and these do not seem to explain differences in efficacy (Katritch et al., 2009) and

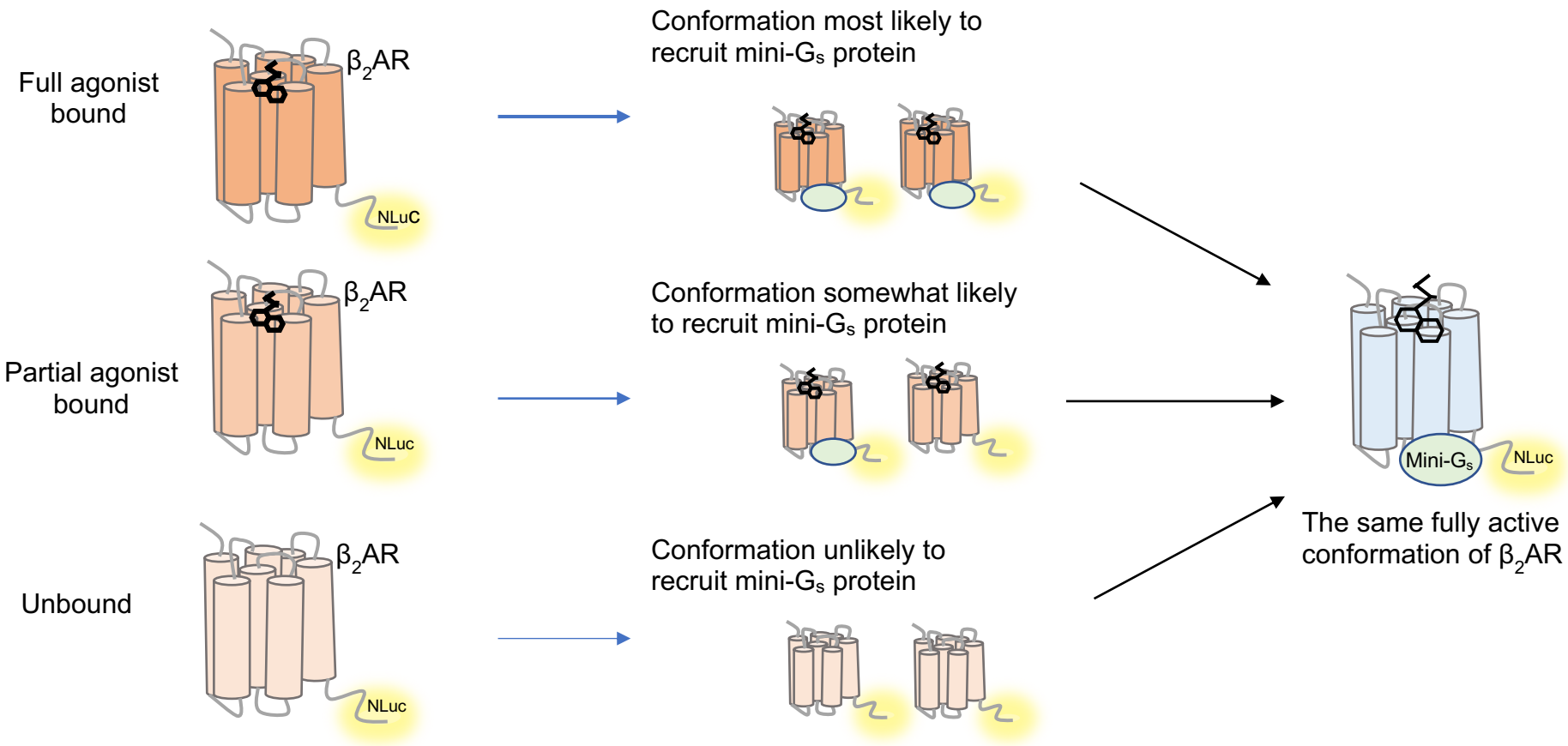

Figure 6.2: A summary of the conformational model of efficacy proposed by this study: agonists of higher efficacy induce a conformation of β_2AR that is more likely to recruit a mini-G_s protein but once bound there is no difference in the β_2AR conformation within the agonist-β_2AR-mini-G_s complex.

support our finding that there was no difference in the agonist-β_2AR-mini-G_s conformation.

6.1.5 Future work

Overall, the main finding of this study was that for these β_2AR agonists at least at the biophysical level, efficacy appeared dependent upon the agonist induced conformation of the β_2AR. Moreover, although there were moderate correlations in G_s activation efficacy and mini-G_s binding data sets, the differences for the eight agonists used, within each data sets were small. Therefore, whilst supported by other studies, these results should be interpreted with caution, considering this, future work should focus on the applicability of this model to a greater range of agonists and GPCRs. It would be particularly interesting to investigate the agonists used by Guo and colleagues (Guo et al., 2012) and Sykes and colleagues (Sykes et al., 2009) as, in contrast to our study, the ligand residence time of the agonists used in these studies was shown to correlate positive with efficacy. Exploration of the applicability of this study to these, and other agonists and receptors would aid understanding of whether there is a general mechanism of efficacy or can be a variety of reasons for efficacy.

Moreover, this study investigated ligand and mini-G_s binding kinetics to the β_2AR in the DDM micelle, therefore considering β_2AR dynamics in isolation from the regulation of the cell. Whilst this approach answers the questions posed in this study at the biophysical level, further work should investigate if the findings of this study are applicable in the native cell environment. Interestingly, Sungkaworn and colleagues (Sungkaworn et al., 2017) investigated the K_{on} and K_{off} of $G\alpha_i$ binding to the α2A receptor in CHO cells in response to a range of agonists using single molecule microscopy and show efficacy is at least partially correlated with K_{on} but not K_{off}. Taken together with this study, this suggests that the conformational model of efficacy proposed in here is relevant to the α2A receptor in the cell environment. Future work could

investigate if this is the case for the eight β_2AR agonists used in this study and other ligands and receptors.

Moreover, particularly if the conformational model of efficacy proposed in this study proved relevant to other agonists and GPCRs, further studies could investigate the conformational differences in the β_2AR when bound to the full range of agonists shown in this study. This could take place using NMR or molecular dynamics simulations. This would show the receptor conformation most likely to recruit and therefore activate G_s protein, understanding this could aid drug design. As discussed above, limitations in structural biology mean that agonist bound GPCR complexes can currently only be obtained in complex with the G protein.

6.2 General conclusion

In summary, this thesis shows the development of novel systems and approaches to study the pharmacology of the isolated β_2AR. Specifically, this study employs alternative approaches to the characterisation of membrane protein preparations, and, using purified mini-G_s proteins a novel approach to probe β_2AR pharmacology. Using these techniques, and eight agonists for the β_2AR, this study provides evidence for a conformational model of efficacy. Whilst this model is supported by literature, further work should investigate the applicability of this model to a greater range of agonists and GPCRs to ascertain if this model provides a general mechanism of efficacy.

Chapter 7

Appendices and references

7.1 Supplementary data

7.1.1 Vector maps

All constructs used in this study were in the vector backbones, pcDNA4TO, pcDNA3.1(+), PJ411 or Clonetech N1. An example of the pcDNA4TO vector containing the sequence for TS-SNAP-β_2AR is shown in figure **7.1.1.** The receptors TS-SNAP-A_{2A}R, TS-SNAP-β_2AR-nLuc and TS-SNAP-A_{2A}R-nLuc were inserted also inserted under the control of the CMV promoter.

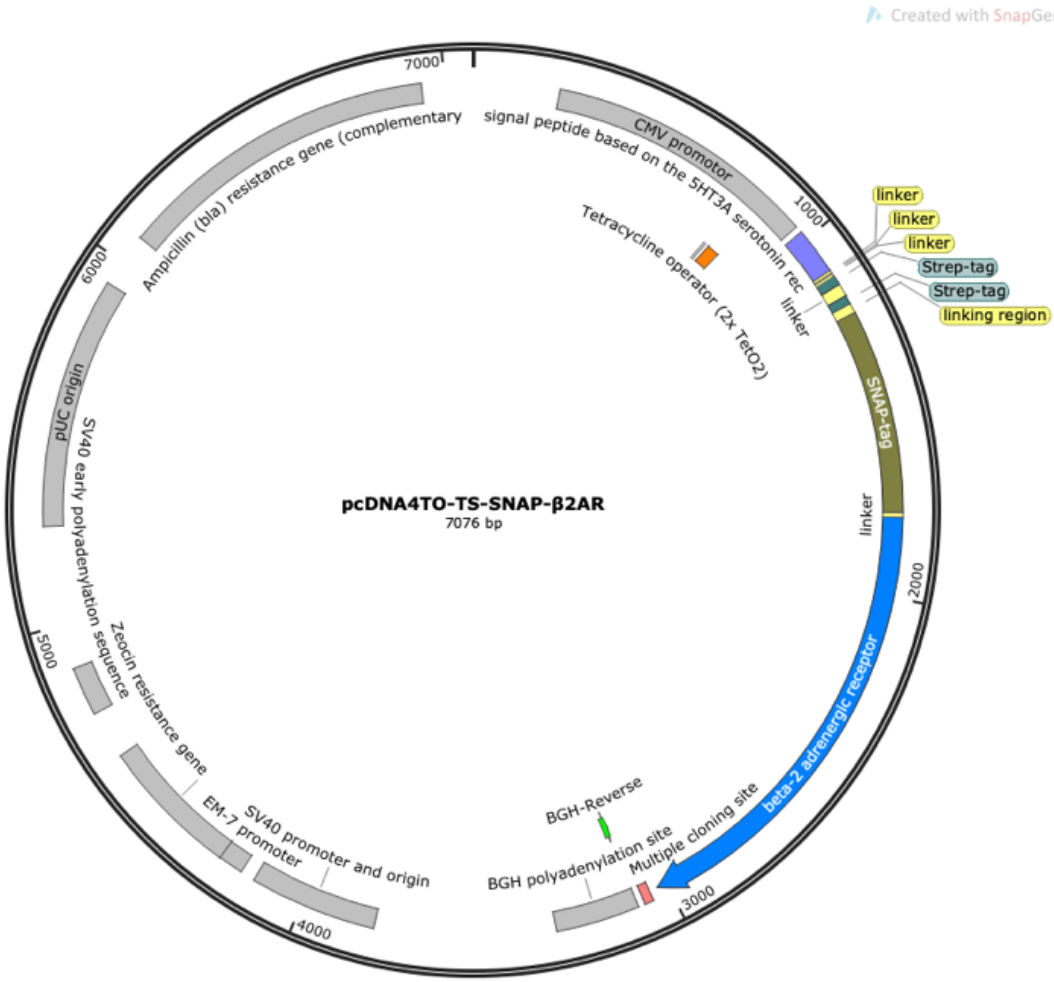

Figure 7.1.1 Map of the pcDNA4TO-TS-SNAP-β_2AR plasmid showing main features and sites of interest. Image obtained with SnapGene Viewer.

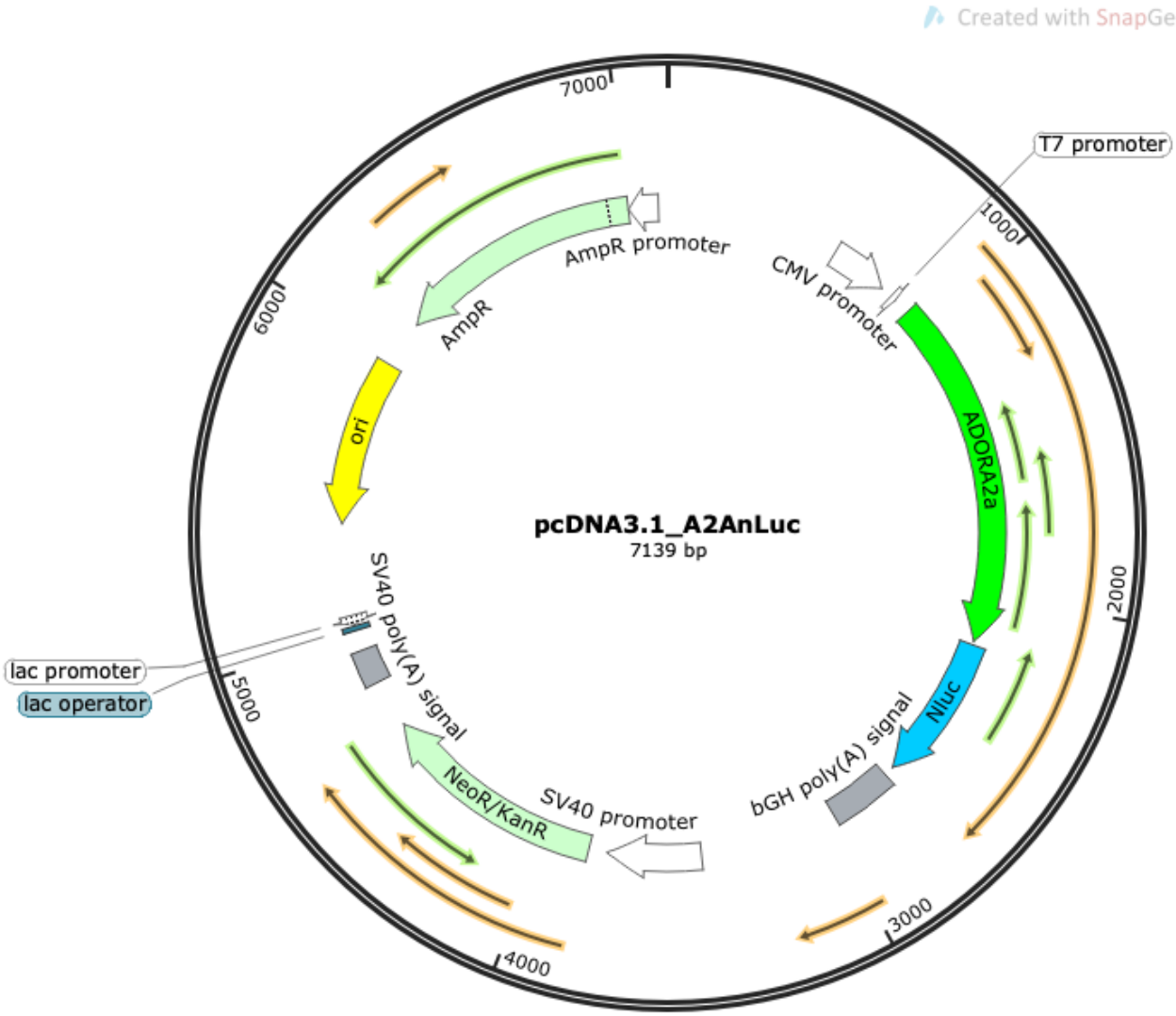

Figure 7.1.2 Map of the pcDNA4TO-TS-SNAP-A_{2A}R plasmid showing main features and sites of interest. Image obtained with SnapGene Viewer.

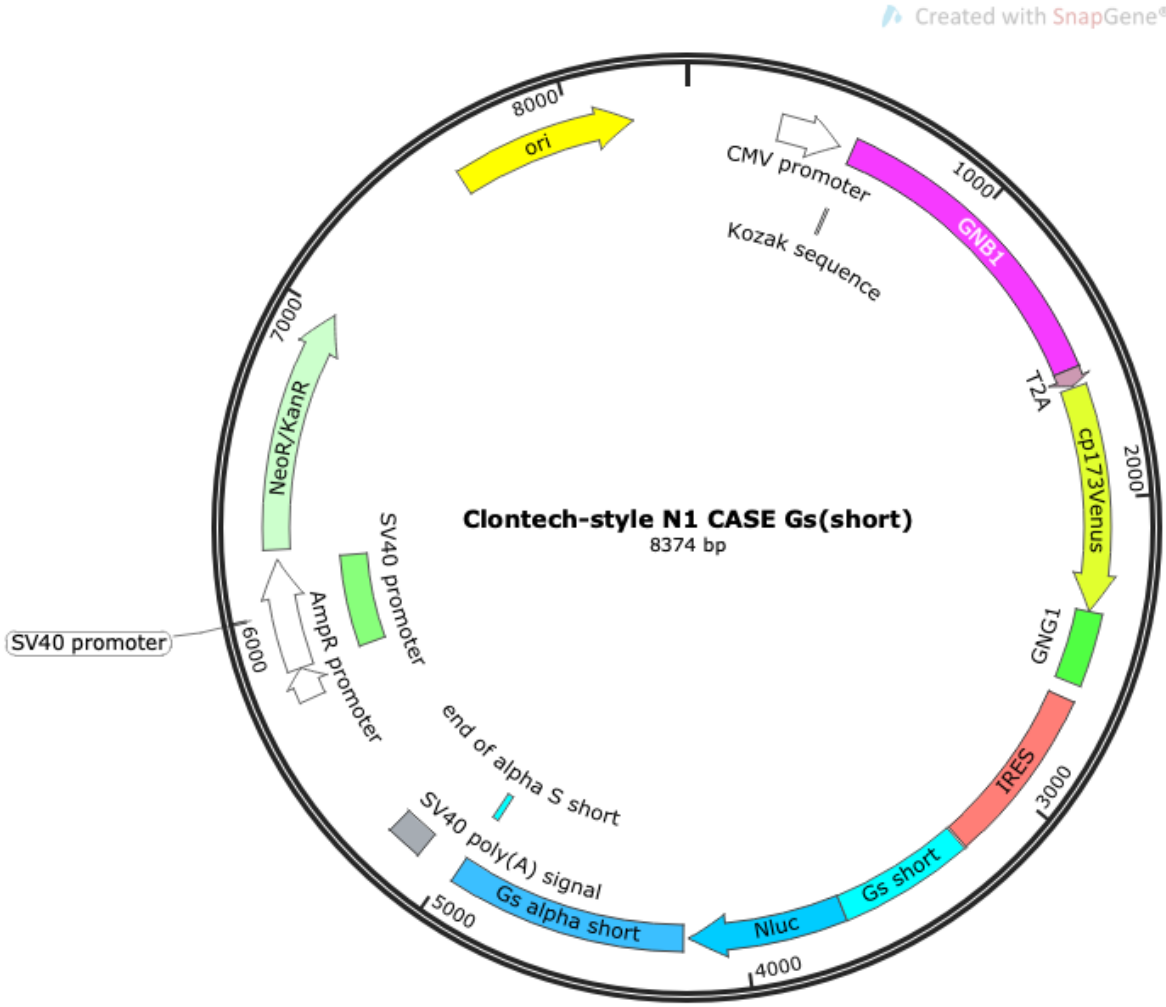

Figure 7.1.3 Map of the Clontech-style N1 CASE Gs plasmid showing main features and sites of interest. Image obtained with SnapGene Viewer.

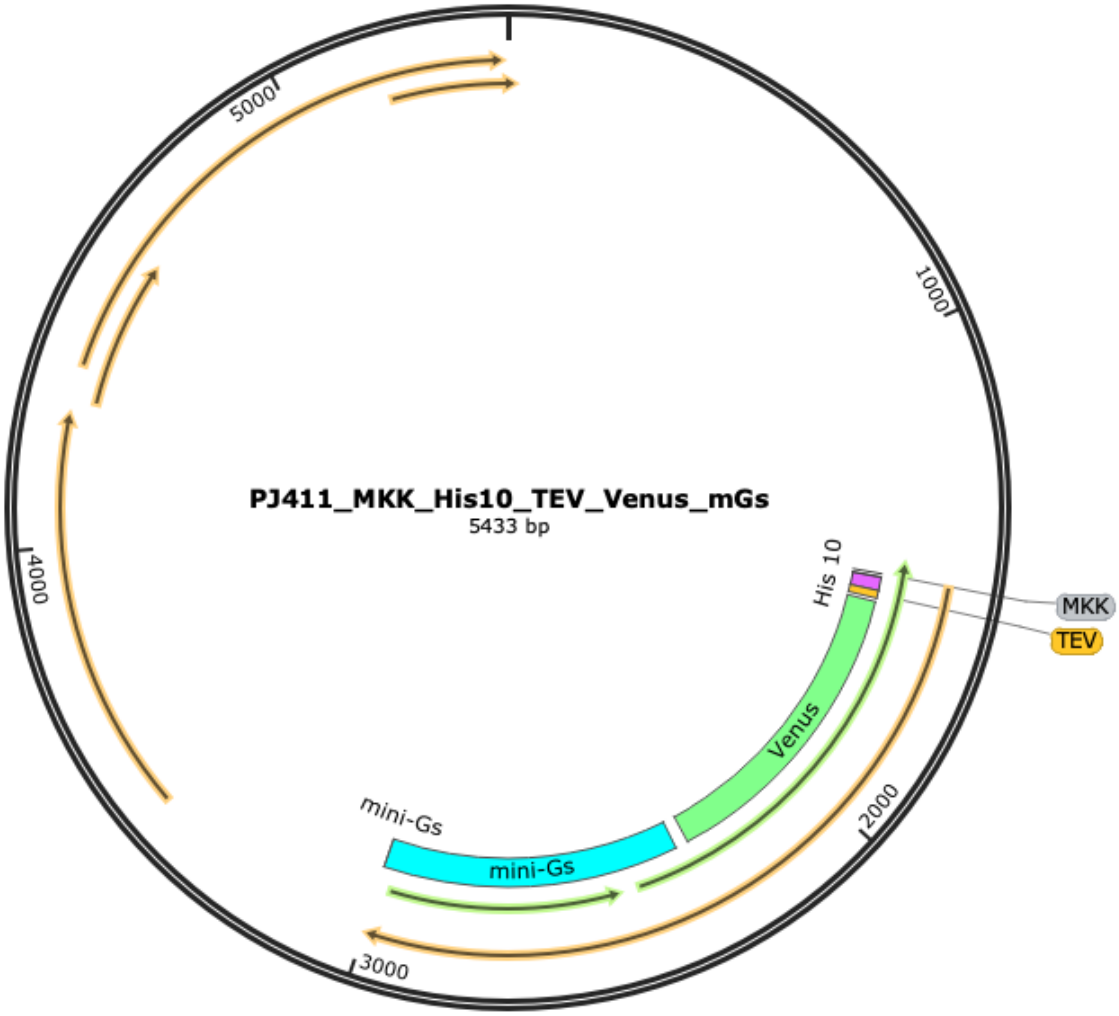

Figure 7.1.4 Map of the PJ411_MKK_His_10_venus_mini-G_s plasmid showing main features and sites of interest. Image obtained with SnapGene Viewer.

7.1.3 Monte carlo simulations of TR-FRET ligand binding assays

Monte Carlo simulations of the tracer and time cycles used in our assay and a hypothetically cold compound with a K_{off} of 0.1min^{-1}, 1 min^{-1}, 3min^{-1} and 10 min^{-1} were run to investigate the limitation of the TR-FRET kinetic ligand binding assay in chapter 4. Motulsky Mahan fits of simulated data with hypothetically cold compound with a K_{off} of 0.1min^{-1}, 1 min^{-1}, 3min^{-1} and 10 min^{-1} are show in tables **7.1.1 to 7.1.4**:

	0	1e6	3e5	1e5	3e4	1e4	Global (shared)
Kinetics of competitive binding							Ambiguous
Best-fit values							
K1	= 4100000	= 4100000	= 4100000	= 4100000	= 4100000	= 4100000	
L	= 75.00	= 75.00	= 75.00	= 75.00	= 75.00	= 75.00	
K2	= 0.08000	= 0.08000	= 0.08000	= 0.08000	= 0.08000	= 0.08000	
K3	~ 3632705	~ 3632705	~ 3632705	~ 3632705	~ 3632705	~ 3632705	~ 3632705
I	= 0.000	= 1000000	= 300000	= 100000	= 30000	= 10000	
K4	~ 36.62	~ 36.62	~ 36.62	~ 36.62	~ 36.62	~ 36.62	~ 36.62
Bmax	99.80	99.80	99.80	99.80	99.80	99.80	99.80

Table 7.1.1: Output of Motulsky Mahan fit to monte carlo simulated TR-FRET ligand binding assay of using 75nM CA200693 (S)-propranolol-green to measure the ligand binding kinetics of 0- 3x10^{-4}M a cold ligand a K_{off} of 10 Min^{-1}.

	0	1e6	3e5	1e5	3e4	1e4	Global (shared)
Kinetics of competitive binding							
Best-fit values							
K1	= 4100000	= 4100000	= 4100000	= 4100000	= 4100000	= 4100000	
L	= 75.00	= 75.00	= 75.00	= 75.00	= 75.00	= 75.00	
K2	= 0.08000	= 0.08000	= 0.08000	= 0.08000	= 0.08000	= 0.08000	
K3	303419	303419	303419	303419	303419	303419	303419
I	= 0.000	= 1000000	= 300000	= 100000	= 30000	= 10000	
K4	3.036	3.036	3.036	3.036	3.036	3.036	3.036
Bmax	99.87	99.87	99.87	99.87	99.87	99.87	99.87

Table 7.1.2: Output of Motulsky-Mahan fit to monte carlo simulated TR-FRET ligand binding assay of using 75nM CA200693 (S)-propranolol-green to measure the ligand binding kinetics of 0- $3x10^{-4}$M a cold ligand a K_{off} of $3Min^{-1}$.

	0	1e6	3e5	1e5	3e4	1e4	Global (shared)
Kinetics of competitive binding							
Best-fit values							
K1	= 4100000	= 4100000	= 4100000	= 4100000	= 4100000	= 4100000	
L	= 75.00	= 75.00	= 75.00	= 75.00	= 75.00	= 75.00	
K2	= 0.08000	= 0.08000	= 0.08000	= 0.08000	= 0.08000	= 0.08000	
K3	84340	84340	84340	84340	84340	84340	84340
I	= 0.000	= 1000000	= 300000	= 100000	= 30000	= 10000	
K4	0.8481	0.8481	0.8481	0.8481	0.8481	0.8481	0.8481
Bmax	99.69	99.69	99.69	99.69	99.69	99.69	99.69

Table 7.1.3: Output of Motulsky-Mahan fit to monte carlo simulated TR-FRET ligand binding assay of using 75nM CA200693 (S)-propranolol-green to measure the ligand binding kinetics of 0- $3x10^{-4}$M a cold ligand a K_{off} of $1Min^{-1}$.

	0	1e6	3e5	1e5	3e4	1e4	Global (shared)
Kinetics of competitive binding							
Best-fit values							
K1	= 4100000	= 4100000	= 4100000	= 4100000	= 4100000	= 4100000	
L	= 75.00	= 75.00	= 75.00	= 75.00	= 75.00	= 75.00	
K2	= 0.08000	= 0.08000	= 0.08000	= 0.08000	= 0.08000	= 0.08000	
K3	10058	10058	10058	10058	10058	10058	10058
I	= 0.000	= 1000000	= 300000	= 100000	= 30000	= 10000	
K4	0.1027	0.1027	0.1027	0.1027	0.1027	0.1027	0.1027
Bmax	100.1	100.1	100.1	100.1	100.1	100.1	100.1

Table 7.1.4: Output of Motulsky Mahan fit to monte carlo simulated TR-FRET ligand binding assay of using 75nM CA200693 (S)-propranolol-green to measure the ligand binding kinetics of 0- $3x10^{-4}$M a cold ligand a K_{off} of $0.1Min^{-1}$.

7.1.4 Analysis of percentage of fast reversible and slow irreversible components of venus- mini-G_s binding to the DDM-TS-SNAP-β_2ARnLuc

For venus-mini-G_s association and dissociation to the DDM-TS-SNAP-β_2ARnLuc the percentage of association that could be attributed to the fast-binding phase was investigated across the different venus-mini-G_s and across ligands, this is summarised in table **7.1.5.**

	3000nM	**1000nM**	**333nM**	**111nM**
Formoterol	71.4±3.0	63.6±6.5	49.9±11.5	23±9.0
Isoprenaline	60.0±12.1	53.5±10.8	41.6±17.7	23±11.0
Salbutamol	66.4±1.6	44.0±9.7	39.6±15.2	52±21.0
C26	78.7±1.4	63.6±3.4	48.3±7.0	27±11.4
Adrenaline	76.5±3.9	66.3±8.1	45.6±11.9	35±13.8
BI-167-107	62.9±13.0	66.1±3.6	51.4±3.2	43±8.5
Salmeterol	70.0±.3.8	48.6±9.1	34.6±9.8	36 ±15.3

Table 7.1.5: Quantification of the percentage of venus-mini-G_s binding DDM-TS-SNAP-β_2AR that could be attributed to the fast association phase at varying [venus-mini-G_s] and in the presence of each β_2AR agonist used in this study. Data are mean of n=3-4 experiments ±SEM.

For venus-mini-G_s dissociation from the agonist bound DDM-TS-SNAP-β_2AR the percentage of complexes that could be dissociated was quantified and is summarised in table **7.1.6.**

	% Dissociated
Formoterol	74.3±4.1
Isoprenaline	73.1±2.1
Salbutamol	72.3±2.2
C26	76.9±1.4
Adrenaline	73.1±2.1
BI-167-107	79.7±4.5
Salmeterol	72.5±1.5

Table 7.1.6: A summary of the percentage of DDM-TS-SNAP-β_2AR: venus-mini-G_s complexes that dissociated with each β_2AR agonist at each concentration. Data are mean of n=3-4 experiments ±SEM.

Alexander, S. P., Christopoulos, A., Davenport, A. P., Kelly, E., Mathie, A., Peters, J. A., Veale, E. L., Armstrong, J. F., Faccenda, E., Harding, S. D., Pawson, A. J., Southan, C., Davies, J. A., Pia Abbracchio, M., Alexander, W., Al-hosaini, K., Bäck, M., Barnes, N. M., Bathgate, R.,Ye, R. D. (2021). The Concise Guide to PHARMACOLOGY 2021/22: G-protein-coupled receptors. *British Journal of Pharmacology*, *178*, 27–156. https://doi.org/10.1111/bph.15538/full

Angers, S., Salahpour, A., Joly, E., Hilairet, S., Chelsky, D., Dennis, M., & Bouvier, M. (2000). *Detection of 2-adrenergic receptor dimerization in living cells using bioluminescence resonance energy transfer (BRET)* (Vol. 97, Issue 7). PNAS. www.pnas.orgcgidoi10.1073pnas.060590697

Bada Juarez, J. F., Muñoz-García, J. C., Inácio dos Reis, R., Henry, A., McMillan, D., Kriek, M., Wood, M., Vandenplas, C., Sands, Z., Castro, L., Taylor, R., & Watts, A. (2020). Detergent-free extraction of a functional low-expressing GPCR from a human cell line. *Biochimica et Biophysica Acta - Biomembranes*, *1862*(3), 183152. https://doi.org/10.1016/j.bbamem.2019.183152

Baker, J. G. (2005). The selectivity of β-adrenoceptor antagonists at the human β1, β2 and β3 adrenoceptors. *British Journal of Pharmacology*, *144*(3), 317–322. https://doi.org/10.1038/sj.bjp.0706048

Ballesteros, J. A., & Weinstein, H. (1995). Integrated methods for the construction of three-dimensional models and computational probing of structure-function relations in G protein-coupled receptors (pp. 366–428). https://doi.org/10.1016/S1043-9471(05)80049-7

Bang, I., & Choi, H.-J. (2015). Structural Features of β2 Adrenergic Receptor: Crystal Structures and Beyond OVERALL STRUCTURE OF BETA2-ADRENERGIC RECEPTOR Molecules and Cells. *Mol. Cells*, *38*(2), 105–111. https://doi.org/10.14348/molcells.2015.2301

Bari, M., Paradisi, A., Pasquariello, N., & Maccarrone, M. (2005). Cholesterol-dependent modulation of type 1 cannabinoid receptors in nerve cells. *Journal of Neuroscience Research*, *81*(2), 275–283. https://doi.org/10.1002/jnr.20546

Berman, H. M., Westbrook, J., Feng, Z., Gilliland, G., Bhat, T. N., Weissig, H., Shindyalov, I. N., & Bourne, P. E. (2000). The Protein Data Bank. In *Nucleic Acids Research* (Vol. 28, Issue 1). http://www.rcsb.org/pdb/status.html

Birnboim, H. C., & Doly, J. (1979). A rapid alkaline extraction procedure for screening recombinant plasmid DNA. *Nucleic Acids Research*, *7*(6), 1513–1523. https://doi.org/10.1093/nar/7.6.1513

Black, J. W., & Leff, P. (1983). Operational models of pharmacological agonism. In *Proc. R. Soc. Lond. B* (Vol. 220). https://royalsocietypublishing.org/

Blackmer, T., Larsen, E. C., Bartleson, C., Kowalchyk, J. A., Yoon, E. J., Preininger, A. M., Alford, S., Hamm, H. E., & Martin, T. F. J. (2005). G protein βγ directly regulates SNARE protein fusion machinery for secretory granule exocytosis. *Nature Neuroscience*, *8*(4), 421–425. https://doi.org/10.1038/nn1423

Bond, R. A., Lefft, P., David Johnsont, T., Milano, C. A., Rockman I, H. A., McMinn II, T. R., Apparsundaram, S., Hyek, M. F., Kenakin, T. P., Allen, L. F., & Robert Lefkowitz, Physiological effects of inverse agonists in transgenic mice with myocardial overexpression of the β2-adrenoceptor. *Nature Mar (1995). 272-6 10.1038/374272a0*

Bouzo-Lorenzo, M., Stoddart, L. A., Xia, L., IJzerman, A. P., Heitman, L. H., Briddon, S. J., & Hill, S. J. (2019). A live cell NanoBRET binding assay allows the study of ligand-binding kinetics to the adenosine A3 receptor. Purinergic Signalling, *15*(2), 139–153. https://doi.org/10.1007/s11302-019-09650-9

Carpenter, B., Nehmé, R., Warne, T., Leslie, A. G. W., & Tate, C. G. (2016). Structure of the adenosine A2A receptor bound to an engineered G protein. *Nature*, *536*(7614), 104–107. https://doi.org/10.1038/nature18966

Carpenter, B., & Tate, C. G. (2016). Engineering a minimal G protein to facilitate crystallisation of G protein-coupled receptors in their active conformation. Protein Engineering, Design and Selection, *29*(12), 583–593. https://doi.org/10.1093/protein/gzw049

Cherezov, V., Rosenbaum, D. M., Hanson, M. A., Kuhn, P., Weis, W. I., Kobilka, B. K., & Stevens, R. C. (2007). RESEARCH ARTICLES High-Resolution Crystal Structure of an Engineered Human β_2-Adrenergic G Protein–Coupled Receptor. *Science*, *318*(November), 1258–1265.

D'ans, J., Breckheimer, K, W., Bonhoeffer, W., Jena; A, Makrides, N., Komodromos, N., Hackerman, B, Conway, J., & Bockris, O. (1952). Application of the theory of diffusion-controlled reactions to enzyme kinetics. In *J. Electro-chem. Soc* (Vol. 56, Issue 26). https://pubs.acs.org/sharingguidelines

Dawaliby, R., Trubbia, C., Delporte, C., Masureel, M., van Antwerpen, P., Kobilka, B. K., & Govaerts, C. (2016). Allosteric regulation of G

protein-coupled receptor activity by phospholipids. *Nature Chemical Biology*, *12*(1), 35–39. https://doi.org/10.1038/nchembio.1960

De Lean, A., Stadel, J. M., & Lefkowitzl, R. J. (1980). A ternary complex model explains the agonist-specific binding properties of the adenylate cyclase-coupled β_2-adrenoceptor, *Journal of biological chemistry (1980)* (Vol. 255, Issue 15) 7108-7117.

Deupi, X., & Kobilka, B. K. (2011). Energy landscapes as a tool to integrate GPCR structure, dynamics and function, *Physiology*. *25*(5), 293–303,https://doi.org/10.1152/physiol.00002.2010.Energy

Dixon, R. A. F., Kobilkat, B. K., Strader: D. J., Benovict, J. L., Dohlmant, H. G., Friellet, T., Bolanowskit, M. A., Bennett, C. D., Rands, E., Diehl, R. E., & Mumford, R. A. Cloning of the gene and cDNA for mammalian β_2-adrenoceptor receptor and homology with rhodopsin.

Dörr, J. M., Koorengevel, M. C., Schäfer, M., Prokofyev, A. V., Scheidelaar, S., Van Der Cruijsen, E. A. W., Dafforn, T. R., Baldus, M., & Killian, J. A. (2014). Detergent-free isolation, characterization, and functional reconstitution of a tetrameric K+ channel: The power of native nanodiscs. *PNAS*, *111*(52), 18607–18612. https://doi.org/10.1073/pnas.1416205112

Downes, G. B., & Gautam, N. (1999). The G protein subunit gene families. *Genomics*, *62*(3), 544–552. https://doi.org/10.1006/geno.1999.5992

Du, Y., Duc, N. M., Rasmussen, S. G. F., Hilger, D., Kubiak, X., Wang, L., Bohon, J., Kim, H. R., Wegrecki, M., Asuru, A., Jeong, K. M., Lee, J., Chance, M. R., Lodowski, D. T., Kobilka, B. K., & Chung, K. Y. (2019). Assembly of a GPCR-G Protein Complex. *Cell*, *177*(5), 1232-1242.e11. https://doi.org/10.1016/j.cell.2019.04.022

Yao, F., Svensjo, T., Winkler, T., Lu, M., Eriksson, C., & Eriksson E.. (1998). Tetracycline repressor, tetR, rather than the cell transcription factor fusion derivatives, regulates inducible gene expression in mammalian cells. *Human gene therapy 9:*1939–1950. 10.1089/hum.1998.9 13-1939

Flock, T., Ravarani, C. N. J., Sun, D., & Venkatakrishnan, A. J. (2016). *Europe PMC Funders Group Universal allosteric mechanism for G α activation by GPCRs*. *524*(7564), 173–179. https://doi.org/10.1038/nature14663.Universal

Galés, C., Rebois, R. V., Hogue, M., Trieu, P., Breit, A., Hébert, T. E., & Bouvier, M. (2005). Real-time monitoring of receptor and G-protein

interactions in living cells. *Nature Methods*, *2*(3), 177–184. https://doi.org/10.1038/nmeth743

Galés, C., van Durm, J., Schaak, S., Pontier, S., Percherancier, Y., Audet, M., Paris, H., & Bouvier, M. (2006). Probing the activation-promoted structural rearrangements in preassembled receptor-G protein complexes. *Nature Structural and Molecular Biology*, *13*(9), 778–786. https://doi.org/10.1038/nsmb1134

Gao, K., Oerlemans, R., & Groves, M. R. (2020). Theory and applications of differential scanning fluorimetry in early-stage drug discovery. *Biophysical Reviews*, *12*(1), 85–104. https://doi.org/10.1007/s12551-020-00619-2

García-Nafría, J., Lee, Y., Bai, X., Carpenter, B. & Tate, C. G. (2018). Cryo-EM structure of 201 the adenosine A_{2A} receptor coupled to an engineered heterotrimeric G protein, *eLife* 7:e35946 https://doi.org/10.1101/267674

George, S., Furness, B., Liang, Y., Nowell, C. J., Christopoulos, A., Wootten, D., George, S., Furness, B., Liang, Y., Nowell, C. J., Halls, M. L., Wookey, P. J., Maso, E. D., Inoue, A., Christopoulos, A., Wootten, D., & Sexton, P. M. (2016). Ligand-Dependent Modulation of G Protein Article Ligand-Dependent Modulation of G Protein Conformation Alters Drug Efficacy. *Cell*, *167*(3), 739-744.e11. https://doi.org/10.1016/j.cell.2016.09.021

Gibson, D. G., Young, L., Chuang, R.-Y., Venter, J. C., Hutchison, C. A., & Smith, H. O. (2009). Enzymatic assembly of DNA molecules up to several hundred kilobases. *Nature Methods*, *6*(5), 343–345. https://doi.org/10.1038/nmeth.1318

Gregorio, G. G., Masureel, M., Hilger, D., Terry, D. S., Juette, M., Zhao, H., Zhou, Z., Perez-Aguilar, J. M., Hauge, M., Mathiasen, S., Javitch, J. A., Weinstein, H., Kobilka, B. K., & Blanchard, S. C. (2017). Single-molecule analysis of ligand efficacy in β2AR-G-protein activation. *Nature*, *547*(7661), 68–73. https://doi.org/10.1038/nature22354

Grime, R. L., Logan, R. T., Nestorow, S. A., Sridhar, P., Edwards, P. C., Tate, C. G., Klumperman, B., Dafforn, T. R., Poyner, D. R., Reeves, P. J., & Wheatley, M. (2021). Differences in SMA-like polymer architecture dictate the conformational changes exhibited by the membrane protein rhodopsin encapsulated in lipid nanoparticles. *Nanoscale*, *13*(31), 13519–13528. https://doi.org/10.1039/d1nr02419a

Guixà-González, R., Albasanz, J. L., Rodriguez-Espigares, I., Pastor, M., Sanz, F., Martí-Solano, M., Manna, M., Martinez-Seara, H., Hildebrand, P. W., Martín, M., & Selent, J. (2017). Membrane

cholesterol access into a G-protein-coupled receptor. *Nature Communications*, *8*. https://doi.org/10.1038/ncomms14505

Gulamhussein, A. A., Uddin, R., Tighe, B. J., Poyner, D. R., & Rothnie, A. J. (2020). A comparison of SMA (styrene maleic acid) and DIBMA (di-isobutylene maleic acid) for membrane protein purification. *Biochimica et Biophysica Acta (BBA) - Biomembranes*, *1862*(7), 183281. https://doi.org/10.1016/j.bbamem.2020.183281

Gulati, S., Jamshad, M., Knowles, T. J., Morrison, K. A., Downing, R., Cant, N., Collins, R., Koenderink, J. B., Ford, R. C., Overduin, M., Kerr, I. D., Dafforn, T. R., & Rothnie, A. J. (2014). Detergent-free purification of ABC (ATP-binding-cassette) transporters. *Biochemical Journal*, *461*(2), 269–278. https://doi.org/10.1042/BJ20131477

Guo, D., Mulder-Krieger, T., IJzerman, A. P., & Heitman, L. H. (2012). Functional efficacy of adenosine A 2A receptor agonists is positively correlated to their receptor residence time. *British Journal of Pharmacology*, *166*(6), 1846–1859. https://doi.org/10.1111/j.1476-5381.2012.01897.x

Hall, M. P., Unch, J., Binkowski, B. F., Valley, M. P., Butler, B. L., Wood, M. G., Otto, P., Zimmerman, K., Vidugiris, G., MacHleidt, T., Robers, M. B., Benink, H. A., Eggers, C. T., Slater, M. R., Meisenheimer, P. L., Klaubert, D. H., Fan, F., Encell, L. P., & Wood, K. v. (2012). Engineered luciferase reporter from a deep-sea shrimp utilizing a novel imidazopyrazinone substrate. *ACS Chemical Biology*, *7*(11), 1848–1857. https://doi.org/10.1021/cb3002478

Halls, M. L., Yeatman, H. R., Nowell, C. J., Thompson, G. L., Gondin, A. B., Civciristov, S., Bunnett, N. W., Lambert, N. A., Poole, D. P., & Canals, M. (2016). Plasma membrane localization of the μ-opioid receptor controls spatiotemporal signaling. *Science Signaling*, *9*(414), 1–14. https://doi.org/10.1126/scisignal.aac9177

Hauser, A. S., Attwood, M. M., Rask-andersen, M., Schiöth, H. B., & Gloriam, D. E. (2017). Trends in GPCR drug discovery : new agents , targets and indications. *Nature Publishing Group*. https://doi.org/10.1038/nrd.2017.178

Heise, C. E., Sullivan, S. K., & Crowe, P. D. (2007). Scintillation proximity assay as a high-throughput method to identify slowly dissociating nonpeptide ligand binding to the GnRH receptor. *Journal of Biomolecular Screening*, *12*(2), 235–239. https://doi.org/10.1177/1087057106297362

Hillenbrand, M., Schori, C., Schöppe, J., & Plückthun, A. (2015). Comprehensive analysis of heterotrimeric G-protein complex

diversity and their interactions with GPCRs in solution. *PNAS 112*(11), E1181–E1190. https://doi.org/10.1073/pnas.1417573112

Huynh, K. Partch, C. (2016). Analysis of protein stability and ligand interactions by thermal shift assay. *Current protocols in protein science, vol (79) 1 28.9.1-28.9.14* https://doi.org/10.1002/0471140864.ps2809s79.Current

Jakubík, J., Randáková, A., Rudajev, V., Zimčík, P., El-Fakahany, E. E., & Doležal, V. (2019). Applications and limitations of fitting of the operational model to determine relative efficacies of agonists. *Scientific Reports*, *9*(1). https://doi.org/10.1038/s41598-019-40993-w

Jamshad, M., Charlton, J., Lin, Y., Routledge, S. J., Bawa, Z., Knowles, T. J., Overduin, M., Dekker, N., Dafforn, T. R., Bill, R. M., Poyner, D. R., & Wheatley, M. (2015). G-protein coupled receptor solubilization and purification for biophysical analysis and functional studies, in the total absence of detergent. *Bioscience Reports*, *35*(2), 1–10. https://doi.org/10.1042/BSR20140171

Katritch, V., Reynolds, K. A., Cherezov, V., Hanson, M. A., Roth, C. B., Yeager, M., & Abagyan, R. (2009). Analysis of full and partial agonists binding to β2- adrenergic receptor suggests a role of transmembrane helix v in agonist-specific conformational changes. *Journal of Molecular Recognition*, *22*(4), 307–318. https://doi.org/10.1002/jmr.949

Kenakin, T. (2016). The mass action equation in pharmacology. *British Journal of Clinical Pharmacology*, *81*(1), 41–51. https://doi.org/10.1111/bcp.12810

Kenakin, T. (2017). Theoretical aspects of GPCR-ligand complex pharmacology. *Chemical Reviews*, *117*(1), 4–20. https://doi.org/10.1021/acs.chemrev.5b00561

Knowles, T. J., Finka, R., Smith, C., Lin, Y. P., Dafforn, T., & Overduin, M. (2009). Membrane proteins solubilized intact in lipid containing nanoparticles bounded by styrene maleic acid copolymer. *Journal of the American Chemical Society*, *131*(22), 7484–7485. https://doi.org/10.1021/ja810046q

Kresge, C. T., Leonowicz, M. E., Roth, W. J., Vartuli, J. C., Beck, J. S. (1992). Isozyme-selective stimulation of phospholipase C-β2 by G protein βγ-subunits. *Nature*, *359*, 710–713.

Lamichhane, R., Liu, J. J., Pljevaljcic, G., White, K. L., Schans, E. van der, & Katritch, V. (2015). Single-molecule view of basal activity and activation mechanisms of the G protein-coupled receptor β_2 AR. 2–7. *PNAS* 17;112 (46):14254-9 https://doi.org/10.1073/pnas.1519626112

Lamichhane, R., Liu, J. J., White, K. L., Katritch, V., Stevens, R. C., Wüthrich, K., & Millar, D. P. (2020). Biased Signaling of the G-Protein-Coupled Receptor β_2AR Is Governed by Conformational Exchange Kinetics. *Structure*, *28*(3), 371-377.e3. https://doi.org/10.1016/j.str.2020.01.001

Leitz, A. J., Bayburt, T. H., Barnakov, A. N., Springer, B. A., & Sligar, S. G. (2006). Functional reconstitution of β_2-adrenergic receptors utilizing self-assembling Nanodisc technology. *BioTechniques*, *40*(5), 601–612. https://doi.org/10.2144/000112169

Liang, Y., Khoshouei, M., Glukhova, A., Furness, S. G. B., Zhao, P., Clydesdale, L., Koole, C., Truong, T. T., Thal, D. M., Lei, S., Radjainia, M., Danev, R., Baumeister, W., Wang, M., Miller, L. J., Christopoulos, A., Sexton, P. M., & Wootten, D. (2018). bound human GLP-1 receptor – G_s complex. *Nature Publishing Group*. https://doi.org/10.1038/nature25773

Liu, J., Horst, R., Katritch, V., Stevens, R., & Wuthrich, K. (2013). Biased signalling pathways in β_2-adrenergic receptor characterized by 19F-NMR. *Science*, *335*(6072), 1106–1110. https://doi.org/10.1126/science.1215802.

Logez, C., Damian, M., Legros, C., Dupré, C., Guéry, M., Mary, S., Wagner, R., M'Kadmi, C., Nosjean, O., Fould, B., Marie, J., Fehrentz, J. A., Martinez, J., Ferry, G., Boutin, J. A., & Baneìres, J. L. (2016). Detergent-free Isolation of Functional G Protein-Coupled Receptors into Nanometric Lipid Particles. *Biochemistry*, *55*(1), 38–48. https://doi.org/10.1021/acs.biochem.5b01040

Logothetis, D., Kurachi, Y., Galper, J., Neer, E., & Clapham DE. (1987). The βγ subunits of GTP-binding proteins activate the muscarinic K+ channel. *Nature* (Vol. 325, Issue 22).

Louvel, J., Guo, D., Agliardi, M., Mocking, T. A. M., Kars, R., Pham, T. P., Xia, L., de Vries, H., Brussee, J., Heitman, L. H., & Ijzerman, A. P. (2014). Agonists for the adenosine A1 receptor with tunable residence time. a case for nonribose 4-amino-6-aryl-5-cyano-2-thiopyrimidines. *Journal of Medicinal Chemistry*, *57*(8), 3213–3222. https://doi.org/10.1021/jm401643m

Machleidt, T., Woodroofe, C. C., Schwinn, M. K., Méndez, J., Robers, M. B., Zimmerman, K., Otto, P., Daniels, D. L., Kirkland, T. A., & Wood, K. v. (2015). NanoBRET-A Novel BRET Platform for the Analysis of Protein-Protein Interactions. *ACS Chemical Biology*, *10*(8), 1797–1804. https://doi.org/10.1021/acschembio.5b00143

Manglik, A., Kim, T. H., Masureel, M., Altenbach, C., Yang, Z., Hilger, D., Lerch, M. T., Kobilka, T. S., Thian, F. S., Hubbell, W. L., Prosser, R. S., & Kobilka, B. K. (2015). Structural insights into the dynamic process of β_2-adrenergic receptor signaling. *Cell*, *161*(5), 1101–1111. https://doi.org/10.1016/j.cell.2015.04.043

Mary, S., Damian, M., Louet, M., Floquet, N., Fehrentz, J.-A., Marie, J., Martinez, J., & Baneres, J.-L. (2012). Ligands and signaling proteins govern the conformational landscape explored by a G protein-coupled receptor. *PNAS*, *109*(21), 8304–8309. https://doi.org/10.1073/pnas.1119881109

Masureel, M., Zou, Y., Picard, L. P., van der Westhuizen, E., Mahoney, J. P., Rodrigues, J. P. G. L. M., Mildorf, T. J., Dror, R. O., Shaw, D. E., Bouvier, M., Pardon, E., Steyaert, J., Sunahara, R. K., Weis, W. I., Zhang, C., & Kobilka, B. K. (2018). Structural insights into binding specificity, efficacy and bias of a β_2AR partial agonist. *Nature Chemical Biology*, *14*(11), 1059–1066. https://doi.org/10.1038/s41589-018-0145-x

McLaughlin, J. N., Shen, L., Holinstat, M., Brooks, J. D., DiBenedetto, E., & Hamm, H. E. (2005). Functional selectivity of G protein signaling by agonist peptides and thrombin for the protease-activated receptor-1. *Journal of Biological Chemistry*, *280*(26), 25048–25059. https://doi.org/10.1074/jbc.M414090200

Miljus, T., Sykes, D. A., Harwood, C. R., Vuckovic, Z., & Veprintsev, D. B. (2020). GPCR Solubilization and Quality Control. In C. Perez & T. Maier (Eds.), *Expression, Purification, and Structural Biology of Membrane Proteins* (pp. 105–127). Springer US. https://doi.org/10.1007/978-1-0716-0373-4_8

Mosslehy, W., Voskoboynikova, N., Colbasevici, A., Ricke, A., Klose, D., Klare, J. P., Mulkidjanian, A. Y., & Steinhoff, H. J. (2019). Conformational Dynamics of Sensory Rhodopsin II in Nanolipoprotein and Styrene–Maleic Acid Lipid Particles. *Photochemistry and Photobiology*, *95*(5), 1195–1204. https://doi.org/10.1111/php.13096

Motulsky, H. J., & Mahan, L. C. (1984). The kinetics of competitive radioligand binding predicted by the law of mass action. *Molecular Pharmacology*, *25*(1), 1–9.

Mukhopadhyay, S. (2005). Chemically Distinct Ligands Promote Differential CB1 Cannabinoid Receptor-Gi Protein Interactions. *Molecular Pharmacology*, *67*(6), 2016–2024. https://doi.org/10.1124/mol.104.003558

Munk, C., Mutt, E., Isberg, V., Nikolajsen, L. F., Bibbe, J. M., Flock, T., Hanson, M. A., Stevens, R. C., Deupi, X., & Gloriam, D. E. (2019). An online resource for GPCR structure determination and analysis. *Nature Methods*, *16*(2), 151–162. https://doi.org/10.1038/s41592-018-0302-x

Nguyen, H. H., Park, J., Kang, S., & Kim, M. (2015). Surface plasmon resonance: A versatile technique for biosensor applications. In *Sensors (Switzerland)* (Vol. 15, Issue 5, pp. 10481–10510). MDPI AG. https://doi.org/10.3390/s150510481

Nikolaev, V. O., Hoffmann, C., Bünemann, M., Lohse, M. J., & Vilardaga, J. P. (2006). Molecular basis of partial agonism at the neurotransmitter α2A-adrenergic receptor and Gi-protein heterotrimer. *Journal of Biological Chemistry*, *281*(34), 24506–24511. https://doi.org/10.1074/jbc.M603266200

Nygaard, R., Zou, Y., Dror, R. O., Mildorf, T. J., Arlow, D. H., Manglik, A., Pan, A. C., Bokoch, M. P., Thian, F. S., Kobilka, T. S., Shaw, D. E., Liu, C. W., Jose, J., Mueller, L., Prosser, R. S., & Kobilka, B. K. (2013). The Dynamic Process of β_2AR-Adrenergic Receptor Activation. *Cell, 152 (3) 532-542* https://doi.org/10.1016/j.cell.2013.01.008

Oluwole, A. O., Danielczak, B., Meister, A., Babalola, J. O., Vargas, C., & Keller, S. (2017). Solubilization of Membrane Proteins into Functional Lipid-Bilayer Nanodiscs Using a Diisobutylene/Maleic Acid Copolymer. *Angewandte Chemie - International Edition*, *56*(7), 1919–1924. https://doi.org/10.1002/anie.201610778

Oluwole, A. O., Klingler, J., Danielczak, B., Babalola, J. O., Vargas, C., Pabst, G., & Keller, S. (2017). Formation of Lipid-Bilayer Nanodiscs by Diisobutylene/Maleic Acid (DIBMA) Copolymer. *Langmuir*, *33*(50), 14378–14388. https://doi.org/10.1021/acs.langmuir.7b03742

Paila, Y. D., Jindal, E., Goswami, S. K., & Chattopadhyay, A. (2011). Cholesterol depletion enhances adrenergic signaling in cardiac myocytes. *Biochimica et Biophysica Acta - Biomembranes*, *1808*(1), 461–465. https://doi.org/10.1016/j.bbamem.2010.09.006

Pándy-Szekeres, G., Munk, C., Tsonkov, T. M., Mordalski, S., Harpsøe, K., Hauser, A. S., Bojarski, A. J., & Gloriam, D. E. (2018). GPCRdb in 2018: Adding GPCR structure models and ligands. *Nucleic Acids Research*, *46*(D1), D440–D446. https://doi.org/10.1093/nar/gkx1109

Philipp, M., Brede, M., & Hein, L. (2002). invited review Physiological significance of 2-adrenergic receptor subtype diversity: one receptor is not enough. *Am J Physiol Regulatory Integrative Comp Physiol*, *283*, 287–295. https://doi.org/10.1152/ajpregu.00123.2002.

Pontier, S. M., Percherancier, Y., Galandrin, S., Breit, A., Galés, C., & Bouvier, M. (2008). Cholesterol-dependent separation of the β_2-adrenergic receptor from its partners determines signaling efficacy: Insight into nanoscale organization of signal transduction. *Journal of Biological Chemistry*, *283*(36), 24659–24672. https://doi.org/10.1074/jbc.M800778200

Rasmussen, S. G. F., Choi, H. J., Fung, J. J., Pardon, E., Casarosa, P., Chae, P. S., Devree, B. T., Rosenbaum, D. M., Thian, F. S., Kobilka, T. S., Schnapp, A., Konetzki, I., Sunahara, R. K., Gellman, S. H., Pautsch, A., Steyaert, J., Weis, W. I., & Kobilka, B. K. (2011a). Structure of a nanobody-stabilized active state of the β_2 adrenoceptor. *Nature*, *469* (7329), 175–181. https://doi.org/10.1038/nature09648

Rasmussen, S. G. F., Choi, H. J., Rosenbaum, D. M., Kobilka, T. S., Thian, F. S., Edwards, P. C., Burghammer, M., Ratnala, V. R. P., Sanishvili, R., Fischetti, R. F., Schertler, G. F. X., Weis, W. I., & Kobilka, B. K. (2007). Crystal structure of the human β_2 adrenergic G-protein-coupled receptor. *Nature*, *450*(7168), 383–387. https://doi.org/10.1038/nature06325

Rasmussen, S. G. F., Devree, B. T., Zou, Y., Kruse, A. C., Chung, K. Y., Kobilka, T. S., Thian, F. S., Chae, P. S., Pardon, E., Calinski, D., Mathiesen, J. M., Shah, S. T. A., Lyons, J. A., Caffrey, M., Gellman, S. H., Steyaert, J., Skiniotis, G., Weis, W. I., Sunahara, R. K., & Kobilka, B. K. (2011a). Crystal structure of the β2adrenergic receptor-Gs protein complex. *Nature*, *477*(7366), 549–557. https://doi.org/10.1038/nature10361

Rosethorne, E. M., Bradley, M. E., Gherbi, K., Sykes, D. A., Sattikar, A., Wright, J. D., Renard, E., Trifilieff, A., Fairhurst, R. A., & Charlton, S. J. (2016). Long receptor residence time of C26 contributes to super agonist activity at the human β_2 adrenoceptor. *Molecular Pharmacology*, *89*(4), 467–475. https://doi.org/10.1124/mol.115.101253

Roth, C. B., Hanson, M. A., & Stevens, R. C. (2009). Stabilization of the β_2-adrenergic Receptor 4-3-5 Helix Interface by Mutagenesis of Glu-1223.41*, A Critical Residue in GPCR Structure.pdf*. *376*(5), 1305–1319.

Routledge, S. J., Jamshad, M., Little, H. A., Lin, Y. P., Simms, J., Thakker, A., Spickett, C. M., Bill, R. M., Dafforn, T. R., Poyner, D. R., & Wheatley, M. (2020). Ligand-induced conformational changes in a SMALP-encapsulated GPCR. *Biochimica et Biophysica Acta - Biomembranes*, *1862*(6). https://doi.org/10.1016/j.bbamem.2020.183235

Samamasb, P., Cotecchialf, S., Costal, T., & Lefkowitzs, R. J. (1993). A mutation-induced activated state of the β_2 adrenergic receptor. Extending the ternary complex model. *J Biol Chem 268(7):4625-36* PMID: 8095262

Schena, G., & Caplan, M. J. (2019). Everything You Always Wanted to Know about β_3AR (But Were Afraid to Ask). *Cells*, *8*(4), 357. https://doi.org/10.3390/cells8040357

Schihada, H., Shekhani, R., & Schulte, G. (2021). Quantitative assessment of constitutive G protein–coupled receptor activity with BRET-based G protein biosensors. *Science Signaling*, *14*(699). https://doi.org/10.1126/scisignal.abf1653

Schiöth, H. B., & Fredriksson, R. (2005). The GRAFS classification system of G-protein coupled receptors in comparative perspective. *General and Comparative Endocrinology*, *142*, 94–101. https://doi.org/10.1016/j.ygcen.2004.12.018

Serrano-Vega, M. J., & Tate, C. G. (2009a). Transferability of thermostabilizing mutations between β-adrenergic receptors. *Molecular Membrane Biology*, *26*(8), 385–396. https://doi.org/10.3109/09687680903208239

Shirdel, S. A., & Khalifeh, K. (2019). Thermodynamics of protein folding: methodology, data analysis and interpretation of data. *European Biophysics Journal*, *48*(4), 305–316. https://doi.org/10.1007/s00249-019-01362-7

Skrzypek, R., Iqbal, S., & Callaghan, R. (2018). Methods of reconstitution to investigate membrane protein function. *Methods*, *147* (February), 126–141. https://doi.org/10.1016/j.ymeth.2018.02.012

Stoddart, L. A., Johnstone, E. K. M., Wheal, A. J., Goulding, J., Robers, M. B., MacHleidt, T., Wood, K. v., Hill, S. J., & Pfleger, K. D. G. (2015). Application of BRET to monitor ligand binding to GPCRs. *Nature Methods*, *12*(7), 661–663. https://doi.org/10.1038/nmeth.3398

Strohman, M. J., Maeda, S., Hilger, D., Masureel, M., Du, Y., & Kobilka, B. K. (2018). Local membrane charge regulates β_2 adrenergic receptor coupling to G_{i3}. *Nature communications 10 (2234)* https://doi.org/10.1038/s41467-019-10108-0

Stroud, Z., Hall, S. C. L., & Dafforn, T. R. (2018). Purification of membrane proteins free from conventional detergents: SMA, new polymers, new opportunities and new insights. *Methods*, *147*, 106–117. https://doi.org/10.1016/j.ymeth.2018.03.011

Sun, C., Benlekbir, S., Venkatakrishnan, P., Wang, Y., Hong, S., Hosler, J., Tajkhorshid, E., Rubinstein, J. L., & Gennis, R. B. (2018). Structure of the alternative complex III in a supercomplex with cytochrome oxidase. *Nature*, *557*(7703), 123–126. https://doi.org/10.1038/s41586-018-0061-y

Sun, D., Ostermaier, M. K., Heydenreich, F. M., Mayer, D., Jaussi, R., Standfuss, J., & Veprintsev, D. B. (2013). *AAscan, PCRdesign and MutantChecker : A Suite of Programs for Primer Design and Sequence Analysis for High-Throughput Scanning Mutagenesis*. *8*(10). https://doi.org/10.1371/journal.pone.0078878

Sungkaworn, T., Jobin, M., Burnecki, K., Weron, A., Lohse, M. J., & Calebiro, D. (2017). Single-molecule imaging reveals receptor–G protein interactions at cell surface hot spots. *Nature Publishing Group*, *550*(7677), 543–547. https://doi.org/10.1038/nature24264

Sykes, D. A., & Charlton, S. J. (2012). Slow receptor dissociation is not a key factor in the duration of action of inhaled long-acting β_2-adrenoceptor agonists. *British Journal of Pharmacology*, *165*(8), 2672–2683. https://doi.org/10.1111/j.1476-5381.2011.01639.x

Sykes, D. A., Dowling, M. R., & Charlton, S. J. (2009). Exploring the mechanism of agonist efficacy: a relationship between efficacy and agonist dissociation rate at the muscarinic M3 receptor. *Molecular Pharmacology*, *76*(3), 543–551. https://doi.org/10.1124/mol.108.054452

Sykes, D. A., Parry, C., Reilly, J., Wright, P., Fairhurst, R. A., & Charlton, S. J. (2014a). Observed drug-receptor association rates are governed by membrane affinity: The importance of establishing "micro-pharmacokinetic/pharmacodynamic relationships" at the β_2-adrenoceptor. *Molecular Pharmacology*, *85*(4), 608–617. https://doi.org/10.1124/mol.113.090209

Sykes, D. A., Stoddart, L. A., Kilpatrick, L. E., & Hill, S. J. (2019). Binding kinetics of ligands acting at GPCRs. *Molecular and Cellular Endocrinology*, *485* (February), 9–19. https://doi.org/10.1016/j.mce.2019.01.018

Tang, A. W., Gilman, A. G., Tang, W., & Gilman, A. G. (1995). Constrcution of a soluble adenylyl cyclase activated by Gs alpha and forskolin. *Science,* 23;268(5218):1769-72. https://10.1126/science.7792604

Tippett, D. N., Hoare, B., Miljus, T., Sykes, D. A., & Veprintsev, D. B. (2020). ThermoFRET: A novel nanoscale G protein coupled receptor thermostability assay functional in crude solubilised membrane preparations. *BioRxiv*. https://doi.org/10.1101/2020.07.07.191957

Triposkiadis, F., Karayannis, G., Giamouzis, G., Skoularigis, J., Louridas, G., & Butler, J. (2009). The Sympathetic Nervous System in Heart Failure. Physiology, Pathophysiology, and Clinical Implications. In *Journal of the American College of Cardiology* (Vol. 54, Issue 19, pp. 1747–1762). https://doi.org/10.1016/j.jacc.2009.05.015

Wacker, D., Fenalti, G., Brown, M. A., Katritch, V., Abagyan, R., Cherezov, V., & Stevens, R. C. (2010). Conserved binding mode of human β2 adrenergic receptor inverse agonists and antagonist revealed by X-ray crystallography. *Journal of the American Chemical Society*, *132* (33), 11443–11445. https://doi.org/10.1021/ja105108q

Wan, Q., Okashah, N., Inoue, A., Nehmé, R., Carpenter, B., Tate, C. G., & Lambert, N. A. (2018). *Mini G protein probes for active G protein – coupled receptors (GPCRs) in live cells*. *293*, 7466–7473. https://doi.org/10.1074/jbc.RA118.001975

Warne, T., Moukhametzianov, R., Baker, J. G., Nehmé, R., Patricia, C., Leslie, A. G. W., Schertler, G. F. X., & Tate, C. G. (2011). *UKPMC Funders Group β1-adrenergic receptor*. *469*(7329), 241–244. https://doi.org/10.1038/nature09746.

Whorton, M. R., Bokoch, M. P., Rasmussen, S. G. F., Huang, B., Zare, R. N., Kobilka, B., & Sunahara, R. K. (2007). A monomeric G protein-coupled receptor isolated in a high-density lipoprotein particle efficiently activates its G protein. *PNAS 104*(18), 7682–7687. https://doi.org/10.1073/pnas.0611448104

Yu, J.-Z., & Rasenick, M. M. (2002). *Real-Time Visualization of a Fluorescent Gs: Dissociation of the Activated G Protein from Plasma Membrane*. http://molpharm.aspetjournals.org

Zarzycka, B., Zaidi, S. A., Roth, B. L., & Katritch, V. (2019). Harnessing ion-binding sites for GPCR pharmacology. *Pharmacological Reviews*, *71*(4), 571–595. https://doi.org/10.1124/pr.119.017863

Zhang, H., Sturchler, E., Zhu, J., Nieto, A., Cistrone, P. A., Xie, J., He, L., Yea, K., Jones, T., Turn, R., di Stefano, P. S., Griffin, P. R., Dawson, P. E., McDonald, P. H., & Lerner, R. A. (2015). Autocrine selection of a GLP-1R G-protein biased agonist with potent antidiabetic effects. *Nature Communications*, *6*(May), 1–13. https://doi.org/10.1038/ncomms9918

Zhang, Y., Yang, F., Ling, S., Lv, P., Zhou, Y., Fang, W., Sun, W., Zhang, L., Shi, P., & Tian, C. (2020). Single-particle cryo-EM structural studies of the β2AR–Gs complex bound with a full agonist formoterol. In *Cell Discovery* (Vol. 6, Issue 1). Springer Nature. https://doi.org/10.1038/s41421-020-0176-9

Zhao, P., & Furness, S. G. B. (2019). The nature of efficacy at G protein-coupled receptors. *Biochemical Pharmacology*, 113647. https://doi.org/10.1016/j.bcp.2019.113647

Zocher, M., Zhang, C., Rasmussen, S. G. F., Kobilka, B. K., & Müller, D. J. (2012). Cholesterol increases kinetic, energetic and mechanical stability of the human β_2-adrenergic receptor. *PNAS*, *109*(50), 3463–3472. https://doi.org/10.1073/pnas.1210373109